



**BROADCAST VS PRECISE GPS
EPHEMERIDES:
A HISTORICAL PERSPECTIVE**

THESIS

David L.M. Warren, BEng (Elec)
Squadron Leader, Royal Australian Air Force

AFIT/GSO/ENG/02M-01

**DEPARTMENT OF THE AIR FORCE
AIR UNIVERSITY**

AIR FORCE INSTITUTE OF TECHNOLOGY

Wright-Patterson Air Force Base, Ohio

APPROVED FOR PUBLIC RELEASE; DISTRIBUTION UNLIMITED.

Report Documentation Page

Report Date 26 Mar 02	Report Type Final	Dates Covered (from... to) Aug 2000 - Mar 2002
Title and Subtitle Broadcast vs Precise GPS Ephemerides a Historical Perspective	Contract Number	
	Grant Number	
	Program Element Number	
Author(s) Squadron Leader, David L. M. Warren, RAAF	Project Number	
	Task Number	
	Work Unit Number	
Performing Organization Name(s) and Address(es) Air Force Institute of Technology Graduate School of Engineering and Management (AFIT/EN) 2950 P Street, Bldg 640 WPAFB, OH 45433-7765	Performing Organization Report Number AFIT/GSO/ENG/02M-01	
Sponsoring/Monitoring Agency Name(s) and Address(es) Major David Goldstein, SMC/CZE 2435 Vela Way Suite 1613 El Segundo, CA 90245-5500	Sponsor/Monitor's Acronym(s)	
	Sponsor/Monitor's Report Number(s)	
Distribution/Availability Statement Approved for public release, distribution unlimited		
Supplementary Notes The original document contains color images.		

Abstract

The Global Positioning System (GPS) Operational Control Segment (OCS) generates predicted satellite ephemerides and clock corrections that are broadcast in the navigation message and used by receivers to estimate real-time satellite position and clock corrections for use in navigation solutions. Any errors in these ephemerides will directly impact the accuracy of GPS based positioning. This study compares the satellite position computed using broadcast ephemerides with the precise position provided by the International GPS Service for Geodynamics (IGS) Final Orbit solution. Similar comparisons have been undertaken in the past, but for only short periods of time. This study presents an analysis of the GPS broadcast ephemeris position error on a daily basis over the entire period 14 Nov 1993 through to 1 Nov 2001. The statistics of these errors were also analysed. In addition, the satellite position computed using the almanac ephemeris was compared to the IGS precise final orbit to determine the long-term effect of using older almanac data. The results of this research provide an independent method for the GPS Joint Program Office (JPO) and the OCS to gauge the direct impact of Kalman filter modifications on the accuracy of the navigational information available to the GPS users. GPS engineers can compare future Kalman filter changes to the historical baseline developed by this thesis and readily assess the significance of each proposed engineering change.

Subject Terms

GPS, Global Positioning, Ephemeris, Ephemerides, Navigation, Error, Almanac, Broadcast

Report Classification

unclassified

Classification of this page

unclassified

Classification of Abstract

unclassified

Limitation of Abstract

UU

Number of Pages

182

The views expressed in this document are those of the author and do not reflect the official policy or position of the U.S. Department of Defense, the U.S. Government, or the Government of the Commonwealth of Australia.

BROADCAST VS PRECISE GPS EPHEMERIDES:
A HISTORICAL PERSPECTIVE

THESIS

Presented to the Faculty

Department of Electrical and Computer Engineering

Graduate School of Engineering and Management

Air Force Institute of Technology

Air University

Air Education and Training Command

In Partial Fulfilment of the Requirements for the

Degree of Master of Science in Space Operations

David L.M. Warren, BEng (Elec)

Squadron Leader, Royal Australian Air Force

March 2002

APPROVED FOR PUBLIC RELEASE; DISTRIBUTION UNLIMITED

BROADCAST VS PRECISE GPS EPHEMERIDES:
A HISTORICAL PERSPECTIVE

David L.M. Warren, BEng (Elec)

Squadron Leader, Royal Australian Air Force

Approved:



John F. Raquet, Ph.D., Major, USAF (Chairman)

11 MAR 2002

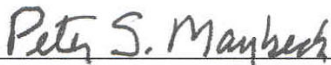
date



Steven Tragesser, Ph.D., (Committee Member)

11 MAR 2002

date



Peter Maybeck, Ph.D., (Committee Member)

11 Mar 2002

date

Acknowledgments

I would like to express my sincere appreciation to my thesis advisor, Major John Racquet for his support and encouragement over the course of my studies. I would also like to thank my committee members, Dr. Steven Tragessor and Dr. Peter Maybeck for their guidance and advice. I have relied heavily upon the support provided by each of the committee members. I have been guided in this research by the efforts of Major David Goldstein, Ph.D. (Chief, Engineering Branch, Navstar GPS JPO) and the staff of the GPS JPO. I would also like to acknowledge the contribution made to my work by Angelyn Moore, Ph.D. (Deputy Director, IGS Central Bureau) and Ms. Carey Noll (Manager, Crustal Dynamics Data Information System) who provided the data files referenced throughout this thesis.

I am very grateful to the Royal Australian Air Force for giving me the opportunity to study at AFIT and experience, for twenty months, American life and culture. While studying has been a privilege for me, my fondest memories will be of the people, social events and places. I must extend a special thank you to Annette, Jo, Lynne and Janet in the International Students Office for their untiring efforts in support of the international families.

To my wife, I can only say 'I love you. Thanks for sticking by me whilst I spent all those nights studying'.

Table Of Contents

	Page
Acknowledgments	v
Table Of Contents	vi
List Of Figures	x
List Of Tables.....	xii
Abstract	xiii
I. Introduction.....	1
Research Objectives.....	2
Motivation.....	2
Summary.....	2
II. Background And Literature Review	4
Introduction.....	4
GPS System Overview	4
Background	4
Space Segment.....	6
Operational Control Segment (OCS)	8
User Segment	10
Space Segment Error Sources.....	10
Earth Oblateness Perturbations	11
Third Body Gravitational Perturbations	12
Solar Radiation Pressure (SRP) Torque	13
Yaw-Bias	13
Fixed Body Tides	14
Earth's Albedo	14
Aerodynamic Torque / Drag	14
Gravity Gradient Torque	15
Satellite Clock Phase Error	15
Non Space Segment Error Sources.....	16
Miscellaneous	16

	Page
Foliage attenuation	16
Selective Availability (SA)	16
Relativistic Effects	17
Multipath	18
Ionosphere	18
Troposphere	19
Scintillation	19
Receiver Noise	20
Geometric Dilution Of Precision (GDOP)	20
GPS Navigational Errors	20
Operational Control Segment Performance Measures	22
Observed Range Deviations (ORD)	22
Estimated Range Deviations (ERDs)	23
NAVigational SOLutions (NAVSOLs)	24
Smoothed Measurement RESidual Generator (SMRES)	24
A Posteriora Analysis	25
Orbit and Clock State Comparisons	26
Laser Ranging Residuals	27
Previous Analysis	28
GPS OCS Performance Analysis and Reporting (GOSPAR)	28
University of New Brunswick Study	29
Other Studies	29
Orbit Generation	30
Broadcast / Almanac Orbit	30
IGS Final Orbit	31
Data Formats.....	32
Broadcast Ephemeris	32
Almanac Ephemeris	32
IGS Final Orbit	33
Summary.....	33
III. Analysis and Modelling Methodologies.....	34
Introduction.....	34
Required Outputs	34
Required Inputs.....	35
Method of Analysis.....	35
Overview of the Process	36
Broadcast Orbit	36
Almanac Orbit	37
Analysis Parameters and Assumptions.....	39
Study Analysis Period	39
Ephemeris Data	39
The Sampling Interval	40
Orbit Analysis.....	42

	Page
Precise Orbit Analysis	42
Broadcast Ephemeris Analysis	42
Almanac Ephemeris Analysis	43
Error Analysis	43
Data Format	49
Summary.....	49
IV. Presentation and Analysis of Results.....	50
Introduction.....	50
Broadcast Orbit Position Error Results.....	50
Outlier Filtering	50
Along-Track, Cross-track and Radial	53
Statistical Analysis	60
3D ACR Broadcast Position Error	65
SISRE	69
Almanac Orbit Position Error Results	72
Outlier Filtering	72
Along-Track, Cross-track and Radial	72
Statistical Analysis	75
SISRE	76
Summary.....	78
V. Summary and Conclusions	79
Summary – Broadcast Ephemeris.....	79
Summary – Almanac Ephemeris	80
Conclusions.....	81
Recommendations.....	82
Appendix A: Data Format	83
Poserr	83
Rms	84
Stats	85
Sisre	86
Appendix B: Along-Track, Cross-track and Radial Broadcast Position Error	87
1 Nov 1994	87
1 Nov 1997	100
1 Nov 2000	113
Appendix C: RMS ACR Broadcast Position Error	127

	Page
Appendix D: 3D ACR Broadcast Position Error	143
Appendix E: Mean 3D ACR Broadcast Position Error.....	159
Bibliography.....	165
Vita	168

List Of Figures

Figure	Page
Figure II-1: GPS Segments	6
Figure II-2: GPS Constellation	7
Figure II-3: Keplarian Orbital Elements	8
Figure II-4: Operational Control Segment	9
Figure II-5: Constellation Orbit-Only SISRE	28
Figure II-6: OCS Ephemeris Generation Process	31
Figure III-1: Broadcast Analysis Process	37
Figure III-2: Almanac Analysis Process	38
Figure IV-1: Satellite broadcast position error - 3 Jan 1997	51
Figure IV-2: Daily outlier data epochs removed	53
Figure IV-3: ACR broadcast orbit position error, 1 Nov 1997, PRN 22, SVN 22	54
Figure IV-4: ACR broadcast orbit position error, 1 Nov 2000, PRN 22, SVN 22	55
Figure IV-5: ACR broadcast orbit position error, PRN 1, SVN 32	57
Figure IV-6: Histogram of ACR broadcast orbit position error, PRN 21, SVN 21	58
Figure IV-7: Histogram of ACR broadcast orbit position error, PRN 2, SVN 13	59
Figure IV-8: Histogram of ACR broadcast orbit position error, PRN 11, SVN 46	60
Figure IV-9: Mean RMS ACR broadcast position error, All active satellites	62
Figure IV-10: RMS ACR broadcast position error, PRN 7, SVN 37	63
Figure IV-11: RMS ACR broadcast position errors, PRN 13	64
Figure IV-12: 3D ACR broadcast orbit position error, PRN 14	66
Figure IV-13: RMS 3D ACR broadcast orbit position error - 1995	68

	Page
Figure IV-14: RMS 3D ACR broadcast orbit position error – 2000	68
Figure IV-15: RMS constellation broadcast orbit-only SISRE	69
Figure IV-16: RMS Block II constellation broadcast orbit-only SISRE	70
Figure IV-17: RMS Block IIR constellation broadcast orbit-only SISRE	71
Figure IV-18: PRN 21 Almanac ACR position error for week 1042 almanac	73
Figure IV-19: PRN 3 Almanac ACR position error for week 1042 almanac	74
Figure IV-20: PRN 13 Almanac ACR position error for week 1042 almanac	75
Figure IV-21: RMS constellation SISRE almanac position error	77
Figure IV-22: RMS constellation SISRE almanac position error	77

List Of Tables

Table	Page
Table II-1: Common GPS Spacecraft Perturbations	11
Table III-1: Antenna Phase Centre Offset	44
Table IV-1: 3D Broadcast Ephemeris Error Statistics	61
Table IV-2: 3D Almanac Ephemeris Error Statistics	76

Abstract

The Global Positioning System (GPS) Operational Control Segment (OCS) generates predicted satellite ephemerides and clock corrections that are broadcast in the navigation message and used by receivers to estimate real-time satellite position and clock corrections for use in navigation solutions. Any errors in these ephemerides will directly impact the accuracy of GPS based positioning.

This study compares the satellite position computed using broadcast ephemerides with the precise position provided by the International GPS Service for Geodynamics (IGS) Final Orbit solution. Similar comparisons have been undertaken in the past, but for only short periods of time. This study presents an analysis of the GPS broadcast ephemeris position error on a daily basis over the entire period 14 Nov 1993 through to 1 Nov 2001. The statistics of these errors were also analysed. In addition, the satellite position computed using the almanac ephemeris was compared to the IGS precise final orbit to determine the long-term effect of using older almanac data.

The results of this research provide an independent method for the GPS Joint Program Office (JPO) and the OCS to gauge the direct impact of Kalman filter modifications on the accuracy of the navigational information available to the GPS users. GPS engineers can compare future Kalman filter changes to the historical baseline developed by this thesis and readily assess the significance of each proposed engineering change.

BROADCAST VS PRECISE GPS EPHEMERIDES: A HISTORICAL PERSPECTIVE

I. Introduction

The NAVigational System using Timing And Ranging (NAVSTAR) Global Positioning System (GPS) Operational Control Segment (OCS) generates predicted satellite ephemerides and clock corrections that are broadcast in the navigation message and used by receivers to estimate real-time satellite position and clock corrections for use in navigation solutions. The generation of the navigation message starts with the OCS's use of a Kalman filter to estimate satellite position, velocity, solar radiation pressure coefficients, clock bias, clock drift; and clock drift rate. These estimated parameters are then used to propagate the satellite position and clock corrections into the future. The propagated values are then fit to a set of equations and the fit coefficients are broadcast in the navigation message.

This study extends the work of the GPS OCS Performance Analysis and Reporting (GOSPAR) Project, over the entire operational lifetime of the GPS program. The primary objective of this research has been to compare the broadcast orbit with precise values. The secondary objective has been to compare the almanac orbit with precise values to determine the effect of age of data on almanac position error.

Research Objectives

The research objectives of this thesis are as follows:

- Compare the GPS broadcast orbit with the International GPS Service (IGS) final orbit over the GPS program's operational history.
- Compare the GPS almanac orbit with the IGS final orbit to determine the effect of age of data on almanac error.

Motivation

Modifications are often made to the OCS Kalman filter to improve the accuracy of the broadcast ephemerides [Spilker 1996-1]. These modifications include updating solar radiation pressure models, satellite mass, ground station coordinates, and process noise covariance values. Unfortunately, there is no independent publicly available procedure for gauging the effect of Kalman filter 'tweaking' on broadcast ephemeris accuracy, when compared to precise orbits.

The results of this thesis provide an independent method for the GPS Joint Project Office (JPO) to gauge the direct impact of Kalman filter modifications on the accuracy of the navigational information available to the Navstar GPS users. GPS JPO engineers can compare future Kalman filter changes to the historical baseline developed by this thesis and readily assess the significance of each proposed engineering change.

Summary

This chapter defined the goals for conducting the research and described the motivation leading to the selection of those goals. Chapter 2 provides the background

necessary to support the research and presents a review of relevant literature in the areas of satellite orbit analysis, GPS error sources and GPS Kalman filter modifications. Chapter 3 explains the methodology used to compare the broadcast ephemerides against the IGS data. Chapter 4 presents the results of the analysis of GPS broadcast and almanac orbit performance. Chapter 5 contains conclusions from the research and recommendations for further research.

II. Background And Literature Review

Introduction

GPS is the premier global navigation system in use today. During its design phase, an error budget allocated tolerances for each major navigation error source. Each of these environmental and non-environmental error sources has been evaluated and their impact on GPS analysed. The many GPS performance analysis methods were discussed, including both operational level and post-performance analysis. This chapter provides the background necessary to support this research and presents a review of relevant literature on satellite orbit analysis, GPS error sources, and the performance of the GPS system.

GPS System Overview

Background

Navstar GPS is a direct result of operational experience obtained from the USAF 621B Project, the USN Research Laboratories TIME navigATION (TIMATION) program, and the Applied Physics Laboratories TRANSIT Navy Navigation Satellite System (NNSS) [Parkinson 1996, pp 4-6]. The GPS program commenced in 1973 as a replacement for the 200-metre accuracy TRANSIT system (finally retired in 1996 [Nelson 2002]). The first group of satellites consisted of two Navigation Technology Satellites (NTS) launched to explore space-based navigational technology. A follow-on contract was let to Rockwell International in 1974 for eleven Block I prototype NAVSTAR satellites. Only ten of the satellites were successfully launched due to a failure of one Atlas F booster. The first satellite was launched in February 1978 and the last in 1985 [Nelson 2002].

To develop an operational navigational system, a contract was let to Rockwell International for 9 Block II and 19 Block IIA satellites. The Block II satellites were launched commencing in August 1989 and concluding in 1990. The Block IIA satellites were launched from 1990 through to 1997 [Nelson 2002]. The Block II / IIA satellites have significantly exceeded their six year design life.

Initial Operating Capability (IOC) and Final Operating Capability (FOC) (full 24-satellite constellation) were achieved on 8 December 1993 and 27 April 1994 respectively [Tutor 2002, USNO 2002]. A contract is currently in place to launch (as required) up to 26 Block IIR replenishment satellites. The Block IIR satellites have enhanced autonomy via cross link ranging, increased radiation hardening [Parkinson 1996, p20] and a design life of ten years [Tutor 2002]. The first Block IIR satellite was unsuccessfully launched in 1997 due to a booster failure and the first successful launch was also in 1997 [Tutor 2002].

A new generation of Block IIF satellites are under development by Boeing (formally Rockwell International). The new satellites have a 12.7-year design life and will be supported by an enhanced ground infrastructure.

Figure II-1 displays the three segments of the GPS system and the communications links used [NRC 1995, p 151]. Each of these segments will be briefly described in the following sections.

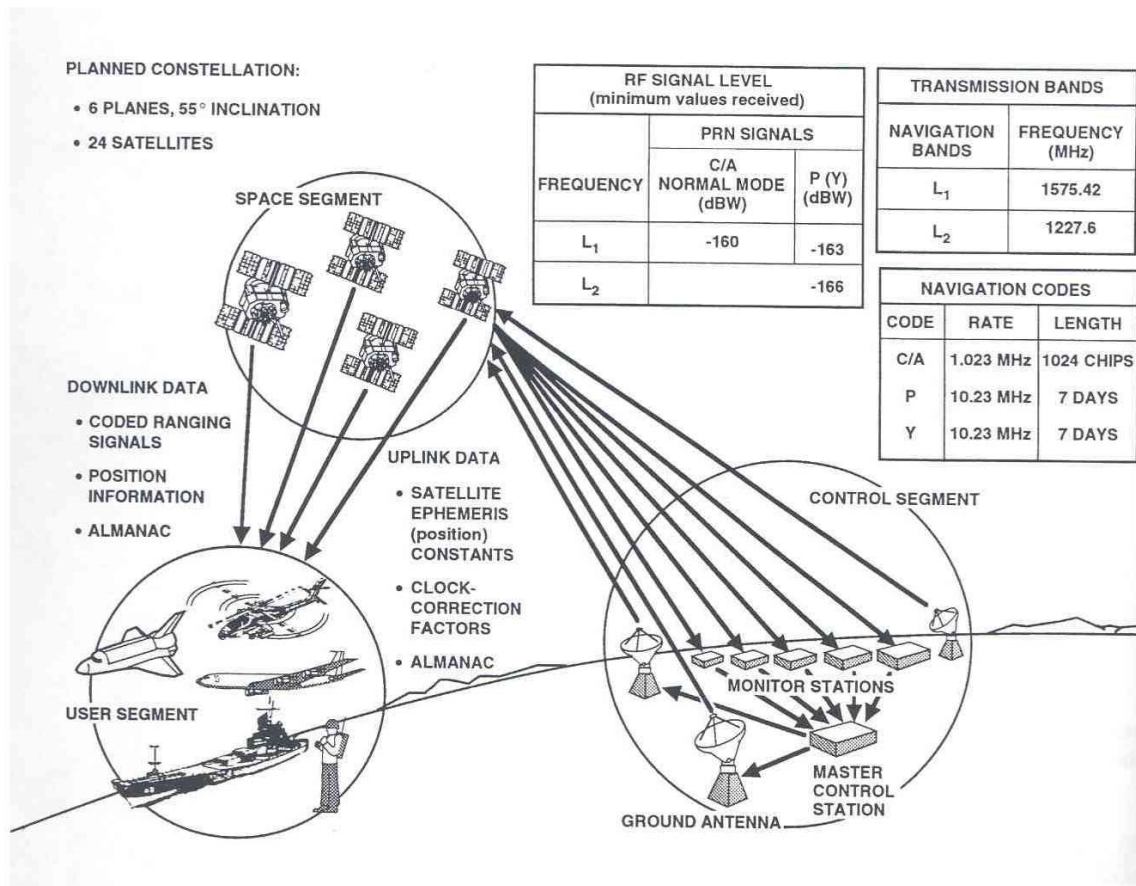


Figure II-1: GPS Segments

Space Segment

Satellite Orbit. The GPS system features a constellation of 24 satellites deployed in six orbital planes, each comprising four satellites. This constellation is sufficient to provide global coverage of approximately five to eight simultaneous satellites [Info 2002]. Each orbit plane is inclined at 55° (nominal) (63° for Block I satellites [Hofmann-Wellenhof 1994, p15]), and each satellite has a period of 12 hrs sidereal time (1 sidereal day = 23 h 56 min 4.009054s), which corresponds to an orbital altitude of 20,162.61 km at the equator.

The GPS orbits also have the following approximate characteristics [Spilker 1996-1, p40]:

- Angular velocity - 1.454×10^{-4} rad/s
- Eccentricity less than 0.02 (nominally zero)
- Earth Centred Inertial (ECI) Orbit velocity - 3.8704 km/s
- Orbit radius - 26561.75 km semi major axis (Mid Earth Orbit (MEO))

Figure II-2 depicts the GPS constellation as derived from the NORAD two-line element set [Kelso 2002, Garmin 2002].



Figure II-2: GPS Constellation

Figure II-3 describes the GPS orbit in terms of Keplerian orbital elements [Hofmann-Wellenhof, p45].

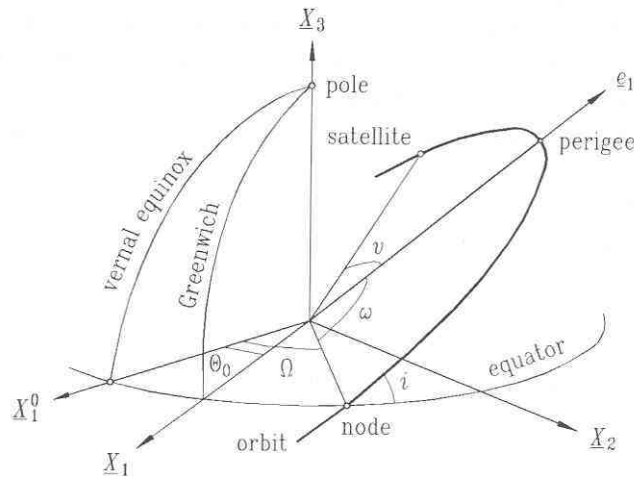


Figure II-3: Keplerian Orbital Elements

Where,

Ω = Right Ascension of Ascending Node (RAAN)

i = Inclination of the Orbital Plane

ω = Argument of Perigee

a = Semi major axis of orbital plane

e = Numerical eccentricity of ellipse

T_0 = Epoch of Perigee Passage

Communication Links. The satellite-to-user downlink operates in the L-Band at 1227 and 1575 MHz. Telemetry and data uplink from the control segment is achieved using an S-Band communications link [Spilker 1996-1].

Operational Control Segment (OCS)

The OCS became operational in 1985 and consists of five monitoring stations (shown in Figure II-4 [Spilker 1996-1, p42]) three-ground antenna upload stations and one Master Control Station (MCS). The stations were selected to provide longitudinal separation and are

located at Hawaii (monitoring station only), Colorado Springs (monitoring station only), Ascension Island, Diego Garcia and Kwajalein Island [Spilker 1996-1]. The MCS is located at Schriever Air Force Base in Colorado Springs and is operated by the 2nd Satellite Operational Squadron (2SOPS) [USNO 2002, Boeing 2002].

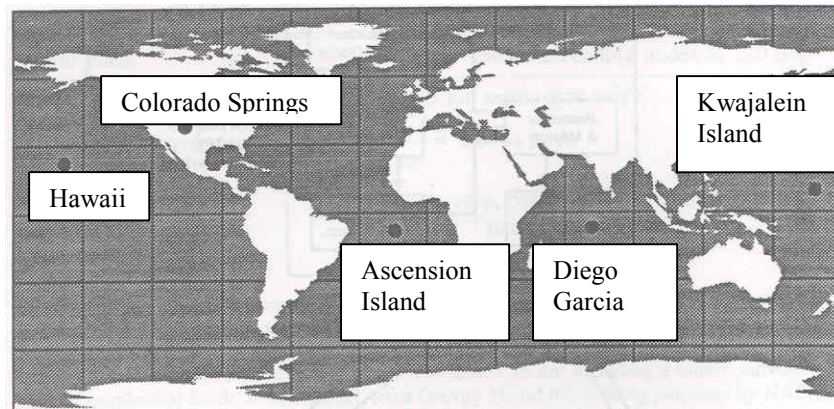


Figure II-4: Operational Control Segment

The OCS has four main objectives:

- Maintain each SV in its proper orbit through small commanded manoeuvres.
- Make corrections to the SV clocks and payload as required.
- Track each SV and generate and upload navigational data to each SV.
- Monitor the constellation and correct for any SV failures.

The MCS receives pseudorange and carrier-phase measurements from each satellite via the monitoring stations. The measurements are fed into a Kalman filter which estimates each satellite's ephemerides, all clock errors, and other navigational information. The MCS formats data for a minimum of fourteen days of uploads, which are then fed to each satellite using the upload stations. Uploads can occur up to three times daily; however, it is typical for only one daily upload to occur [Spilker 1996-1 p42].

User Segment

The user segment consists of all GPS receivers that track and decode the GPS signal for the purposes of determining precise position or time information [Spilker 1996-1, p45]. Possible uses include land, air, maritime, and space navigation, SV orbit determination, kinematic survey, time transfer, and attitude determination. The user segment may also monitor variations in the GPS signal over time to determine environmental variations (such as ionospheric changes).

Space Segment Error Sources

If the GPS navigational message contains errors in each satellite's location, that error will translate to a user position error. The radial component of a satellite's ephemeris error is normally the smallest; however, it has the largest impact on the user's calculated position. Along-track and cross-track components are larger than the radial component by an order of magnitude but have little impact of the resultant user position error [Roulston 2000, p50].

The primary force on an Earth-orbiting satellite is the gravitational attraction that results from the Earth's mass, which can be modelled as a uniform density sphere. Equation (1) describes the two-body equation of motion derived by Isaac Newton for a satellite orbiting the Earth:

$$\frac{d^2 \bar{r}}{dt^2} + \left(\frac{\mu}{r^3}\right) \bar{r} = 0 \quad (1)$$

Forces that cause deviations from the above ideal model are called perturbations. For the GPS constellation, minor inaccuracies in the orbital path of each satellite can translate to

major discrepancies in navigational solutions. Table II-1 shows the effect of common spacecraft perturbations [Beutler 2001].

Table II-1: Common GPS Spacecraft Perturbations

Perturbation	Approximate effect on a GPS satellite	
	Acceleration (m/s ²)	Orbital Error after one day (m)
Two-Body Term of Earth's Gravitational Field	0.59	∞
Earth Oblateness – J2 Term	5×10^{-5}	10,000
Lunar Gravitational Attraction	5×10^{-6}	3,000
Solar Gravitational Attraction	2×10^{-6}	800
Earth's Gravitational Field – Other Terms	3×10^{-7}	200
Solar Radiation Pressure (Direct)	9×10^{-8}	200
Solar Radiation Pressure (Y-Bias)	5×10^{-10}	2
Fixed Body Tides	1×10^{-9}	0.3
Earth's Albedo	1.1×10^{-9}	0.3
Atmospheric Drag	0	Negligible
Gravity Gradient Torque	Negligible	Negligible

Earth Oblateness Perturbations

The Earth is non-spherical — it bulges at the equator and is flattened ($f = 1 / 298.257$) at the poles. The uneven distribution of the Earth's mass causes perturbations from the above ideal Newtonian gravitational force. The effect of this oblateness on a satellite can be determined by taking the gradient of the Earth's gravitational potential, which is expressed as a function of zonal coefficients, which map the Earth's gravitational field.

The dominant effect of the non-spherical Earth is a secular (linear with time) variation of right ascension of the ascending node and argument of perigee due to Earth oblateness, mapped by the J_2 (0.00108263) zonal coefficient. The effect of lower level zonal coefficients is significantly less than the impact of the J_2 zonal coefficient [Spilker 1996-2, p164].

Third Body Gravitational Perturbations

The relatively small gravitational effects on a satellite due to each non Earth solar system body (Sun, Moon and near planets) perturbs the satellite away from the natural Earth-satellite two body motion. The exact force each body exerts on the satellite is dependent upon the distance between that body and the satellite. The sun and moon cause periodic (less than one orbit) variations in all of the orbital elements. However, only right ascension of the ascending node, argument of perigee, and mean anomaly experience secular variations. The secular variation in mean anomaly due to third body perturbations is negligible. The secular variations for right ascension of the ascending node and argument of perigee due to third body perturbations are both significant, especially for MEO orbits [Spilker 1996-2, p168].

Gravitational perturbations dominate for near-Earth orbits; however, due to the orbital accuracy and precision required for the GPS system, they are still significant even at MEO [Cook 2001, p2-4]. Hofman-Wellenhof provides a detailed discussion of the perturbations and their formulas [Hofman-Wellenhof 1994].

Solar Radiation Pressure (SRP) Torque

SRP is the impingement of photons of light upon a satellite's surface, which imparts energy to that surface via an exchange of momentum [Hofman-Wellenhof 1994, p1-2]. Variations in SRP across a satellite's exposed surface generate a resultant torque. SRP varies across a satellite's orbit as orbital characteristics and attitude change. Variations in a satellite's cross-sectional area incident to the sun, time periods eclipsed by the Earth, and reflection off satellite surfaces all vary the SRP imparted onto a satellite [Hofman-Wellenhof 1994, p1-2].

A prime example of the effects of SRP is the 30-metre ECHO balloon satellite launched in 1960. At an altitude of 1852 km, ECHO experienced a 3.5 km / day decrease in perigee height due to SRP [Hofman-Wellenhof 1994, p1-2]. SRP is the dominant non-gravitational force on a MEO satellite, and therefore it is the largest non-gravitational error source for a GPS orbit [Springer 1999, pp 673-676].

Yaw-Bias

Yaw misalignment within the GPS satellite's attitude control system results in a misalignment of the satellite's solar radiation panels. Solar radiation pressure on these misaligned panels results in a rotational force around the zenith-axis. Thermal radiation along the y-axis (cross-track) accentuates the rotational force [Hofman-Wellenhof 1994, p54].

Fixed Body Tides

When two objects interact, they stretch slightly along the symmetric line between them. For the Earth this stretching results in a bulge towards bodies such as the moon; this bulge consists of both crustal deformation and ocean tides [Tidal Forces 2002]. The impact of these tides on the GPS constellation is very small.

Earth's Albedo

A small portion of the solar radiation incident upon the Earth is reflected back out into space. The effect is called albedo. The solar radiation pressure on GPS satellites (due to albedo) is minimal and the effect on the GPS satellites orbit is very small [Tidal Forces 2002, p58].

Aerodynamic Torque / Drag

Aerodynamic torque is any force applied to a vehicle that results from drag between that vehicle and atmospheric particles. Drag particularly affects Low Earth Orbit (LEO) satellites since the concentration of particles decreases with altitude. Aerodynamic drag slows a satellite, which decreases its orbital altitude. The leading edge of a satellite is rarely an aerodynamically consistent surface and this is accentuated by a satellite's rotation. These inconsistencies cause the aerodynamic drag to vary across the leading edge; any uneven drag generates a rotational force on the satellite [Wertz 1999, p145].

Aerodynamic drag due to the bulk of the Earth's atmosphere has negligible affect on the MEO GPS constellation; however, drag due to particles within the Van Allen Belt is significant. The concentration of particles within the Van Allen Belt increases exponentially with increases in the Sun Spot Number (SSN). The relationship between particle

concentration (and therefore drag) and SSN has been modelled for low solar activity, but it is difficult to predict for an active solar cycle [Wertz 1999, p145].

An example of the impact of aerodynamic drag is the Skylab space station. A significant factor that contributed to Skylab's loss was the expansion of the ionosphere due to increased solar activity, which increased aerodynamic drag and degraded Skylab's orbit [Springer 1999, p1-3].

Gravity Gradient Torque

The gravitational force between two bodies is inversely proportional to R^2 where R is the distance between them. This relationship between gravitational force and distance causes a rotational force on the satellite, which tends to align the satellite's longest axis (about which the moment of inertia is minimal) with the local vertical. The effect of this gravitational gradient is that it adds an extra rotational force that complicates modelling of the above major perturbations. The gravity gradient is difficult to model due to changing geometry of the Earth, Sun and Lunar gravitational sources with respect to GPS satellites [Weisal 1995, p149].

Satellite Clock Phase Error

Each of the satellite clocks is subject to clock drift and frequency errors. Individual clocks can vary by as much as one second from GPS system time. An offset correction is transmitted in the navigational message, which each receiver can use to correct for clock phase errors. Clock deviations not accounted for in the offset correction can cause an approximate error of up to 0.31 metres in equivalent range; however, for a non-differential

receiver this error is indistinguishable from ephemeris errors, so they are combined in the ephemeris error budget [NRC 1995, p161].

Non Space Segment Error Sources

Miscellaneous

Many miscellaneous control functions performed onboard a satellite can convert momentum from the process to satellite rotational movement. Examples of these processes include fluid ventilation, antennae distribution, solar panels distribution, movement of instruments, deploying arms and appendices, opening or closing doors and lens covers, and redistribution of fuel.

Foliage attenuation

The GPS signal is attenuated as it passes through foliage. This attenuation can be sufficient to cause a GPS receiver to lose frequency lock on a satellite.

Selective Availability (SA)

SA was activated on 4 July 1991 at 0400UT [Nelson 2002] and then deactivated on GPS day 123 (02 May 00) at 0407Z [OA 2001]. SA is the intentional degradation of the SPS signal by introducing a time varying bias. Since SA bias varies between satellites and due to its low frequency period, SA can be mostly removed by averaging the signal over time. SA is introduced by manipulating the navigational message orbit data (epsilon) and / or the satellite clock frequency (dither) [USNO 2002]. When activated, SA is the single largest error source for GPS [NA 1991].

Relativistic Effects

Albert Einstein's theories of special and general relativity account for the gravitational effects of Earth magnetic field and Earth rotation. The relative velocities of the satellite and the user cause an average increase in satellite clock frequency as observed by any stationary observer.

Einstein's theories include three influences. The first influence includes time dilation and red shift. Time dilation is the effect that a moving clock runs slower than a stationary clock from the perspective of the stationary user (7 μs slower for GPS). Red shift is the effect that clocks in a weaker gravitational potential run faster compared to clocks in a stronger gravitational potential (45 μs faster for GPS). The net result of the first influence is that the GPS signal frequencies were set lower during design to allow for the 38 μs faster clock [Nelson 2002].

The second influence is that residual eccentricity in the satellite orbit causes periodic variations in the time dilation and red shift observed by a user. Therefore a receiver must be designed to account for these variations [Nelson 2002].

As the GPS signal propagates from the satellite to the user, the receiver inertial position with respect to the satellite changes. This is the third influence, called the Sagnac Effect; and it is especially evident when the receiver is onboard a moving platform. The receiver must also correct this effect [Nelson 2002].

Multipath

Multipath communications occur when propagation conditions allow, or force, a transmitted radio wave to reach the receiving antenna by two or more propagation paths. There are three primary mechanisms by which multipath communications can occur: refraction, reflection, and diffraction. Each of these mechanisms occurs when a propagating radio wave encounters refractive index irregularities in the earth's atmosphere or structural and terrain obstructions on the surface of the earth [Crowe 1999, p6]. Multipath due to reflections close to the receiver are especially detrimental to GPS signals [Overview 2002].

Ionosphere

Ionospheric scintillation is produced by electron density fluctuation in the ionosphere, the most significant of which occurs at the F2 Layer peak at an altitude of 225 to 400 km above the earth's surface. The varying electron densities cause fluctuations in the scatter, refraction, and diffraction effects experienced by transiting electromagnetic waves. These variations may result in signal cancellation or reinforcement, which is observed as rapid changes in the characteristics of the received signal. Factors influencing the severity of ionospheric impact include the time of year, local time of day, the level of solar activity, level of geomagnetic activity, user latitude and satellite height [Tascione 1994, p113].

The primary effects of the ionosphere on GPS signals are group delay of the signal and an advance of the carrier phase. The intensity of the signal modifications varies with signal path and with ionospheric electron density. Another minor impact of the ionosphere is Faraday rotation, which changes the angle of arrival of the signal. Faraday rotation has an insignificant impact on the GPS signal [Tascione 1994, p113]. By comparing the

propagation time of the L1 and L2 GPS signals, Precise Positioning Service (PPS) users can remove most of the ionospheric interference [Spilker 1996-1, p51].

Troposphere

Tropospheric scintillations are produced when transiting radio waves pass through regions of the atmosphere that are subject to refractive index fluctuations with time and height. These fluctuations are caused by high humidity gradients and temperature inversion layers and generally occur in the lowest few kilometres of altitude. The effects are strongly correlated with season, local time of day, and with local climate and latitude [Pollock 2001, p10]. Since the troposphere is comprised of non-ionised gas, it is non-dispersive to RF signals. The troposphere does however cause a group delay of the GPS signal of approximately 2.6 metres at zenith and greater than 20 metres at elevations less than 10 degrees [Spilker 1996-1, p52]. Simple models are used to remove the bulk of the tropospheric error. To remove more of the tropospheric error, complex models requiring precise temperature, pressure and humidity are needed [Overview 2002].

Scintillation

Scintillation describes the rapid fluctuations in the characteristics of a radio wave caused by time-dependent and small-scale irregularities in the transmission path. Scintillation effects can be produced in the ionospheric and tropospheric regions of the earth's atmosphere; however, occurrences of scintillation are rare [Tascione 1994, p123].

Receiver Noise

Even the best GPS receivers introduce extra errors into the signal measurement path, both due to environmental and thermal noise. Noise sources include analogue-to-digital quantisation, and tracking loop design. Most of these extra noises are essentially white in nature and therefore can be removed by averaging or smoothing [NRC 1995, p161].

Geometric Dilution Of Precision (GDOP)

GDOP is a measure of the geometric relationship between the receiver position and the positions of each of the satellites used in the navigational calculation. GPS navigational errors are magnified by the range vector differences between the receiver and the satellites used to calculate the navigational solution. The volume of the shape described by the unit vectors from the receiver to each satellite used for the position fix is inversely proportional to the GDOP of the constellation [Overview 2002]. Since each ranging error is multiplied by the appropriate GDOP term, geometric error is the second most significant non-environmental error source for GPS [Dias 2002].

GPS Navigational Errors

Several DoD and commercial organisations routinely monitor the accuracy of the GPS PPS and Standard Positioning Service (SPS). The GPS navigation accuracy specifications called for 16 metre 50% Spherical Error Probable (SEP) and 100 metre 95% 2 Dimensional (2D) Root Mean Square (RMS), for the PPS and SPS systems respectively [Malys 1997, p376]. These specifications were developed through operational experience gained from the USN TIMATION program, the USAF 621B Project, the USN NNSS project, and through simulations [Parkinson 1996, pp 4-6].

The above GPS real-time user accuracy specifications comprise ‘Signal-In-Space’ (SIS) and User-Equipment (UE) error components. The SIS Range Error (SISRE) is a measure of the fidelity of the navigation messages broadcast by the GPS satellites, and its accuracy is the responsibility of the OCS [Malys 1997, p376].

The UE Range Error (UERE) comprises receiver noise, tropospheric refraction, uncompensated ionospheric effects, multipath effects, and any other errors induced by a user’s local environment. UERE is dependent upon the receiver design and the environment in which a receiver is used. The original SPS GPS error budget allocated 6 metres to SISRE and 3.6 metres to UERE [Van Dierendonck 1980]. User Navigational Error is a measure of the total navigational error experienced by a user for defined equipment in a known environment.

$$UNE(1\sigma) = GDOP \sqrt{SISRE^2 + UERE^2} \quad (2)$$

where

$$\begin{aligned} GDOP &= \text{Geometric Dilution Of Precision} \\ UERE &= \text{Composite of all UE Range Errors} \end{aligned}$$

SISRE is the RMS of many individual SISRE values approximated using:

$$SISRE = \sqrt{(R - CLK)^2 + \left(\frac{1}{49}\right)(A^2 + C^2)} \quad (3)$$

where

$$\begin{aligned} R &= \text{Radial Ephemeris Error} \\ A &= \text{Along-track Ephemeris Error} \\ C &= \text{Cross-track Ephemeris Error} \\ CLK &= \text{SV Clock Phase Error (wrt GPS time)} \end{aligned}$$

Operational Control Segment Performance Measures

The OCS monitors three performance measures every 15 minutes to track the quality of the navigational message: Observed Range Deviations (ORDs), Estimated Range Deviations (ERDs), and NAVigational SOLutions (NAVSOLs). The OCS also monitors the Kalman filter estimates every 24 hours using a tool called Smoothed Measurement RESidual Generator (SMRES). These performance measures are described in the sections that follow.

Observed Range Deviations (ORD)

Using the broadcast navigational message, the World Geodetic System 1984 (WGS-84) coordinates of each Air Force monitor station, and the Kalman filter estimates for each station's clock offsets from GPS time, the OCS calculates the range to each satellite. The difference between that range and the measured smoothed pseudorange is the ORD for that satellite [Malys 1997, p377].

The RMS ORD is calculated for each station after calculating the ORD to all visible satellites. Since ORDs contain errors due to UEREs such as receiver and propagation effects, they do not provide a direct measure of SISRE by themselves; however, they do correlate with the residuals of the OCS Kalman filter estimation process [Malys 1997, p377]. Typical ORD RMS values in early 1997 were 2.3 metres [LMFS 1996].

Estimated Range Deviations (ERDs)

The OCS computes the orbit and satellite clock differences between the broadcast navigational message and the corresponding real-time Kalman filter states for each satellite. In this calculation the real-time Kalman filter orbit and clock estimates are treated as ‘truth’.

The orbit and clock differences are then projected onto the Line-Of-Sight (LOS) between the satellite and a fictitious ground site. The OCS selects a set of fictitious ground sites distributed evenly around the globe. At any given epoch, a set of ERDs is computed for each satellite for the subset of fictitious ground sites, which are visible from that satellite. The maximum and RMS ERDs are also computed for each satellite [Malys 1997, p377].

A set of 32 globally distributed sites, selected by the 2nd Space Operations Squadron (2SOPS), is spaced around the earth in five latitude bands. ERDs are a useful real-time tool to monitor the prediction error inherent in the broadcast navigation messages. When the prediction error exceeds a specified threshold, operators schedule a ‘contingency upload’ for that satellite.

ERD thresholds for contingency upload were set at 8 metres prior to 1997 and 5 metres after 1997 [Malys 1997, p377]. If no uploads are needed in a 24-hour period, then a once-a-day upload is performed. Careful monitoring of the ERDs can optimise the performance of GPS over a geographic region. Typical RMS ORD values in 1996 were 2.3 metres and 2.1 metres in 1997 [Malys 1997, p377]. The change between 1996 and 1997 was due to Kalman filter modifications made under the GPS Accuracy Improvement Initiative (AII) program and the 2SOPS Ephemeris Enhancement Endeavour (EEE) program [Malys 1997, Crum 1997].

NAVigational SOLutions (NAVSOLs)

Ionospherically corrected smoothed pseudoranges for at least four satellites in view of each monitoring station are used to calculate the 3D position of the monitoring station. The method used to calculate position is the same as for any generic PPS user.

The calculated positions are then compared to known monitor station locations. The error in the position location reflects errors in the GPS navigational message. However, it also includes receiver related errors, signal propagation errors, and DOP effects. Typical RMS 3D NAVSOL values in 1996 were 6 metres [Malys 1997, p377].

Smoothed Measurement RESidual Generator (SMRES)

SMRES is an offline independent analysis tool developed by Applied Research Laboratories of the University of Texas [Malys 1997, p377]. The OCS uses SMRES to evaluate the fidelity of the Kalman filter estimates for each satellite shortly after the end of each day. SMRES computes pseudorange residuals for all tracking stations operated by the National Imagery and Mapping Agency (NIMA) using the Kalman filter orbit and clock estimates and the known WGS-84 coordinates for each monitoring station.

The pseudoranges are corrected using standard data corrections such as L1 / L2 frequency ionospheric correction, tropospheric correction, relativistic correction, and signal propagation delay. SMRES doesn't rely on station clock estimates for the OCS Kalman filter, but instead it uses a linear model (clock phase and frequency covering the 24 hour period) to estimate each station's caesium clock. This linear model is later removed from the daily residuals at each station. This lack of dependence on the OCS filter, coupled with the

geographic diversity offered by the NIMA stations, allow the SMRES process to provide an independent assessment of GPS performance [Malys 1997, p377].

Daily RMS residuals for all NIMA stations and for all Air Force and NIMA combined stations are computed. The RMS value is calculated for each satellite, each monitor station, and for the entire constellation. The RMS values are edited to remove corrupted data (using a mean ± 3 -sigma filter). The estimates are given as a function of Age Of Data (AOD), where the Kalman filter estimates are zero AOD. These RMS residuals are then used to characterise the performance of the zero AOD Kalman filter states.

Constellation RMS values that exceed a 3.2 metre tolerance and individual satellite RMS residuals that exceed a 4.2 metre tolerance are flagged for investigation. This method allows detection of anomalous station performance and provides the 2SOPS with a mechanism to isolate a source of suspicious results. Typical RMS constellation SMRES residuals in 1996 were 1.3 metres and reduced to less than 0.8 metres in 1997, due to tuning by 2SOPS [Malys 1997, p377].

A Posteriora Analysis

Various test systems have been developed to enable OCS to quantify the effects of OCS algorithm improvements and to characterise Kalman filter performance and broadcast navigational message accuracy. Some of these systems were developed by the OCS, NIMA, Aerospace Corporation, Overlook Systems Technology, Lockheed Martin Federal Systems and the Naval Surface Warfare Centre Dahlgren Division [Malys 1997, p378].

Orbit and Clock State Comparisons

The primary method used for a posteriora analysis is a comparison of the OCS Kalman filter orbit and clock estimates with a set of more accurate post-fit ephemeris and clock estimates. The NIMA GPS precise orbit and clock estimates are normally used, since they were developed from data collected by multiple PPS stations and therefore provide clock estimates in addition to precise ephemeris.

The advantages of this method of a posteriora analysis include:

- Allows isolation of ephemeris from clock components in total SISRE,
- Facilitates characterisation of SISRE as a function of AOD (prediction span),
- Isolates SISRE from total User Ranging Error (URE),
- Editing of corrupt data generally not necessary,
- Can be projected along lines of sight to a specific location or user trajectory.

The results of these a posteriora analyses are usually presented as RMS SISRE values assuming that the NIMA data is a truth source. The satellite clock differences and the radial, along-track, and cross-track orbit differences at any given epoch are combined to get an individual SISRE for each satellite.

Equation (3) on page 21 is generally used for calculating the approximate SISRE. However, the formula does vary between studies due to organisational legacies. The RMS value can be calculated for each individual satellite over a selected period or for the entire constellation.

IGS precise orbits are sometimes used to calculate SISRE. The IGS uses an order of magnitude more stations than NIMA and therefore provides more accurate precise ephemeris and clock estimates. However since most IGS stations use SPS receivers, they include the effects of SA. IGS clock states cannot be directly compared to NIMA PPS clock states, so CLK in Equation (3) is normally set to zero and the SISRE is classified as ‘orbit-only’.

In 1996, the RMS SISRE for the Kalman filter estimates, when compared to the IGS final orbit, was 1.3 metres. The orbit-only RMS SISRE (compared to IGS final orbit) was 1.5 metres. A high correlation (correlation coefficient of 0.7 to 0.8) between the radial orbit and the clock differences results in the total SISRE being less than the orbit-only SISRE. The RMS orbit-only SISREs for the NIMA precise orbits (compared to IGS) were approximately 0.3 metres [LMFS 1996]. Since October 1996, when the NIMA implemented several estimation improvements the NIMA RMS, orbit-only SISREs have been in the range of 0.1 to 0.15 metres [Malys 1997, p378].

Laser Ranging Residuals

Satellite Laser Ranging (SLR) observations of GPS satellites have been collected using NASA’s Laser Reflector Array (LRA) since November 1993 [Utexus 2002]. Satellites 35 and 36 were both equipped with laser retro-reflector arrays prior to launch. Each array consists of 32 fused quartz corner cubes arranged on a flat panel in rows of four or five cubes. Observations of these two satellites from 1993, 1994, and 1995 were processed by the Naval Surface Warfare Center, Dahlgren Division (NSWCDD) to independently validate the OCS Kalman filter orbit estimates, the NIMA orbit estimates and the IGS orbits [LMFS 1996, GPS35/36].

Since SLR is independent of SV clock state estimates, it is interpreted as orbit-only SISRE. SLR RMS residuals in the period 1993 to 1995 were 1.3 metres [Malys 1997, p379]

Previous Analysis

The orbit and clock state comparison technique compared against NIMA precise estimates has been the primary post-performance assessment tool. Figure II-5 shows independently reported values of the constellation RMS SISRE measured over the last twelve years. Most samples consisted of only a few weeks of data within each year. Years without SISRE values have had insufficient analysis.

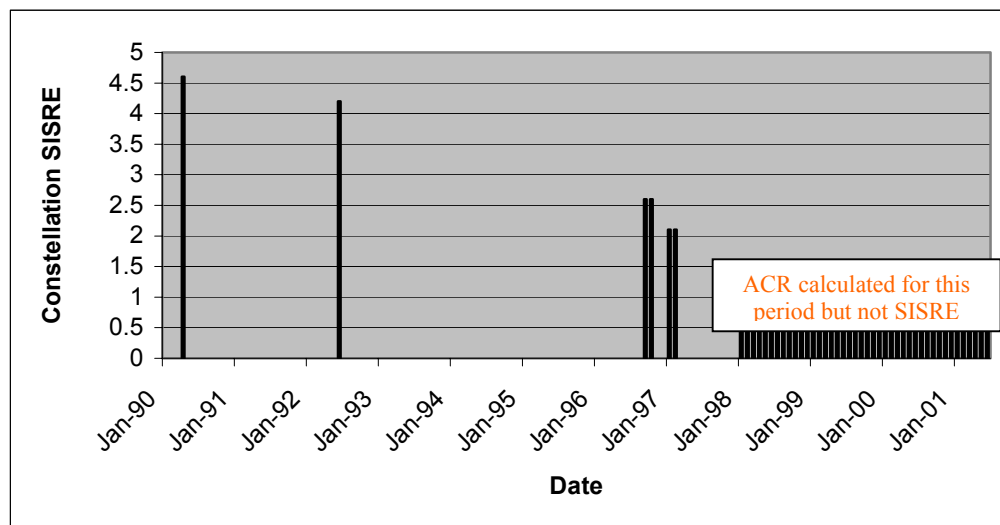


Figure II-5: Constellation Orbit-Only SISRE

GPS OCS Performance Analysis and Reporting (GOSPAR)

The most comprehensive study into GPS performance was undertaken by Overlook Systems Technology Inc and Lockheed Martin Federal Systems as part of the GOSPAR Project [LMFS 1996]. The GOSPAR project enabled the GPS Joint Project Office to examine the PPS performance attributes over an extended period on time on a global scale.

UERE, Universal Coordinated Time (UTC) Time Transfer Bias and Accuracy, Mission Effectiveness, and System Response Time were calculated to establish a top-level OCS performance baseline. The project aims were to assess how the dynamics of the operational environment affect GPS performance and to define a standard methodology for evaluating system performance. The study analysed data from 5 March 1996 through to 11 August 1997, but focussed on April 1997 [LMFS 1996].

University of New Brunswick Study

The University of New Brunswick has undertaken the most comprehensive study to date on the accuracy of the broadcast ephemeris message [Langley 2000]. The study determined the along-track, cross-track, radial and 3D broadcast position error, and the SISRE value for every day since 1 Jan 1999 and published the data at <http://gauss.gge.unb.ca/grads/orbit/>.

Other Studies

Zumberge and Bertiger from JPL studied the accuracy of the broadcast ephemeris for 7 Oct 1993 [Zumberger 1996, pp585-591]. They did not calculate SISRE, but their broadcast position error results were similar to those detailed in Chapter 4.

Jefferson and Bar-Sever from JPL studied the broadcast ephemeris over a two-year period 1 Jan 1998 to 29 Feb 2000 [Jefferson 2000, pp391 - 395]. They focussed on the influence of geographical location on broadcast position errors. They encountered the same outlier problem as discussed in Chapter 4.

Orbit Generation

Broadcast / Almanac Orbit

Figure II-6 describes the process used by the OCS to generate the broadcast and almanac ephemerides [Russell 1980, p76]. All ground stations determine ranging measurements to those satellites in view and feed that information to the MCS. The measurements received by the MCS include L1 pseudorange measurements, L1 – L2 pseudorange difference measurements, and integrated L1 doppler measurements. The corrector makes modifications to the measurements to account for known biases such as ionospheric delay, general and special relativistic effects, gravitational red shift, tropospheric refraction, satellite and ground stations antenna phase centre offsets, Earth rotation, and time tag correction [Russell 1980, p76].

A smoother is used to apply a bandpass filter of that filters out values that exceed the data's mean ± 3 -sigmas. The smoother then fits (using least squares) the measurements to a polynomial, which results in smoothed range and delta range measurements. A Kalman filter is used to produce estimates of the following states: satellite position and velocity, solar radiation pressure, satellite clock bias, satellite clock frequency offset, satellite clock drift rate, ground station clock bias and frequency offset, tropospheric residual bias, and polar wander residuals [Russell 1980, p76].

A predictor is used to propagate the Kalman filter states throughout the prediction span (12 hours), and the polynomial coefficients of this prediction are uploaded to the satellites as broadcast ephemerides [Russell 1980, p77].

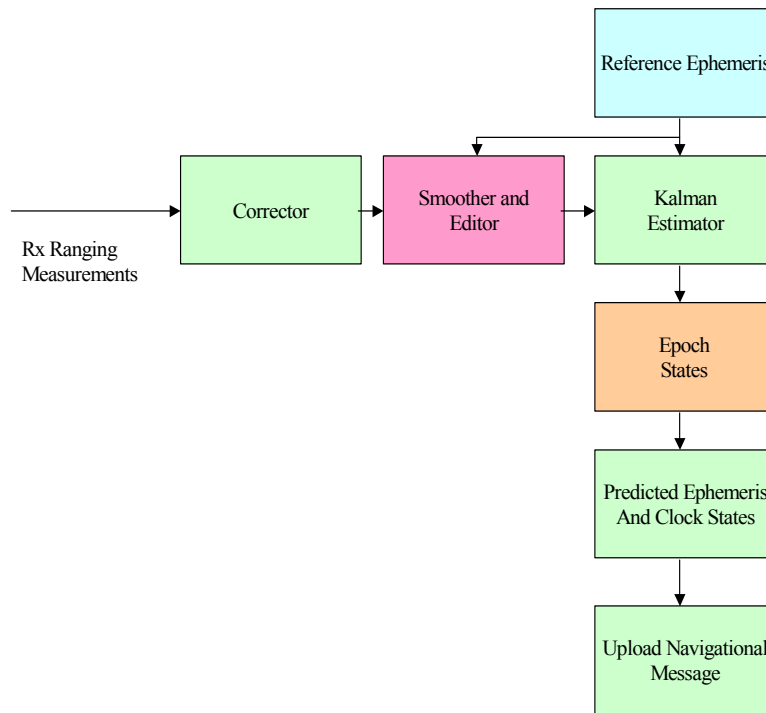


Figure II-6: OCS Ephemeris Generation Process

IGS Final Orbit

The IGS station network consists of 288 (as of 8 Feb 2002) tracking stations equipped with dual-frequency receivers. The data collected from these sites is fed to one of seven analysis centres. Each centre uses different software, measurement models, and orbit models to give independent solutions. The IGS Central Bureau develops the precise final orbit from a weighted average combination of the orbits received from each analysis centre [Roulston 2000, p48].

By allowing each analysis centre the flexibility to develop its own models and procedures, the IGS analysis process removes the likelihood of software or modelling biases. The analysis software used varies between analysis centres and includes Bernese GPS

software V4.1, ESOC BAHN, GPSOBS and BATUSI, GFZ EPOS.P.V2, NOAA page 5, MIT/SIO GAMIT v. 9.72 and GLOBK v. 4.17, and JPL GIPSY/OASIS II Version 2.6 [IGS-Analysis 2002]. Comparison with SLR data has determined that the final orbit solution is consistently better than the seven individual analysis orbits [Roulston 2000, p48].

Data Formats

Broadcast Ephemeris

Broadcast ephemeris files have two common formats: a receiver dependent binary format and a receiver independent format. The binary format of the broadcast ephemeris is the native format used by each receiver to store the ephemeris parameters.

The Receiver Independent Exchange (RINEX) format was first published in 1980 and has undergone many modifications in the last 22 years. The format consists of three types of ASCII text files: the observation data file containing the range data, the meteorological data file, and the navigation message file [Hofman-Wellenhof 1994, p201]. Only the navigation message format was used for this thesis. Hofman-Wellenhof provides a detailed description of the RINEX format [Hofman-Wellenhof 1994, pp200-204], as does the CDDIS website [CDDIS-RINEX 2002].

Almanac Ephemeris

Three standards formats are used to transmit almanac files: the original receiver-dependent binary file, the YUMA format file, and the SEM format file. The binary format of the almanac ephemeris is the native format used by each receiver to store the ephemeris parameters.

The YUMA format file is an ASCII file that contains multiple satellite almanac records, each consisting of the almanac data and a description of its content. Details of the YUMA format can be found on the US Coast Guard website [YUMA 2002].

The SEM format file is also an ASCII file that contains multiple satellite ephemeris records. However, in the SEM format, each record does not contain a description of its content. Details of the SEM format can be found at the US Coast Guard website [SEM 2002].

IGS Final Orbit

The IGS final orbit is published in SP3 format. SP3 is an industry standard ASCII format used to record satellite navigation observation records. A detailed history of the SP3 format can be found at the CDDIS website [CDDIS-SP3 2002], the NIMA Website [NIMA-SP3 2002], and the IGS website [IGS-SP3 2002].

Summary

The focus of this study is the analysis of GPS navigational errors using post-processing techniques. A review of the available literature indicated that similar studies have been undertaken with regard to GPS errors. Each of these studies was confined to a small sample period within the history of the GPS program. All of these studies assume that GPS SISRE for each sample period can be extrapolated for an entire year. Orbit generation techniques were detailed, as were the resultant file formats.

III. Analysis and Modelling Methodologies

Introduction

The purpose of this chapter is to describe and support the methods used to achieve the objectives of this research and to define the scope and limitations of the methods chosen. The outputs required from the research are defined, followed by the required inputs. An overview of the method used to meet the objectives is provided, followed by an overview of the analysis process. The assumptions and restrictions needed to establish a baseline for the analyses are defined. The methods used to obtain and present the results are then defined, and finally the data format is outlined.

Required Outputs

As stated in Chapter 1, the intent of this thesis is to:

- Compare the satellite orbit computed using the GPS broadcast ephemerides with the IGS precise orbit over as much of the GPS program's operational history as possible.
- Compare the satellite position computed using the GPS almanac ephemerides with the IGS precise orbit to determine the effect of age of data on almanac accuracy.

Required Inputs

The following data was required to complete the research:

- GPS Broadcast ephemerides for the entire study time period
- GPS Almanac ephemerides for sample weeks
- IGS Precise orbits for the entire study time period

Method of Analysis

Either simulation or direct analysis of historical data could be used to generate the results required to satisfy the requirements of this research. However, since analysis of historical data is more accurate and the data is readily available over the Internet, this method was selected.

Given that direct computation is the most appropriate method for conducting the analysis, the selection of the most appropriate software packages was based on several factors, including the availability of standard and tailorable reports within each of the packages, the user interface provided by each application, the packages' numerical computation capabilities, and the format of relevant research work undertaken by other students (and applicable to this thesis). For these reasons, MATLAB R12 was selected for this thesis.

Overview of the Process

Broadcast Orbit

The processes used to achieve the broadcast objectives of this study were undertaken in a linear order as described below and in Figure III-1.

MATLAB routines were written to undertake the following:

- a. Convert RINEX format broadcast ephemeris data to binary format.
- b. Load broadcast ephemerides and precise orbit data, allowing for variations in data format over the study time period.
- c. Calculate the position of each satellite for all selected time epochs using the broadcast ephemerides. Correct the broadcast orbits for satellite antenna offsets. Compare the broadcast orbit to the precise orbit to determine the satellite position error (see page 43). Filter corrupt broadcast data epochs (see page 50). Calculate error values for each satellite and RMS values for the entire constellation, for each day of the study time period. Translate the position error to satellite body reference frame.
- d. Calculate Signal In Space Range Error (SISRE) for each satellite and RMS values for the entire constellation, for each day of the study time period.
- e. Plot and analyse position error and SISRE data.

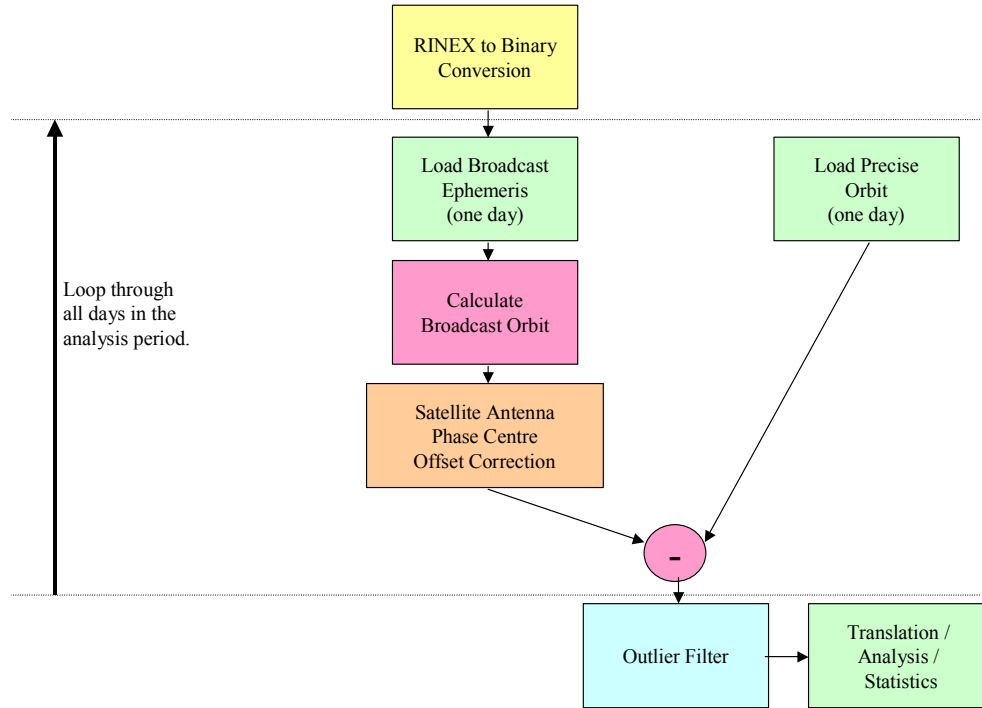


Figure III-1: Broadcast Analysis Process

Almanac Orbit

The processes used to achieve the almanac objectives of this study were undertaken in a linear order as described below and in Figure III-2. The almanac orbit was calculated using a single almanac ephemeris compared to each day's precise orbit.

MATLAB routines were written to undertake the following:

- a. Load almanac ephemerides and precise orbit data, allowing for variations in data format over the study time period.
- b. Calculate the position of each satellite for all selected time epochs using the almanac ephemerides. Correct the almanac orbits for satellite antenna offsets (see page 43). Compare the almanac orbit to the precise orbit to determine the

satellite position error. Calculate error values for each satellite and RMS values for the entire constellation, for each day of the study time period.

Translate position error to a satellite body reference frame.

- c. Calculate Signal In Space Range Error (SISRE) for each satellite and RMS values for the entire constellation, for each day of the study time period.
- d. Plot and analyse position error and SISRE data.

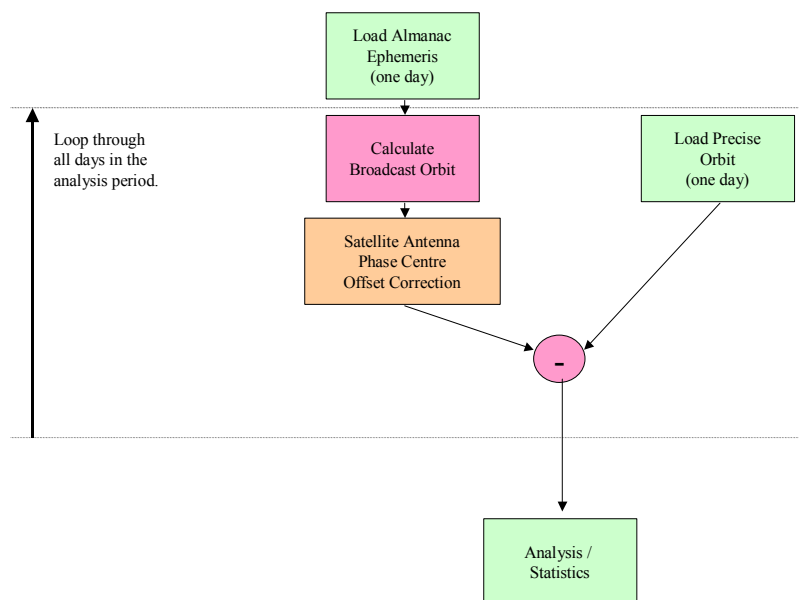


Figure III-2: Almanac Analysis Process

Analysis Parameters and Assumptions

Study Analysis Period

Since the primary aim of this thesis was to perform an historical analysis of ephemeris error, the ideal study period would commence when the GPS system reached Final Operating Capability (FOC) on 17 July 95 [Pace 1995, p246]. However, since ephemeris data is readily available prior to 1995, the study period was expanded to include the interval 14 Nov 1993 through to 1 Nov 2001. Most importantly, the routines and processes developed for use in the analysis can be applied to any data set.

Ephemeris Data

Broadcast Ephemerides

Broadcast ephemerides were obtained from the Crustal Dynamics Data Information System (CDDIS) website managed by the National Aeronautics and Space Administration (NASA) Goddard Space Flight Center in Greenbelt Maryland [CDDIS 2002]. The CDDIS web site maintains broadcast ephemeris records from 1992 GPS week 0570 through to the present. Data is stored in RINEX format as compressed (zip) files. Uncompressed, the broadcast data set for this study consists of 3533 RINEX files. The accuracy of broadcast orbit is 2.60 metres (1- σ) [IGS-Products 2002].

Precise Orbits

Precise orbits were obtained from the IGS website managed by the Jet Propulsion Laboratory of the California Institute of Technology [IGS-Products 2002]. The IGS website provides GPS data to the scientific community [IGS 2002].

The IGS web site maintains precise orbit records from 1992 GPS week 649 through to the present. Data is stored in SP3 format as compressed (zip) files. The accuracy of IGS final orbit data is generally less than 0.05 metres ($1-\sigma$) [IGS 2002].

Almanac Ephemerides

Almanac ephemerides were obtained from the US Coast Guard Navigation Centre GPS Almanac Website [USCG-Almanac 2002]. The USCG website maintains almanac ephemeris records from 1990 through to the present. Data is stored in both YUMA and SEM formats. Almanac ephemerides variables are a subset of the broadcast ephemeris variables and are used by GPS receivers to assist in initial acquisition of satellites. The accuracy of almanac orbit exceeds 2.60 metres ($1-\sigma$) [IGS-Products 2002].

The Sampling Interval

The following reasoning is applied for selecting a suitable interval for sampling the location of satellites in the constellation:

- The sample interval chosen should seek to provide a balance between the resolution achieved and the resource requirements required for undertaking the analysis.

- The interval should be based on the requirements of the fastest moving satellites. At an altitude of 21,162.6 km (ECI at equator), GPS satellites travel at approximately 3.87 km/s [Spilker 1996, p40].
- If a sample interval of one minute is chosen, approximately 2.5 Gbyte of data is required to represent the precise and broadcast orbits over the study analysis period. Resourcing this analysis posed considerable concerns and extrapolation of the precise orbit to intermediate data points introduced unnecessary interpolation errors.
- The interval should be small enough to capture variations in the GPS orbit. The orbital errors are highly correlated over time and therefore sampling at a higher rate than once every 15 minutes would provide little extra orbit information.

A sample interval of 15-minutes was therefore chosen. The primary reason for choosing a 15-minute interval was to avoid the considerable data storage and processing overheads, while providing sufficient data to analyse the position error and achieve the aims of this thesis.

Orbit Analysis

Precise Orbit Analysis

The precise orbit was determined by loading all available orbit records. These records provided precise satellite positions at 15-minute intervals.

Broadcast Ephemeris Analysis

The broadcast orbits were determined from the broadcast ephemeris using the method described in ICD-GPS-200C. Exact details of this procedure are outlined in ICD-GPS-200C Table 20-IV. The ephemeris data is normally uploaded every 12 hours and normally remains valid for a period 2 hours either side of the Time Of Ephemeris (TOE) broadcast as part of the GPS navigational message [Weiss 1994, p295]. The position of each satellite was determined using the broadcast ephemeris at 15-minute intervals that coincided with the IGS orbit epochs.

The difference between the calculated broadcast orbit and the precise orbit was calculated. This broadcast position error, in the ECEF WGS-84 reference frame, was then translated to a spacecraft body reference frame comprised of along-track (satellite's direction of motion), cross-track (tangential to along-track and radial) and radial (vector from centre of Earth to satellite) components.

The positions provided by the IGS are in the International Terrestrial Reference Frame (ITRF), which is consistent with the Earth Centred, Earth Fixed (ECEF) WGS-84 frame within a few centimetres [Malys 1997-2]. For this reason a transformation between ITRF and WGS-84 was not considered necessary for the purposes of this analysis.

Almanac Ephemeris Analysis

The almanac orbits were determined from the almanac ephemeris using the method described in ICD-GPS-200C. Exact details of this procedure are outlined in ICD-GPS-200C Table 20-IV. The position of each satellite was determined using the almanac ephemeris at 15-minute intervals that coincide with the IGS orbit epochs. The almanac orbit was determined using a single GPS almanac and compared to the precise orbit for multiple days. The difference between the calculated almanac orbit and the precise orbit was calculated.

This almanac position error, in the ECEF WGS-84 reference frame, was then translated to a body reference frame comprising of along-track, cross-track and radial components. Again, coordinate transformation between the WGS-84 and ITRF reference frames was not considered necessary.

The almanac position error was calculated for two periods: precise orbit period 1 Jan 2000 to 1 Nov 2001 against 1 Jan 2000 almanac and precise orbit period 1 Jan 2001 to 1 Nov 2001 against 1 Jan 2001 almanac.

Error Analysis

Satellite Antenna Phase Centre Offset

The broadcast and almanac orbits are determined relative to the spacecraft's antenna phase centre whilst the IGS orbits are determined relative to the spacecraft's centre of mass. A correction (Table III-1) was applied to the broadcast and almanac orbits to correct for the offset between each GPS satellite's antenna phase centre and its centre of mass. The offset values used, shown in Table III-1, were supplied by the IGS [IGS-Analysis 2002].

Table III-1: Antenna Phase Centre Offset

Block	A (m)	C (m)	R (m)
I	0.2100	0.0000	0.8540
II/IIA	0.2794	0.0000	1.0259
IIR	0.0000	0.0000	1.2053

The offset is from satellite centre of mass to antenna phase centre (metres).

The difference between the precise and broadcast orbits was determined for each precise epoch. The broadcast position error results were analysed by calendar year and over the entire study interval. The difference between the precise and almanac ephemerides was determined for each precise epoch. The almanac position error results were analysed over the two study intervals defined above.

Statistics

The following statistics were calculated to characterise the position errors:

- Minimum satellite ACR broadcast position error – To obtain this value, all epochs for the sample day were filtered to separate each individual satellite. The minimum value for each axis (along-track, cross-track and radial) was then calculated for each satellite.
- Minimum constellation ACR broadcast position error – The minimum value for each axis (along-track, cross-track and radial) was calculated using all epochs for all satellites on the sample day.
- Maximum satellite ACR broadcast position error – To obtain this value, all epochs for the sample day were filtered to separate each individual satellite. The maximum value for each axis (along-track, cross-track and radial) was then calculated for each satellite.

- Maximum constellation ACR broadcast position error – The maximum value for each axis (along-track, cross-track and radial) was calculated using all epochs for all satellites on the sample day.
- Mean satellite ACR broadcast position error – To obtain this value, all epochs for the sample day were filtered to separate each individual satellite. The mean value for each axis (along-track, cross-track and radial) was then calculated for each satellite.
- Mean constellation ACR broadcast position error – The mean value for each axis (along-track, cross-track and radial) was calculated using all epochs for all satellites on the sample day.
- Median satellite ACR broadcast position error – To obtain this value, all epochs for the sample day were filtered to separate each individual satellite. The median value for each axis (along-track, cross-track and radial) was then calculated for each satellite.
- Median constellation ACR broadcast position error – The median value for each axis (along-track, cross-track and radial) was calculated using all epochs for all satellites on the sample day.
- Standard deviation of satellite ACR broadcast position error – To obtain this value, all epochs for the sample day were filtered to separate each individual satellite. The standard deviation value for each axis (along-track, cross-track and radial) was then calculated for each satellite.

- Standard deviation of constellation ACR broadcast position error – The standard deviation value for each axis (along-track, cross-track and radial) was calculated using all epochs for all satellites on the sample day.
- 90th percentile of satellite ACR broadcast position error – To obtain this value, all epochs for the sample day were filtered to separate each individual satellite. The MATLAB routine *prctile* was used to calculate the 90th percentile value for each axis (along-track, cross-track and radial) for each satellite.
- 90th percentile of constellation ACR broadcast position error – The MATLAB routine *prctile* was used to calculate the 90th percentile value for each axis (along-track, cross-track and radial) using all epochs for all satellites on the sample day.
- ACR broadcast position error – Raw broadcast position error for each time epoch.
- RMS satellite ACR broadcast position error – To obtain this value, all epochs for the sample day were filtered to separate each individual satellite. Equation (4) (next page) was then used to obtain the daily RMS of all ACR broadcast position errors for each satellite.
- RMS constellation ACR broadcast position error – Equation (4) was used to calculate the daily RMS of all ACR broadcast position errors for each sample day.

- 3D satellite broadcast position error – To obtain this value, all epochs for the sample day were filtered to separate each individual satellite. Equation (5) was then used to calculate the 3D position error for each time epoch.
- 3D constellation RMS broadcast position error – Equation (6) was used to calculate the daily RMS of all 3D broadcast position errors for each sample day.
- Broadcast satellite SISRE – To obtain this value, all epochs for the sample day were filtered to separate each individual satellite. Equation (3) (page 21) was then used to calculate the orbit-only SISRE calculated for each time epoch.
- RMS broadcast satellite SISRE – To obtain this value, all epochs for the sample day were filtered to separate each individual satellite. Equation (7) (page 49) was used to calculate the daily RMS of all SISRE values for each satellite.
- RMS constellation Broadcast SISRE – Equation (7) was used to calculate the daily RMS of all SISRE values for each sample day.

All broadcast values were calculated relative to IGS final orbit. All of the above statistics were also calculated for the almanac ephemeris relative to the IGS final orbit. Each of these statistics were analysed over time, over the constellation, and over satellite block type.

The equation for RMS is

$$RMS = \sqrt{\frac{1}{n} \sum_{i=1}^n (dX_i)^2} \quad (4)$$

where

n = number of epochs for satellite

i = epoch for the satellite

dX_i = broadcast orbit position error in the any reference direction with respect to IGS final orbit for a satellite at epoch.

The equation for 3D error is

$$3D_i = \sqrt{dA_i^2 + dC_i^2 + dR_i^2} \quad (5)$$

where

i = epoch for the satellite

dA_i = broadcast orbit position error in the along-track direction with respect to IGS final orbit for a satellite at epoch.

dC_i = broadcast orbit position error in the cross-track direction with respect to IGS final orbit for a satellite at epoch.

dR_i = broadcast orbit position error in the radial direction with respect to IGS final orbit for a satellite at epoch.

The equation for 3D RMS error is

$$RMS_{3D} = \sqrt{\frac{1}{n} \sum_{i=1}^n (dA_i^2 + dC_i^2 + dR_i^2)} \quad (6)$$

where

n = number of epochs for satellite k

dA_i, dC_i, dR_i = see Equation (5).

The equation for RMS SISRE error is

$$SISRE_{RMS} = \sqrt{\frac{1}{n} \sum_{i=1}^n (SISRE_i)^2} \quad (7)$$

where

n = number of epochs in day

i = epoch

Data Format

The file data formats used in this research are detailed at Appendix A.

Summary

This chapter described the objectives, methodology, processes and assumptions underlying the research. Several specialized routines have been developed to process, analyse and present the data required in the analysis. The reason these routines were required and appropriate descriptions of the functions performed by them have also been provided. The compromises and assumptions that were necessary to limit the scope of the work and the resources required to achieve the desired outcome were described. With the processes and methodology described, the results of the research can now be presented.

IV. Presentation and Analysis of Results

Introduction

The purpose of this chapter is to present the results of the analyses used to characterise the broadcast and almanac ephemeris error over the study period. The along-track, cross-track and radial position errors were analysed using the techniques defined in Chapter 3.

This chapter provides an analysis of the results obtained for the comparison of the orbit determined from the broadcast ephemeris with the orbit provided by the IGS final orbit. The same analysis follows using the almanac ephemeris.

Broadcast Orbit Position Error Results

Outlier Filtering

Initial analysis showed occasional extreme position error values (outliers) due to errors within the broadcast ephemeris. Figure IV-1 shows the broadcast position error for a typical day relative to the IGS final orbit. It can be clearly seen that the large position error deviations between successive epochs are not consistent with a realistic satellite orbit. The errors are generated by corrupted individual ephemeris terms, and occur within only a few epochs in each of the affected broadcast ephemeris files. Using a broadcast file from a different source removed the epochs previously affected, but it introduced errors at other epochs. A previous broadcast ephemeris study revealed that the errors are not due to format conversions between the raw binary receiver data and the ASCII standard RINEX formatted navigational file [Jefferson 2000, p393].

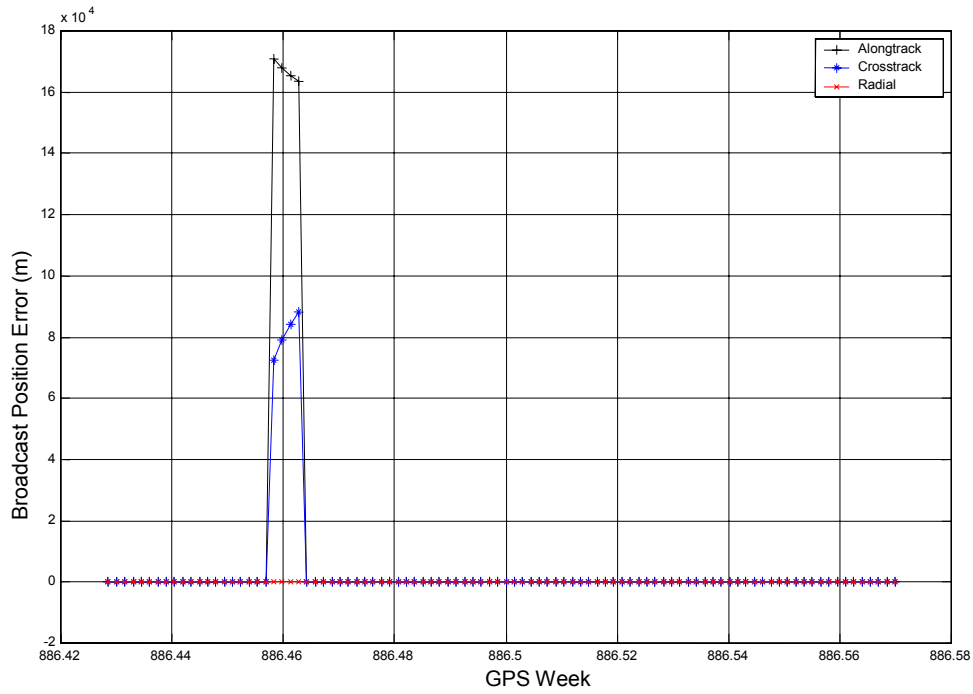


Figure IV-1: Satellite broadcast position error - 3 Jan 1997
Typical day for a typical PRN, relative to the IGS final orbit
No epochs removed
along-track (red), cross-track (blue) and radial (black)

The ideal solution would be to identify which source provided an error-free broadcast ephemeris for each individual day and use that data. One potential source for error-free broadcast ephemeris could be the GPS JPO, however this data was not readily available. To remove the outlier values from the calculations, a number of other methods were explored, and they are described in the sections that follow.

Outlier Removal – X Sigma Filter

The first attempted method was to apply mean \pm X-sigma filters ($X = 1, 2, 3, 4$) to the data for each day, thereby eliminating outlier values. However it was found that this method removed a large number of valid data points in addition to the outliers and resulted in a data set too small for meaningful use.

Outlier Removal – 90th Percentile Filter

The second method attempted was to calculate the 90th percentile point in the data for each day and then remove values that exceeded this 90th percentile value. Again this method removed a large number of valid data points in excess of the outliers and resulted in a data set too small for meaningful use.

Outlier Removal – 30-Metre Filter

The along-track, cross-track, and radial position errors were calculated for the entire study period and it was determined that in all cases the values in each axis were either less than 30 metres or were extremely large outliers (km or greater error). Therefore, an outlier filter was set to remove individual satellite epochs that exceeded the 30-metre limit in any one of the along-track, cross-track and radial coordinate axis's. As shown in Figure IV-2, this filtering process removed a consistently low percentage of the data points across the study period. Once these outliers were removed, the results were more consistent over successive epochs. The peak at week 930 is due to increased data corruption in the broadcast ephemeris files obtained from the CDDIS website over this period.

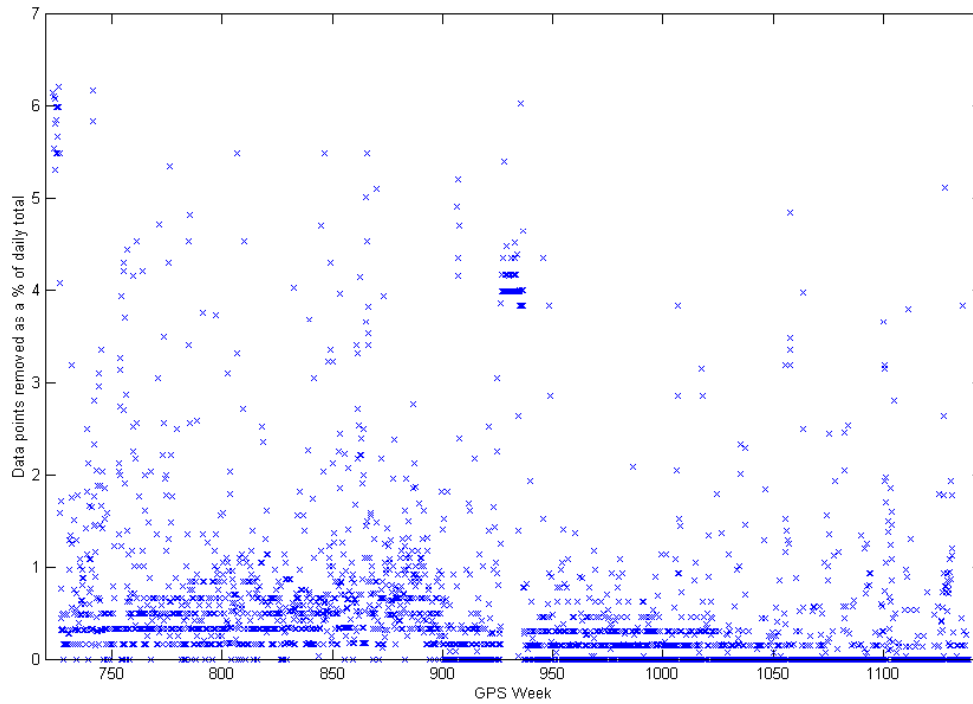


Figure IV-2: Daily outlier data epochs removed
Percentage of total daily data epochs
14 Nov 1993 – 1 Nov 2001

Along-Track, Cross-track and Radial

Along-track, cross-track, and radial broadcast position errors relative to the IGS final orbit were determined using the methods outlined in Chapter 3. Figure IV-3 is a representative sample plot of ACR broadcast orbit position error for PRN 22 (SVN 22) for 1 Nov 1997. Figure IV-4 is a plot of ACR broadcast orbit position error for PRN 22 (SVN 22) for 1 Nov 2000. Appendix B contains plots for each satellite in the constellation for 1 Nov 1994, 1 Nov 1997, and 1 Nov 2000.

The kink shown in the along-track component of Figure IV-3 is due to an ephemeris upload being undertaken. Both figures show a periodic trend that is consistent with the GPS constellation's 12-hour orbit. The point in the centre of the plot where the along-track, cross-

track, and radial components all equal zero is only a coincidence for this sample day. Switching between different ephemeris sets causes small kinks in each component. As can be seen in Appendix B, the figures shown for PRN 22 (SVN 22) are consistent with other satellites in the GPS constellation and consistent across the study analysis period.

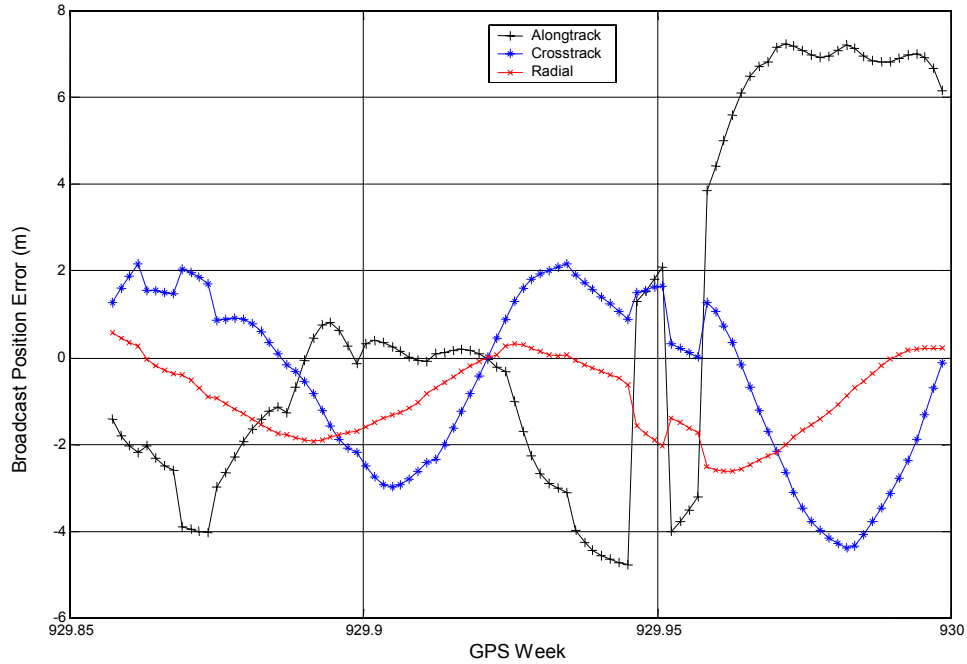


*Figure IV-3: ACR broadcast orbit position error, 1 Nov 1997, PRN 22, SVN 22
with respect to IGS final orbit
along-track (red), cross-track (blue) and radial (black)*

By studying various ACR plots and the results for PRN 2 (SVN 13) over the entire study period, it was determined that the cross-track component tends to have twice the magnitude of the along-track component. Also, the along-track component has approximately three times the amplitude of the radial component. This is consistent with previous studies that determined that the uncertainty in the radial component is 3-4 times better than the along-track and cross-track components [Roulston 2000, p50]. This difference

between the along-track / cross-track and radial components is due to the GPS pseudorange being more sensitive to changes in the radial direction than in other directions [Zumberge 1996, p587].

The GOSPAR project showed that the 12-hour period terms are not due to longitude or latitude movement of the satellite [Conley 2000, p373]. Position error does, however, vary significantly with longitude, due to the ephemeris upload pattern employed by the OCS, which is dictated by fixed ground stations [Conley 2000, p373].

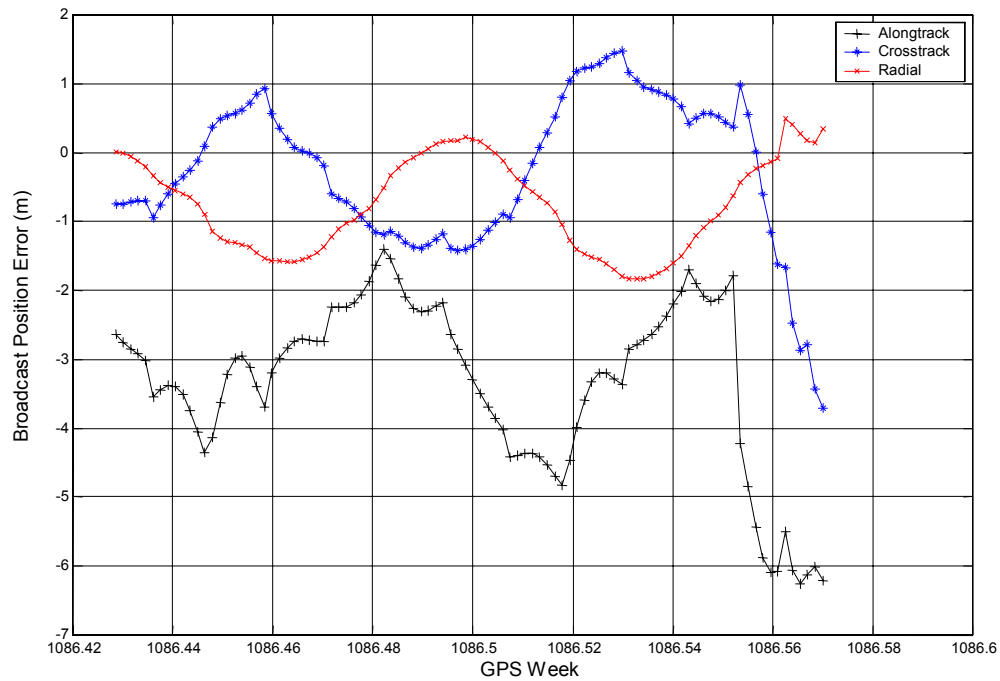


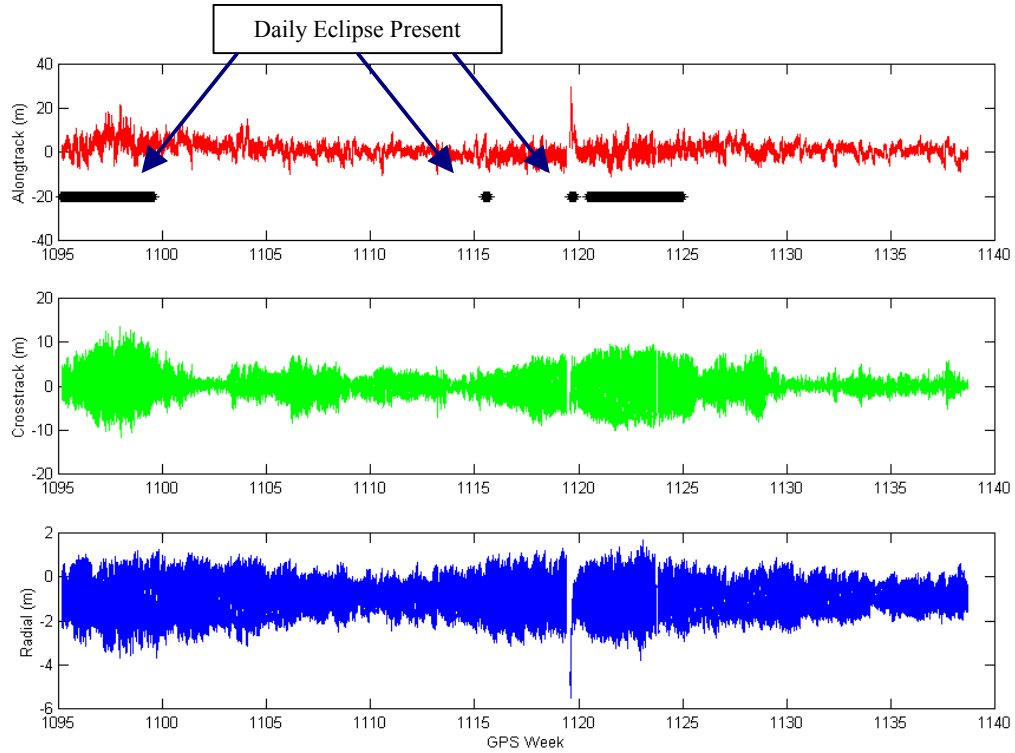
*Figure IV-4: ACR broadcast orbit position error, 1 Nov 2000, PRN 22, SVN 22
with respect to IGS final orbit
along-track (red), cross-track (blue) and radial (black)*

Weiss stated that Kalman filter residual errors could generate the 12-hour periodic terms, especially a consistent error in the orbit eccentricity [Weiss 1994, p296]. The satellite antenna phase centre offset detailed in Chapter 3 is provided in the along-track, cross-track,

and radial reference frame. This satellite body reference frame assumes a fixed satellite attitude, which provides for static offset values between the antenna phase centre and the satellite's centre of mass. Any variation in the satellite's attitude will modify the offset values. Small variations (oscillations) are permitted within a satellite's attitude control system, these variations result in changing broadcast position errors.

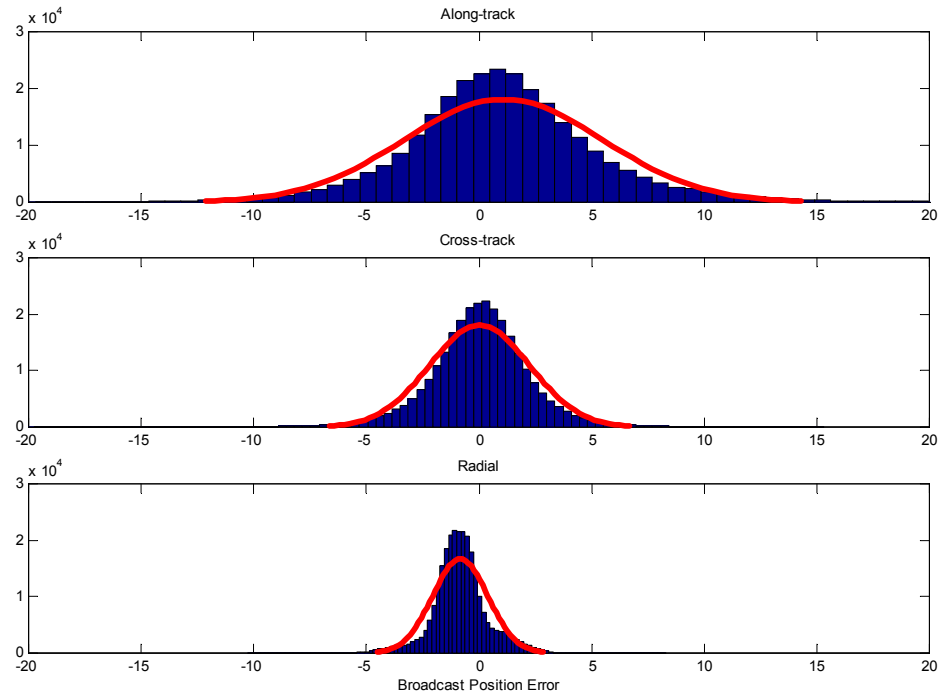
The along-track axis is weakly correlated with the cross-track axis (9.55%) and the radial axis (6.44%) over the study period. This reflects the fact that due to the satellite's high along-track velocity, small variations in the along-track component have very little impact on the radial and cross-track components. The cross-track and radial axis's are highly correlated (30.91%), a reflection of the low magnitude of the radial and cross-track velocity components.

Figure IV-5 is a plot of along-track, cross-track, and radial broadcast position error for PRN 1 (SVN 32) for the year 2001. Superimposed on the along-track plot (at -20 metres) are the periods of the SVN 32 orbit that include a daily eclipse of the satellite by the Earth. As can be seen from the plot, the along-track, cross-track, and radial position errors increase when the satellite moves into eclipse. The likely cause of this increased error is that the Kalman filter models used by the OCS to predict the orbits are optimised for a direct sunlight orbit, because it is more difficult to model the eclipsed satellite orbit. The results shown for PRN 1 are consistent with the results obtained for other satellites in the constellation.



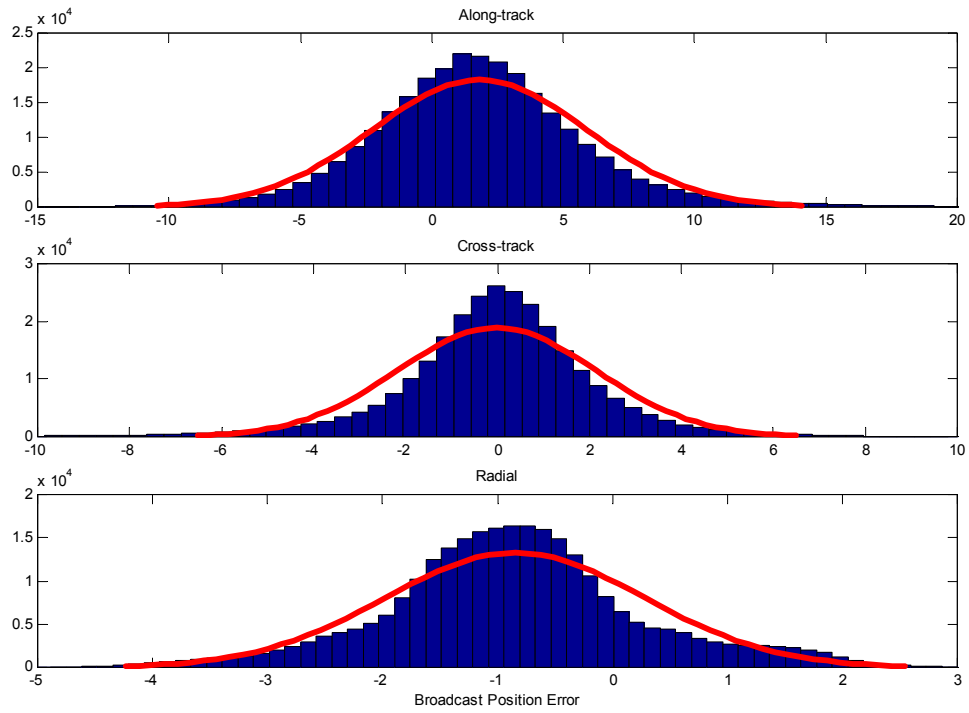
*Figure IV-5: ACR broadcast orbit position error, PRN 1, SVN 32
1 Jan 2001 to 1 Nov 2001, with respect to IGS final orbit
along-track (red), cross-track (green) and radial (blue)*

Figure IV-6 shows a histogram of the daily mean ACR broadcast position errors for PRN 21 (SVN 21) over the entire study period. Superimposed on the histogram are normal gaussian distribution curves based upon the same ACR position errors. As can be seen from Figure IV-6 the along-track and cross-track distributions over the analysis period are approximately zero-mean gaussian. The radial distribution is skewed to a peak at -1 metre rather than following a gaussian curve.



*Figure IV-6: Histogram of ACR broadcast orbit position error, PRN 21, SVN 21
14 Nov 1993 to 1 Nov 2001, with respect to IGS final orbit
Normal Gaussian distribution function superimposed in red on each plot*

By plotting the histograms for various Block II (Figure IV-6 & Figure IV-7) and IIR (Figure IV-8) satellites, it was determined that the radial negative bias is present in both Block II and IIR satellites. The fact that both satellite versions are affected indicates that the most likely cause of this offset is a combination of an OCS Kalman filter bias and an error in the radial satellite antenna offset value used for this study.



*Figure IV-7: Histogram of ACR broadcast orbit position error, PRN 2, SVN 13
14 Nov 1993 to 1 Nov 2001, with respect to IGS final orbit
Normal Gaussian distribution function superimposed in red on each plot*

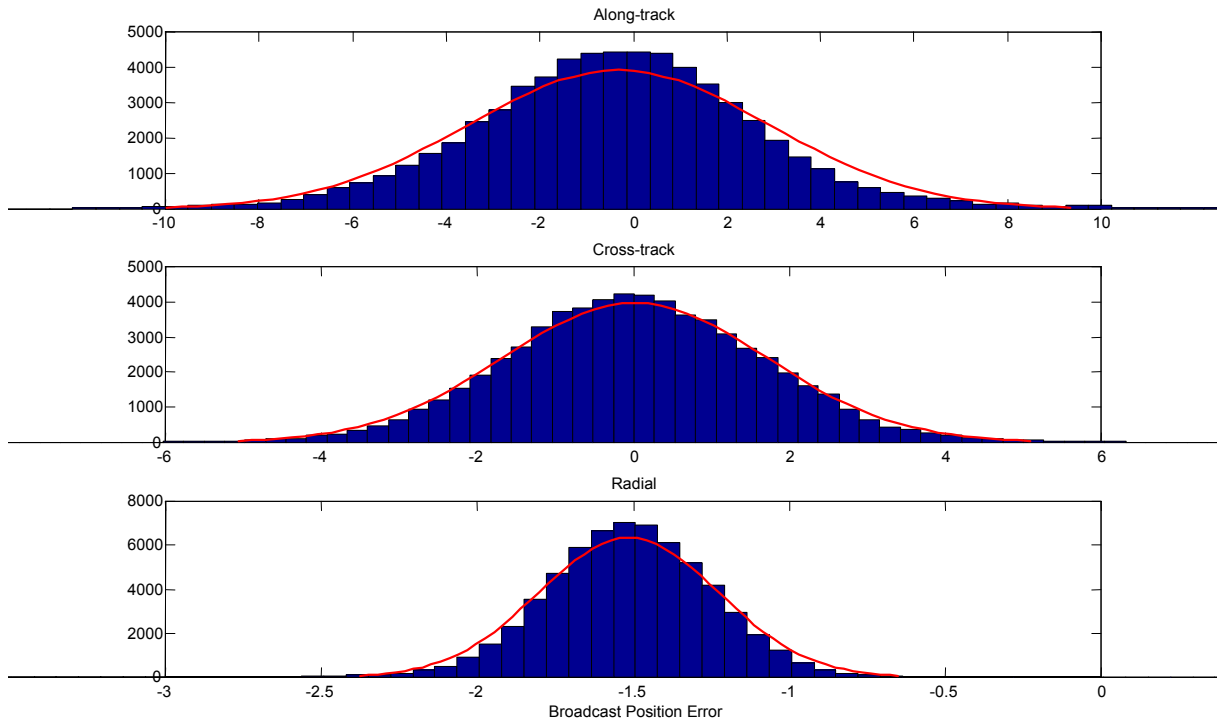


*Figure IV-8: Histogram of ACR broadcast orbit position error, PRN 11, SVN 46
3 Jan 2000 to 1 Nov 2001, with respect to IGS final orbit
Normal Gaussian distribution function superimposed in red on each plot*

Statistical Analysis

The statistics outlined in Chapter 3 (Statistics section) were calculated. Table IV-1 lists the statistics determined by calculating the relevant statistic for each of the along-track, cross-track, and radial components (eg: minimum along-track, cross-track, and radial) for each time epoch. The 3D value (Equation (5)) was calculated for each epoch and the RMS of the 3D values was determined across various time intervals.

The 3D mean, 3D median, and 3D standard deviation gradually decrease from 1993 through to 1998 and then increase slightly from 1999 through to 2001. The overall 3D mean for the study period is 2.88 metres. The reduction in the standard deviation indicates an

overall improvement in the accuracy for the GPS broadcast ephemeris. The most probable cause of the decrease in the standard deviation across the 1993 to 1998 period is OCS Kalman filter improvements and the introduction of more accurate clocks to the satellite constellation.

Table IV-1: 3D Broadcast Ephemeris Error Statistics

Year	Minimum / Maximum (m)	Mean (m)	Median (m)	Standard Deviation (m)	90th Percentile (m)	Maximum – Minimum (m)
1993 (*1)	1.735 / 67.59	3.721	3.882	5.624	8.964	65.85
1994	1.110 / 45.25	3.541	3.613	5.127	8.651	44.14
1995	1.980 / 44.73	3.424	3.470	4.410	7.704	42.75
1996	1.928 / 48.96	2.911	3.010	4.366	6.400	47.04
1997	1.346 / 46.36	2.686	2.769	3.273	4.863	45.02
1998	1.593 / 41.00	2.524	2.582	3.027	4.430	39.41
1999	1.482 / 40.69	2.494	2.545	3.106	4.559	39.21
2000	1.452 / 45.31	2.630	2.700	3.406	5.052	43.86
2001 (*2)	1.695 / 43.85	2.663	2.690	3.064	4.684	42.15
1993 – 2001 (*1, *2)	1.110 / 67.59	2.877	2.943	3.767	5.868	66.48

*1 – 14 Nov 1993 onwards. *2 – 1 Jan 2001 though to 1 Nov 2001.

Figure IV-9 shows the mean of the RMS ACR broadcast position errors for all active satellites in the constellation for each day across the period from 1 Nov 1993 to 1 Nov 2001. The along-track and cross-track mean position errors are consistently higher than the radial mean error, due to the sensitivity of the increased GPS pseudorange to changes in the radial direction than in other directions [Zumberge 1996].

The large reduction in the mean values that occurred at week 900 will be explained later in this chapter. To determine the cause of the gradual increase in mean value from 1999 through to 2001, the RMS ACR broadcast position errors were plotted for each satellite and included in Appendix C.

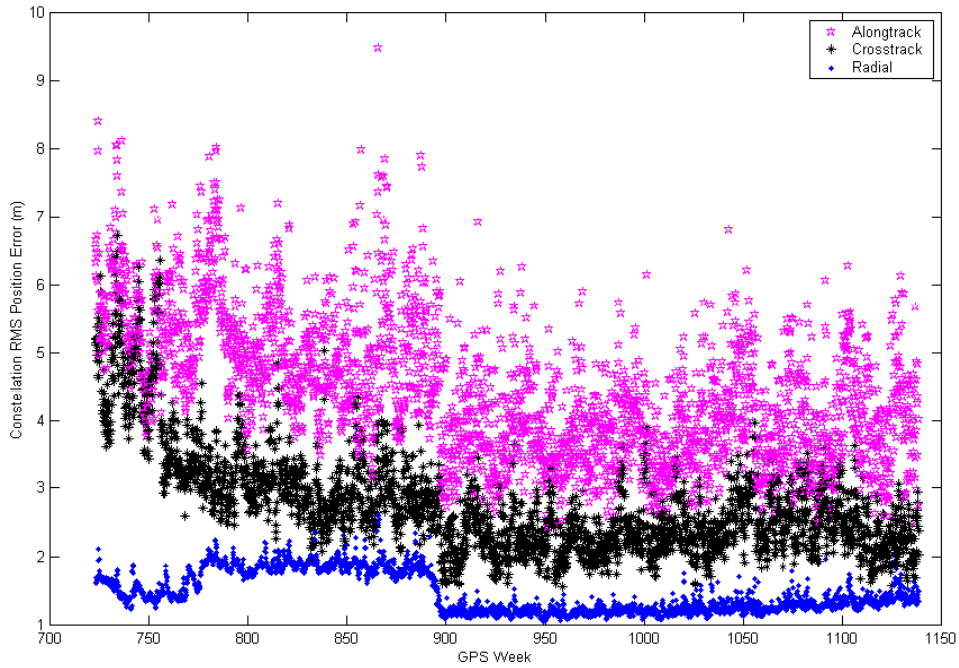


Figure IV-9: Mean RMS ACR broadcast position error, All active satellites

*Mean value across the constellation for each day
14 Nov 1993 – 1 Nov 2001
along-track (pink), cross-track (black) and radial (blue)*

Figure IV-10 shows the plot of the RMS ACR broadcast position error for PRN 7 (SVN 37) for the entire study period. SVN 37 is a Block IIA satellite and it does not show an increase in its RMS values during the interval 1999 to 2001. Figure IV-10 and the figures in Appendix C prove that the increase in the constellation RMS position error shown in Figure IV-9 is not due to the block IIA satellites.

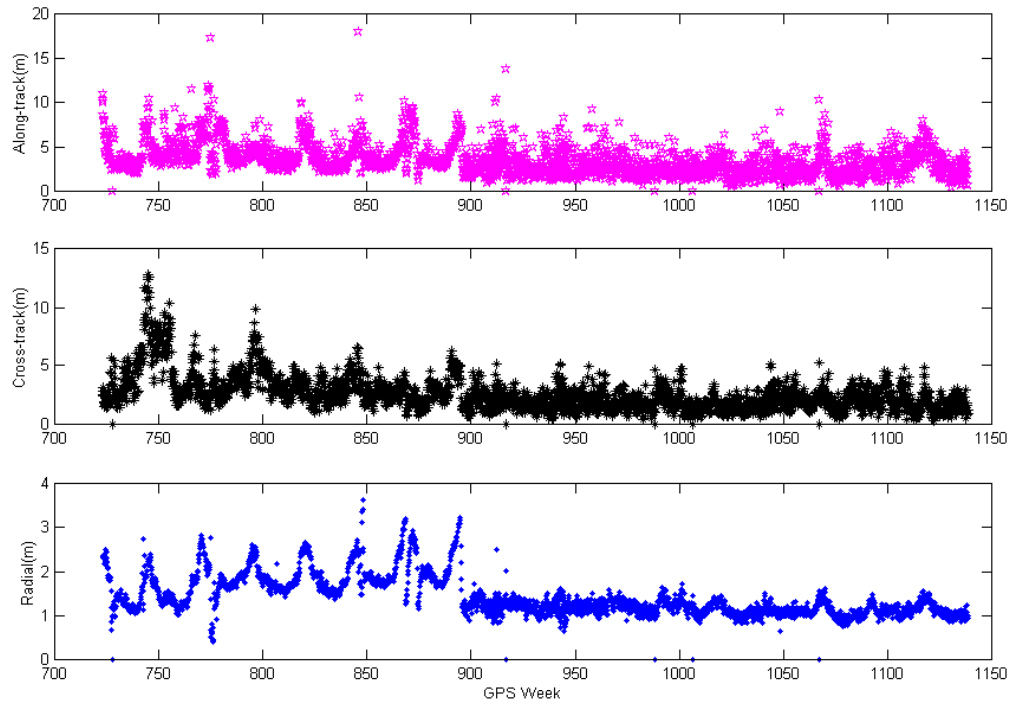


Figure IV-10: RMS ACR broadcast position error, PRN 7, SVN 37

*Daily RMS of all epochs
14 Nov 1993 – 1 Nov 2001
along-track (pink), cross-track (black) and radial (blue)*

Figure IV-11 shows the plot of the RMS ACR broadcast position error for PRN 13 (SVN 43) for the entire study period. After week 920 (31 Jan 1998), SVN 43 is a Block IIR satellite. Over the period 31 Jan 1998 to 1 Nov 2001, PRN 13 (SVN 43) consistently had a higher RMS position error than SVN 37 (see Figure IV-10). From Figure IV-10 and Figure IV-11 and the other plots in Appendix C, it was determined that the increase in the RMS ACR broadcast position error during the period 1999 to 2001 was related to the introduction of Block IIR satellites into the GPS constellation.

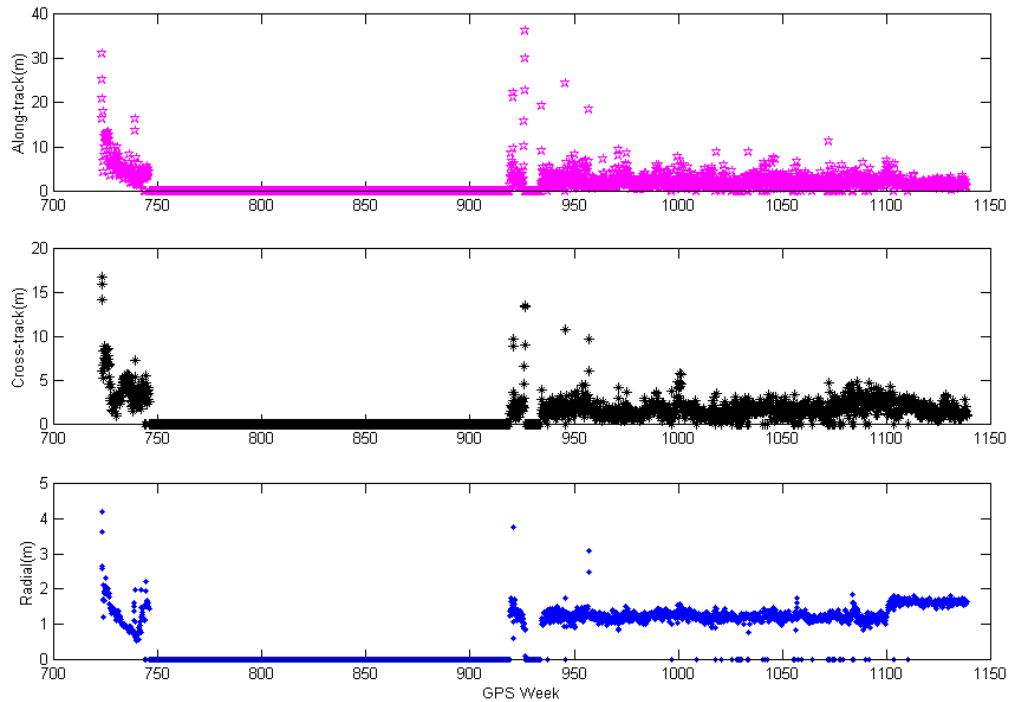


Figure IV-11: RMS ACR broadcast position errors, PRN 13

*SVN 43 after week 920, SVN 9 prior to week 750
 Daily RMS of all epochs, 14 Nov 1993 – 1 Nov 2001
 along-track (pink), cross-track (black) and radial (blue)*

Discussions with the GPS JPO have determined that the improved performance of the Block IIR rubidium clocks has decreased the OCS measured ORDs and therefore increased the time interval between contingency ephemeris uploads. The reduction in the ephemeris upload frequency increases the ephemeris age of data. As the age of data increases, so does the ephemeris position error and the mean position error. The GPS JPO has confirmed that the improved clock performance has decreased the overall URE. By researching the long term GPS system clock performance, it would be possible to confirm that the clock performance has improved and that the full constellation SISRE (not orbit-only) has been reduced. Further research of clock performance is recommended as a future thesis topic.

The increase in the broadcast position error was not identified until this thesis was conducted. If the OCS implemented the same upload frequency employed prior to the introduction of the Block IIR satellites, the broadcast position error would decrease (compared to current upload scheme) and the overall accuracy of the GPS system would improve.

3D ACR Broadcast Position Error

3D ACR broadcast position errors relative to the IGS final orbit were determined for each satellite for each epoch. The three-dimensional errors for each epoch were calculated using Equation (6) detailed on page 48.

Figure IV-12 shows the 3D ACR broadcast position errors for PRN 14 (SVN 14 prior to 1990 and SVN 41 after Dec 2000) over the entire study period. Each point on the plot represents the 3D ACR broadcast position error for one time epoch. This figure demonstrates a maximum 3D ACR broadcast position error of 26 metres, a minimum error of 0.16 metres, and a mean error of 5.33 metres. These values are consistent with the constellation statistics listed in Table IV-1. Plots of the 3D ACR broadcast position error for each satellite are included in Appendix D.

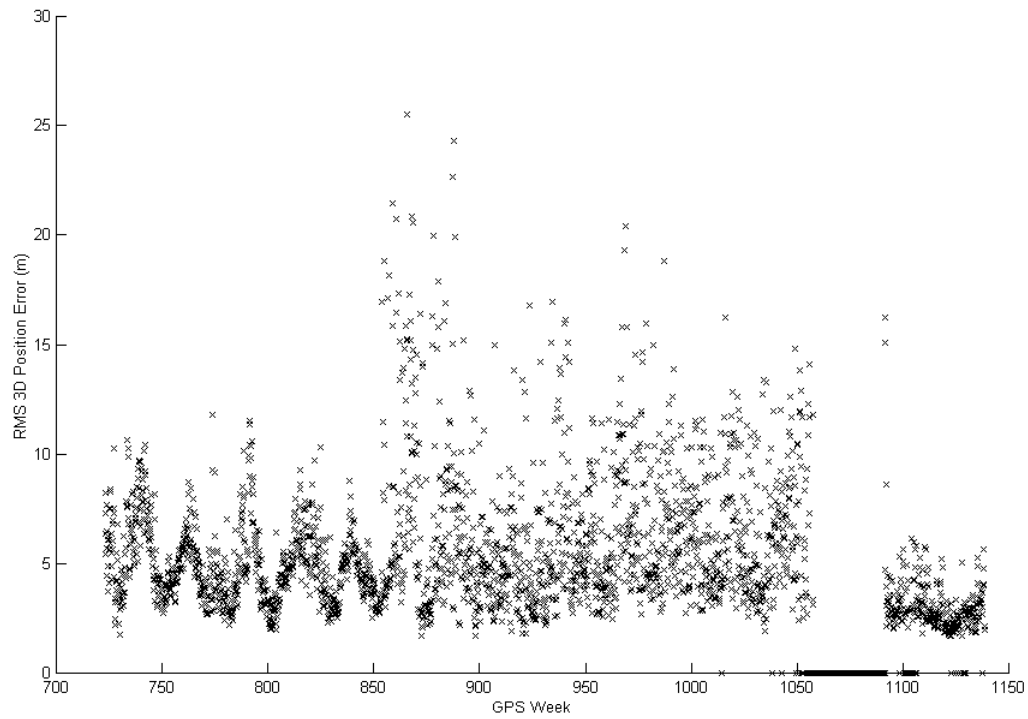


*Figure IV-12: 3D ACR broadcast orbit position error, PRN 14
SVN 41 after week 1090, SVN 14 prior to week 1052
with respect to IGS final orbit
14 Nov 93 – 1 Nov 01*

The RMS 3D ACR broadcast position error was determined for each calendar year and for the entire study period. The RMS value was determined using Equation (4) (page 48), which provides the mean of all 3D ACR values for each satellite over the analysis period.

Figure IV-13 and Figure IV-14 show the mean 3D ACR broadcast error for each satellite number for all of 1995 and 2000 respectively. The mean constellation 3D ACR broadcast position error dropped from 5.3 metres to 3.9 metres over the period, indicating an improvement in the accuracy of the GPS broadcast position over the 1995 to 2000 interval.

All PRNs that are operational in both 1995 and 2000 show a reduction in RMS 3D ACR error, except for PRNs 15 and 18. PRNs 15 and 18 are Block II satellites that have been operational since 20 Oct 1990 and 16 Feb 1990, respectively.

These are aging satellites, and the gradual increase in RMS 3D ACR error shown above is consistent with component aging. In 2000, PRN 15 was known to have problems with its reaction wheel during eclipse; this could be the source of the increased error relative to 1995 [Roulston 2000, p53]. Plots of the RMS 3D ACR broadcast error for each satellite number for each calendar year and for the entire study period are included in Appendix E.

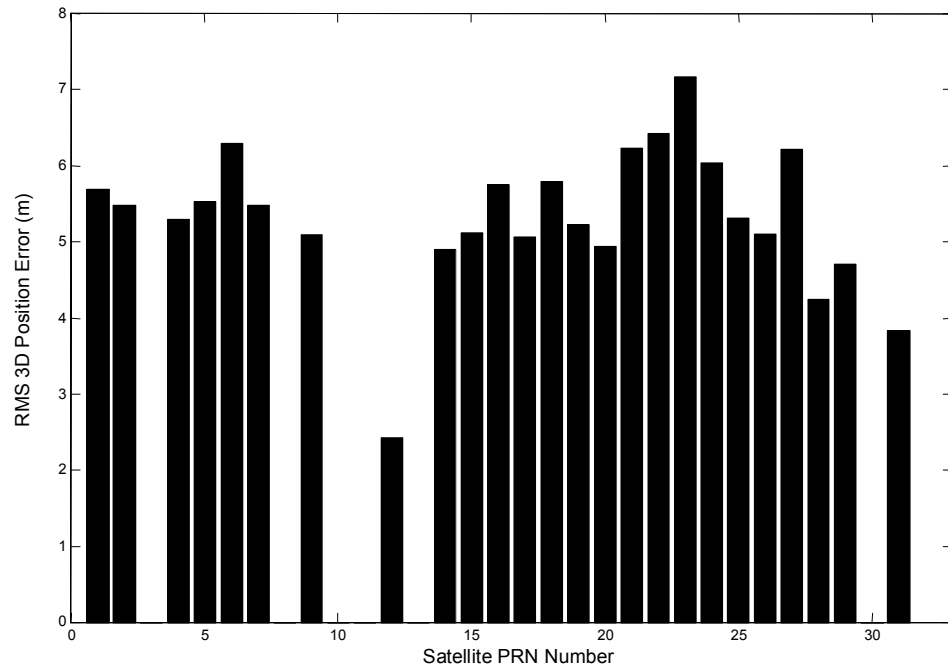


*Figure IV-13: RMS 3D ACR broadcast orbit position error - 1995
with respect to IGS Final Orbit*

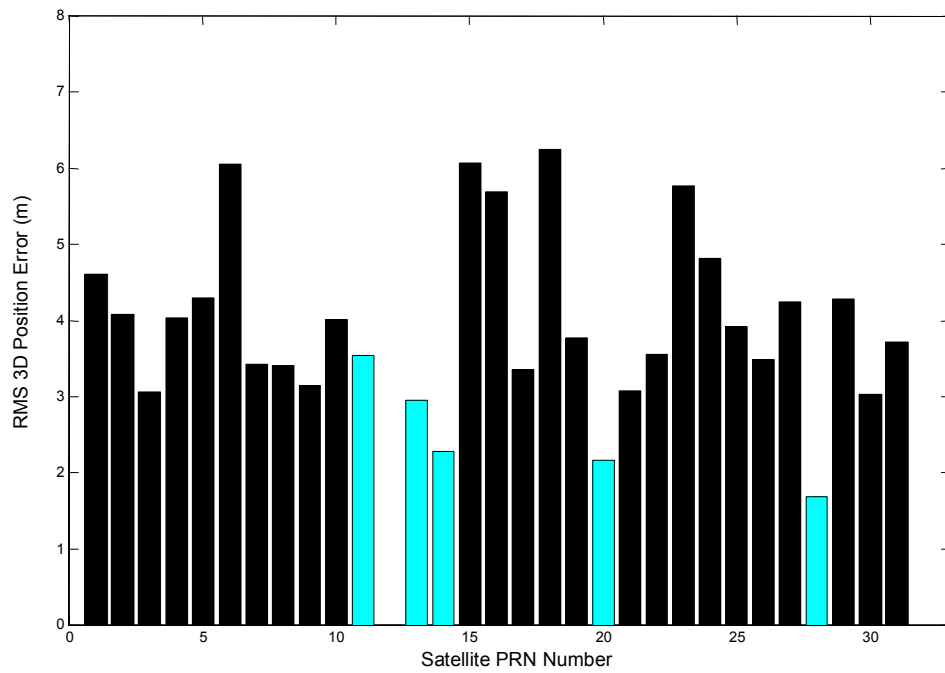


*Figure IV-14: RMS 3D ACR broadcast orbit position error – 2000
with respect to IGS Final Orbit, blue bars show Block IIR satellites*

SISRE

Constellation orbit-only SISRE was determined by evaluating Equation (3) (page 21) for each satellite and then using Equation (4) (page 48) to determine the RMS value across all satellites for each time epoch. Figure IV-15 shows that the RMS constellation orbit-only SISRE is consistent, but with a slight upward trend, from GPS week 900 through to 1 Nov 2001. The large reduction in the mean from 1.7 metre to 1.3 metre (23%) that occurred in GPS week 900 (6-12 Apr 1997) coincides with the initial stages of the GPS AII program, which made modifications to the OCS Kalman filter, added six NIMA tracking stations into the GPS satellite tracking network, and implemented a new navigational upload scheme which reduced prediction error [Malys 1997, pp380-382].

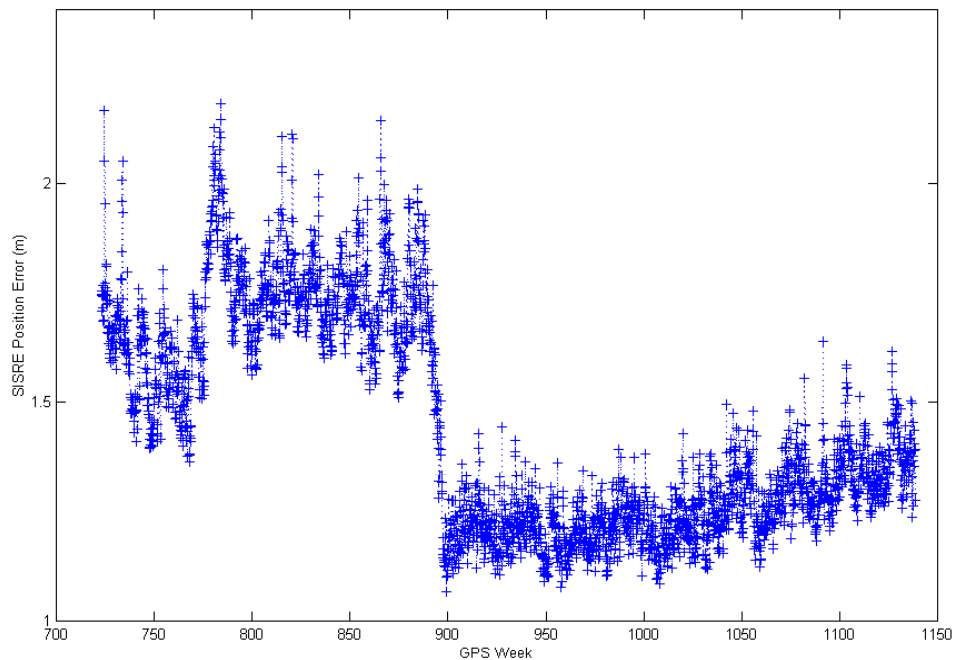


Figure IV-15: RMS constellation broadcast orbit-only SISRE

*14 Nov 1993 – 1 Nov 2001
with respect to IGS Final Orbit*

The 2SOPS Ephemeris Enhancement Endeavour (EEE) also introduced Kalman filter process noise modifications in early 1997, causing a 20% drop in the ORD values [Crum 1997]. The reduction in constellation orbit-only SISRE is consistent with the reduction in mean constellation radial position error shown in Figure IV-9. Since constellation SISRE is a combination of each satellite's SISRE, once again the slight upward trend is due to the introduction of Block IIR satellites into the constellation.

Figure IV-16 and Figure IV-17 show constellation orbit-only SISRE for all of the block II and block IIR satellites respectively. The figures show the influence of the block IIR satellites on the constellation orbit-only SISRE.

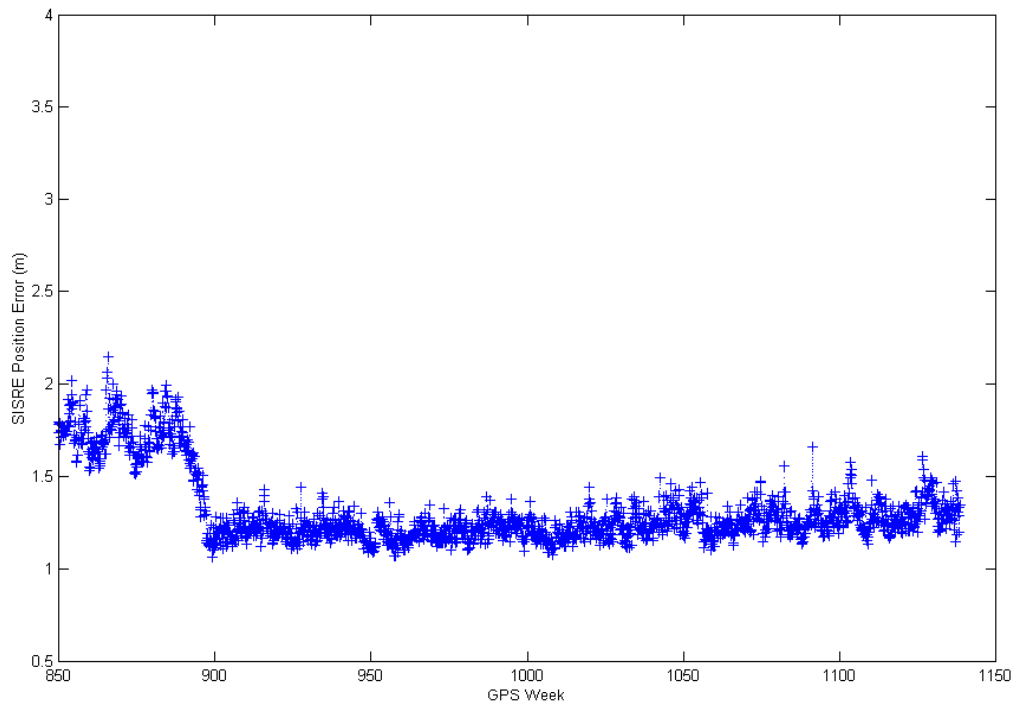
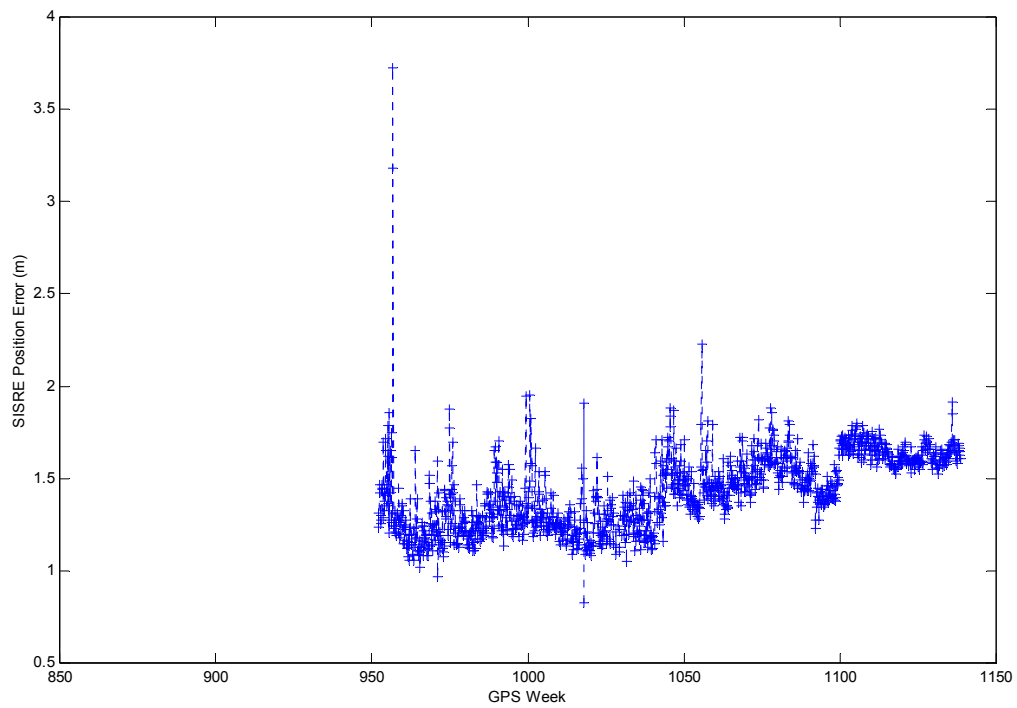


Figure IV-16: RMS Block II constellation broadcast orbit-only SISRE

*1 Jan 1997 – 1 Nov 2001
with respect to IGS Final Orbit*



*Figure IV-17: RMS Block IIR constellation broadcast orbit-only SISRE
1 Jan 1997 – 1 Nov 2001
with respect to IGS Final Orbit*

Almanac Orbit Position Error Results

Outlier Filtering

The almanac position error was determined using the procedure outlined in Chapter 3 for two time periods: 1 Jan 2000 to 1 Nov 2001 (compared to the week 1042 almanac) and 1 Jan 2001 to 1 Nov 2001 (compared to the week 1095 almanac). The position error that resulted was not filtered since the almanac position orbit did not experience the source dependant extreme outlier values that were evident in the broadcast orbit.

Along-Track, Cross-track and Radial

It can be seen from Figure IV-18 and Figure IV-19 (ACR position error for PRNs 21 (SVN 21) and 2 (SVN 13), respectively) that the magnitude and sign of the position error varies with PRN. It was also determined that whilst the cross-track and radial components are approximately zero mean, the mean of the along-track errors deviated from the zero line in either the positive or negative direction.

The period 1 Jan 2001 to 1 Nov 2001 was then analysed against the 1 Jan 2001 almanac and it was determined that, as expected, the ACR and 3D position errors also vary depending upon which almanac ephemeris data was used. This variation combined with the overwhelming effect of orbital corrections makes it very difficult to predict the long-term almanac position error based on the almanac ephemeris.

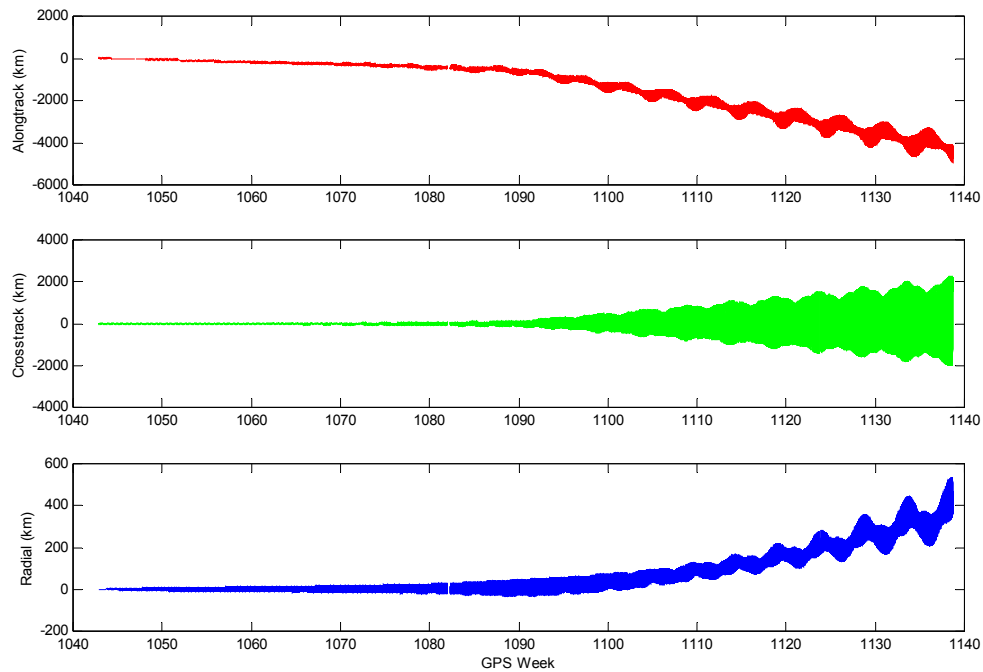


*Figure IV-18: PRN 21 Almanac ACR position error for week 1042 almanac
with respect to IGS final orbit, 1 Jan 2000 – 1 Nov 2001*

The large errors in the almanac orbit occur because the almanac does not model mean motion difference or harmonic corrections to argument of latitude, orbit radius, and angle of inclination. The precision of the almanac's semi major axis, eccentricity, argument of perigee, and rate of right ascension terms are also lower than the broadcast orbit.

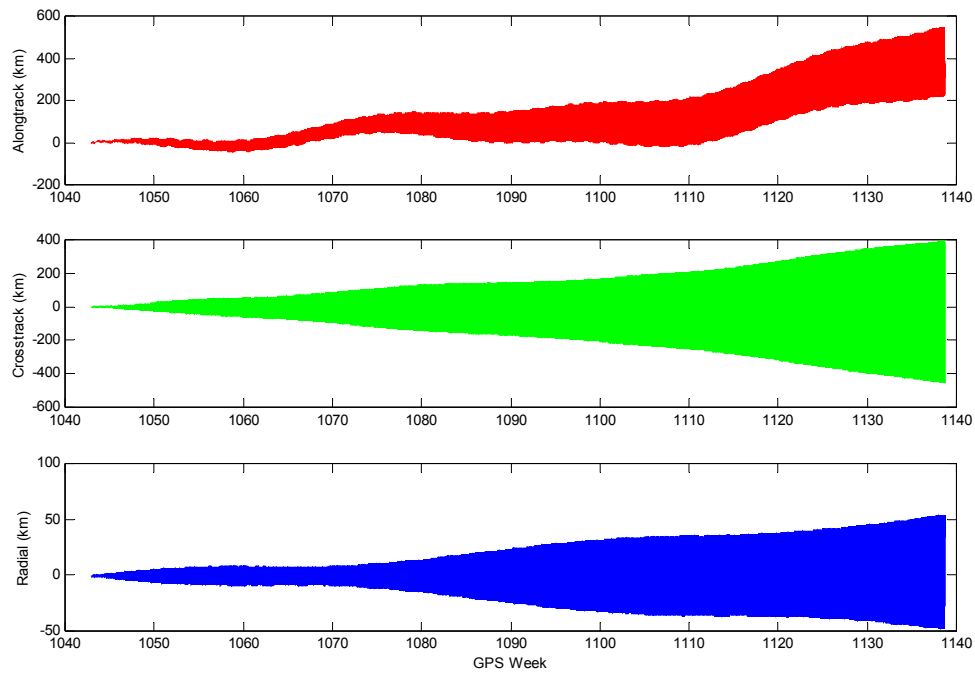


*Figure IV-19: PRN 3 Almanac ACR position error for week 1042 almanac
with respect to IGS final orbit, 1 Jan 2000 – 1 Nov 2001*

Figure IV-20 shows the effect of either a propulsive event or a momentum wheel dump on the accuracy of the almanac orbit. These manoeuvre events represent a large unknown influence on the almanac orbit and are impossible to compensate for without details of planned orbital corrections.

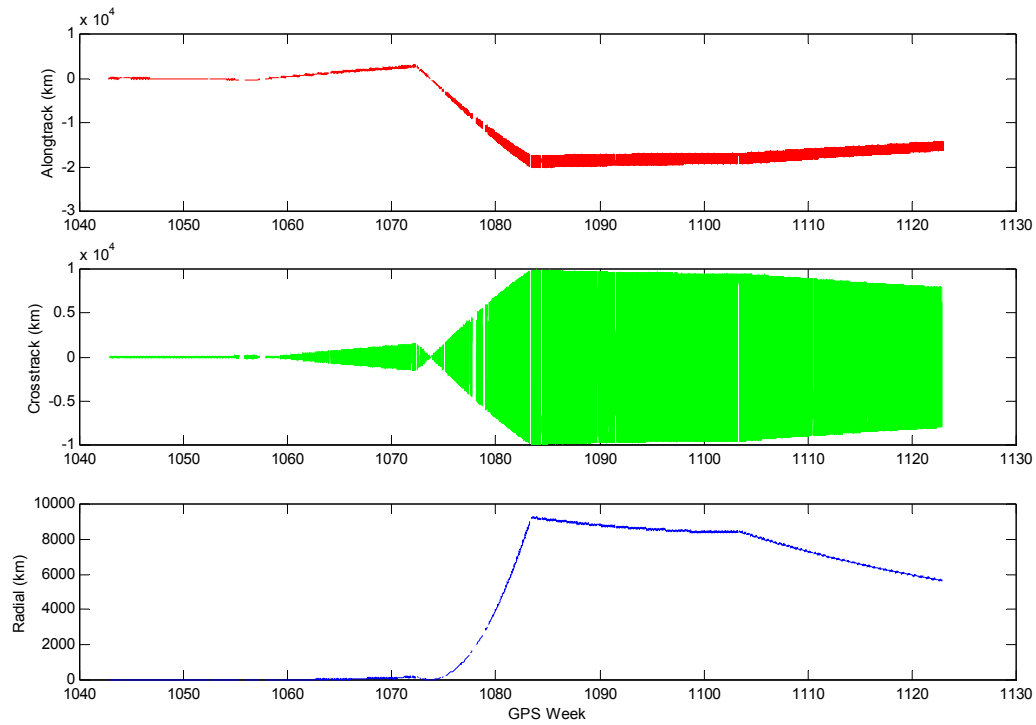


*Figure IV-20: PRN 13 Almanac ACR position error for week 1042 almanac
with respect to IGS final orbit, 1 Jan 2000 – 1 Nov 2001*

Statistical Analysis

The statistics outlined in Chapter 3 (Statistics section) were calculated. Table IV-2 lists the statistics determined by calculating the relevant statistic for each of the along-track, cross-track, and radial components (eg: minimum along-track, cross-track, and radial) for each time epoch. The 3D value (Equation (5)) was calculated for each epoch and the RMS of the 3D values was determined across various time intervals.

All statistics increase rapidly with increasing age of almanac data. The lower fidelity of the almanac ephemeris results in a lower fidelity orbit solution, which is greatly affected by unmodelled perturbing forces.

Table IV-2: 3D Almanac Ephemeris Error Statistics

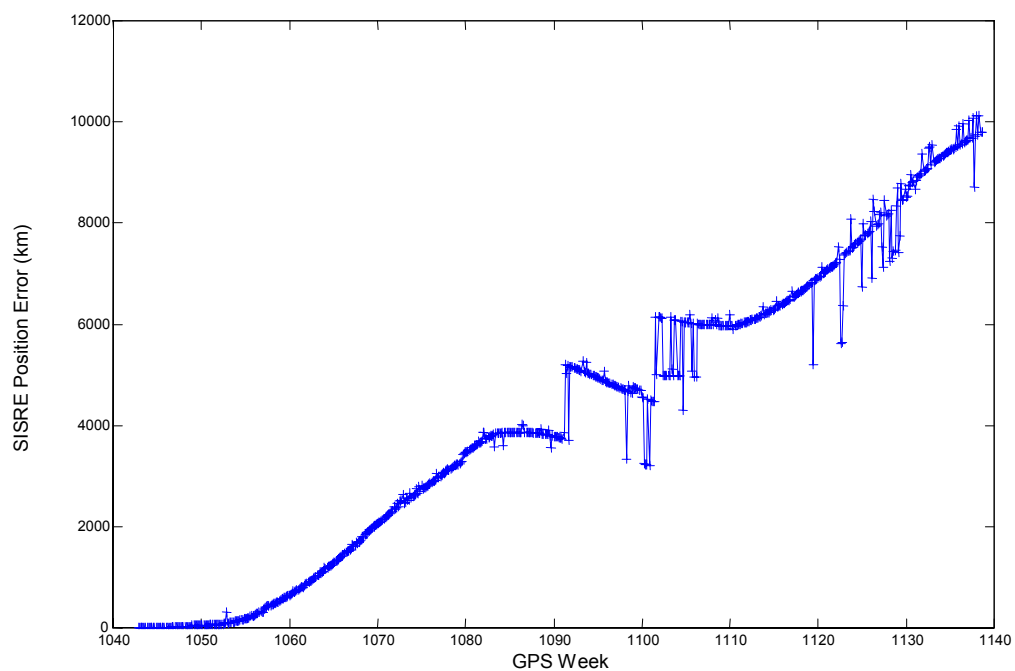
Age of Data	Minimum / Maximum (km)	Mean (km)	Median (km)	Standard Deviation (km)	90th Percentile (km)	Maximum – Minimum (km)
7 Days	0.85 / 12.84	2.39	2.43	1.59	2.97	11.99
14 Days	0.85 / 203	7.20	7.35	3.52	8.46	202.21
1 Month	0.9 / 1056	28.1	28.3	12.1	33.0	1055.4
3 Months	1.0 / 26751	310	307	127	363	26750
Half Year	1.0 / 43839	1485	1481	544	1673	43839
All 2000	1.0 / 53147	4059	4051	1236	4391	53146
2000 – 2001 (*1)	1.0 / 56912	7461	7449	2315	8159	56911

*1 – Until 1 Nov 2001

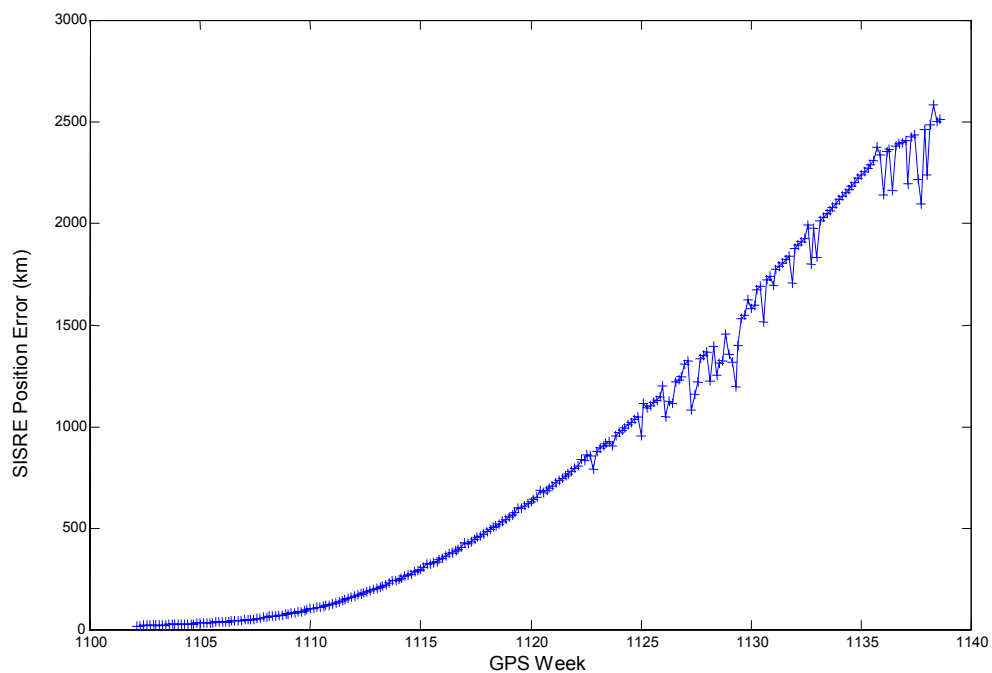
SISRE

Figure IV-21 and Figure IV-22 show the Constellation orbit-only SISRE for the same almanacs and time periods as Figure IV-18 and Figure IV-19. Satellites that obviously underwent propulsive events were removed from the SISRE calculation.

Both figures show a similar structure independent of the almanac used. The constellation orbit-only SISRE initially increases quadratically with a magnitude that is consistent with the values in ICD-GPS-200C (3.6 km – 300 km 1-sigma URE for long term operations (m)).



*Figure IV-21: RMS constellation SISRE almanac position error
Week 1042 Almanac, Orbit-only, with respect to IGS final orbit, 1 Jan 2000 – 1 Nov 2001*



*Figure IV-22: RMS constellation SISRE almanac position error
Week 1095 almanac, Orbit-only, with respect to IGS final orbit, 1 Jan 2001 – 1 Nov 2001*

Summary

This chapter detailed the results of the broadcast and almanac analyses over the study period. The along-track, cross-track, and radial position errors were analysed using the techniques in Chapter 3. Along-track, cross-track, and radial position error, 3D position error, RMS along-track, cross-track, and radial position error and constellation orbit-only SISRE were analysed.

V. Summary and Conclusions

This study extended the work of the University of New Brunswick [Langley 2000] and the GOSPAR project [LMFS 1996] over the entire GPS operational lifetime. Whilst the GOSPAR project concentrated on a small period and the Langley study concentrated on current results, this study analysed the long-term errors within the broadcast ephemeris. In addition, this research analysed the impact of age-of-data on almanac accuracy.

Summary – Broadcast Ephemeris

Relevant literature on satellite orbit analysis, GPS error sources, and the performance of the GPS system was researched. The study period was selected to maximise the length of the analysis period, whilst still ensuring that valid broadcast ephemeris and precise orbit data was available.

The broadcast orbit was calculated from the broadcast ephemeris using the GPS Interface Control Document (ICD) procedure. The broadcast orbit was corrected for the offset from the satellite phase centre to the satellite centre of mass. The broadcast orbit position error between the broadcast orbit and the IGS precise orbit was calculated for each data epoch.

Corrupt broadcast ephemeris files introduced extreme outlier values into broadcast orbit. The extreme broadcast orbit values translated to extreme outlier values in the position error. Many methods were tested to remove these outliers, and a 30 metre filter was finally implemented.

The original goal of this research was to compare the GPS broadcast orbit with the IGS final orbit over the GPS program's operational history. This comparison was conducted by analysing the broadcast orbit position error over the study period, 14 Nov 1993 to 1 Nov 2001. Traditional statistics were calculated for the position error, as well as orbit specific statistics like SISRE and 3D broadcast position error.

The evaluation showed that the broadcast orbit has a mean error of 2.88 metres (14 Nov 1993 – 1 Nov 2001) and 2.66 metres (2001). The mean 3D position error for most satellites has decreased across the analysis period. The mean constellation orbit-only SISRE was 1.7 metres until GPS week 900 when it dropped to 1.3 metres, as a result of the introduction of Kalman filter changes under the 2SOPS EEE program [Crum 1997].

The position error increases when a satellite's orbit passes through a period of eclipse. The RMS position error and its associated statistics increased over the period 1999 to 2001, due to increased ephemeris age-of-data that results from a decrease in the ephemeris upload frequency. The reduced upload frequency is a result of the increased clock accuracy on the Block II-R satellites.

Summary – Almanac Ephemeris

The almanac orbit was calculated from a selected week's almanac ephemeris using the GPS ICD procedure. The almanac orbit was corrected for the offset from the satellite phase centre to the satellite centre of mass. The almanac orbit position error between the almanac orbit and the IGS precise orbit was calculated for each data epoch.

The secondary goal of this research was to compare the GPS almanac orbit with the IGS final orbit to determine the impact of age-of-data on almanac position error. This comparison was conducted by analysing the almanac orbit position error over two overlapping time periods. Traditional statistics were calculated for the position error, as well as orbit-specific statistics like SISRE and 3D almanac position error.

The position error between the almanac and the IGS final orbits is dependent upon PRN and the almanac used. The constellation orbit-only SISRE initially increases quadratically with a magnitude that is consistent with the values in ICD-GPS-200C.

All position error statistics increase rapidly with increasing age of almanac data. The lower fidelity of the almanac ephemeris results in a lower fidelity orbit solution, which is greatly affected by unmodelled perturbing forces.

Conclusions

The results of this thesis provide an independent method for the GPS JPO to gauge the direct impact of Kalman filter modifications on the accuracy of the navigational information available to the Navstar GPS users. This research provided the GPS JPO with an independent data set against which GPS JPO engineers can compare future Kalman filter changes and readily assess the significance of each proposed engineering change. This research determined the broadcast orbit position error for the period 14 Nov 1993 to 1 Nov 2001, in both yearly segments and for the entire time period.

This research identified a previously unknown increase in the broadcast ACR position error over the period 1999 to 2001 and identified likely causes for this increase. Major Kalman

filter modifications were located within the data and the positive impact of these modifications on broadcast position error was verified.

Recommendations

Further research can be undertaken to determine the position error due to satellite ephemeris clock errors. This research would enable the JPO to determine the impact of the increased clock accuracy on the Block II-R satellites and explain why the overall ORD values have decreased over the 1999 to 2001 period, even though the orbit-only position errors have increased. It is recommended that the data produced by this thesis be made available to other agencies for further study.

Further research could be undertaken at thesis or doctorate level to determine accurate time dependant values for the satellite antenna phase centre offsets. The effect of solar cycle on broadcast ephemeris error could also be a topic for future study.

Appendix A: Data Format

Data is stored in four files types as follows:

- x-poserr.mat,
- x-rms.mat,
- x-stats.mat, and
- x-sisre.mat.

Where x denoted the time period of the data, eg: 2001.

Poserr

Poserr is a cell array with m records, where m is the number of days in the analysis period. Each record contains seven data structures:

prn: An array (n x 1) of the PRN values corresponding to the position errors.

svn: An array (n x 1) of the SVN values corresponding to the position errors.

dpos_ECEF: An array (n x 3) of ECEF position errors. Not corrected for satellite antenna offset.

dpos_ACR: An array (n x 3) of ACR position errors. Corrected for satellite antenna offset.

time: An array (n x 1) of time values corresponding to the position errors.

removed: number of data epochs removed by outlier filter.

dpos_bad: An array (removed x 3) of removed ECEF position errors that exceed the outlier filter limit (defined in Chapter 4).

time_ref: An array (n x 1) of time-tagged reference values. Format is $www.x$, where x is the fraction of week www .

Where

n = the number of data points for a particular day.

Rms

Rms is a cell array with m records, where m is the number of days in the analysis period. Each record contains four data structures:

sv: An array (32 x 3) of daily satellite RMS ACR position errors.

sv3D: An array (n x 1) of 3D satellite ACR position errors error for each time epoch.

const: Constellation RMS ACR position error (1 x 3).

const3D: 3D constellation RMS ACR position error (1 x 1).

Where

n = the number of data points for a particular day.

Stats

Stats is a cell array with m records, where m is the number of days in the analysis period. Each record contains twelve data structures:

svmin: An array ($s \times 3$) of daily minimum satellite ACR position error.

svmax: An array ($s \times 3$) of daily maximum satellite ACR position error.

svmean: An array ($s \times 3$) of daily mean satellite ACR position error.

svsd: An array ($s \times 3$) of daily satellite ACR position error standard deviation.

svmed: An array ($s \times 3$) of daily satellite median ACR position error.

sv90: An array ($s \times 3$) of daily 90th percentile satellite ACR position error.

constmin: Daily minimum constellation ACR position error (1×3).

constmax: Daily maximum constellation ACR position error (1×3).

constmean: Daily mean constellation ACR position error (1×3).

constsd: Daily constellation ACR position error standard deviation (1×3).

constmed: Daily constellation ACR median position error (1×3).

const90: Daily 90th percentile constellation ACR position error (1×3).

Where

s = the number of satellites used in the analysis for a particular day.

Sisre

Sisre is a cell array with m records, where m is the number of days in the analysis period. Each record contains three data structures:

raw: An array ($n \times 1$) of SISRE satellite position error for each epoch.

rms_sv: An array (32×1) of RMS satellite SISRE calculated for each day.

rms_const: Daily RMS constellation SISRE (1×1).

Where

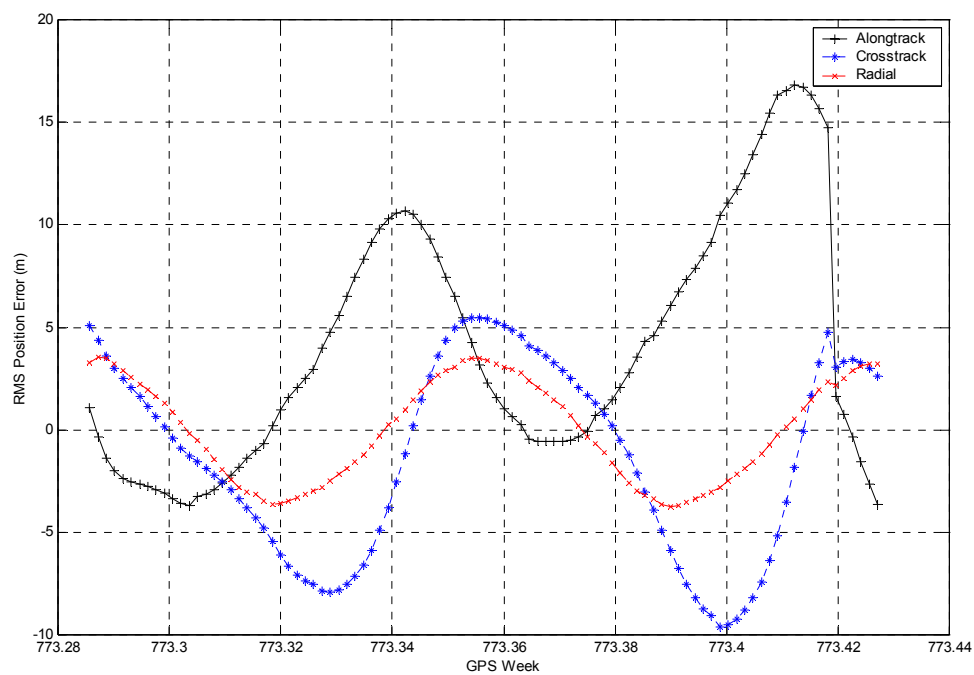
n = the number of data points for a particular day.

Appendix B: Along-Track, Cross-track and Radial Broadcast Position Error

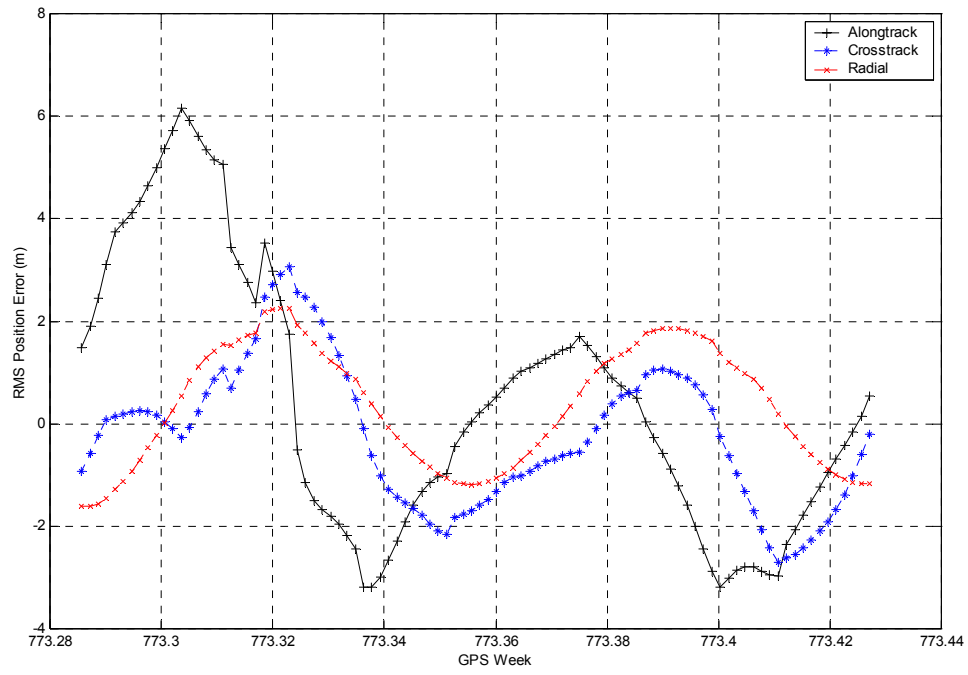
PRNs not listed were not present in the constellation on the sample day.

1 Nov 1994

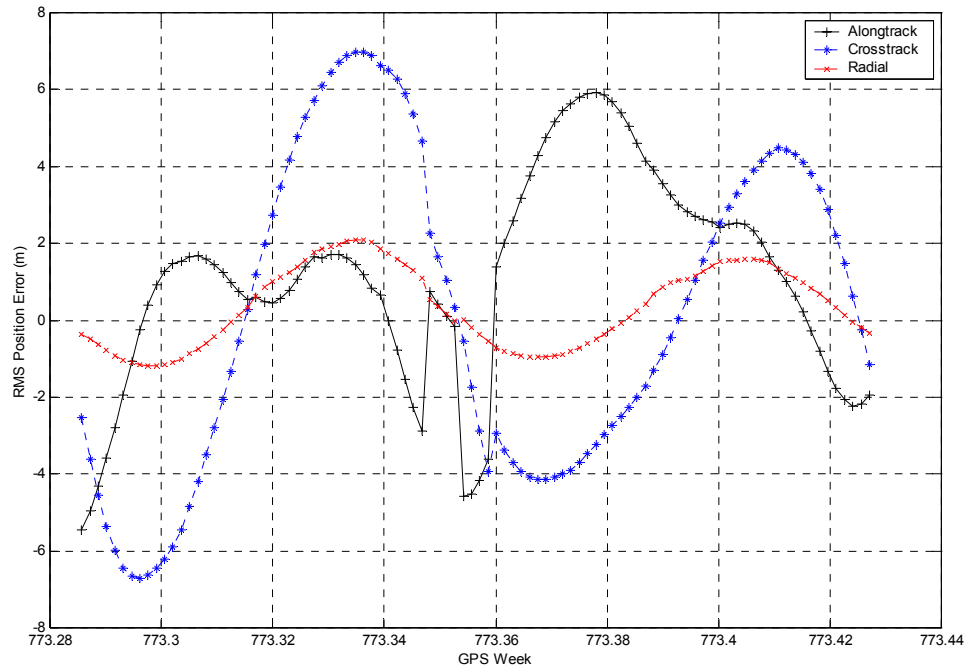
PRN 1 – SVN 32 (Block II)



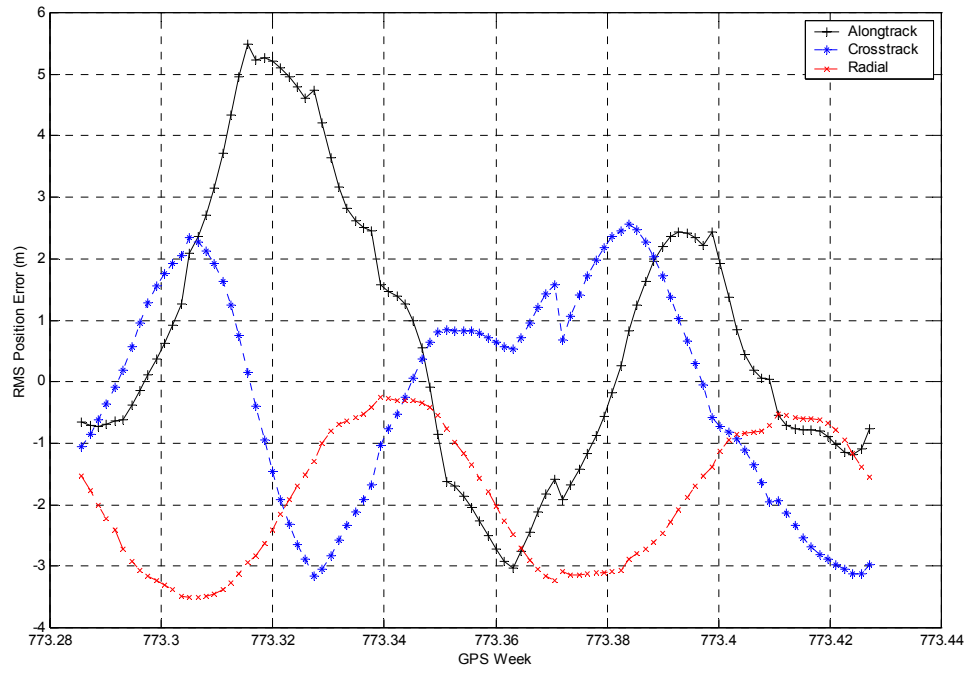
PRN 2 – SVN 13 (Block II)



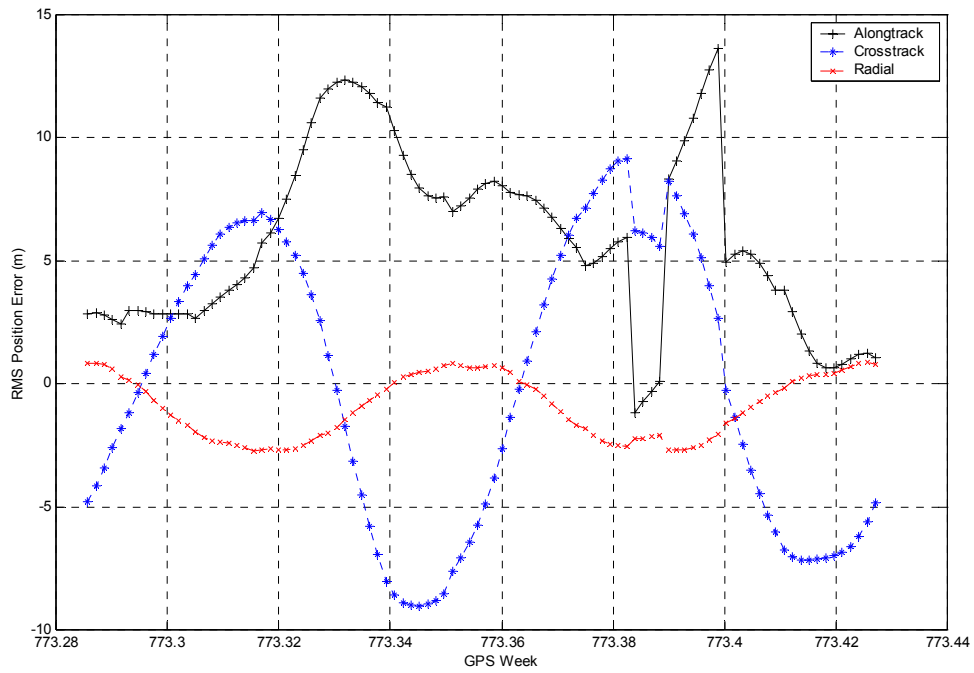
PRN 4 – SVN 34 (Block II)



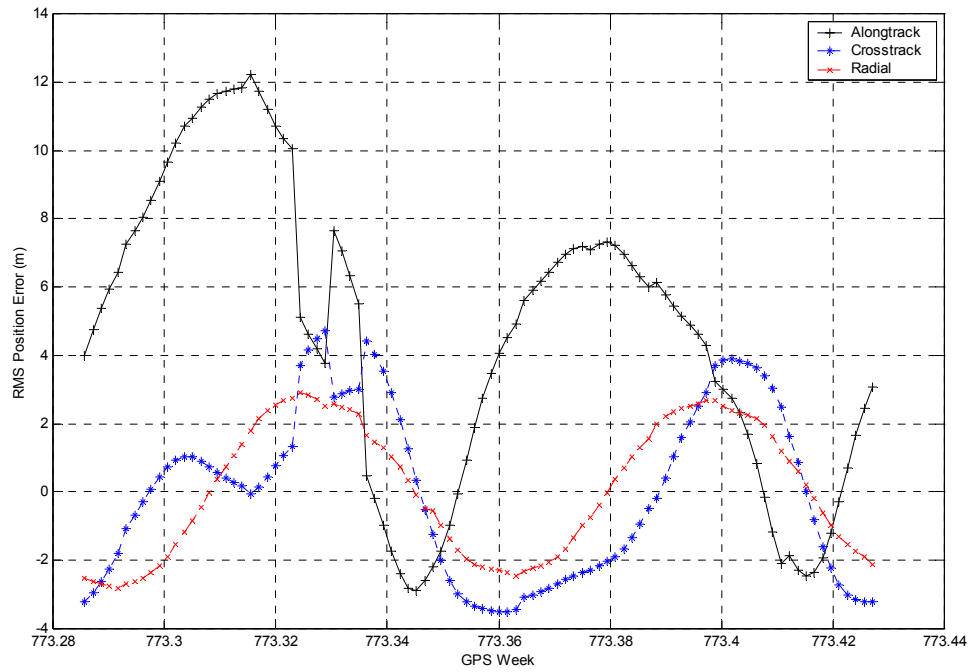
PRN 5 – SVN 35 (Block II)



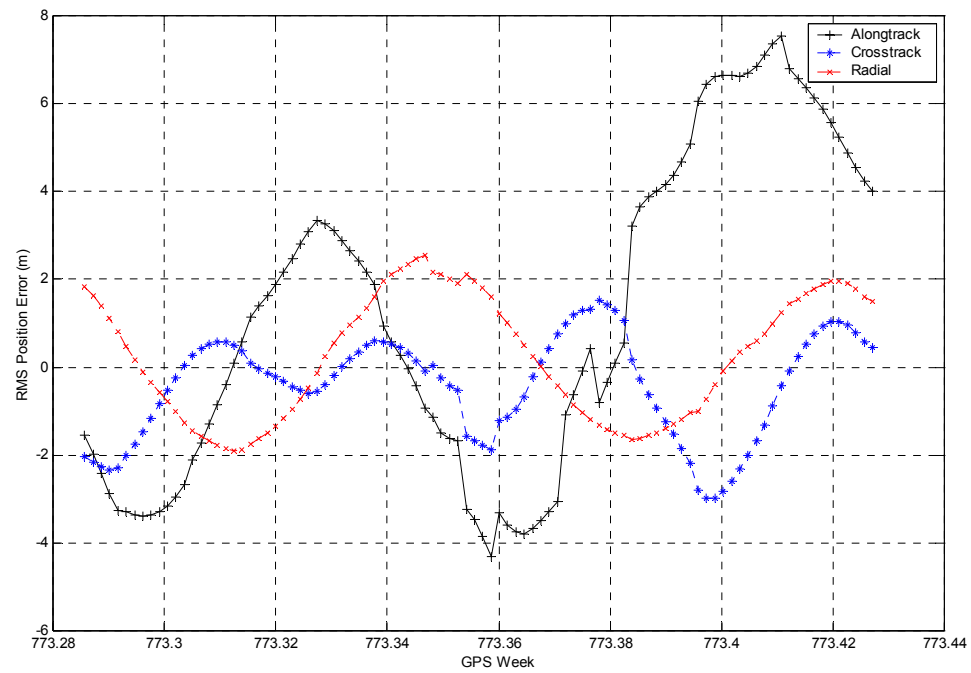
PRN 6 – SVN 36 (Block II)



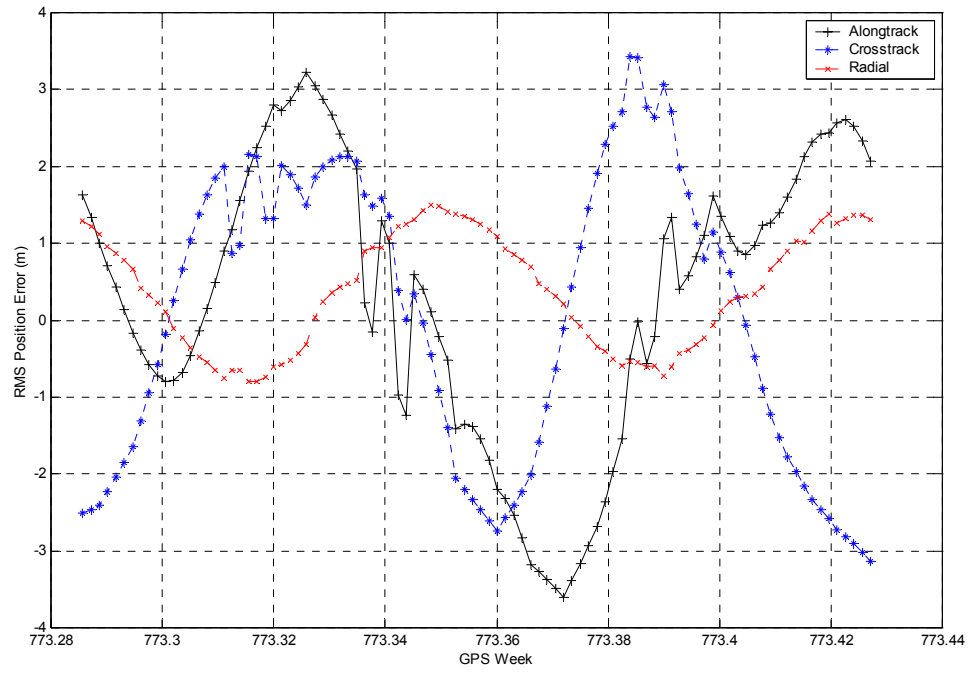
PRN 7 – SVN 37 (Block II)



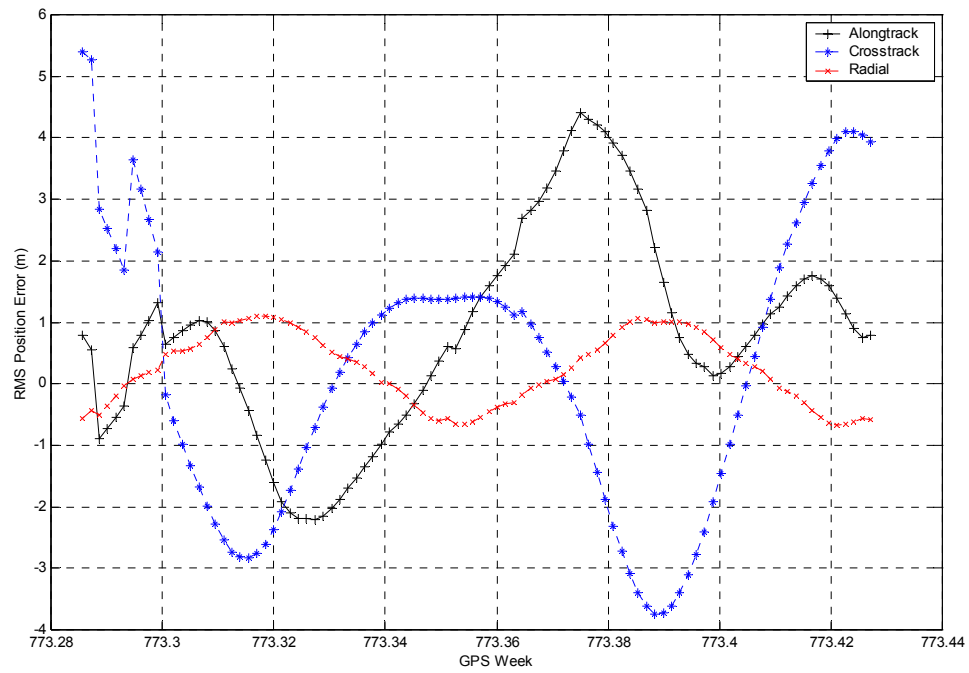
PRN 9 – SVN 39 (Block II)



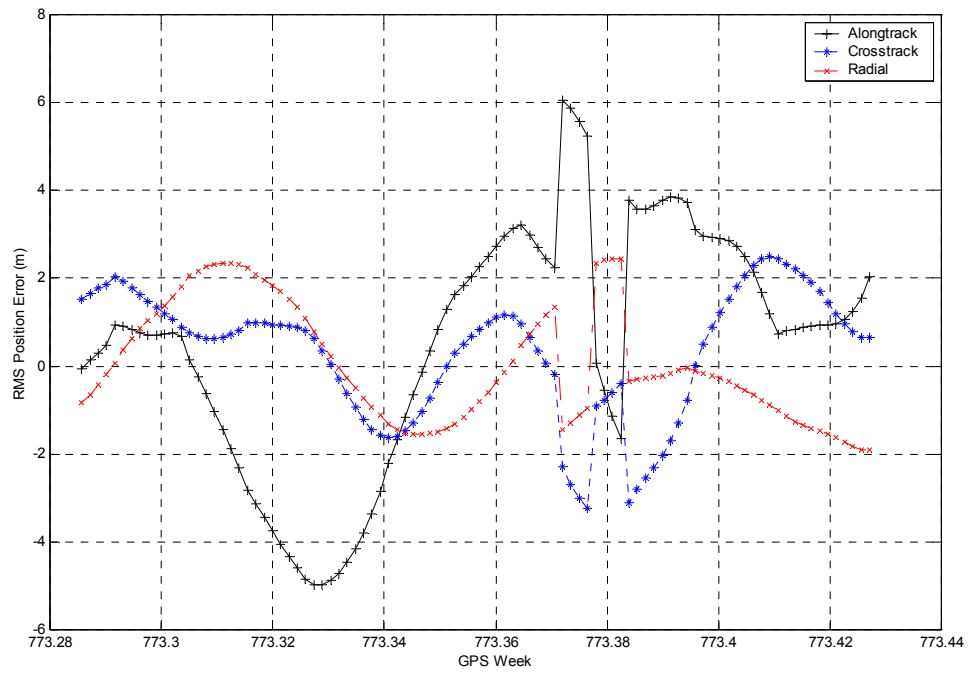
PRN 12 – SVN 10 (Block I)



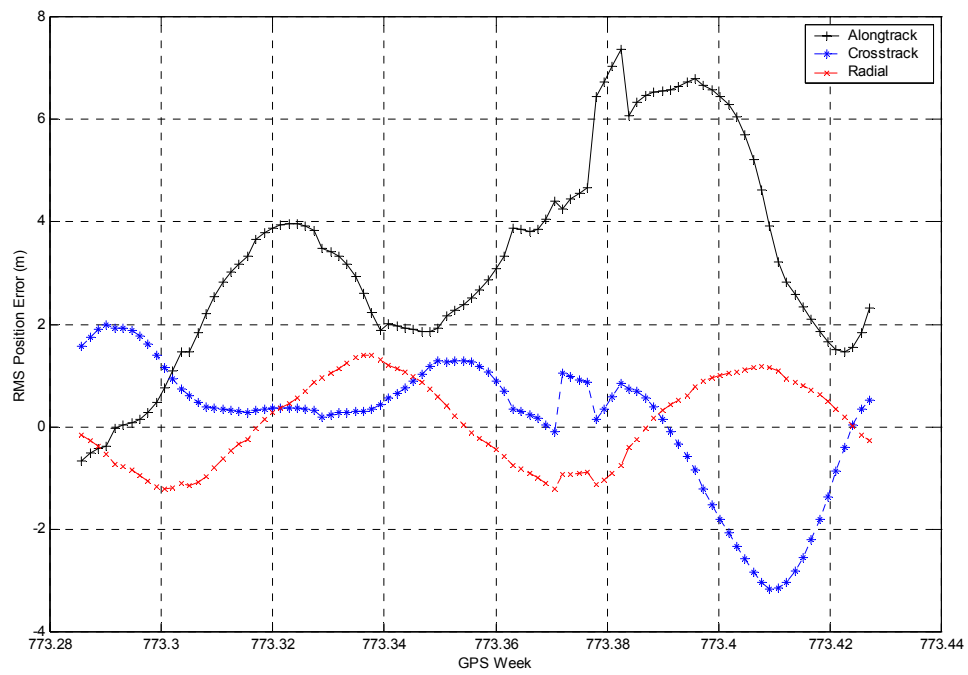
PRN 14 – SVN 14 (Block II)



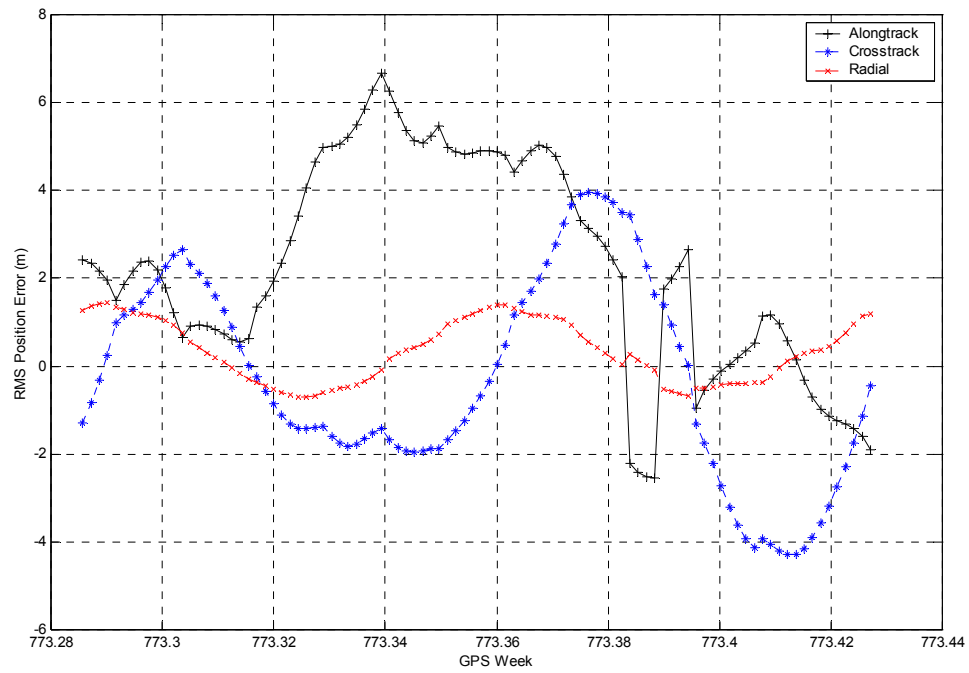
PRN 15 – SVN 15 (Block II)



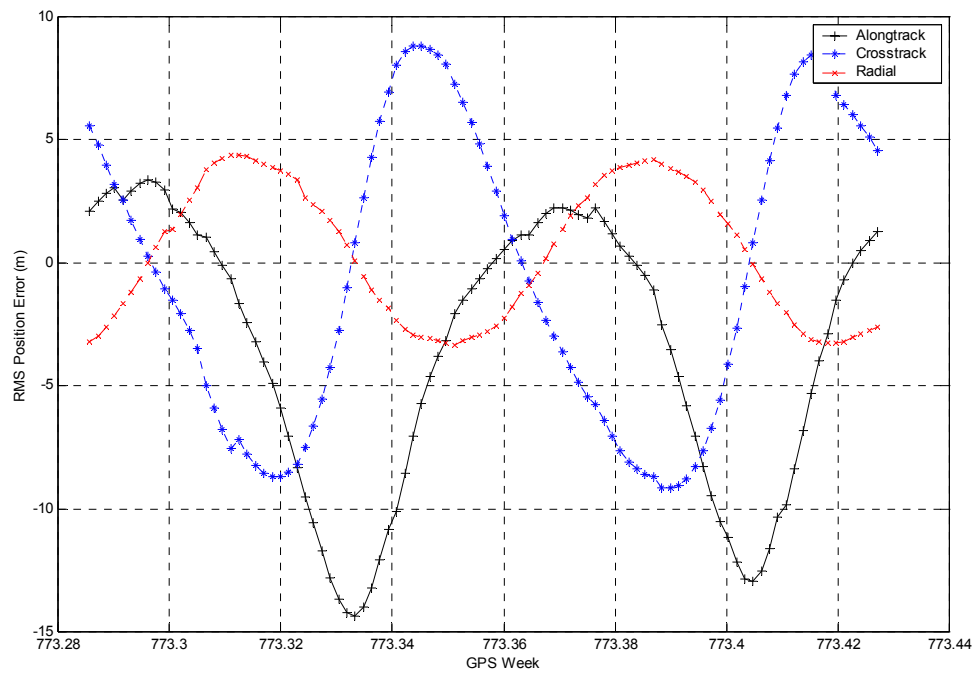
PRN 16 – SVN 16 (Block II)



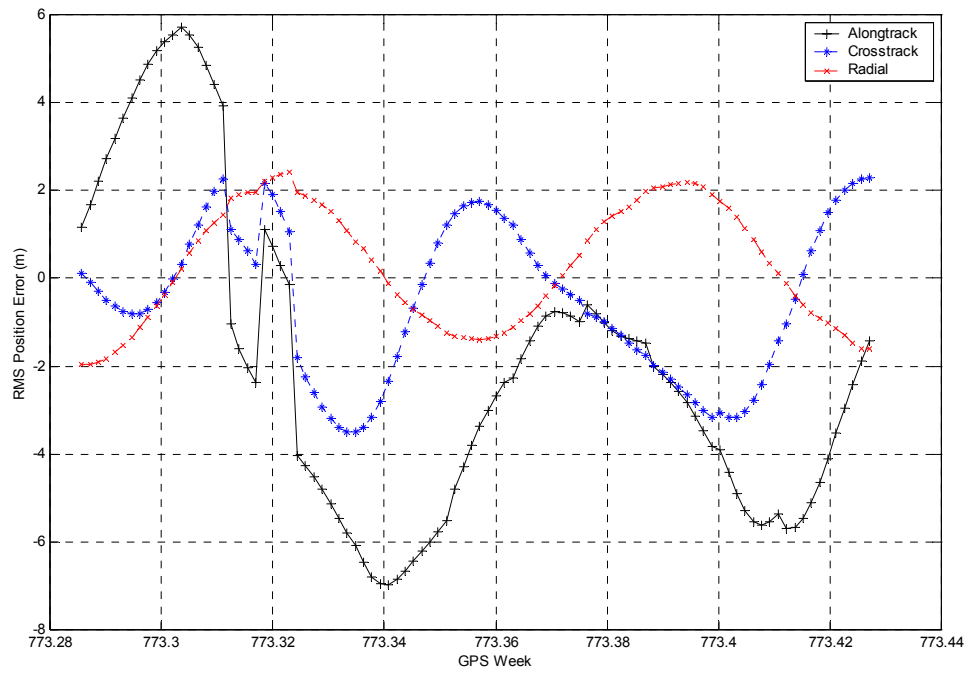
PRN 17 – SVN 17 (Block II)



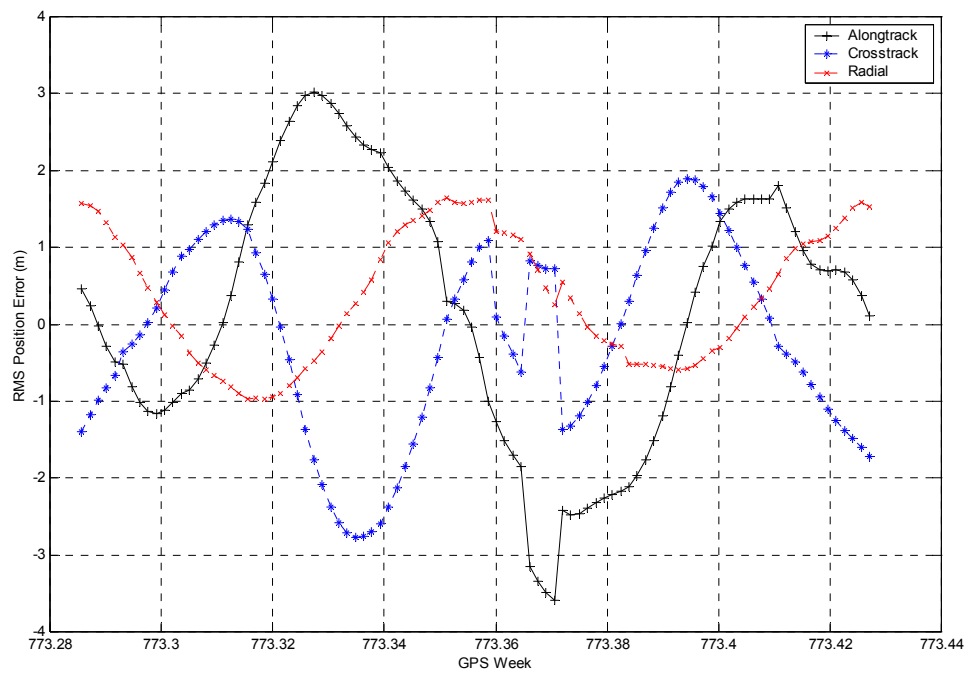
PRN 18 – SVN 18 (Block II)



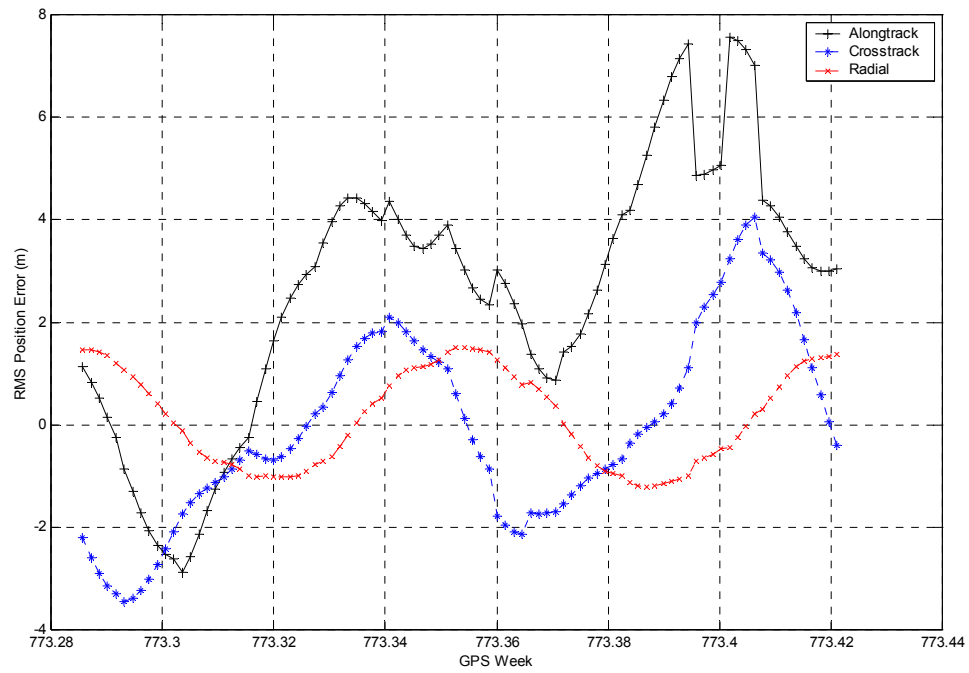
PRN 19 – SVN 19 (Block II)



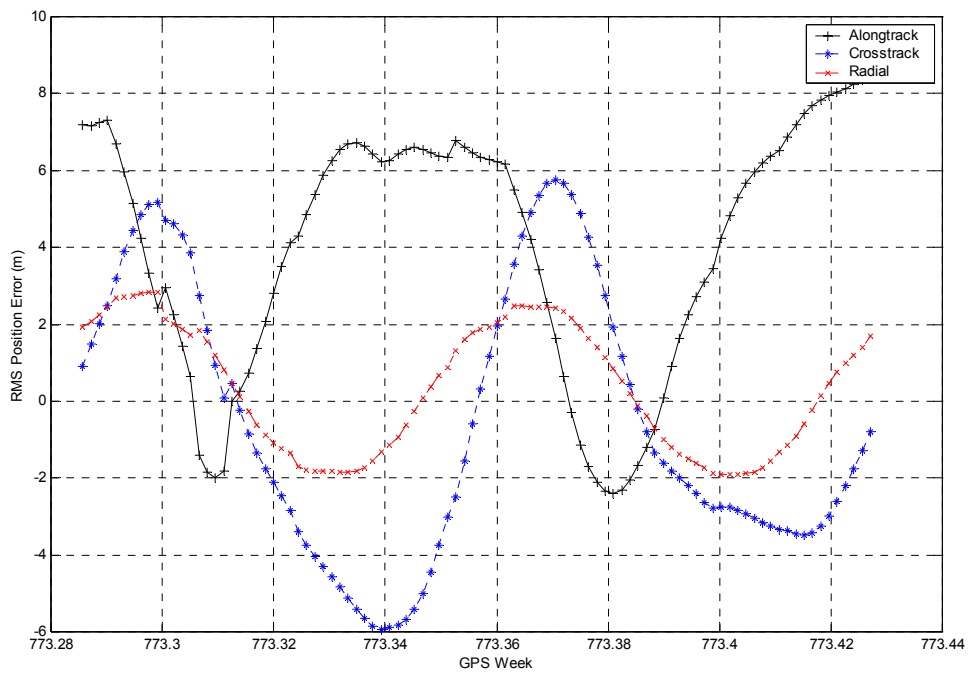
PRN 20 – SVN 20 (Block II)



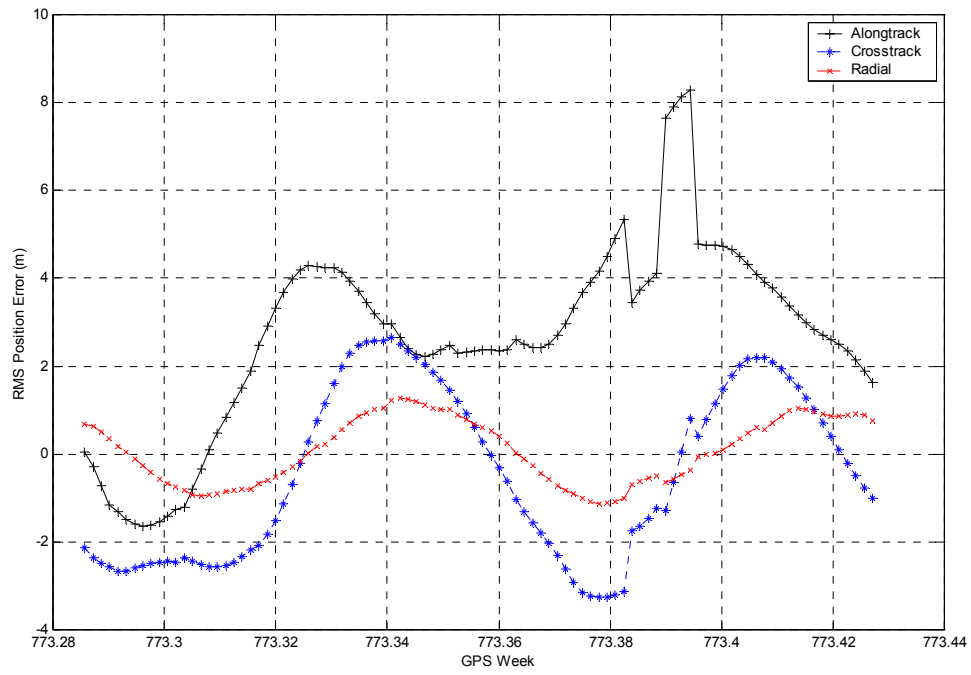
PRN 21 – SVN 21 (Block II)



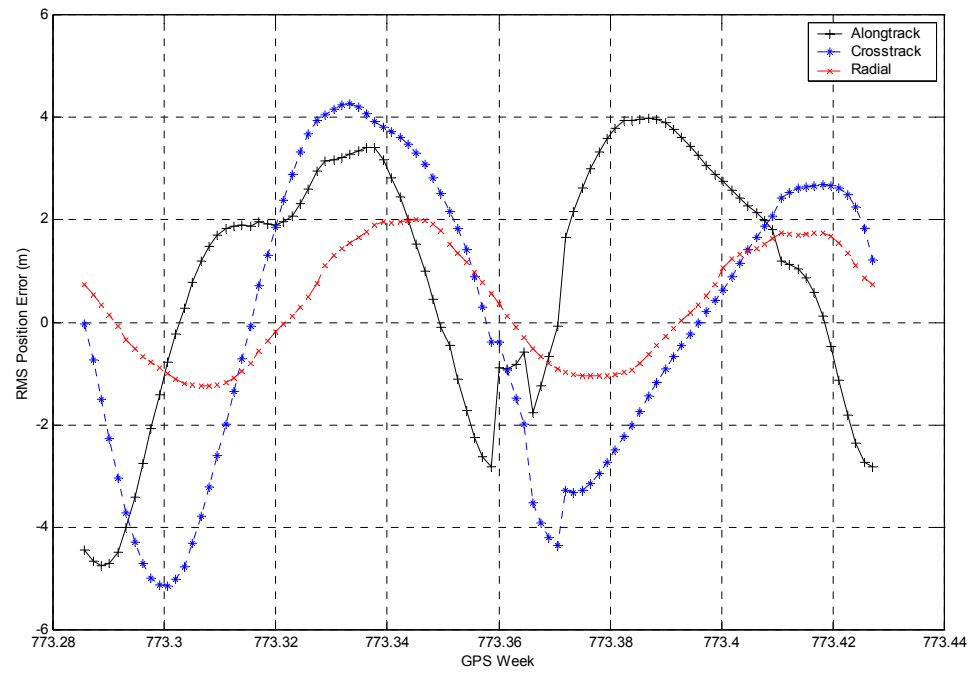
PRN 22 – SVN 22 (Block II)



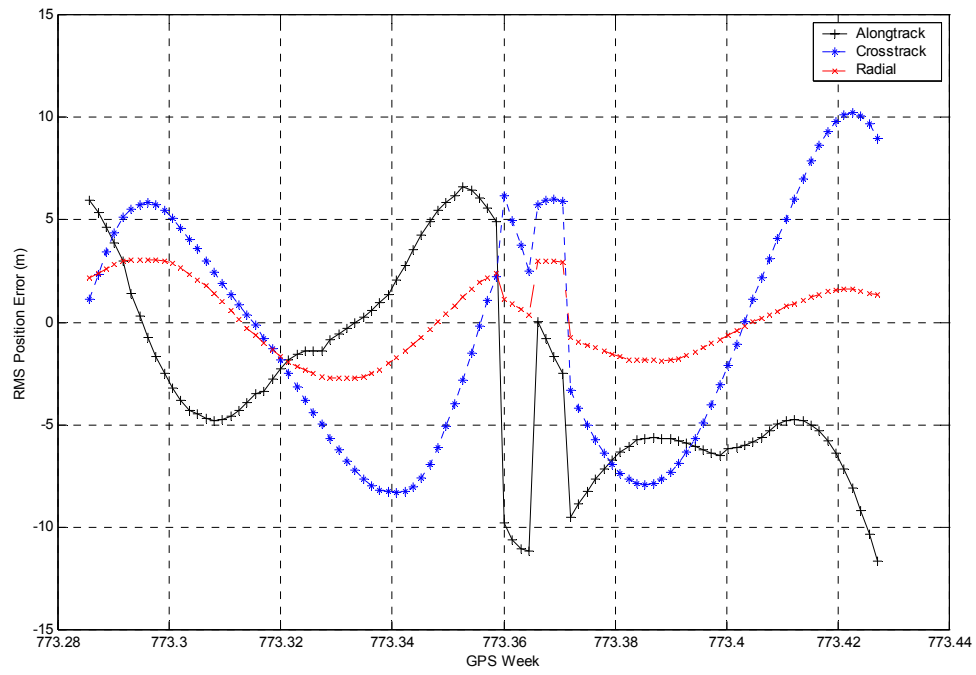
PRN 23 – SVN 23 (Block II)



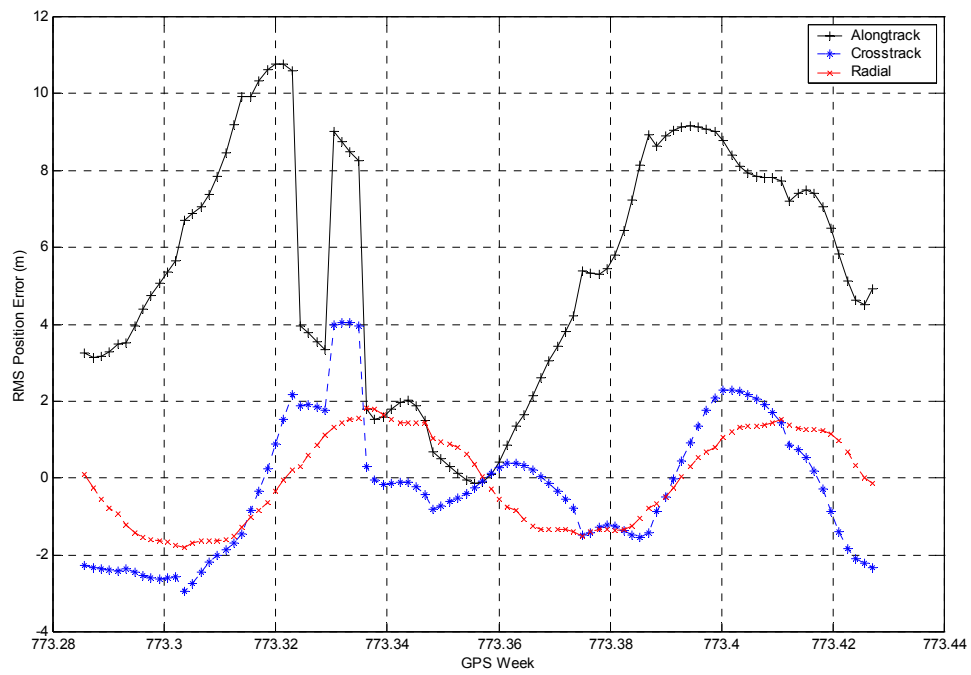
PRN 24 – SVN 24 (Block II)



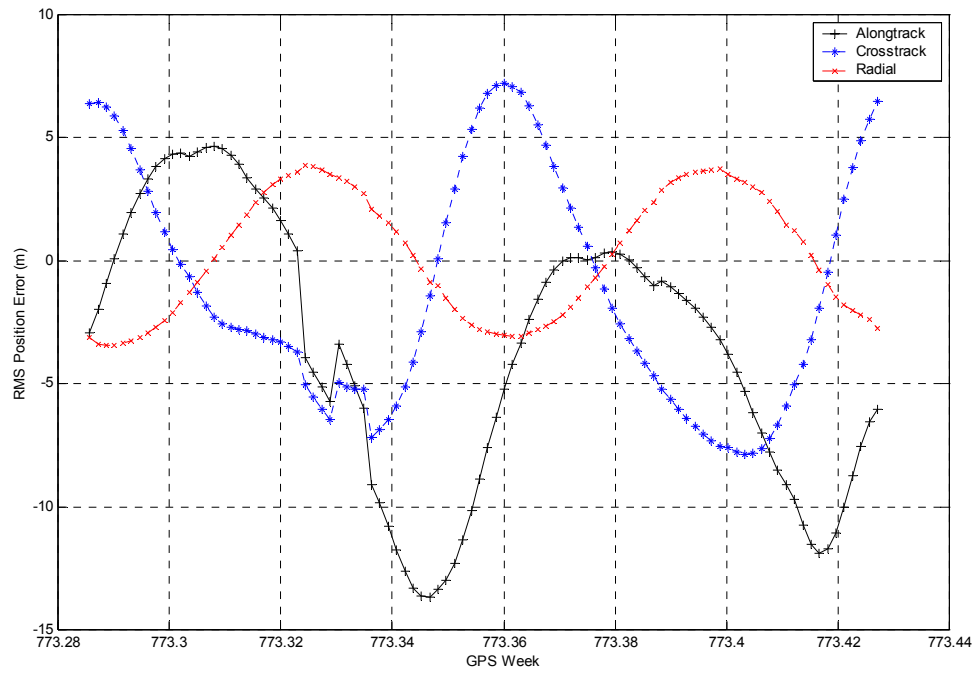
PRN 25 – SVN 25 (Block II)



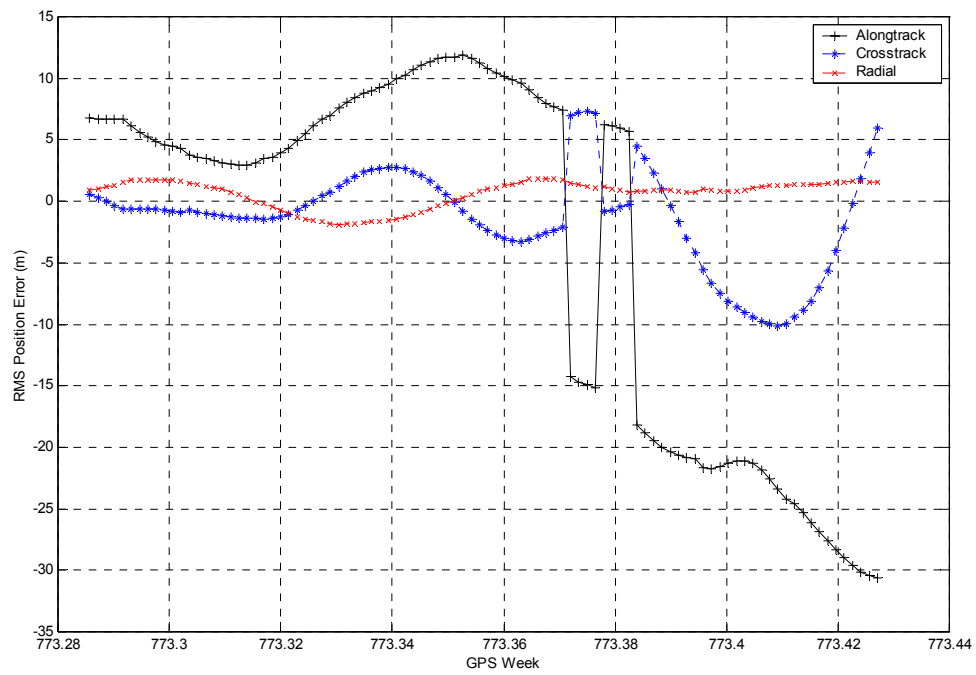
PRN 26 – SVN 26 (Block II)



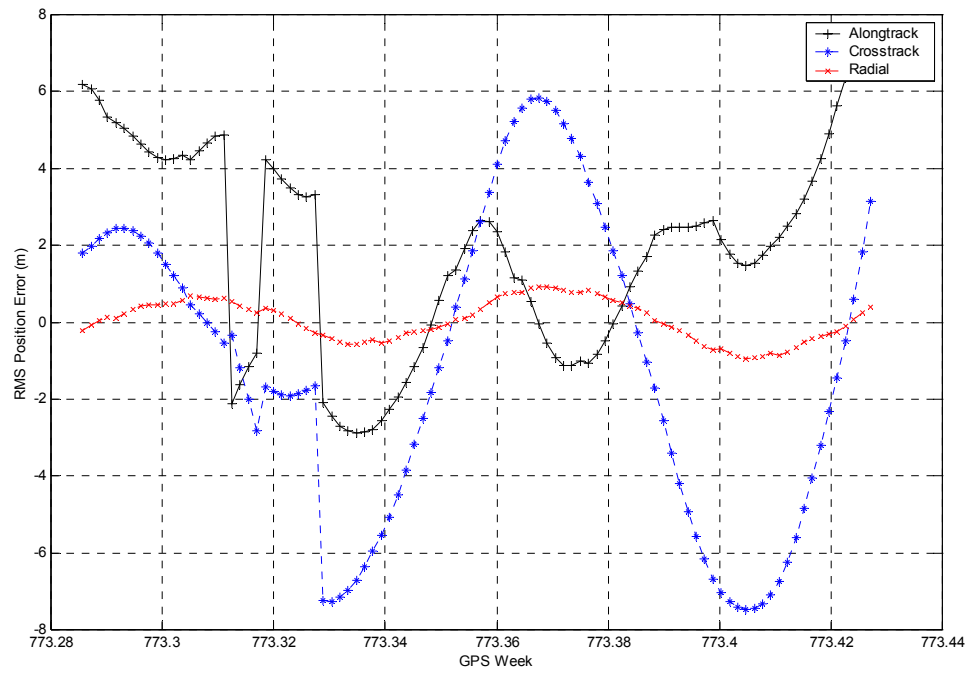
PRN 27 – SVN 27 (Block II)



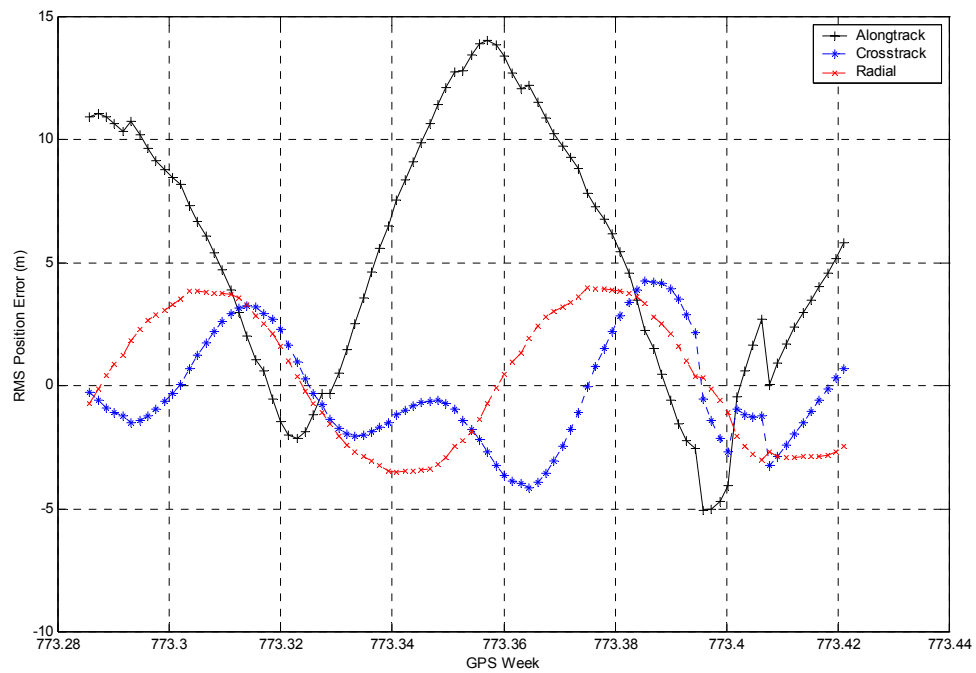
PRN 28 – SVN 28 (Block II)



PRN 29 – SVN 29 (Block II)

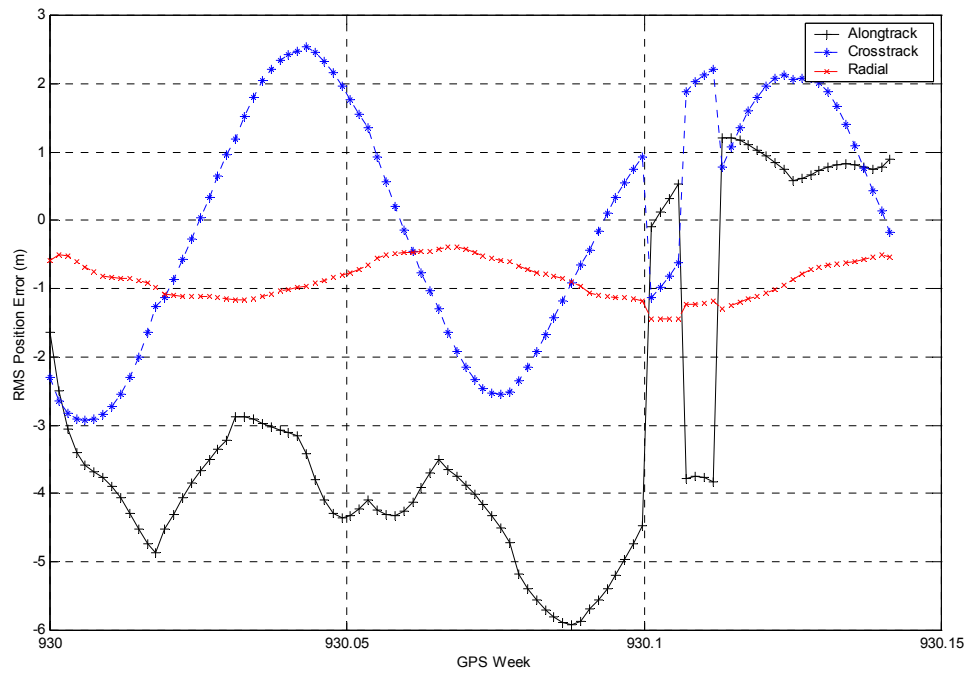


PRN 31 – SVN 31 (Block II)

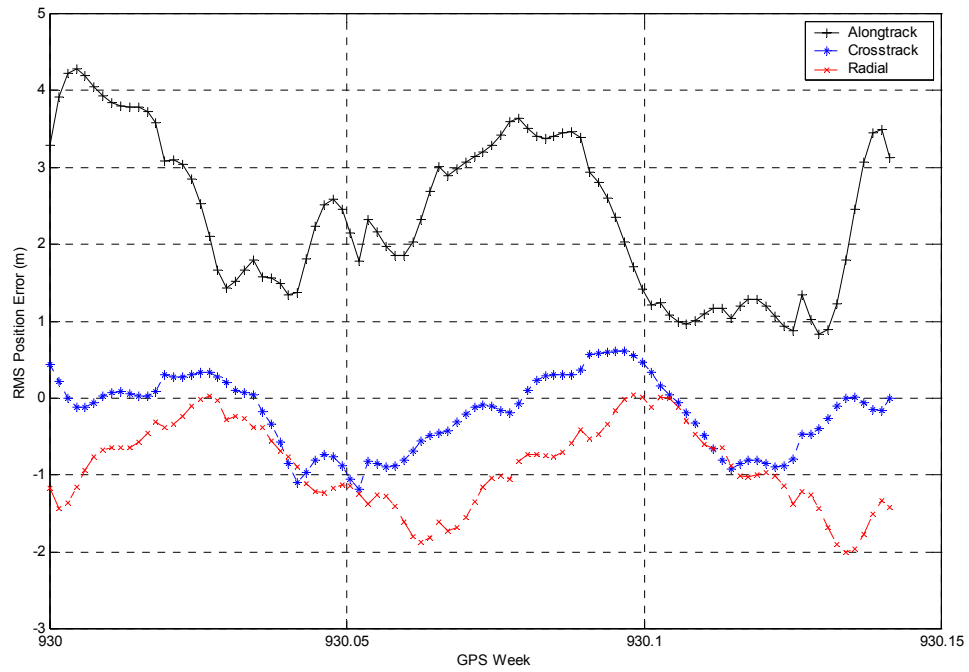


1 Nov 1997

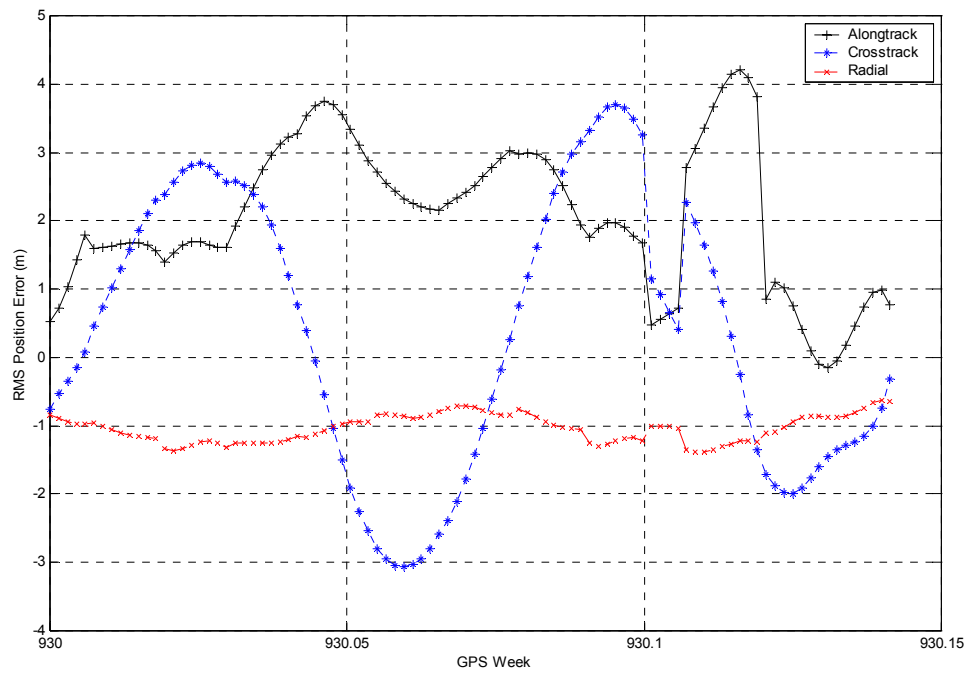
PRN 1 – SVN 32 (Block II)



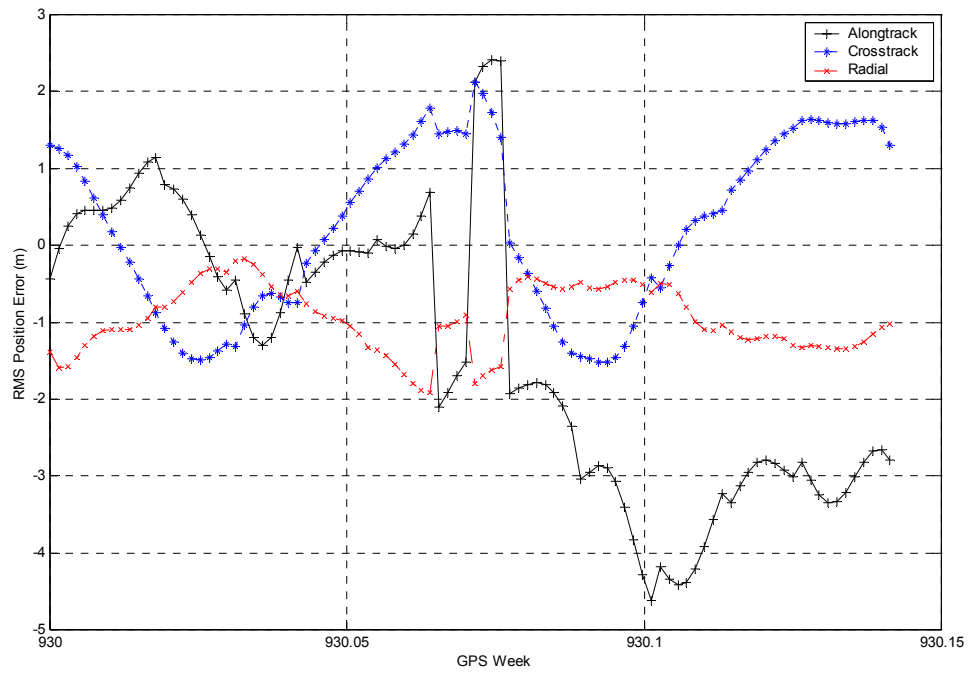
PRN 2 – SVN 13 (Block II)



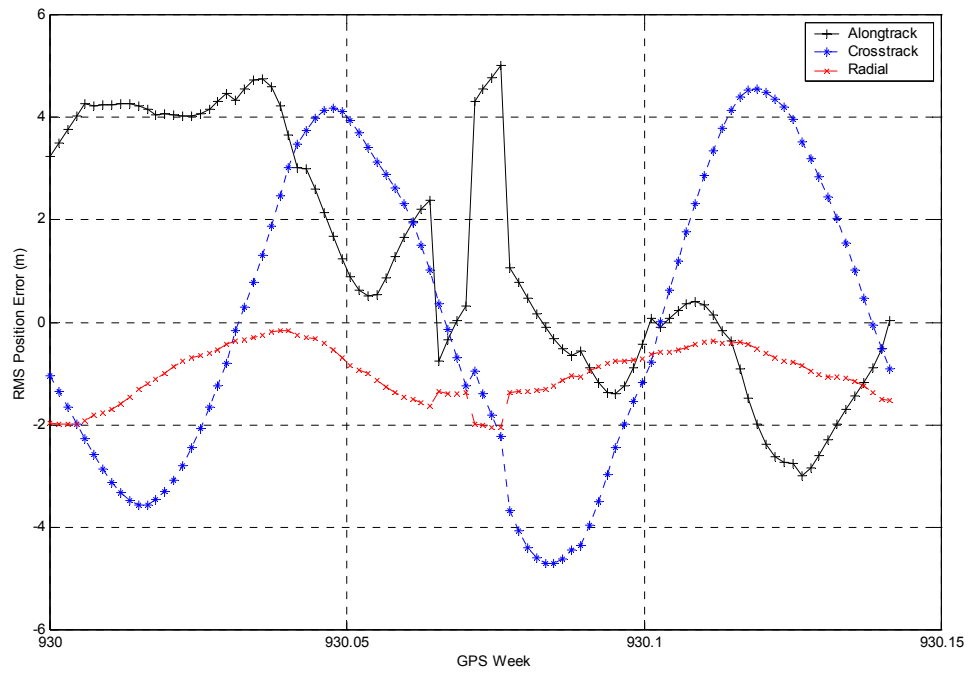
PRN 3 – SVN 33 (Block II)



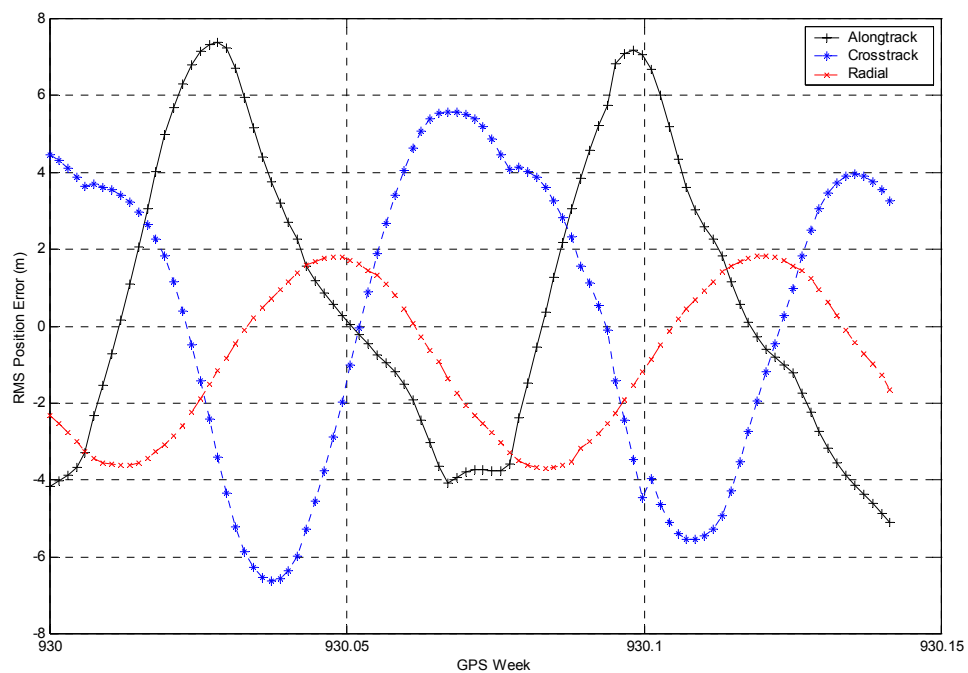
PRN 4 – SVN 34 (Block II)



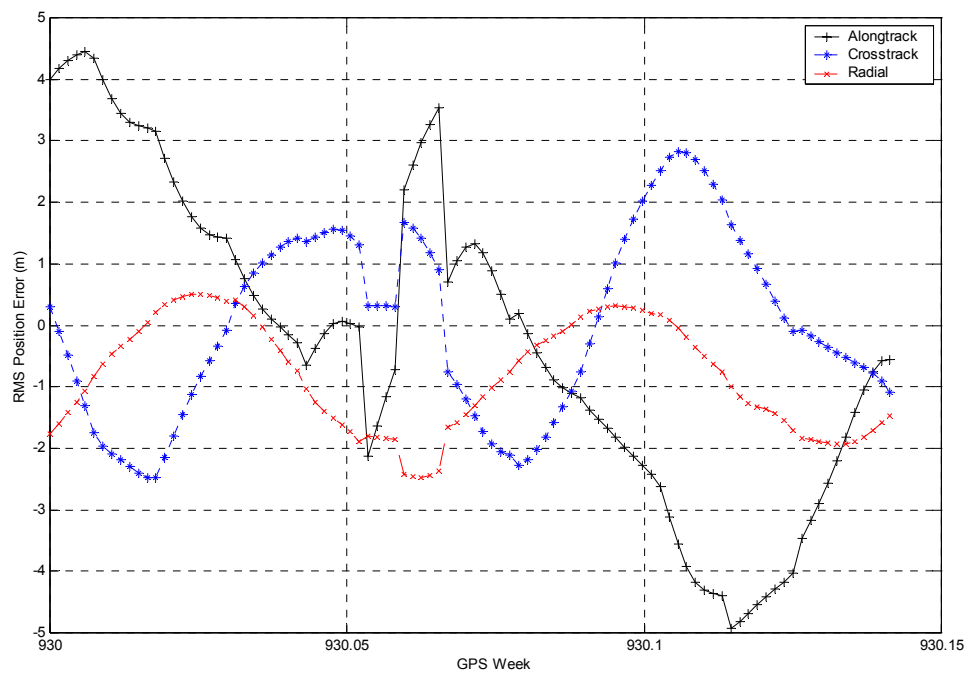
PRN 5 – SVN 35 (Block II)



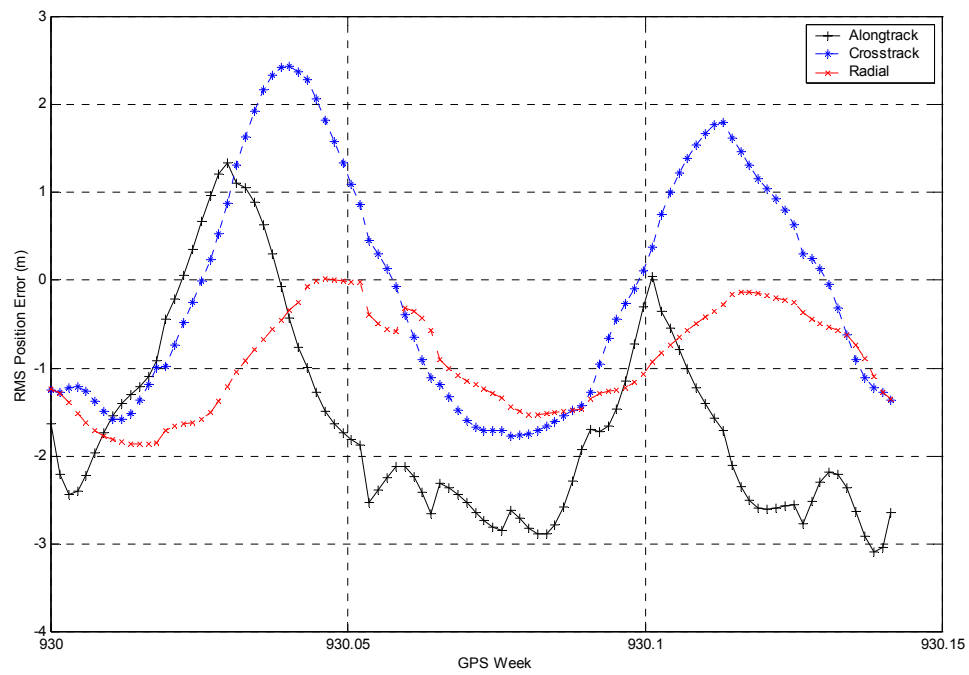
PRN 6 – SVN 36 (Block II)



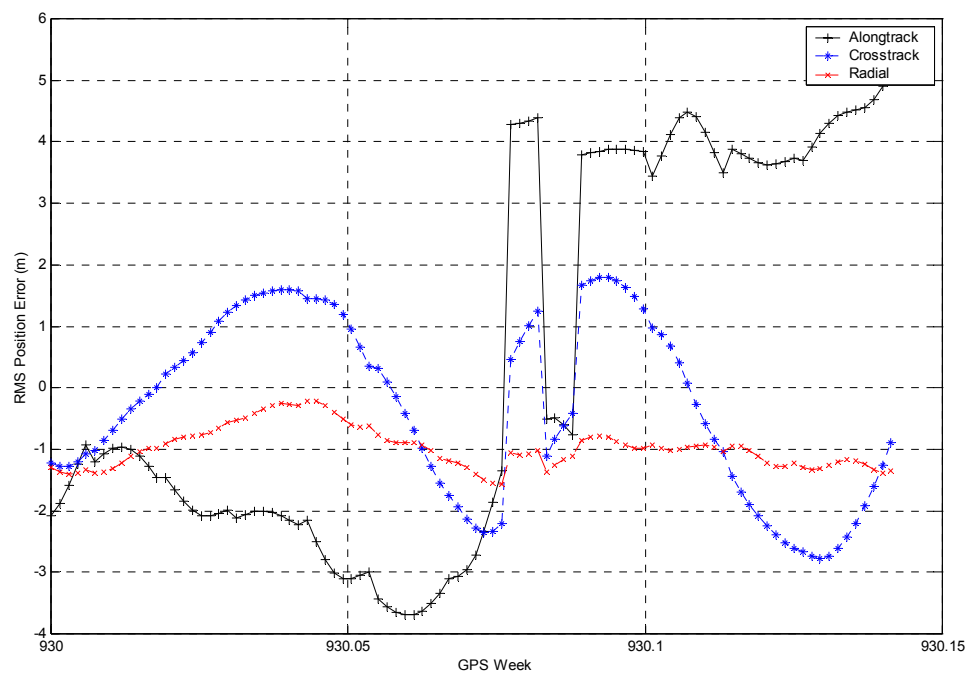
PRN 7 – SVN 37 (Block II)



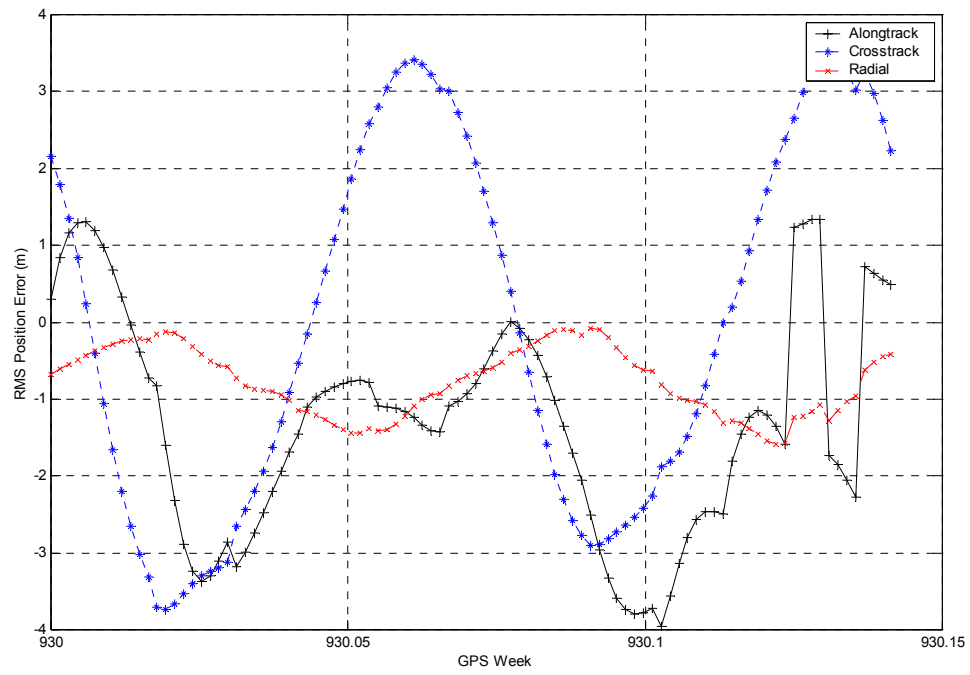
PRN 9 – SVN 39 (Block II)



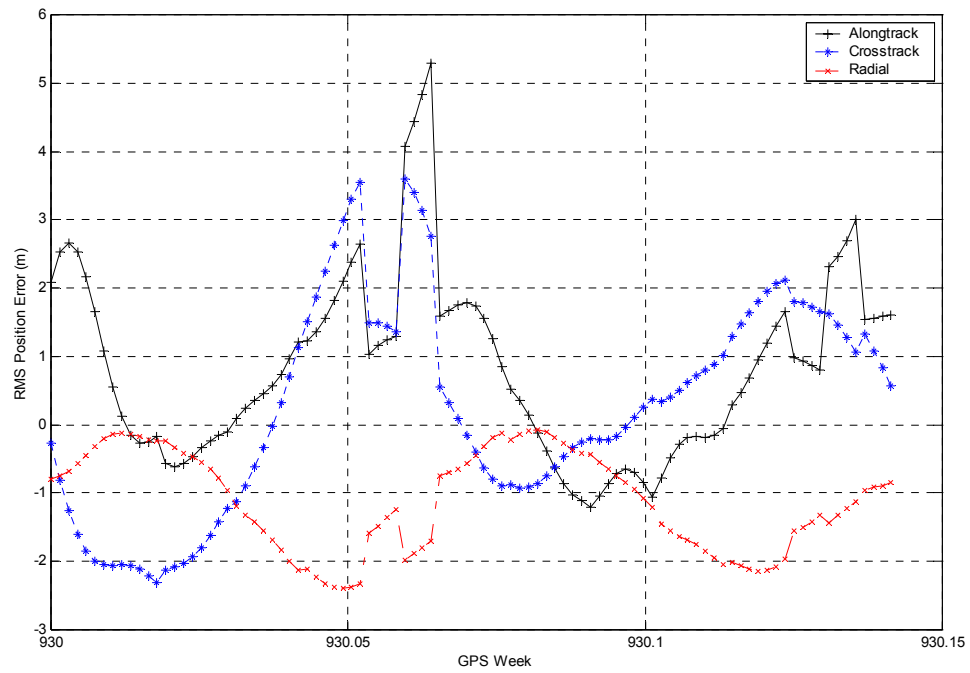
PRN 10 – SVN 40 (Block II)



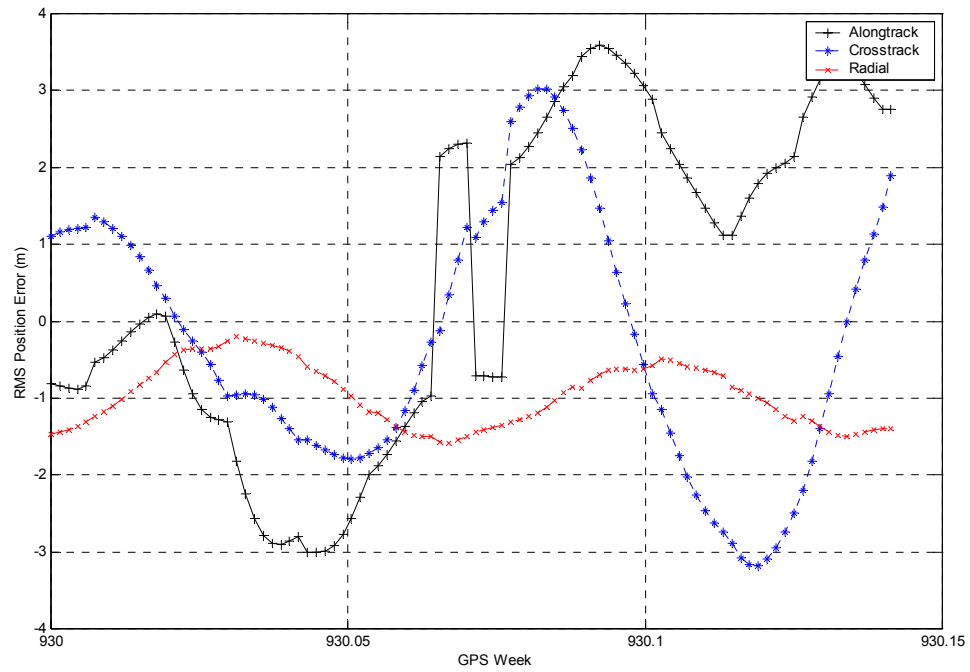
PRN 14 – SVN 14 (Block II)



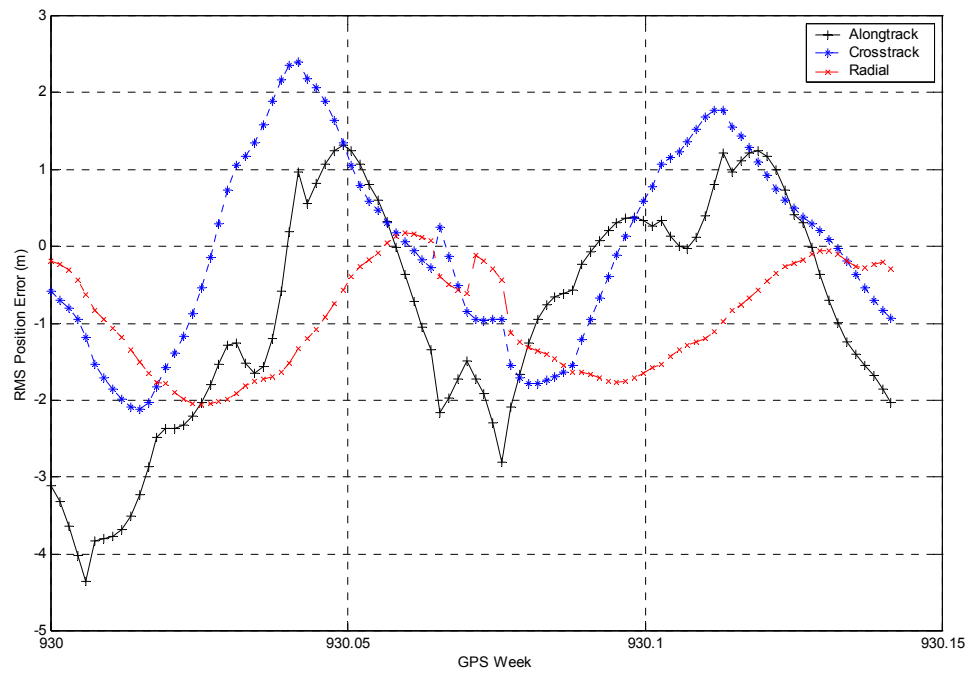
PRN 15 – SVN 15 (Block II)



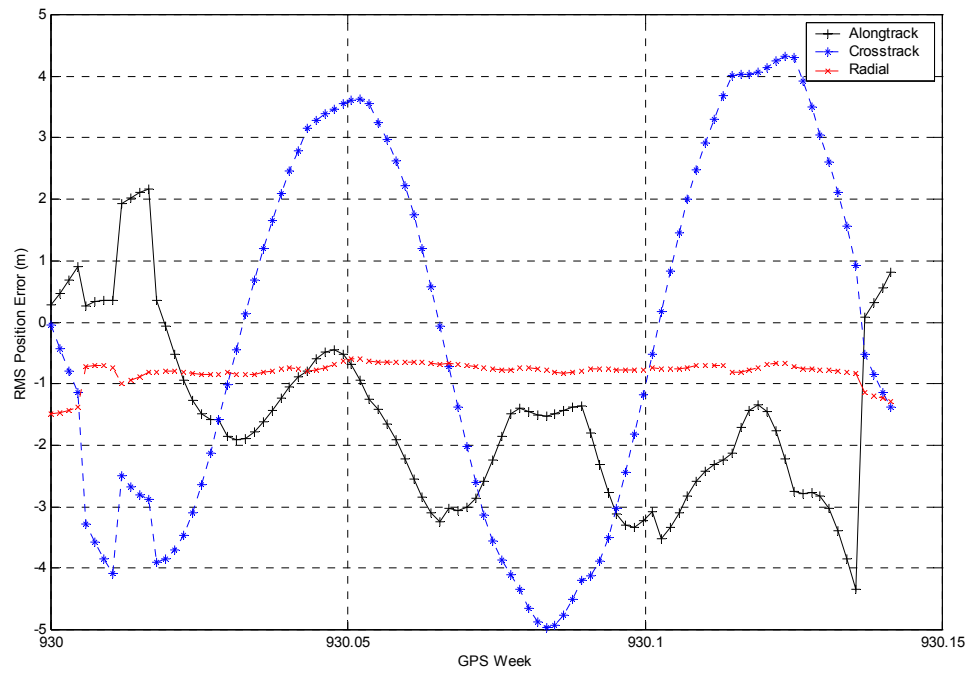
PRN 16 – SVN 16 (Block II)



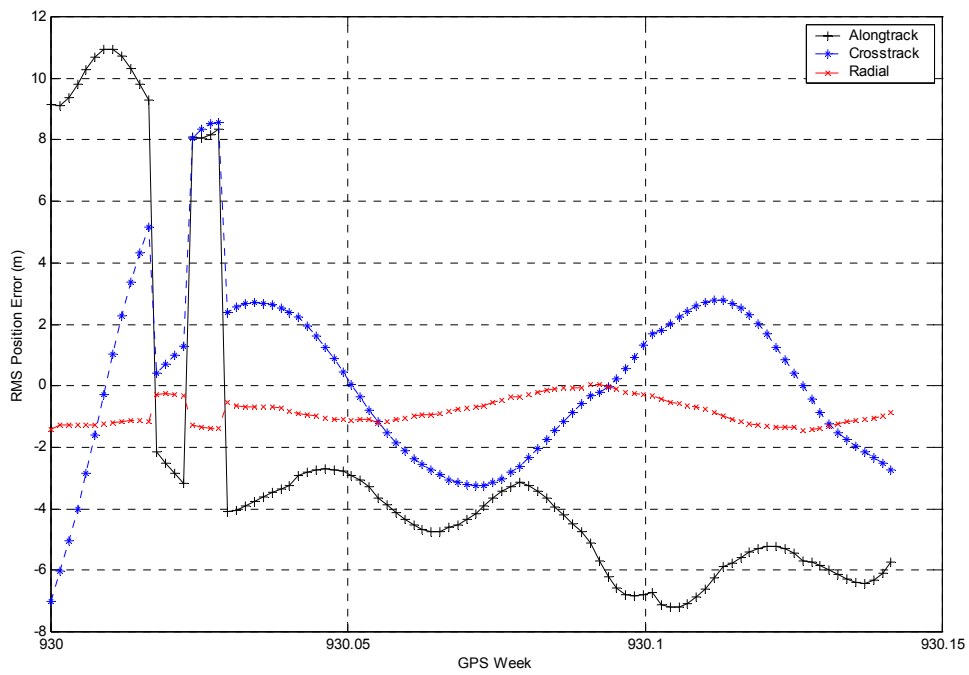
PRN 17 – SVN 17 (Block II)



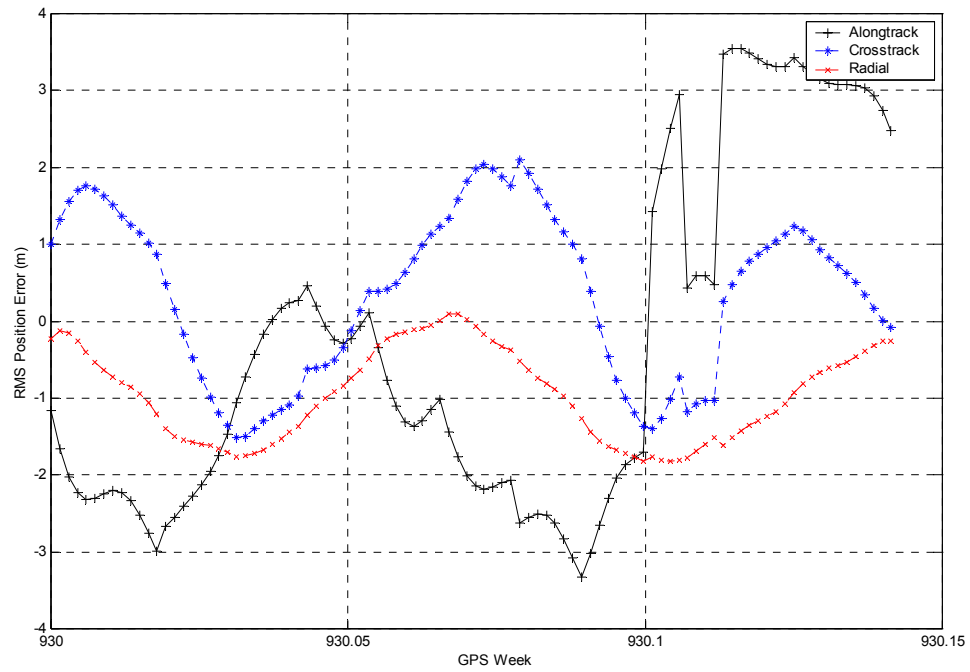
PRN 18 – SVN 18 (Block II)



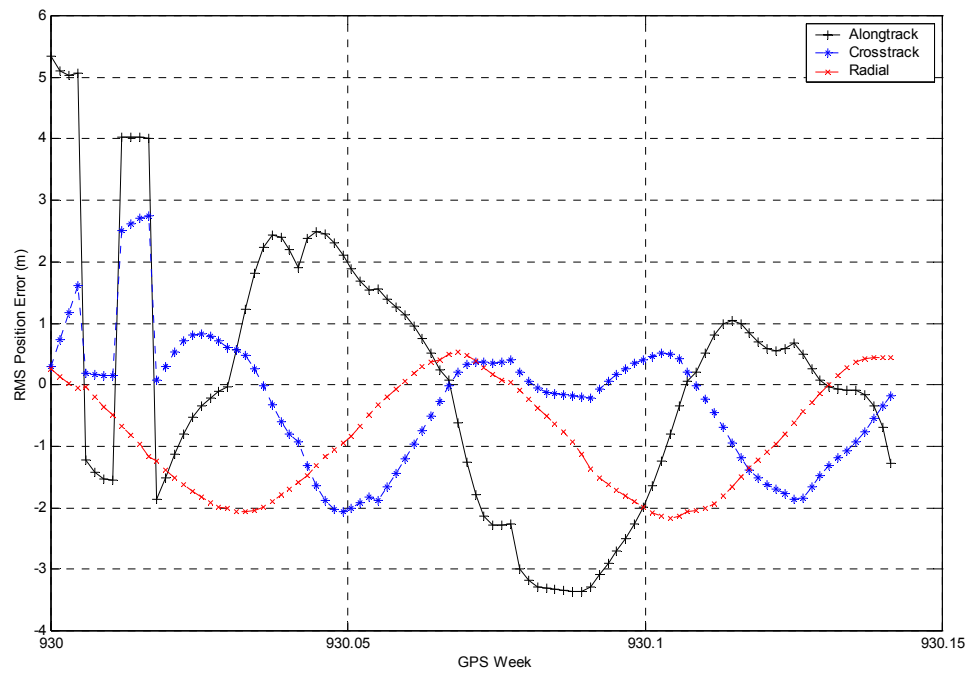
PRN 19 – SVN 19 (Block II)



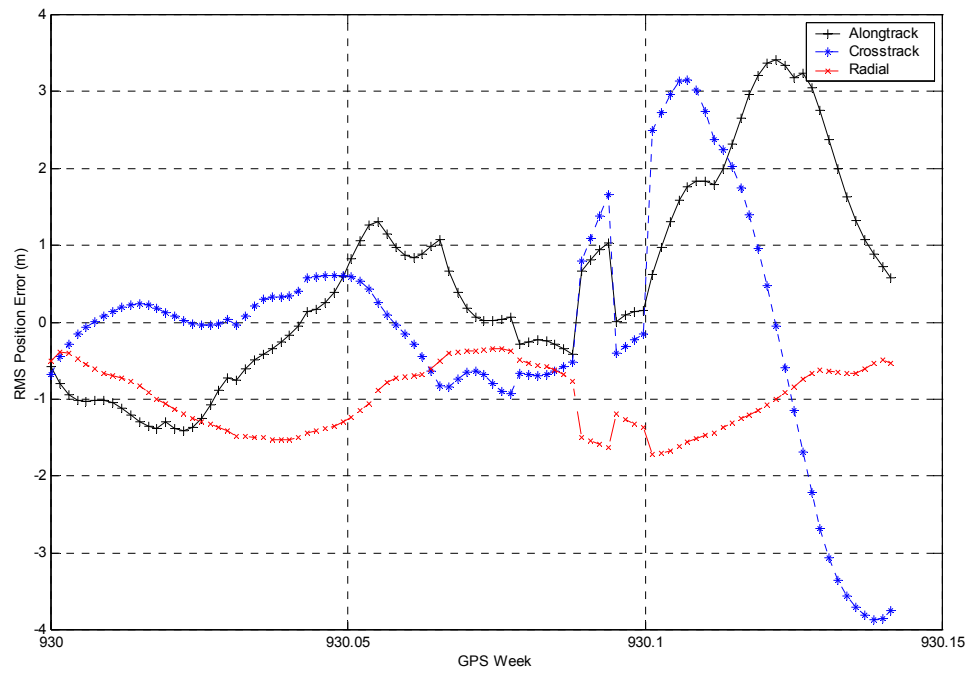
PRN 21 – SVN 21 (Block II)



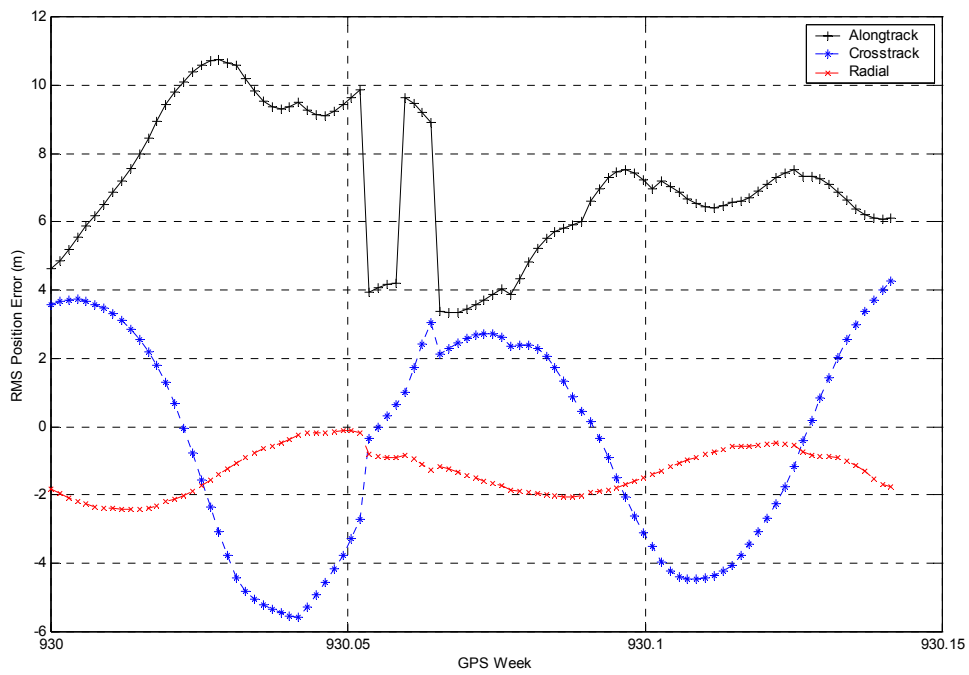
PRN 22 – SVN 22 (Block II)



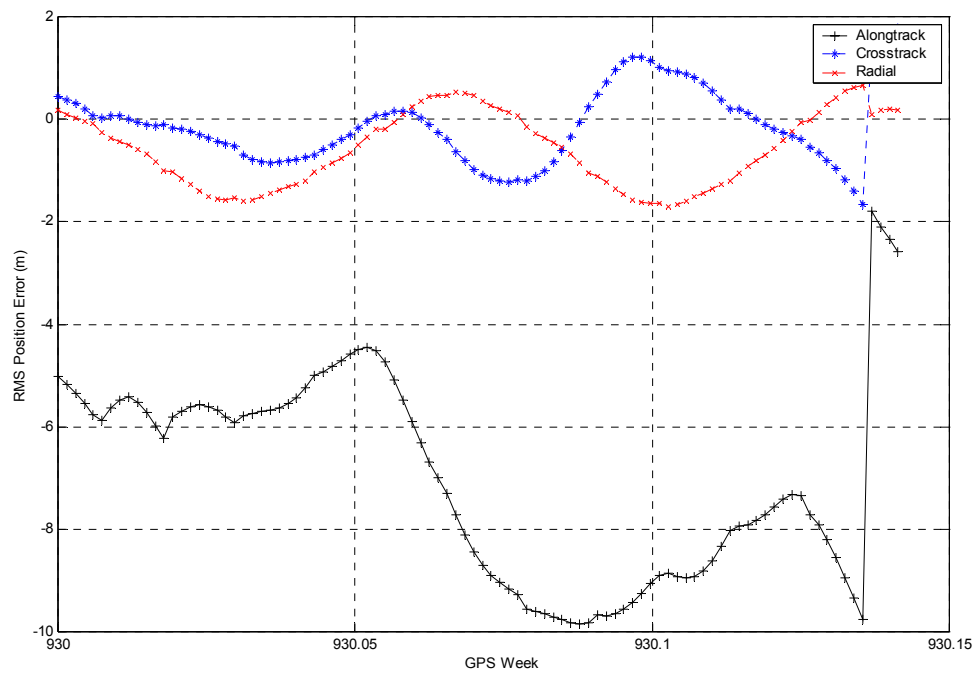
PRN 23 – SVN 23 (Block II)



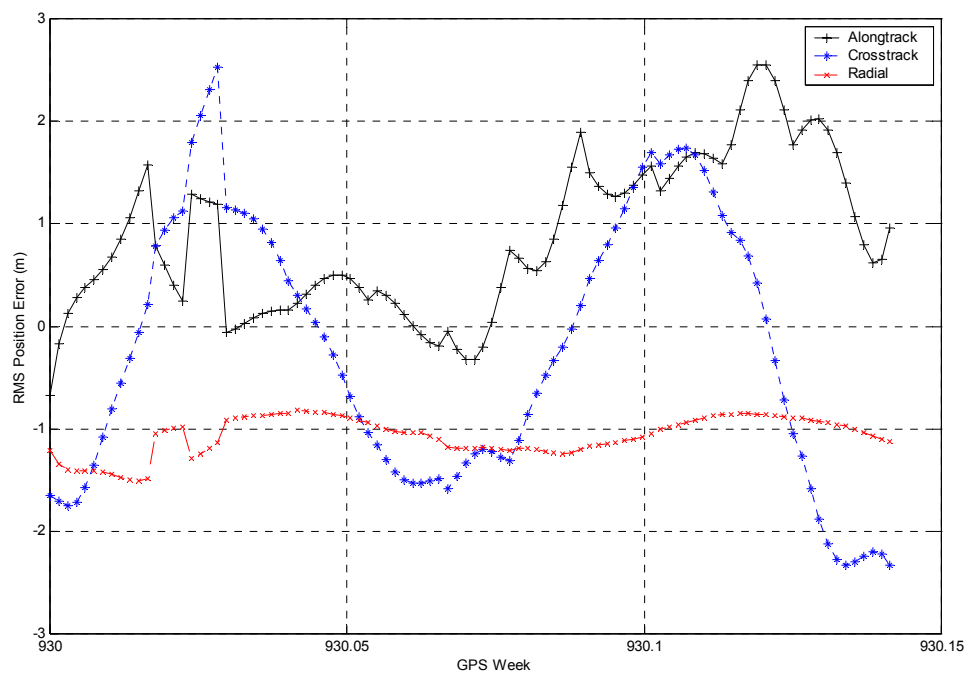
PRN 24 – SVN 24 (Block II)



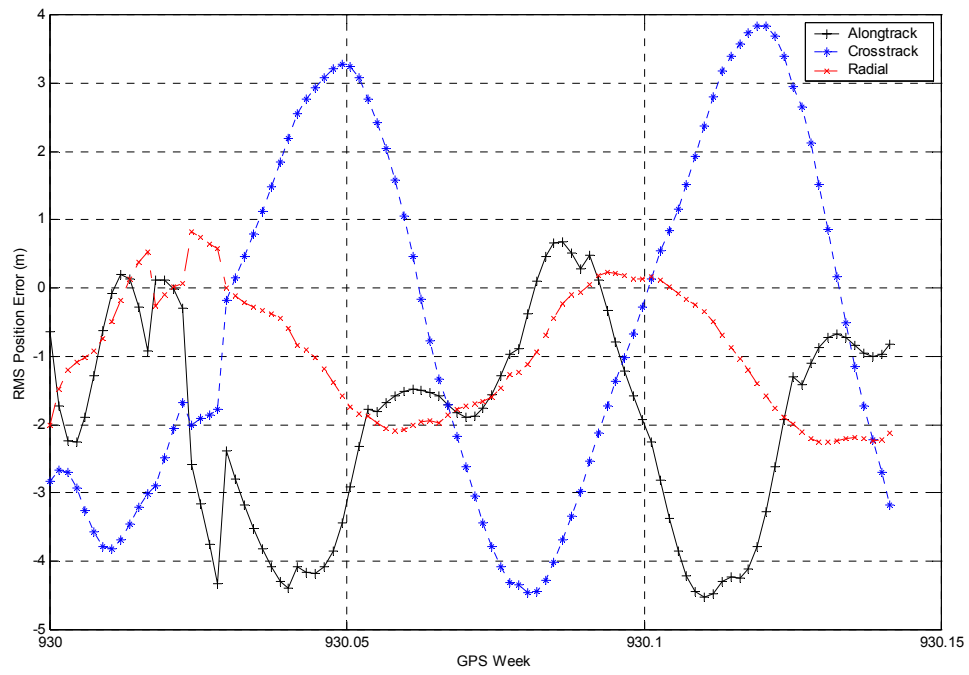
PRN 25 – SVN 25 (Block II)



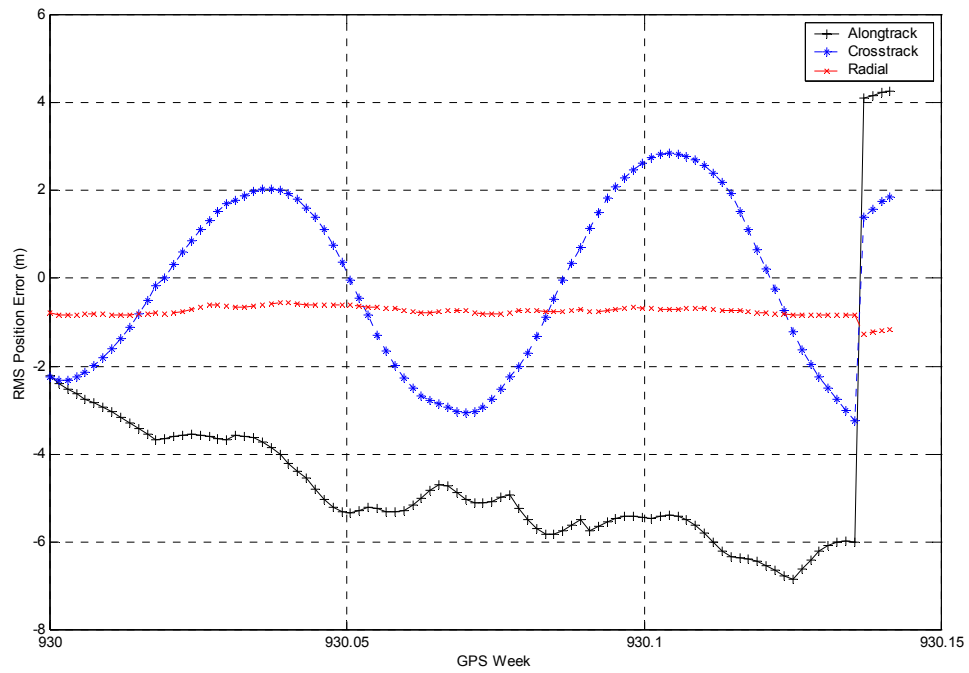
PRN 26 – SVN 26 (Block II)



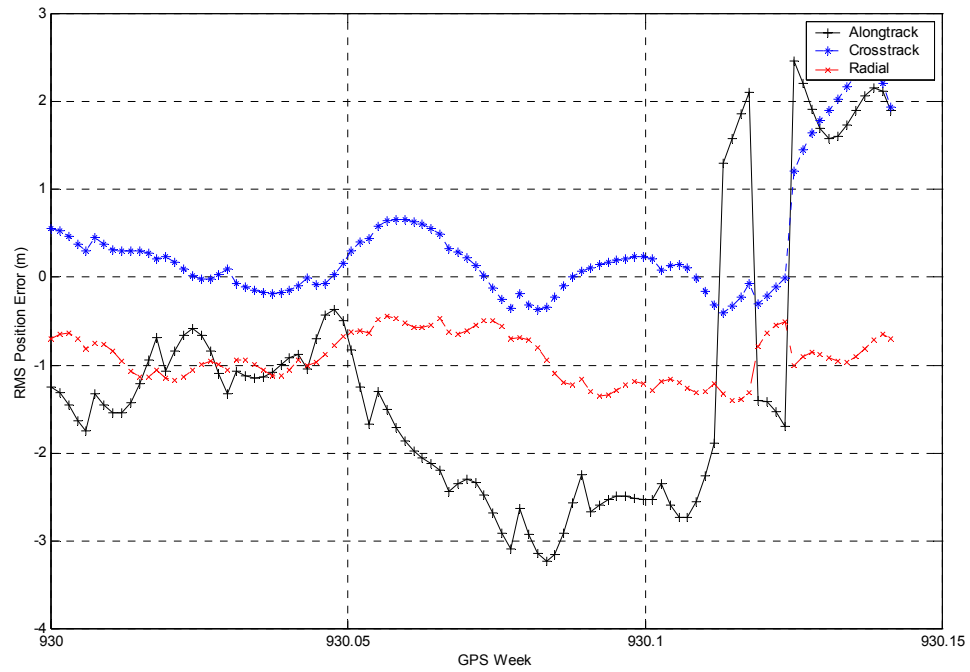
PRN 27 – SVN 27 (Block II)



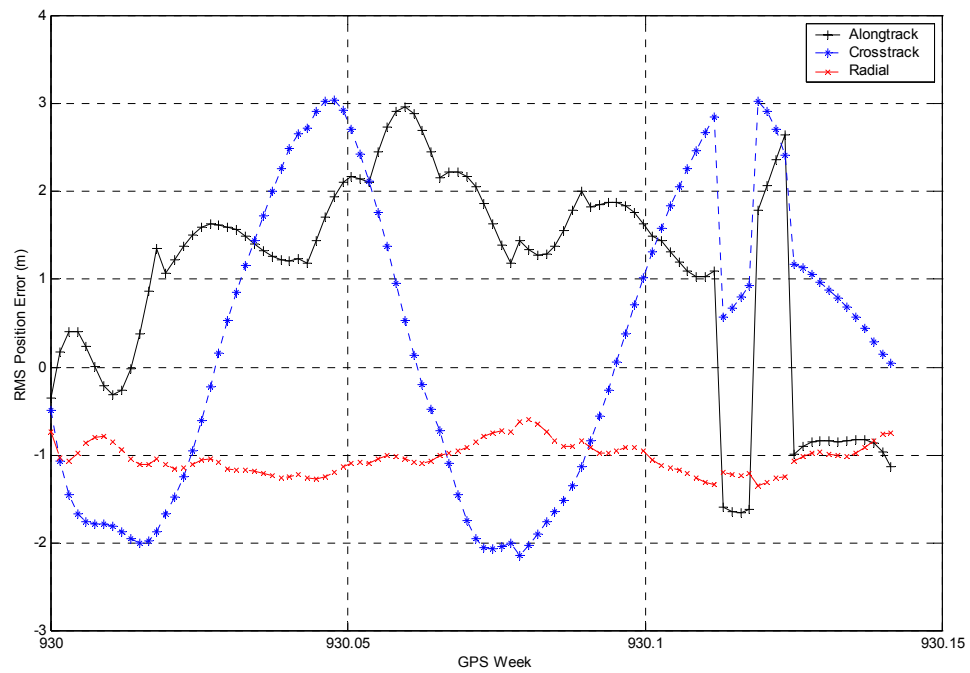
PRN 29 – SVN 29 (Block II)



PRN 30 – SVN 30 (Block II)

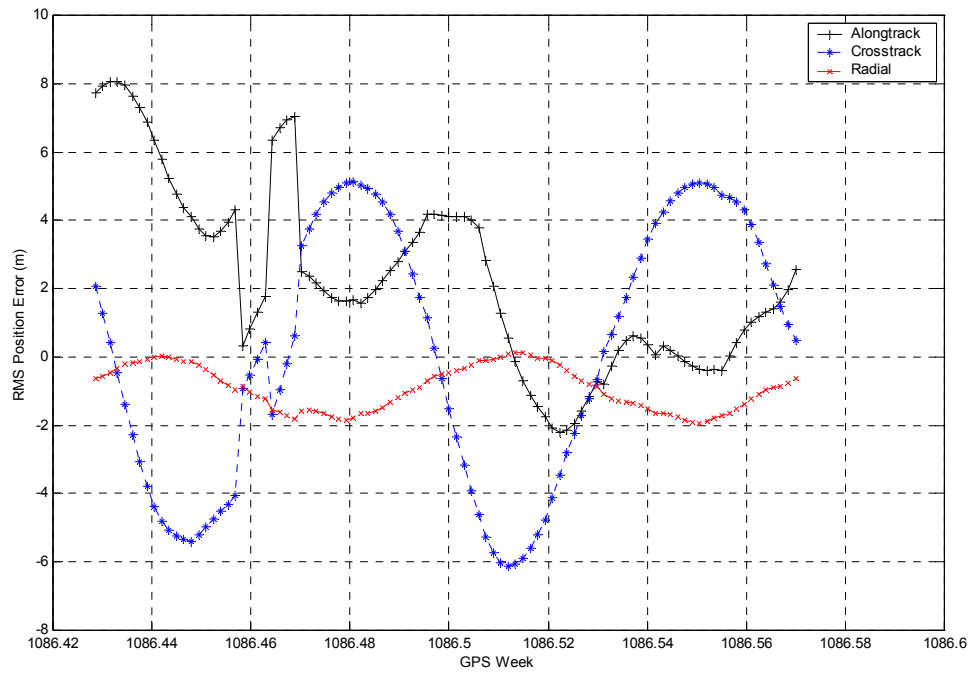


PRN 31 – SVN 31 (Block II)

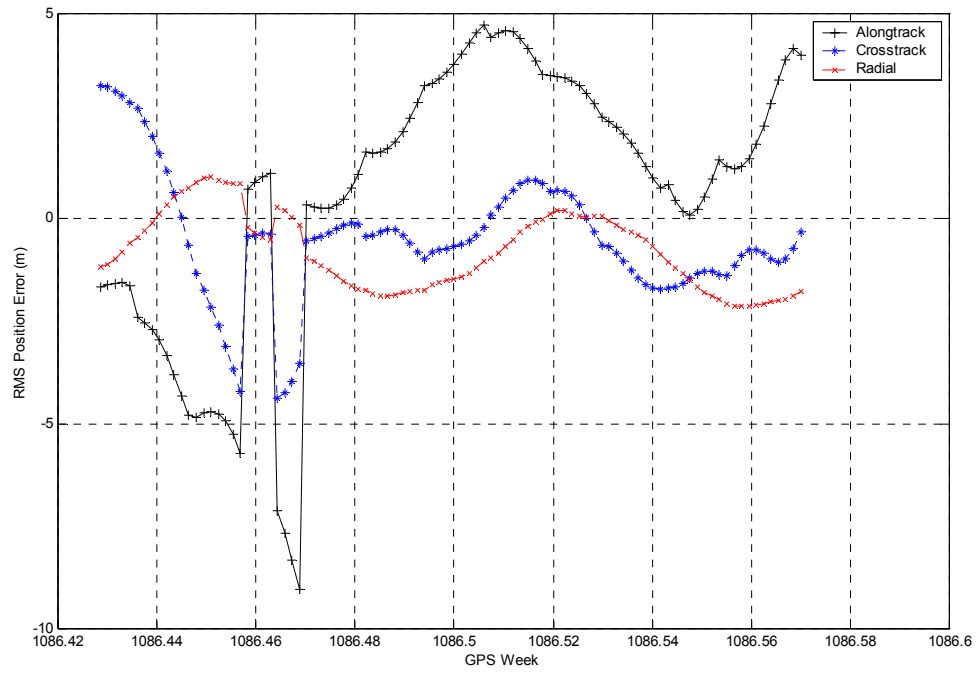


1 Nov 2000

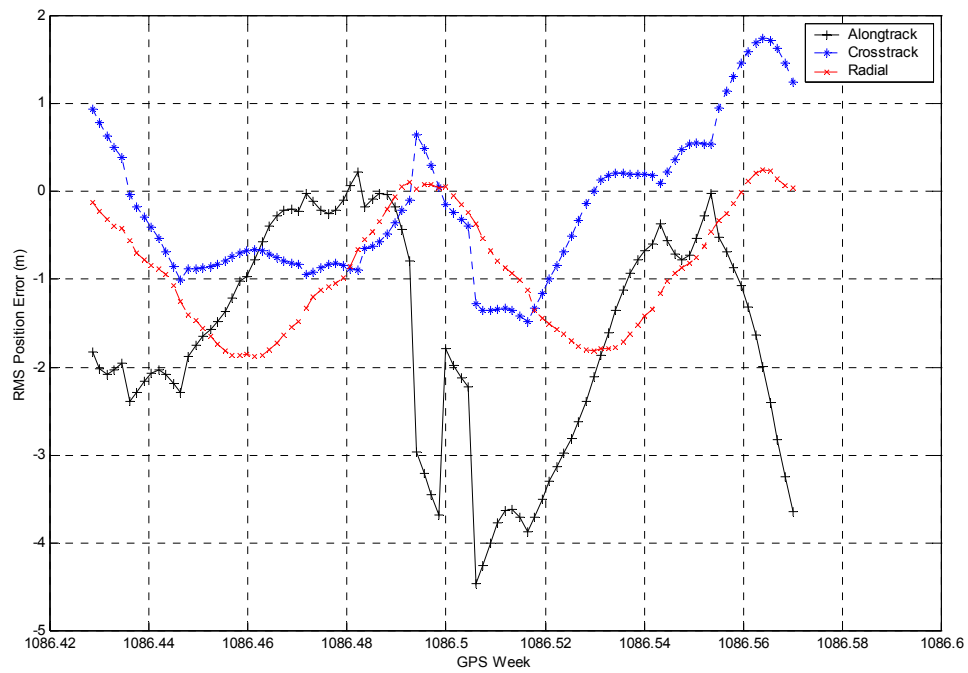
PRN 1 – SVN 32 (Block II)



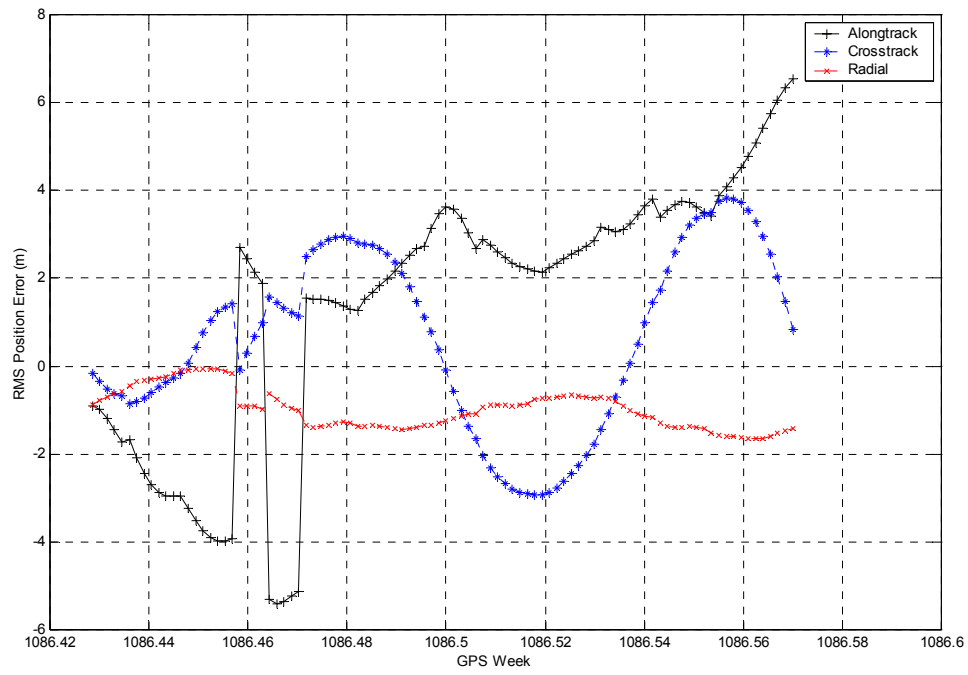
PRN 2 – SVN 13 (Block II)



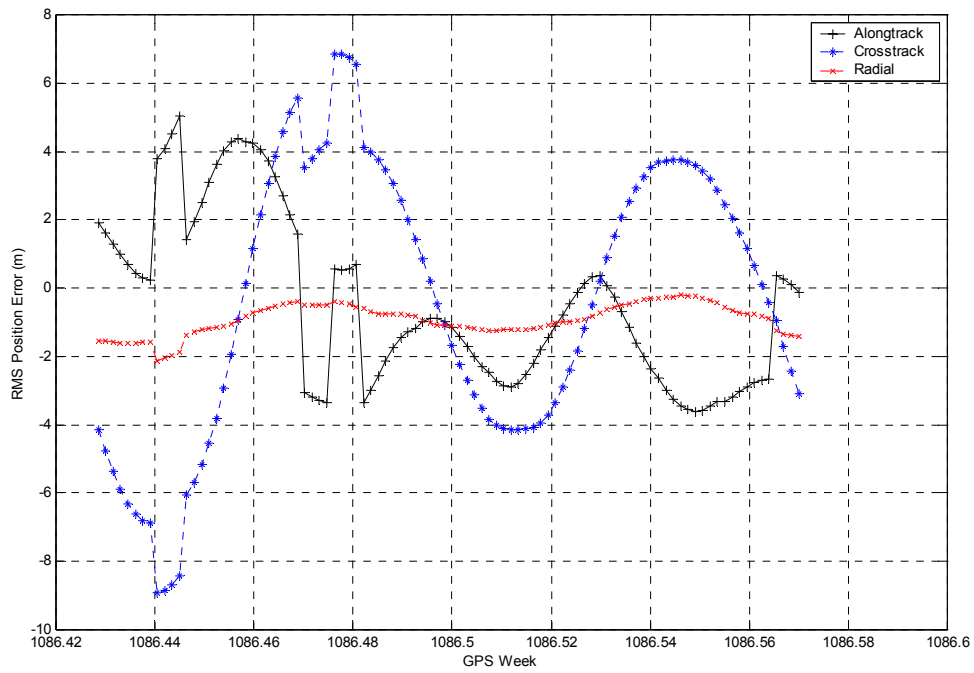
PRN 3 – SVN 33 (Block II)



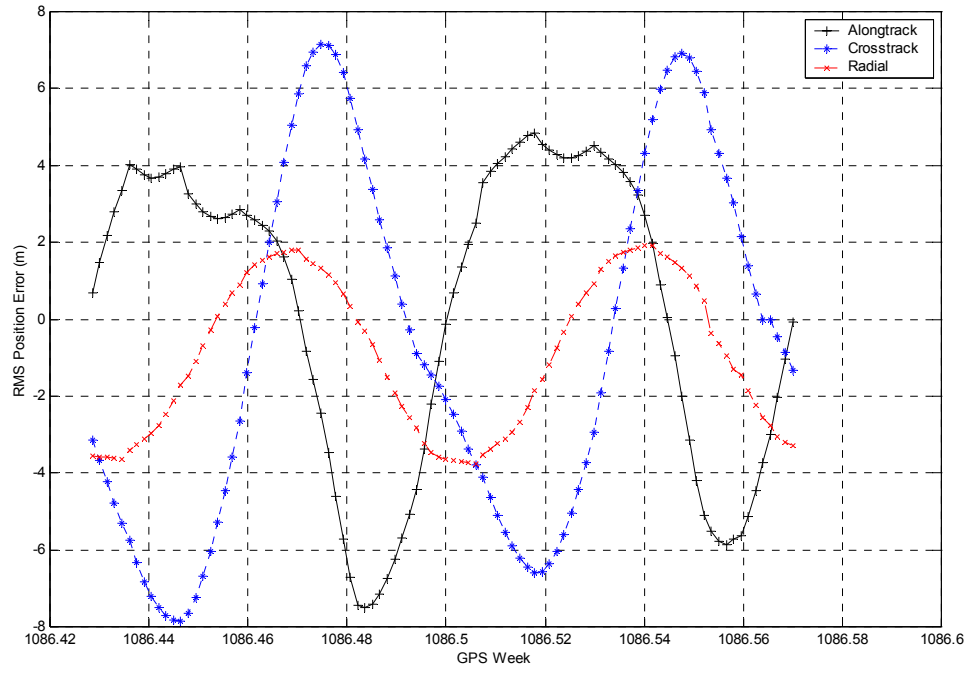
PRN 4 – SVN 34 (Block II)



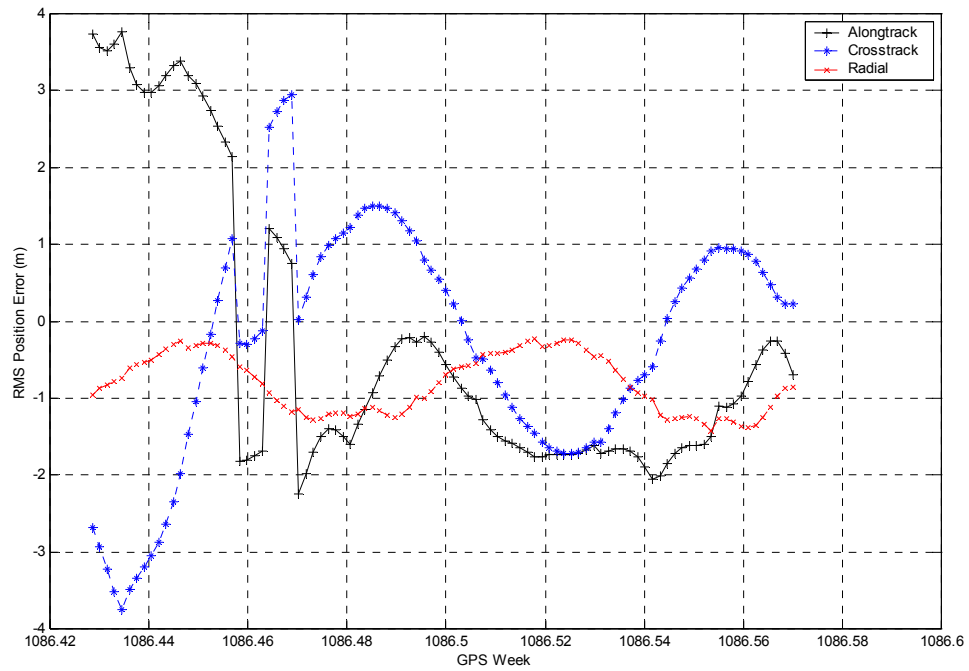
PRN 5 – SVN 35 (Block II)



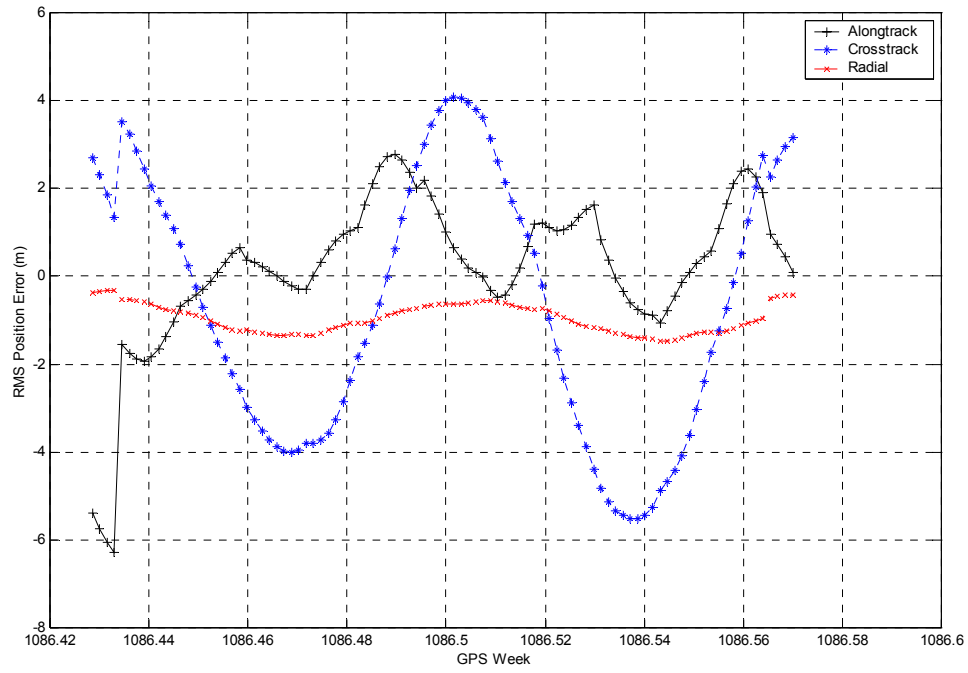
PRN 6 – SVN 36 (Block II)



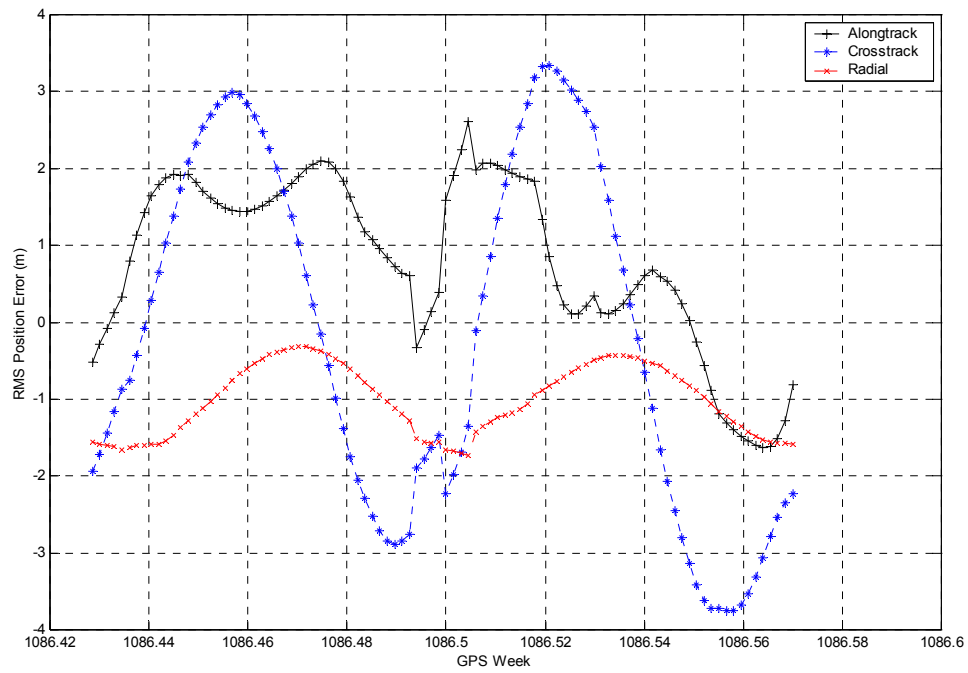
PRN 7 – SVN 37 (Block II)



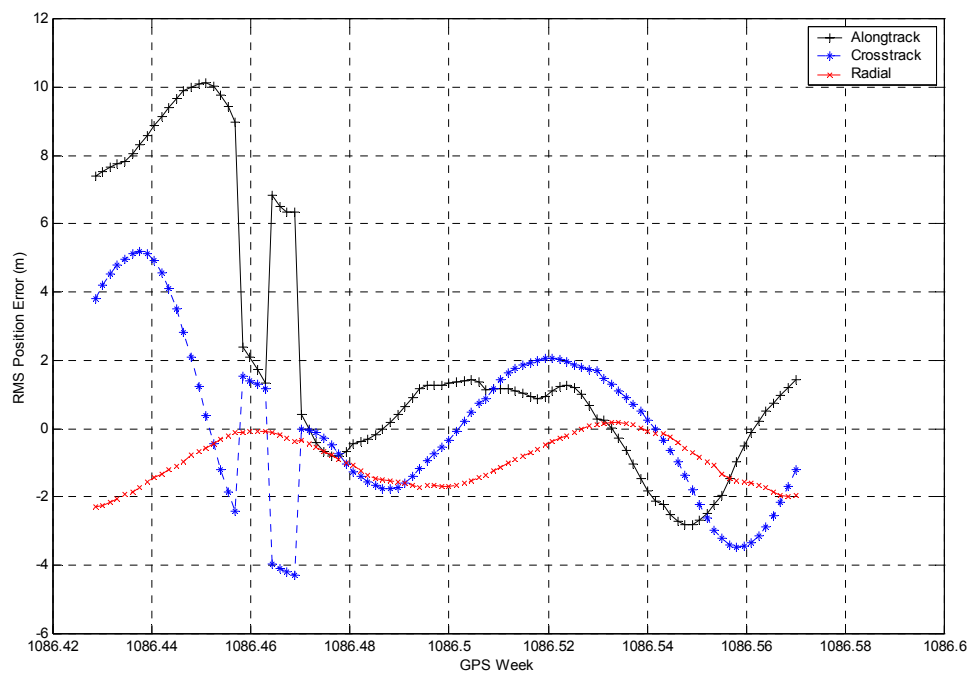
PRN 8 – SVN 38 (Block II)



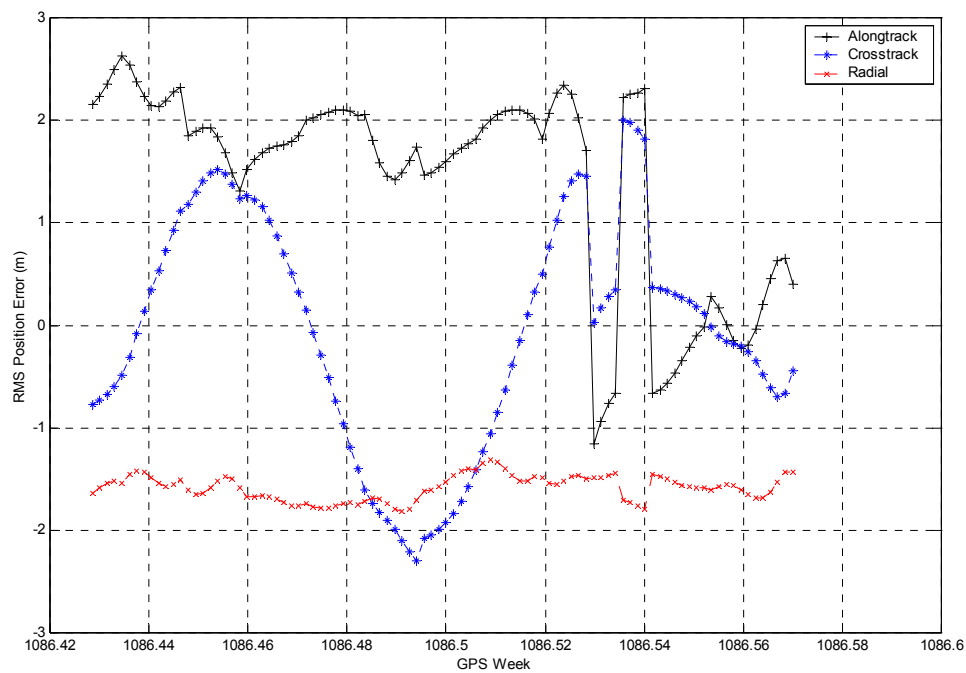
PRN 9 – SVN 39 (Block II)



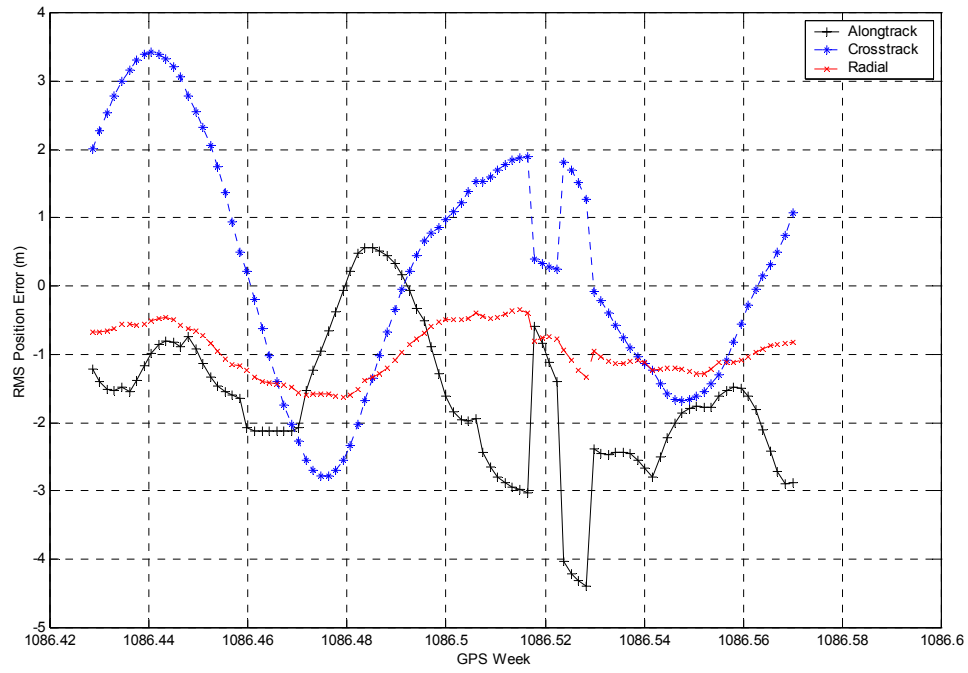
PRN 10 – SVN 40 (Block II)



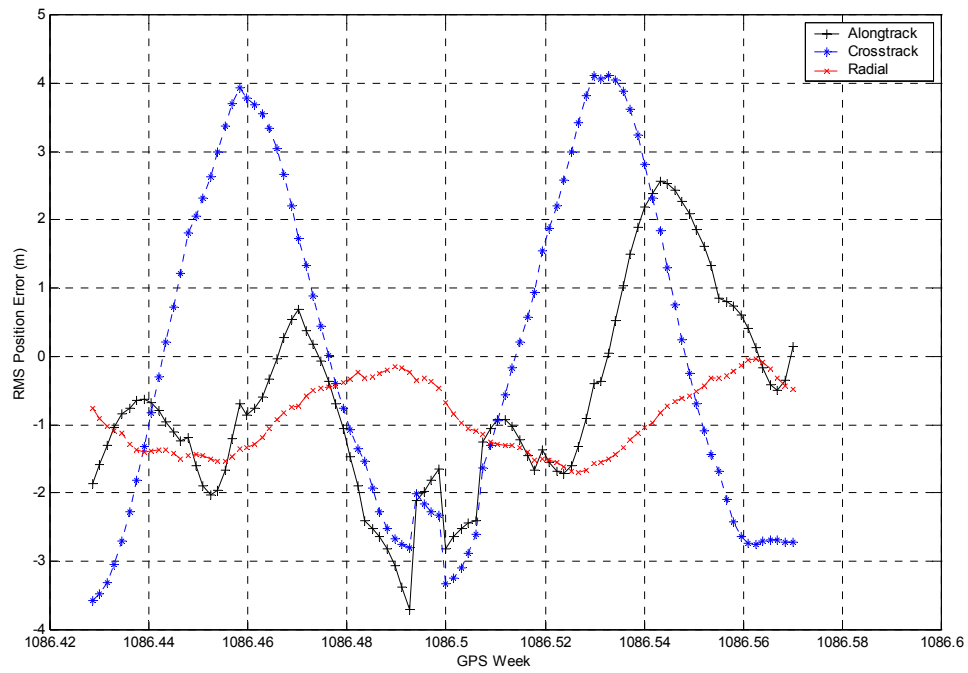
PRN 11 – SVN 46 (Block II-R)



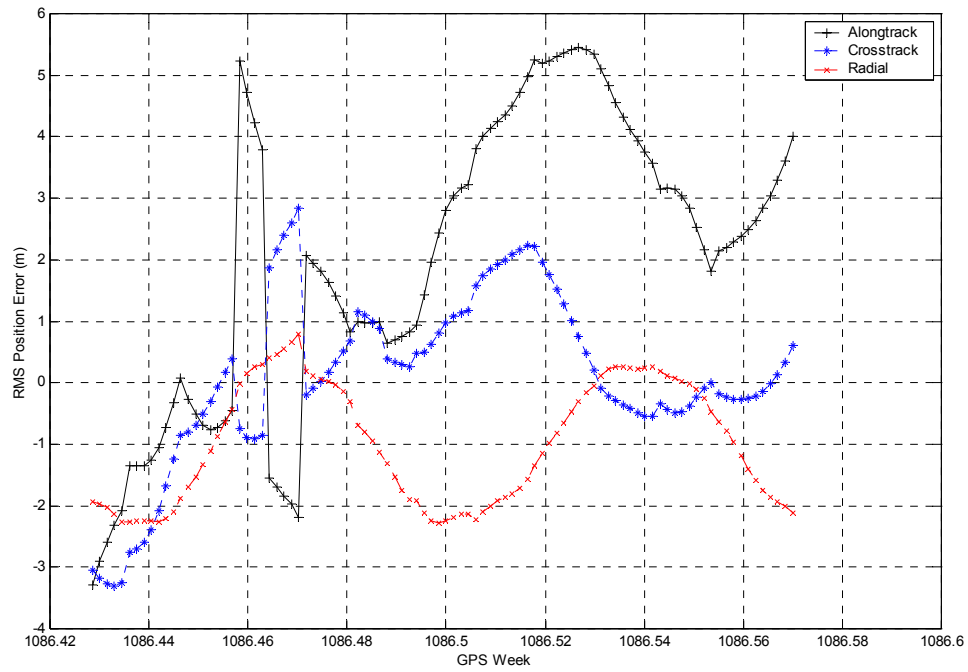
PRN 13 – SVN 43 (Block II-R)



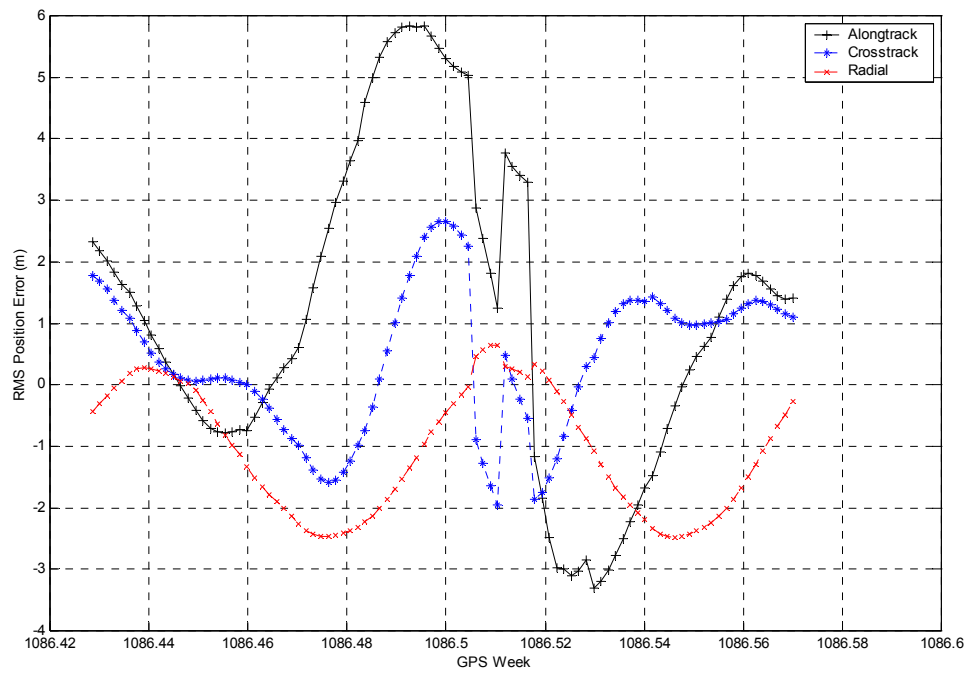
PRN 15 – SVN 15 (Block II)



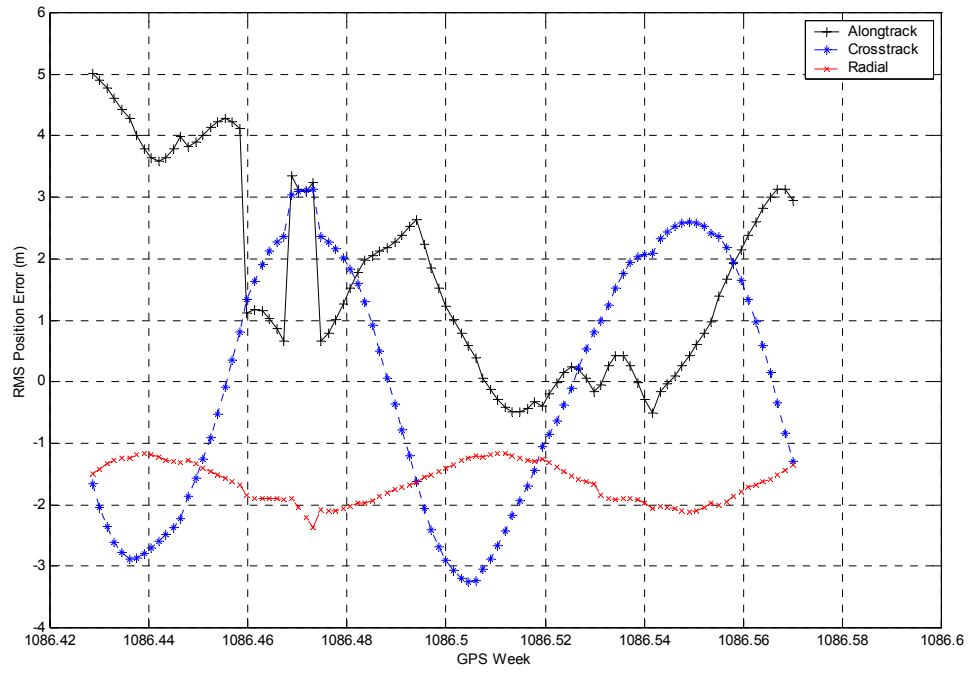
PRN 17 – SVN 17 (Block II)



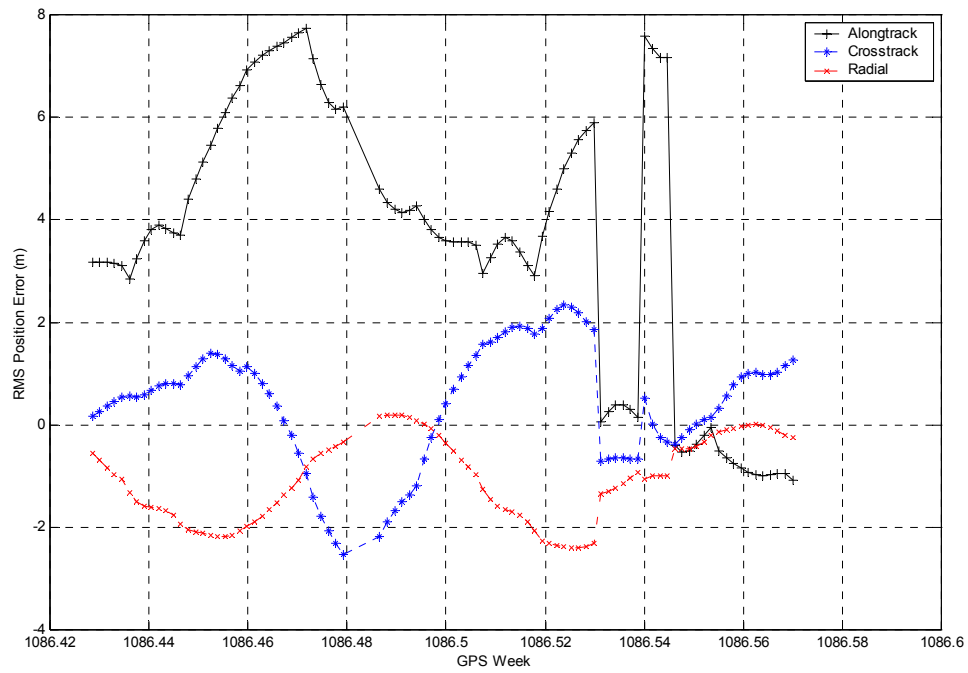
PRN 19 – SVN 19 (Block II)



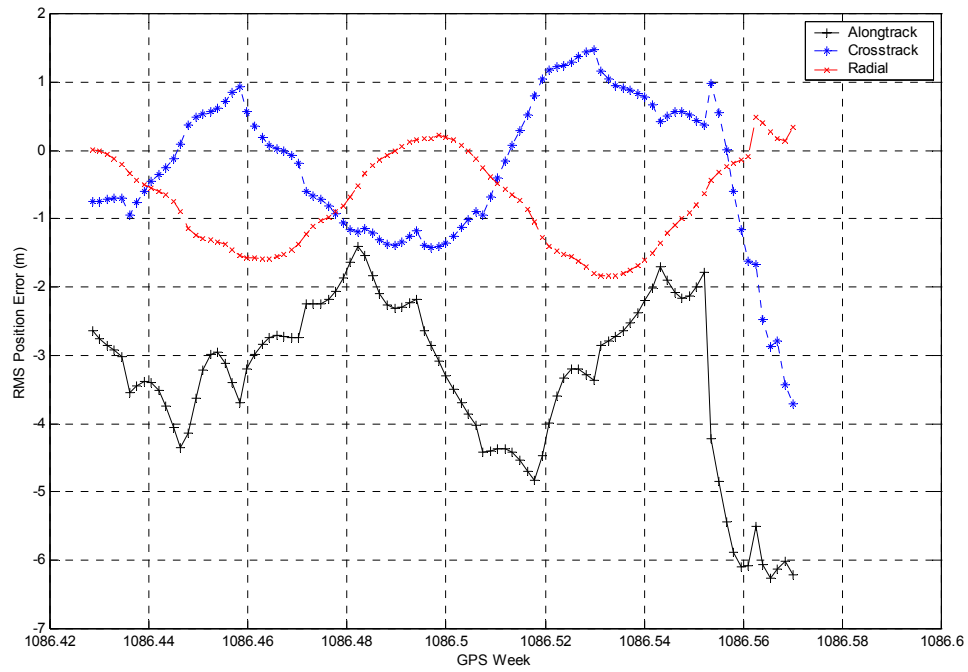
PRN 20 – SVN 51 (Block II-R)



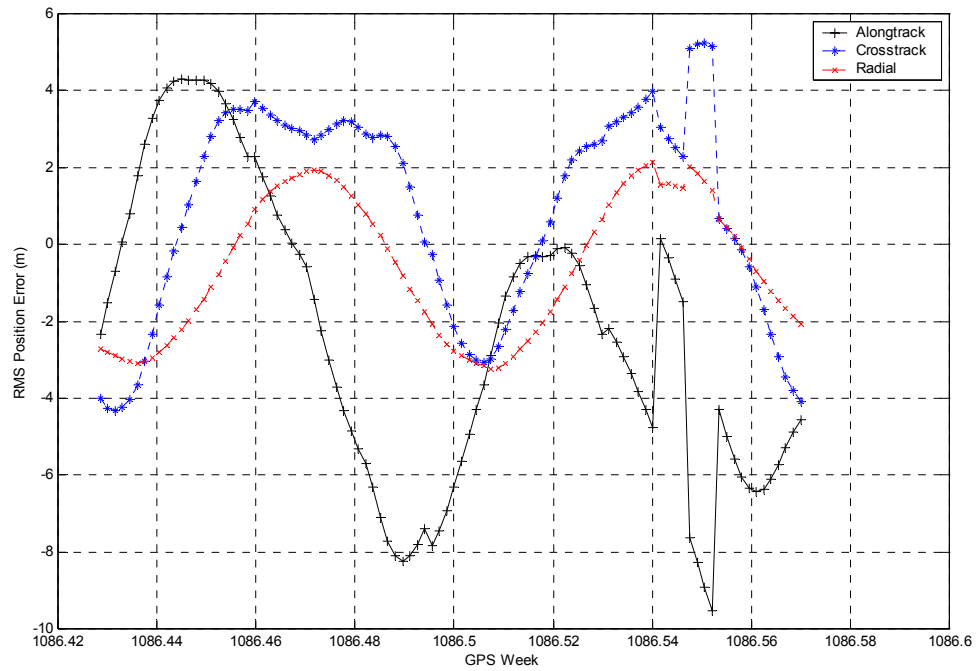
PRN 21 – SVN 21 (Block II)



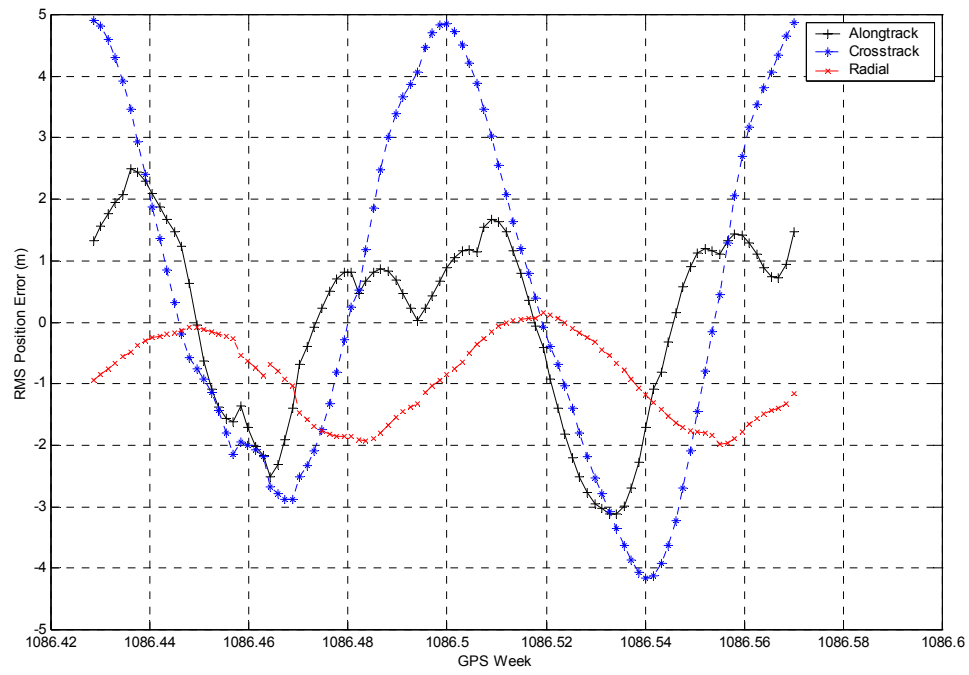
PRN 22 – SVN 22 (Block II)



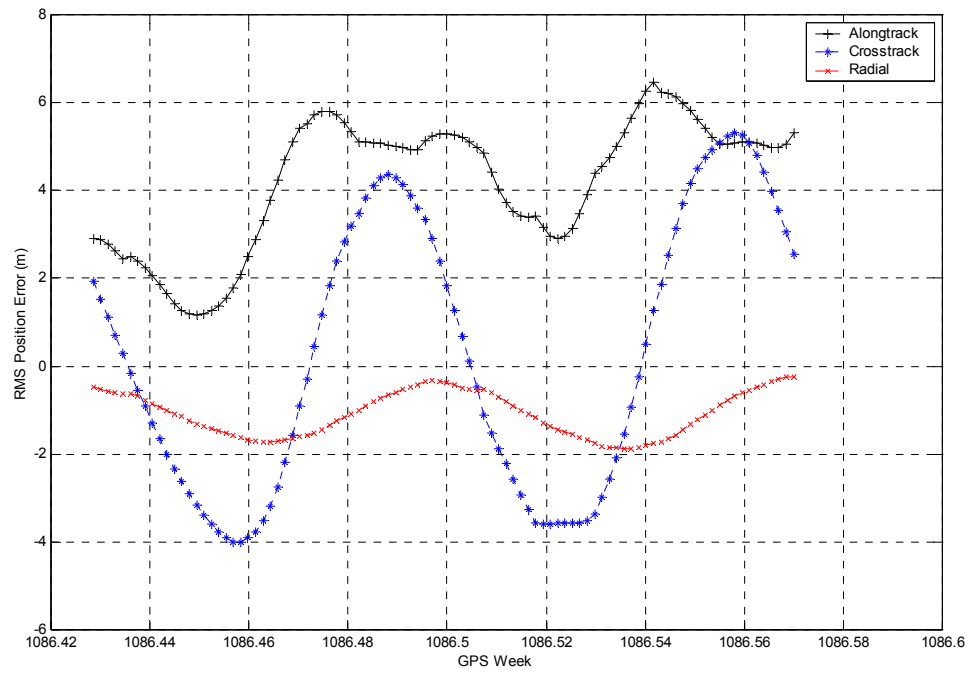
PRN 23 – SVN 23 (Block II)



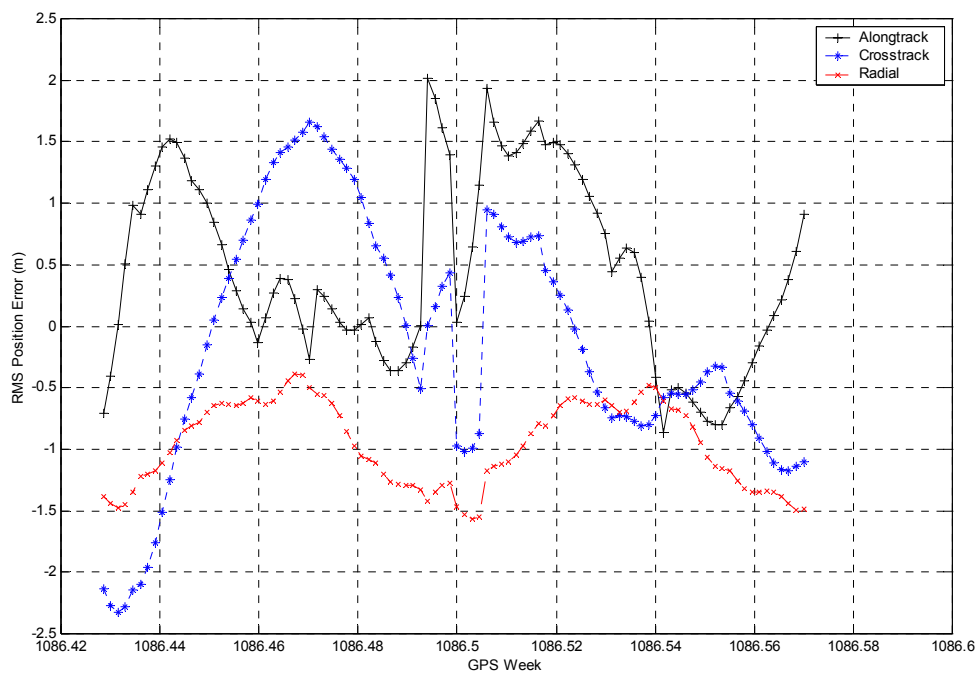
PRN 24 – SVN 24 (Block II)



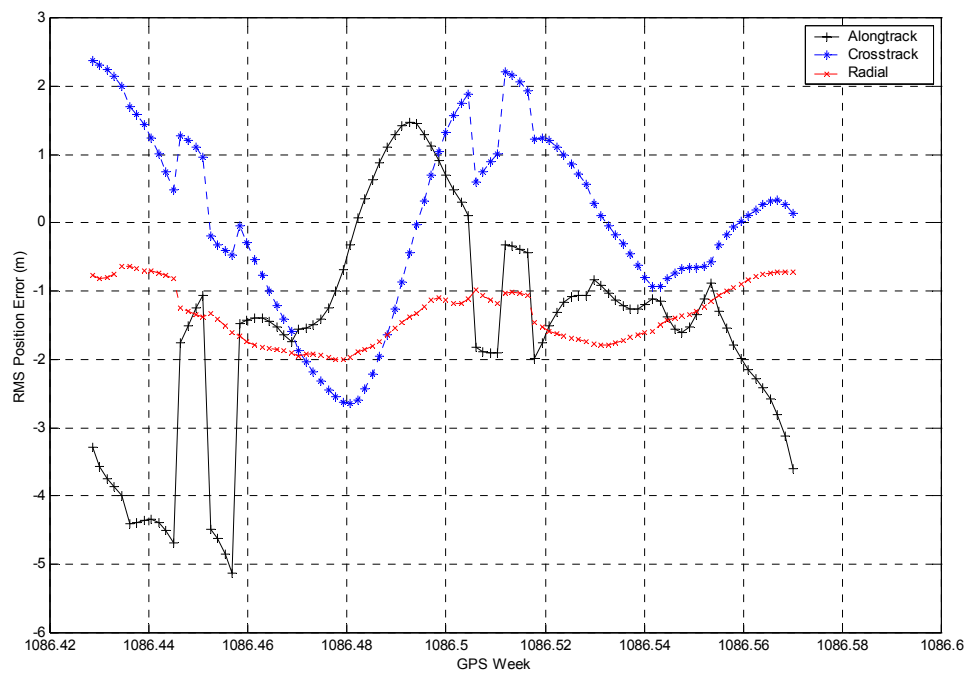
PRN 25 – SVN 25 (Block II)



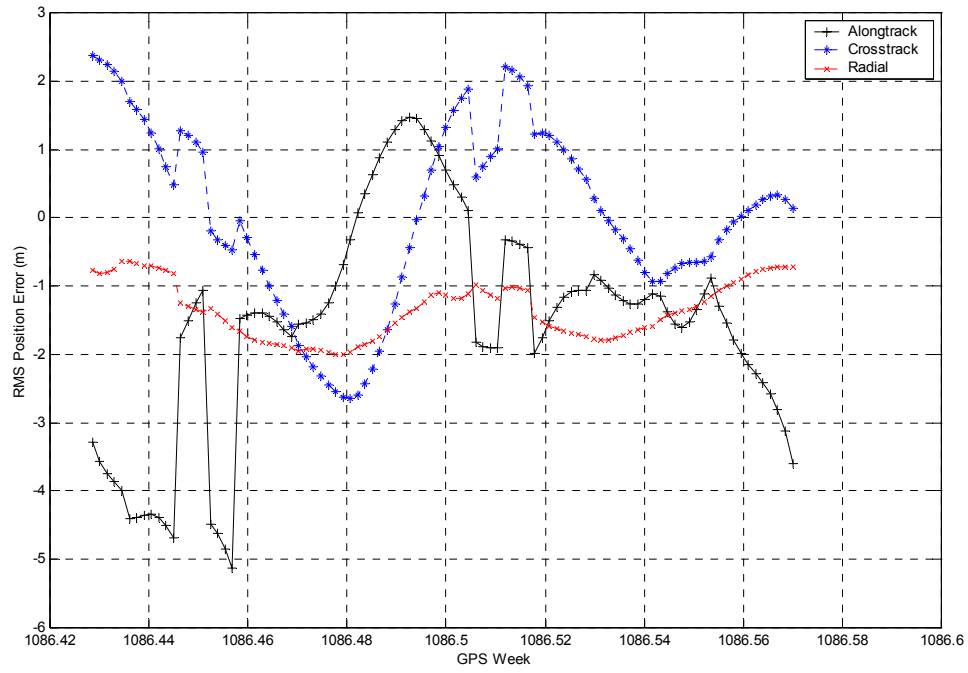
PRN 26 – SVN 26 (Block II)



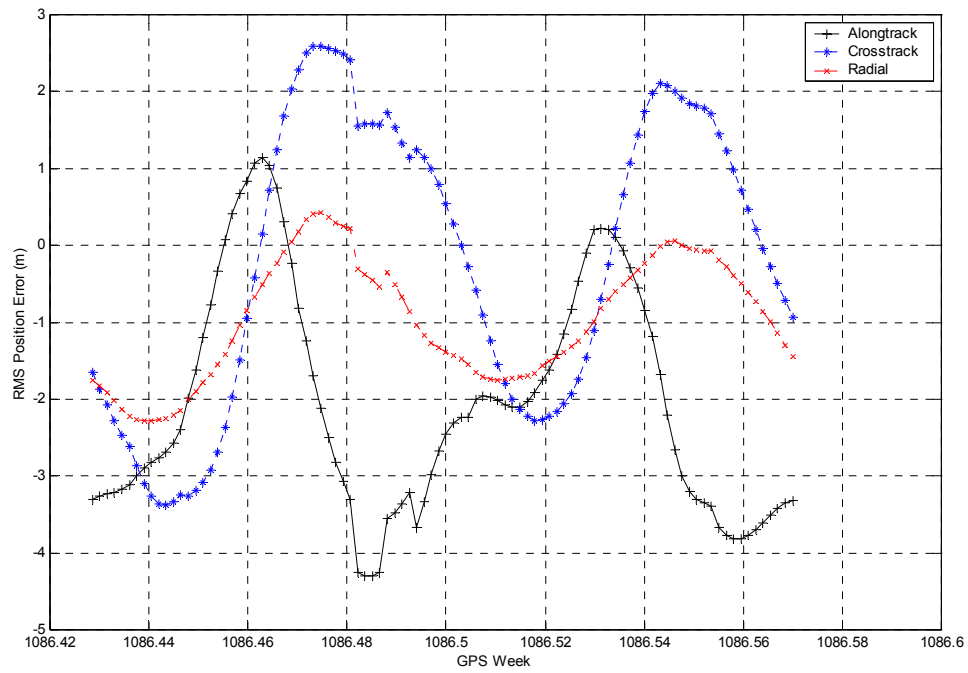
PRN 28 – SVN 44 (Block II-R)



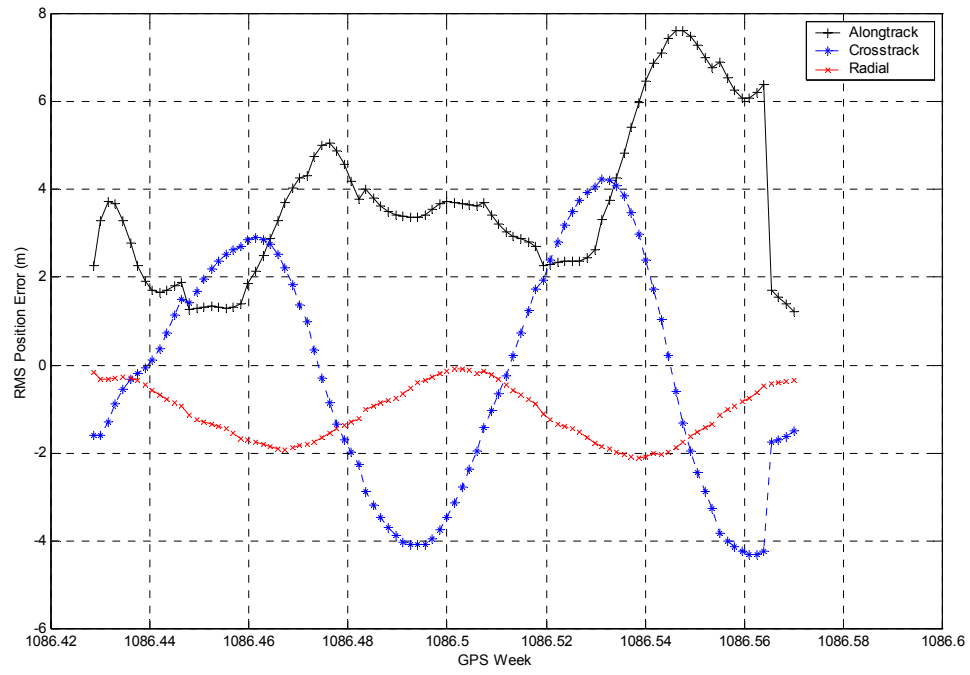
PRN 29 – SVN 29 (Block II)



PRN 30 – SVN 30 (Block II)

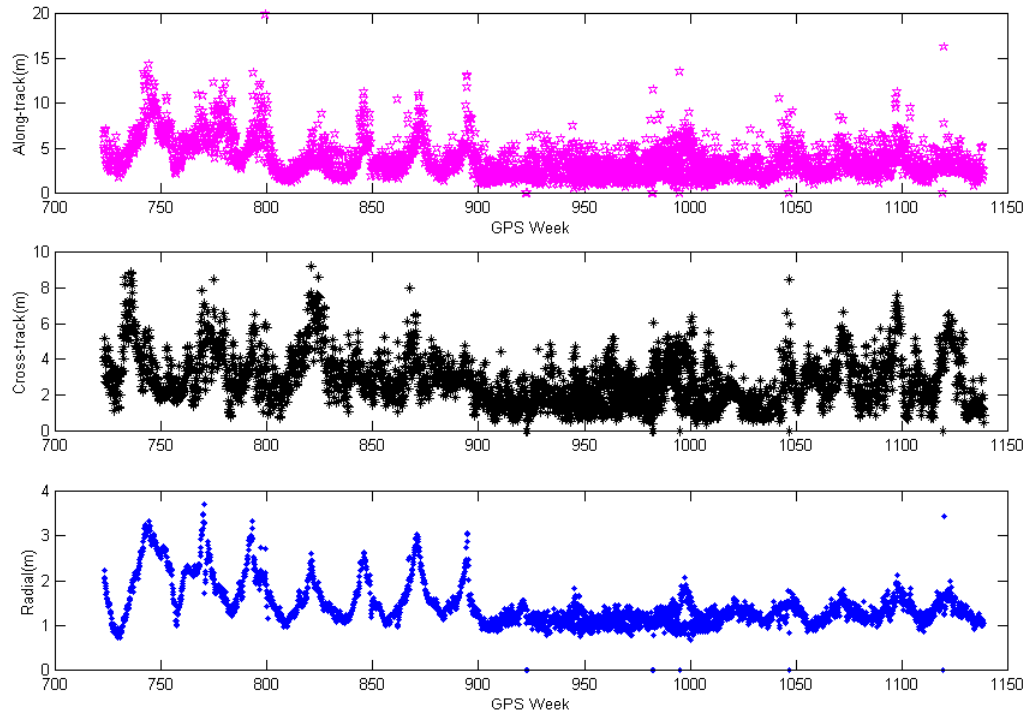


PRN 31 – SVN 31 (Block II)

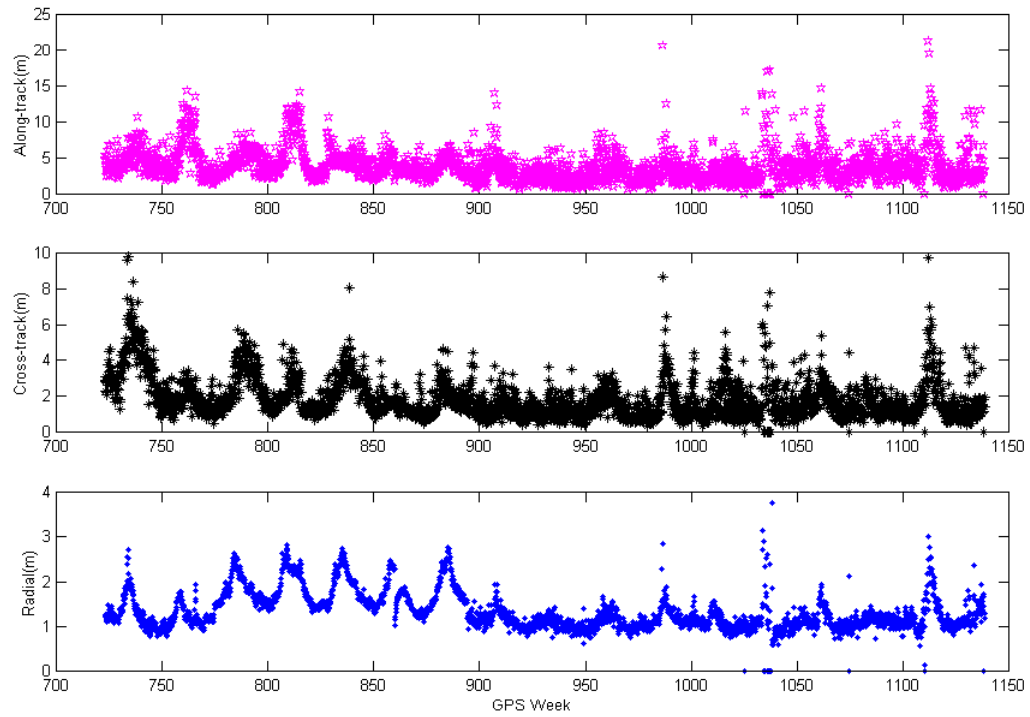


Appendix C: RMS ACR Broadcast Position Error

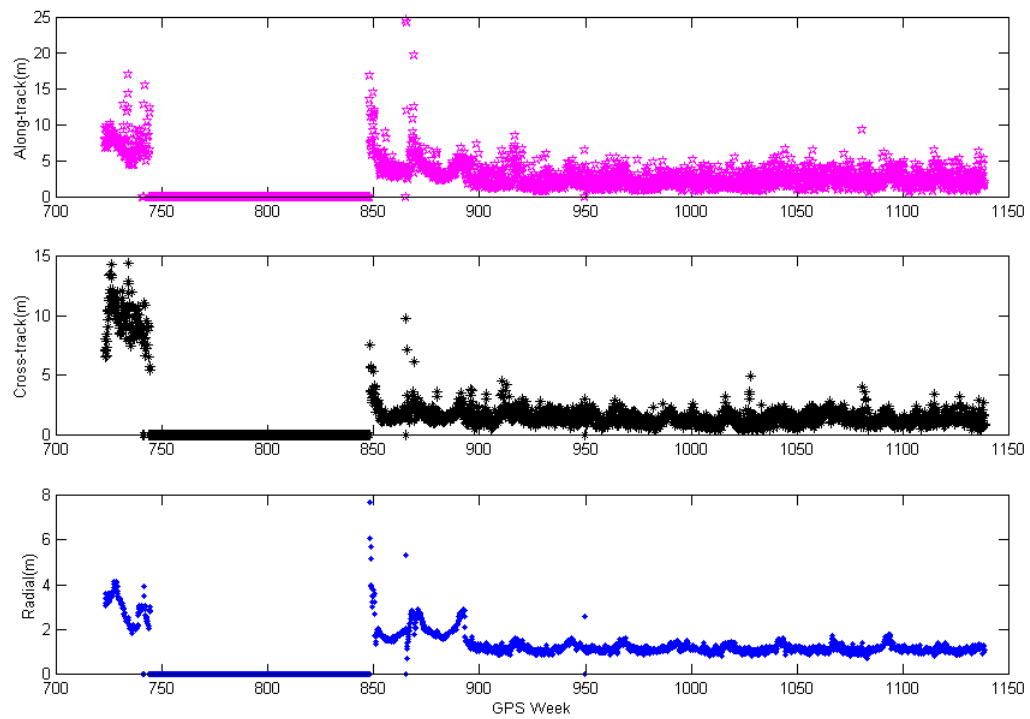
PRN 1 – SVN 32 (Block II)



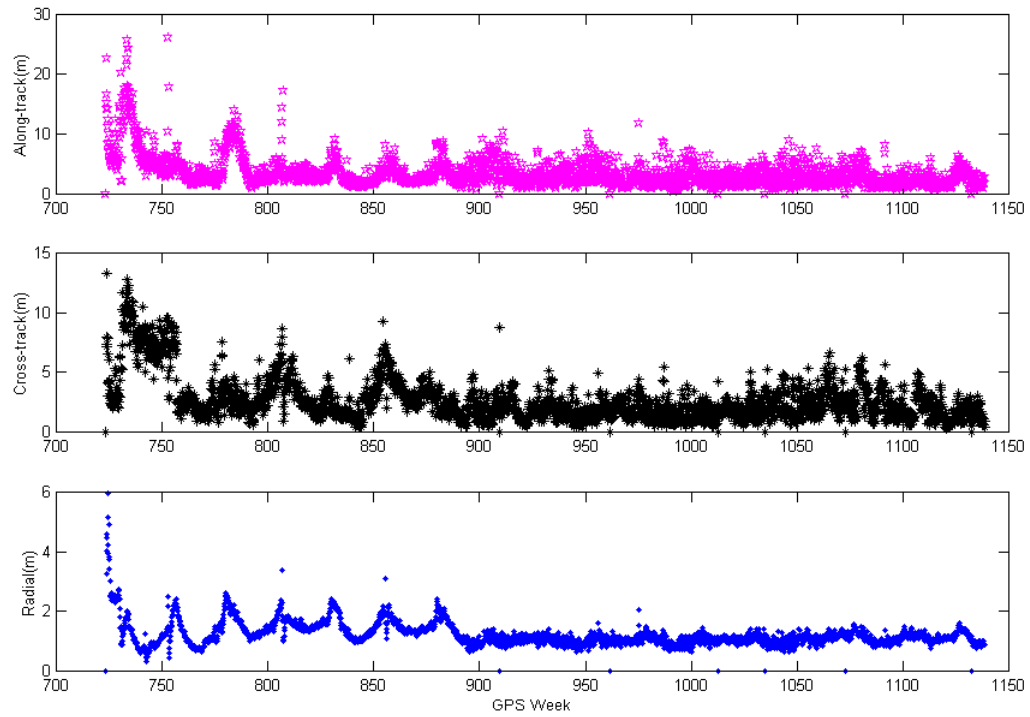
PRN 2 – SVN 13 (Block II)



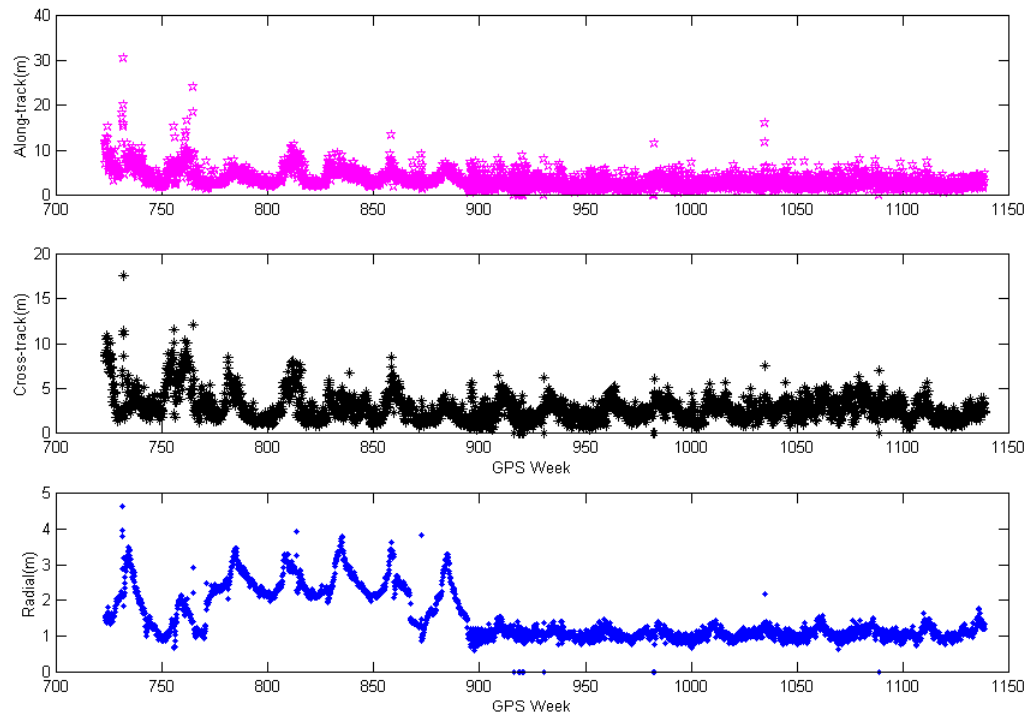
PRN 3 – Prior to week 740 - SVN 11 (Block I). After week 850 – SVN 33 (Block II)



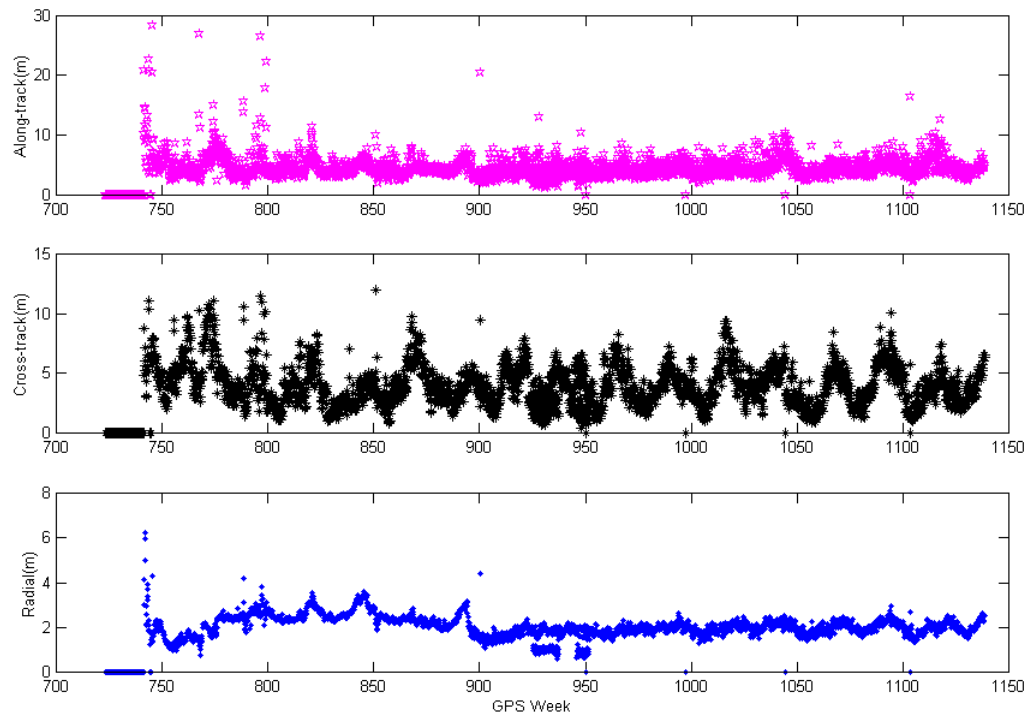
PRN 4 – SVN 34 (Block II)



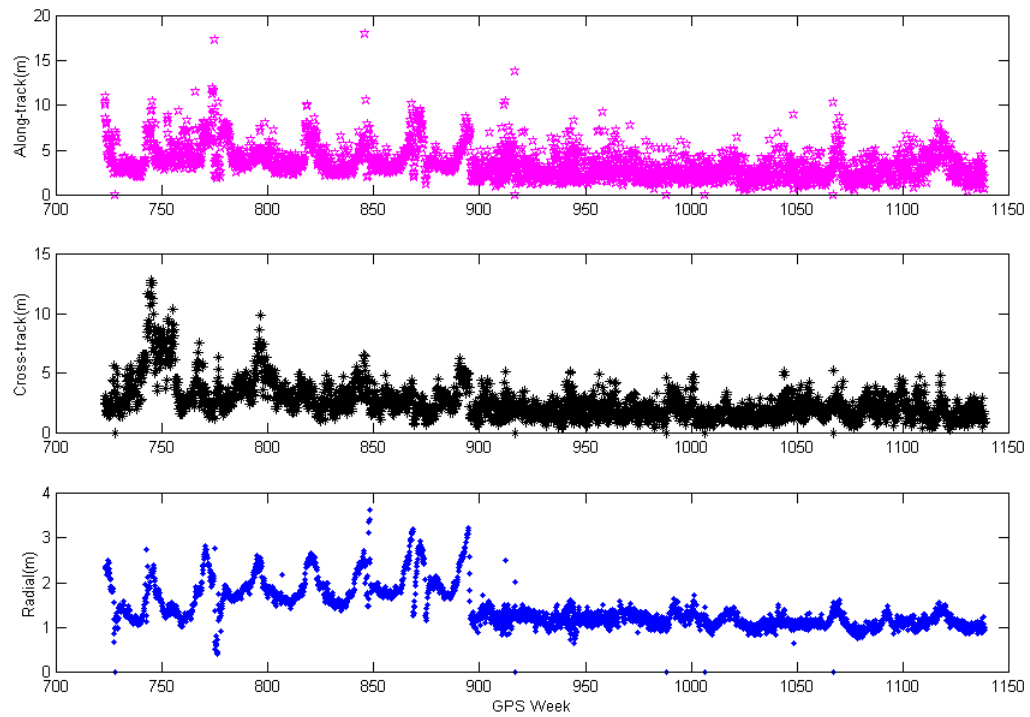
PRN 5 – SVN 35 (Block II)



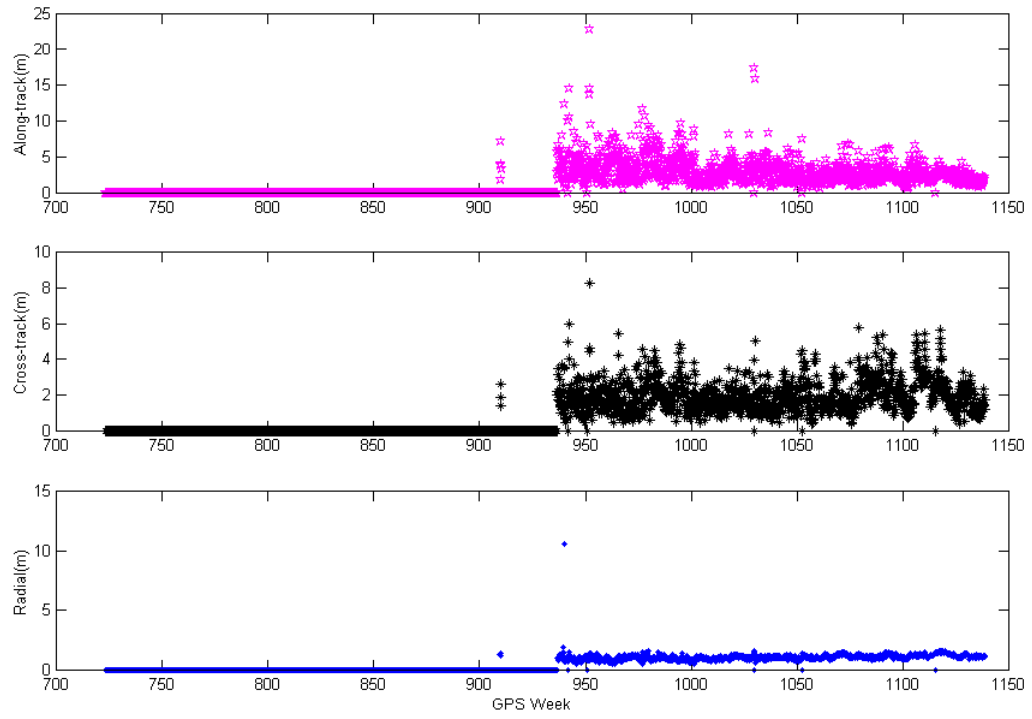
PRN 6 – SVN 36 (Block II)



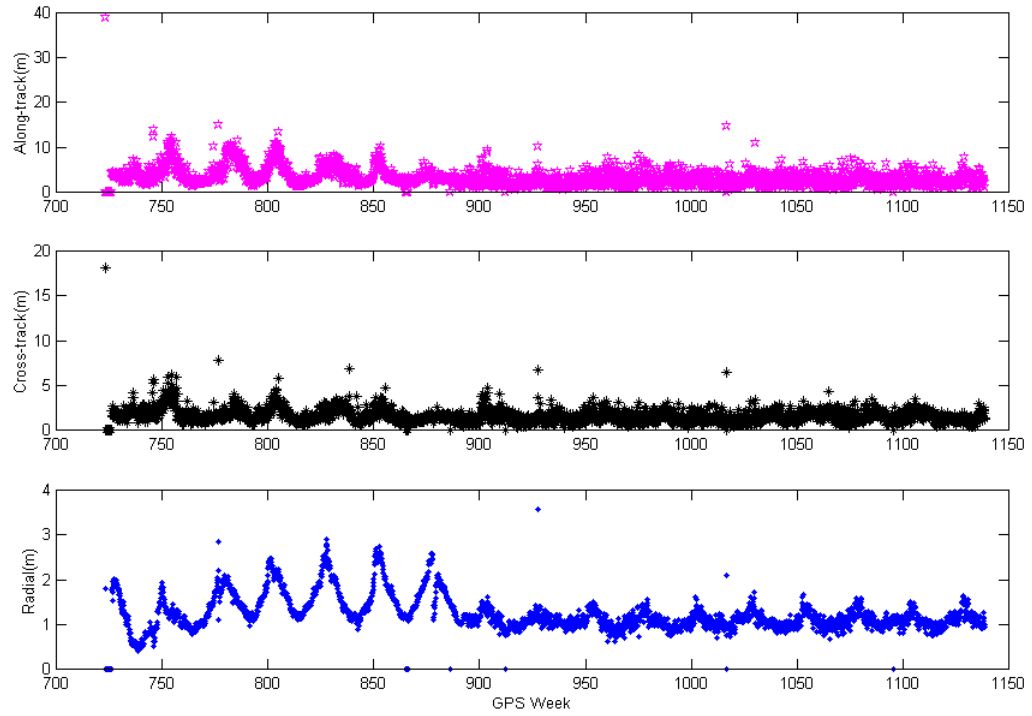
PRN 7 – SVN 37 (Block II)



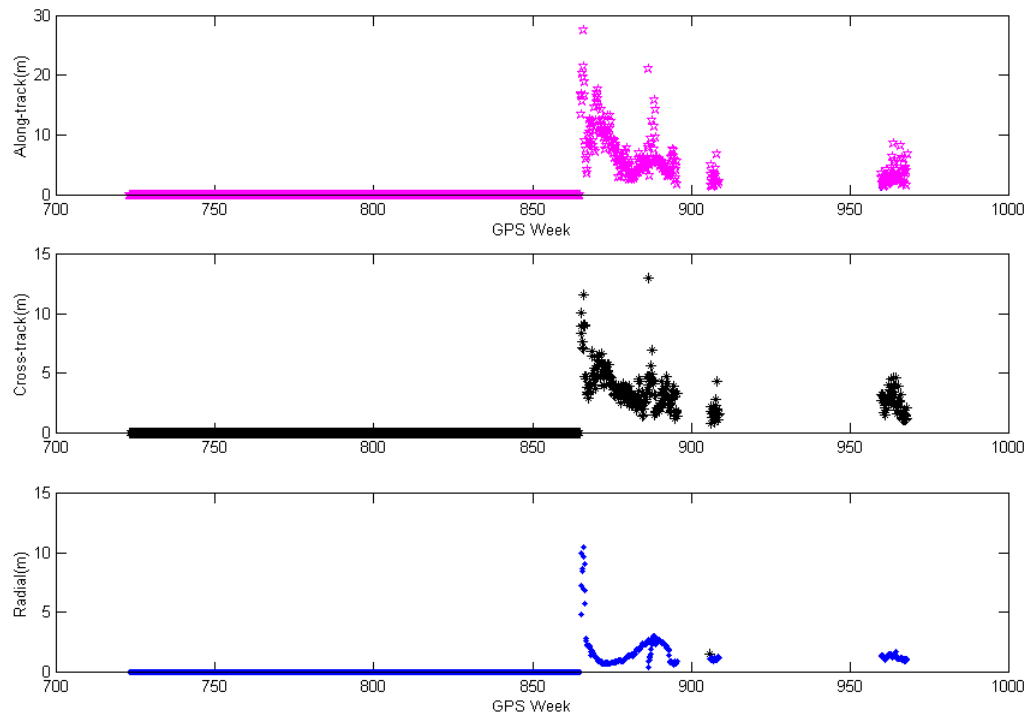
PRN 8 – SVN 38 (Block II)



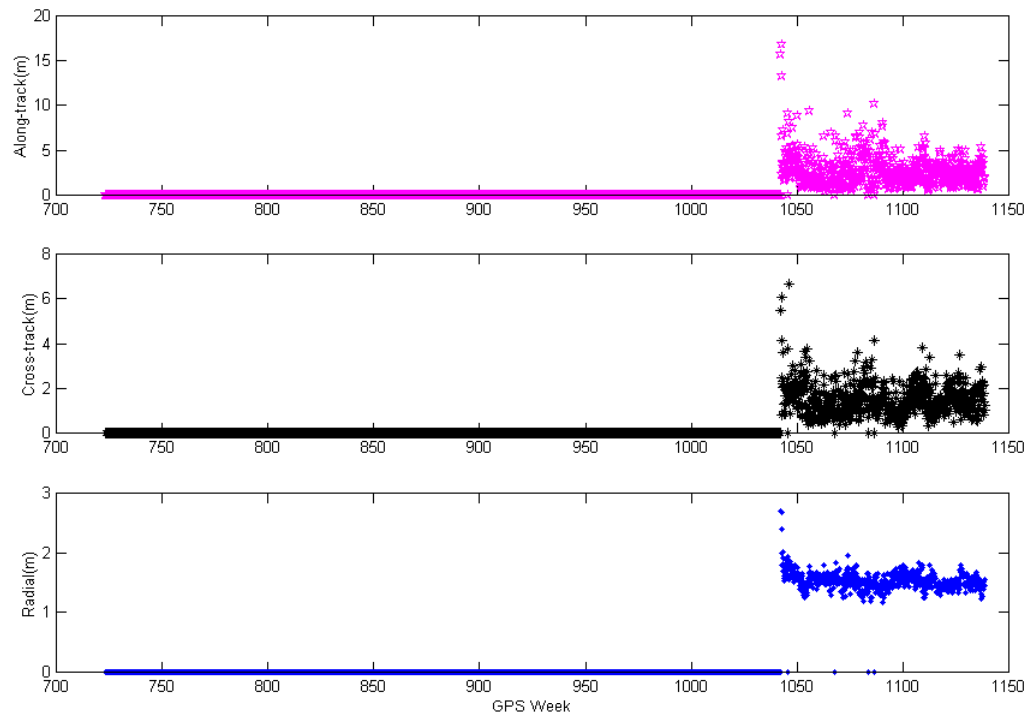
PRN 9 – SVN 39 (Block II)



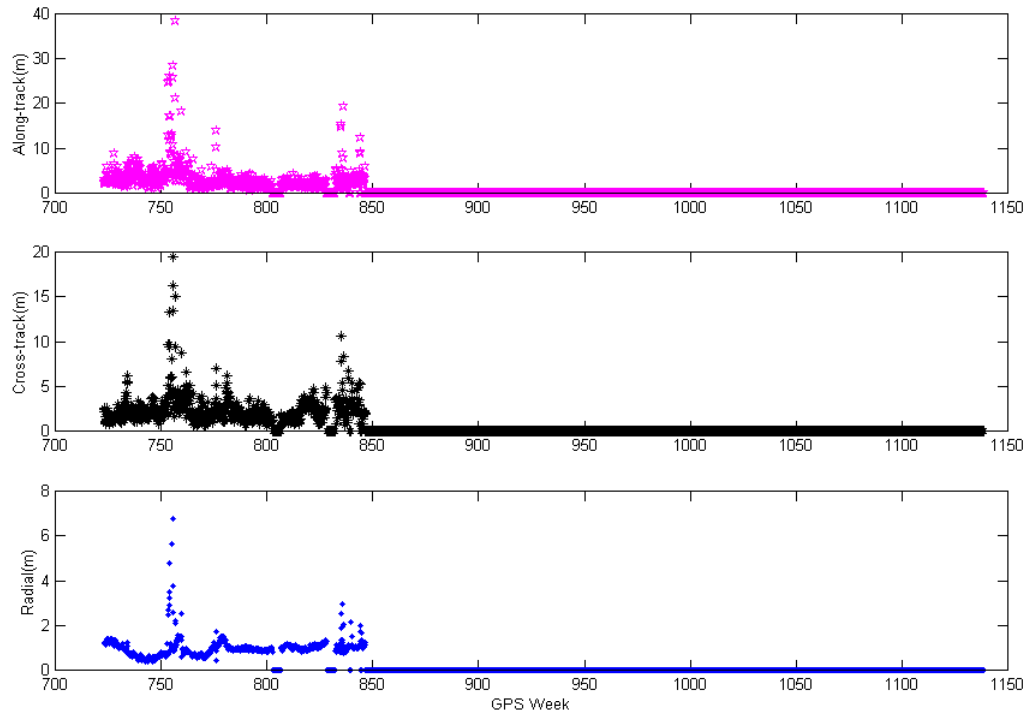
PRN 10 – SVN 40 (Block II)



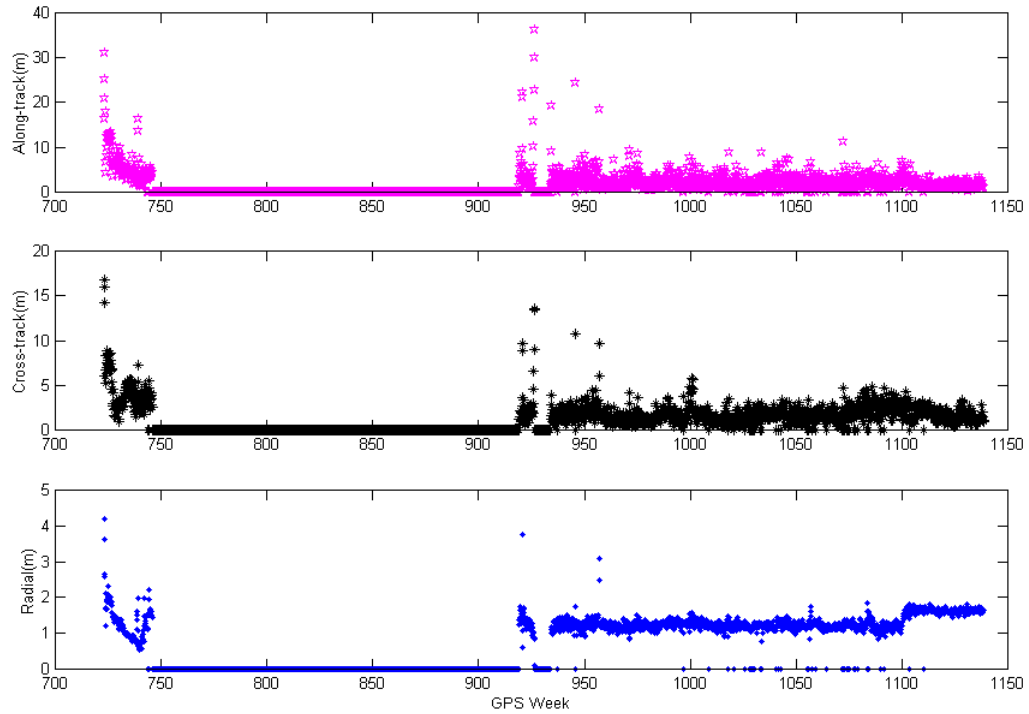
PRN 11 – SVN 46 (Block II-R)



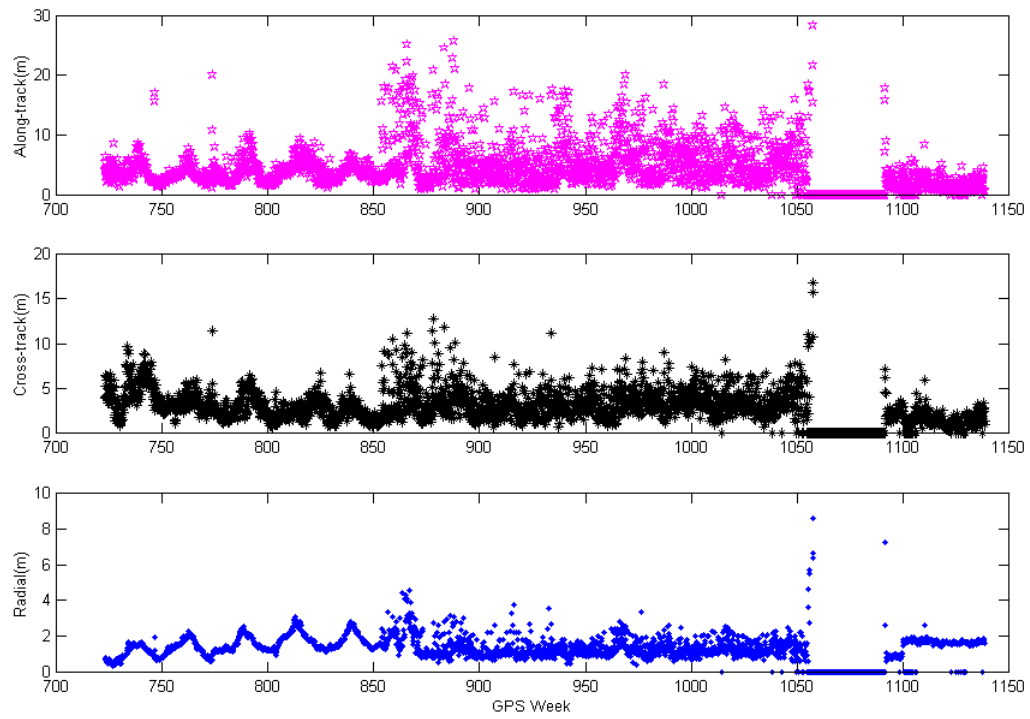
PRN 12 – SVN 10 (Block I)



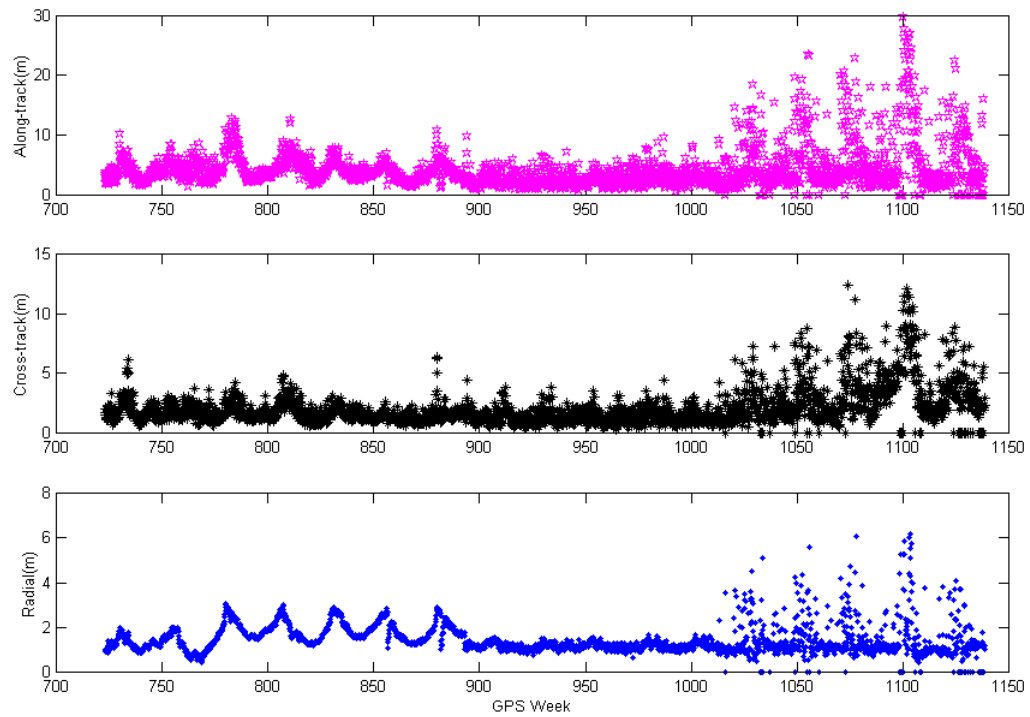
PRN 13 – Prior to week 750 – SVN 9 (Block I). After week 920 – SVN 43 (Block II-R)



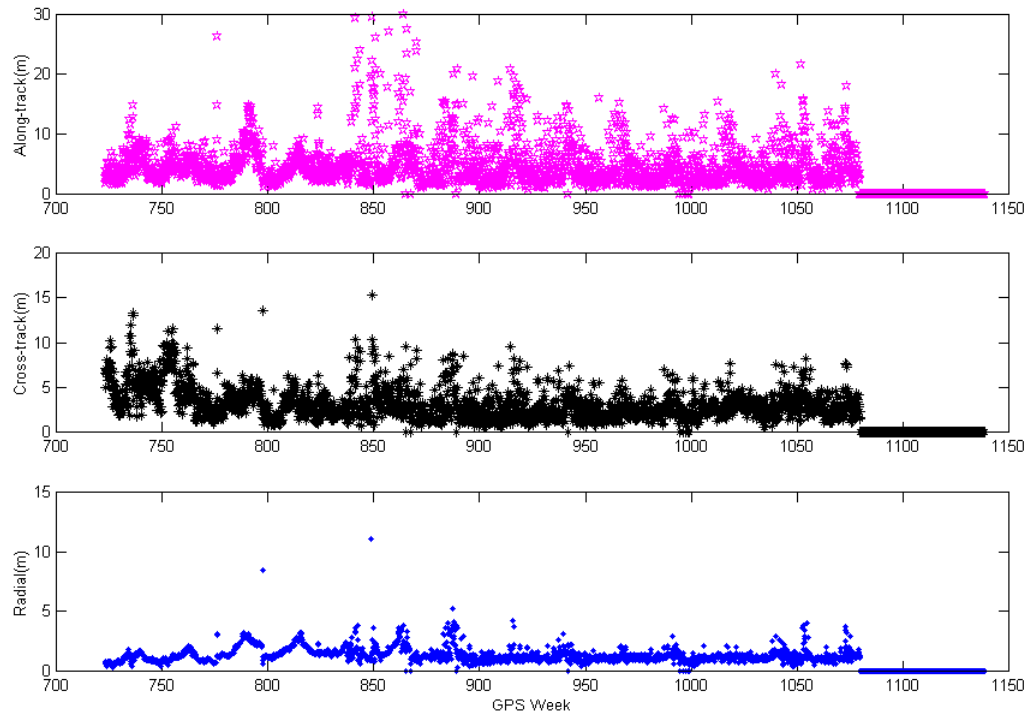
PRN 14 – Prior to week 1060 – SVN 14 (Block II). After week 1090 – SVN 41 (Block II-R)



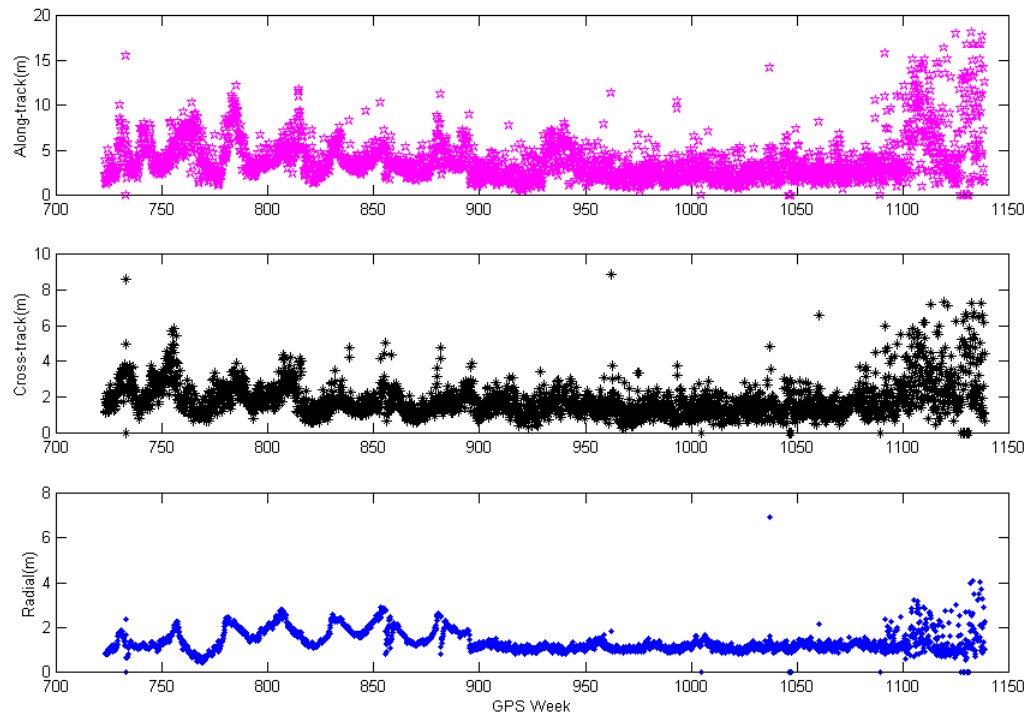
PRN 15 – SVN 15 (Block II)



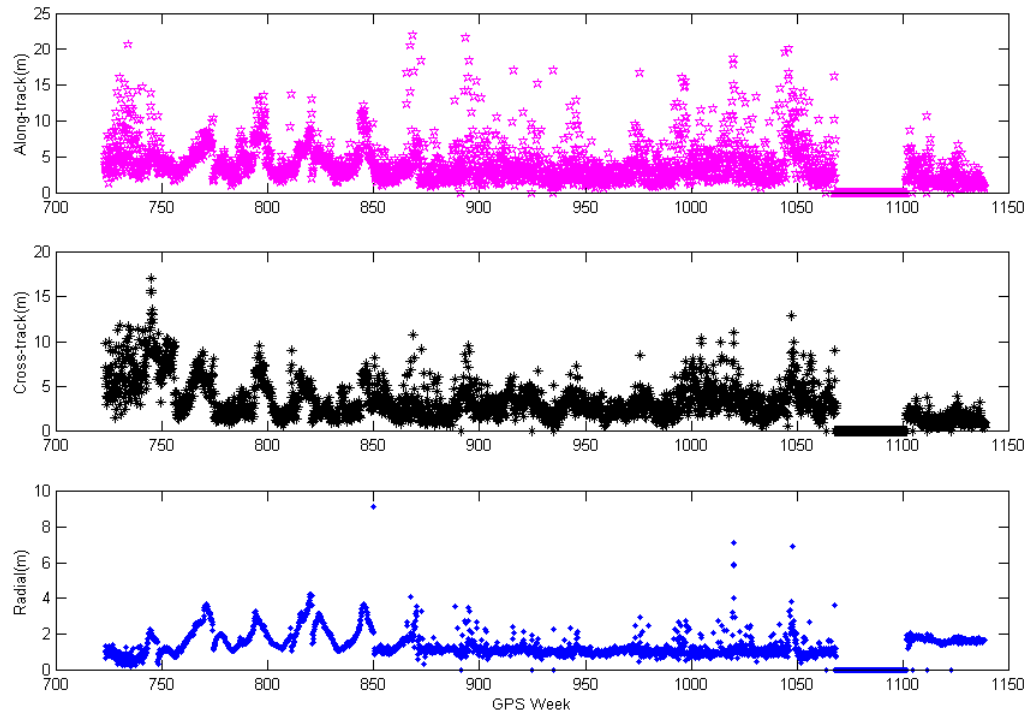
PRN 16 – SVN 16 (Block II)



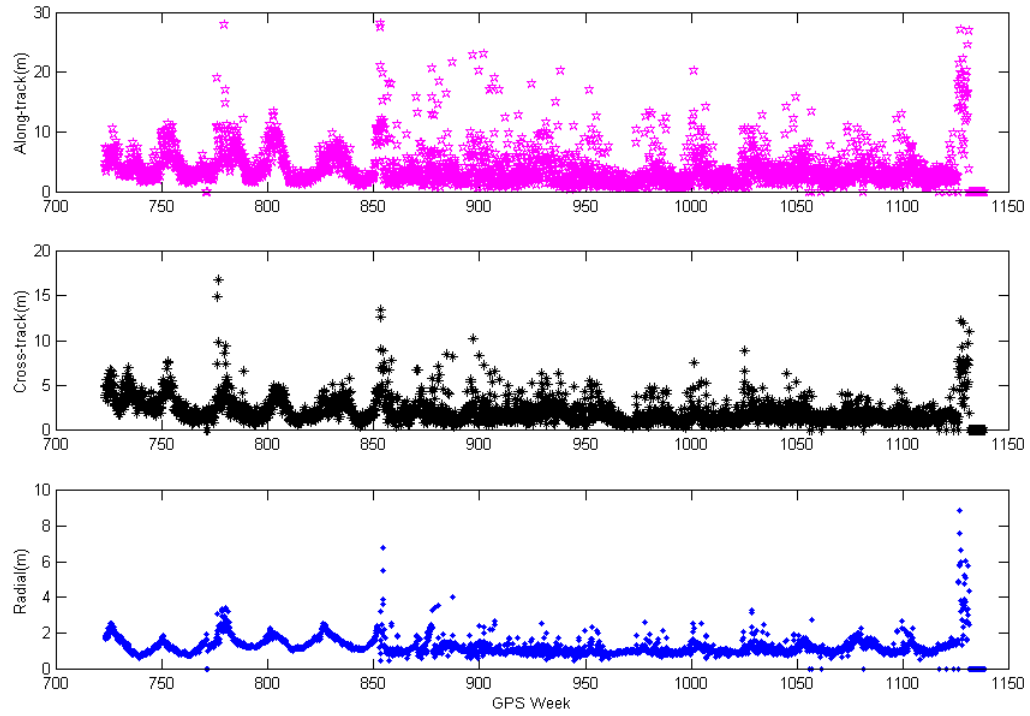
PRN 17 – SVN 17 (Block II)



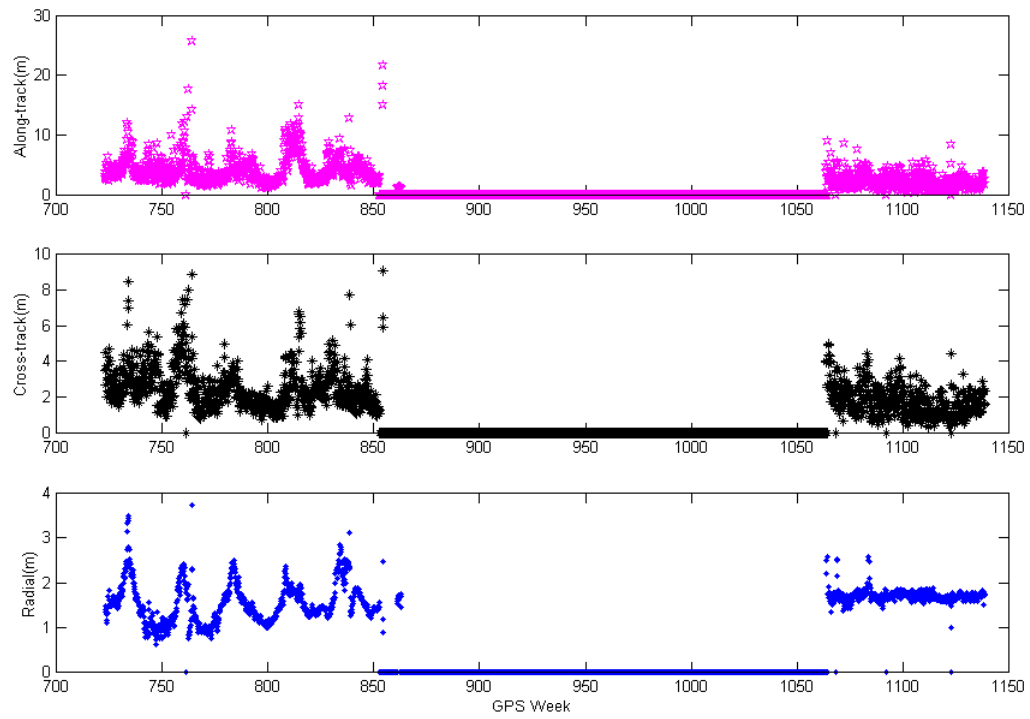
PRN 18 – SVN 18 (Block II)



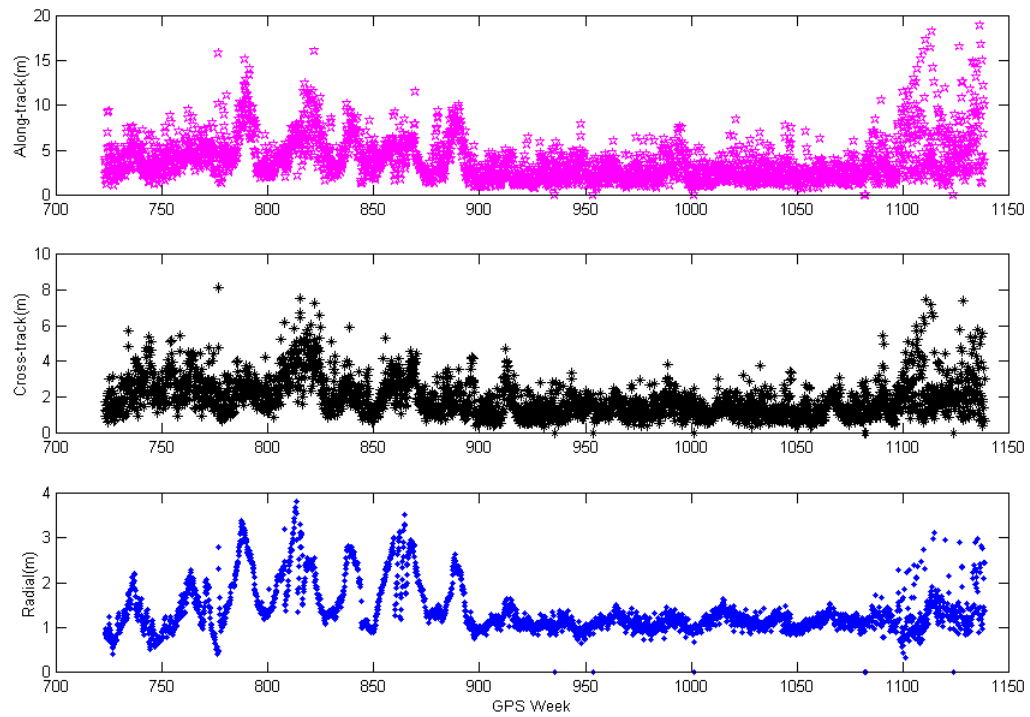
PRN 19 – SVN 19 (Block II)



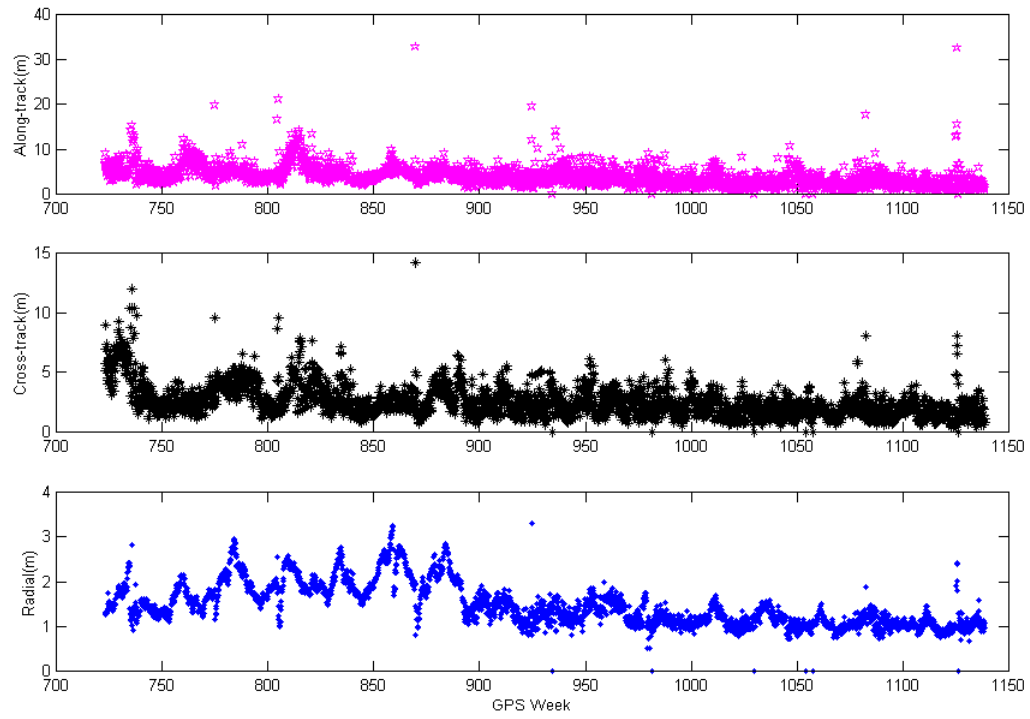
PRN 20 – Prior to week 860 – SVN 20 (Block II). After week 1060 – SVN 51 (Block II-R)



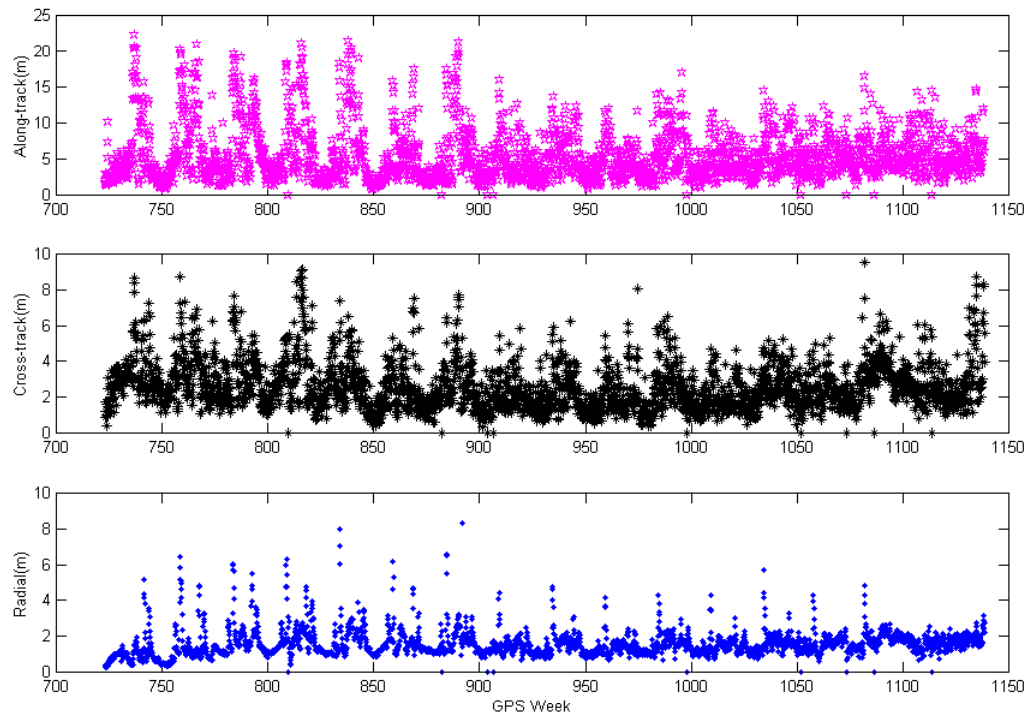
PRN 21 – SVN 21 (Block II)



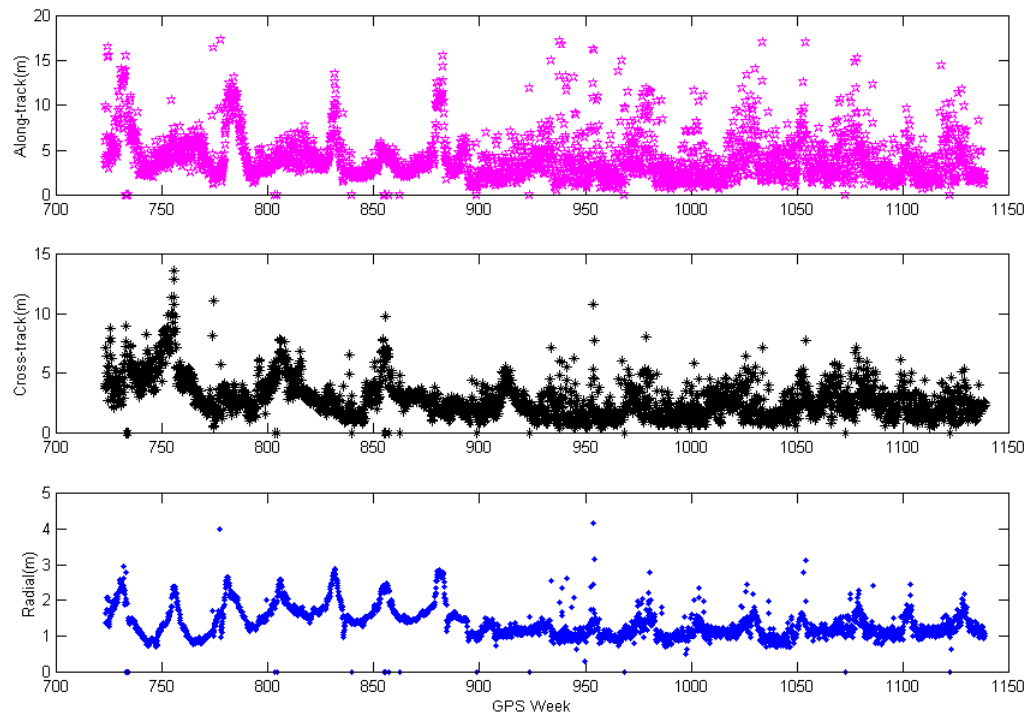
PRN 22 – SVN 22 (Block II)



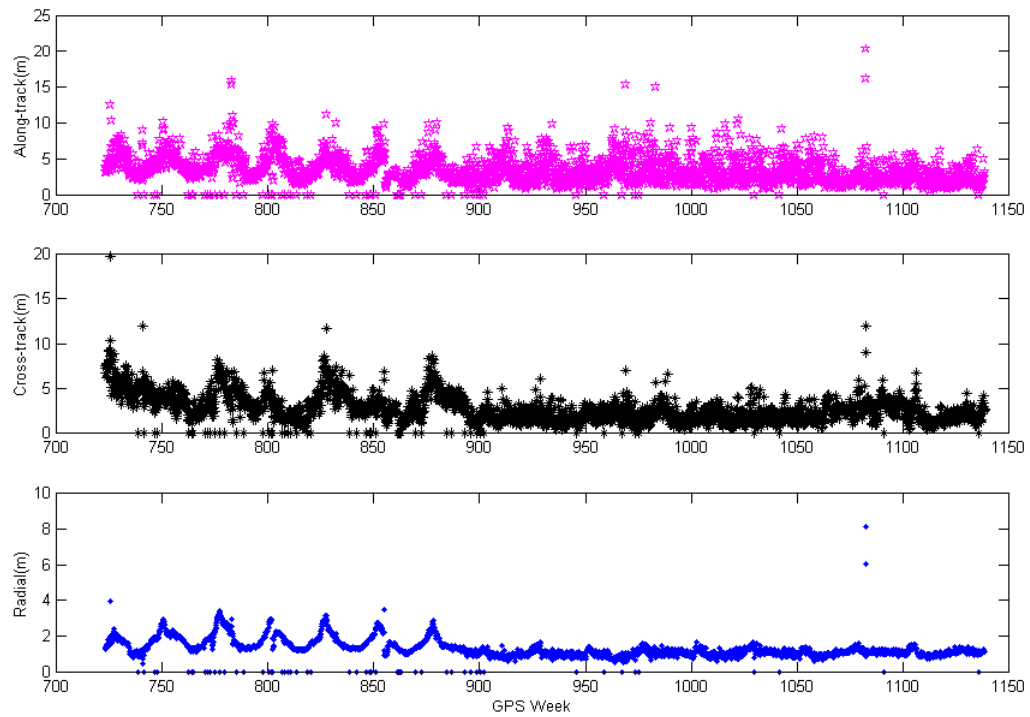
PRN 23 – SVN 23 (Block II)



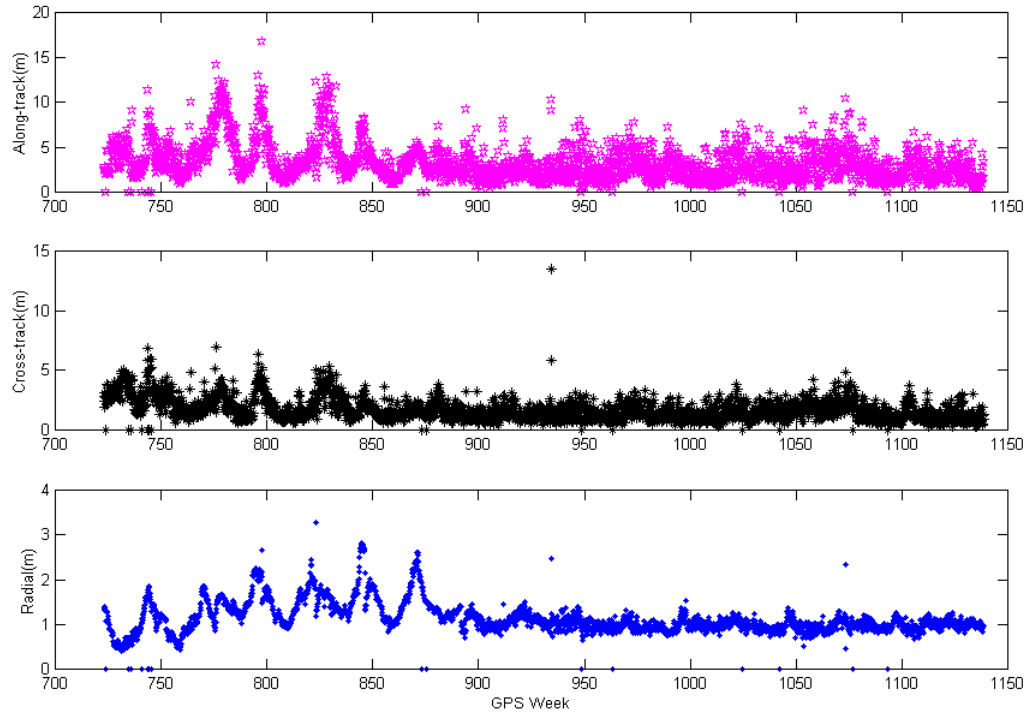
PRN 24 – SVN 24 (Block II)



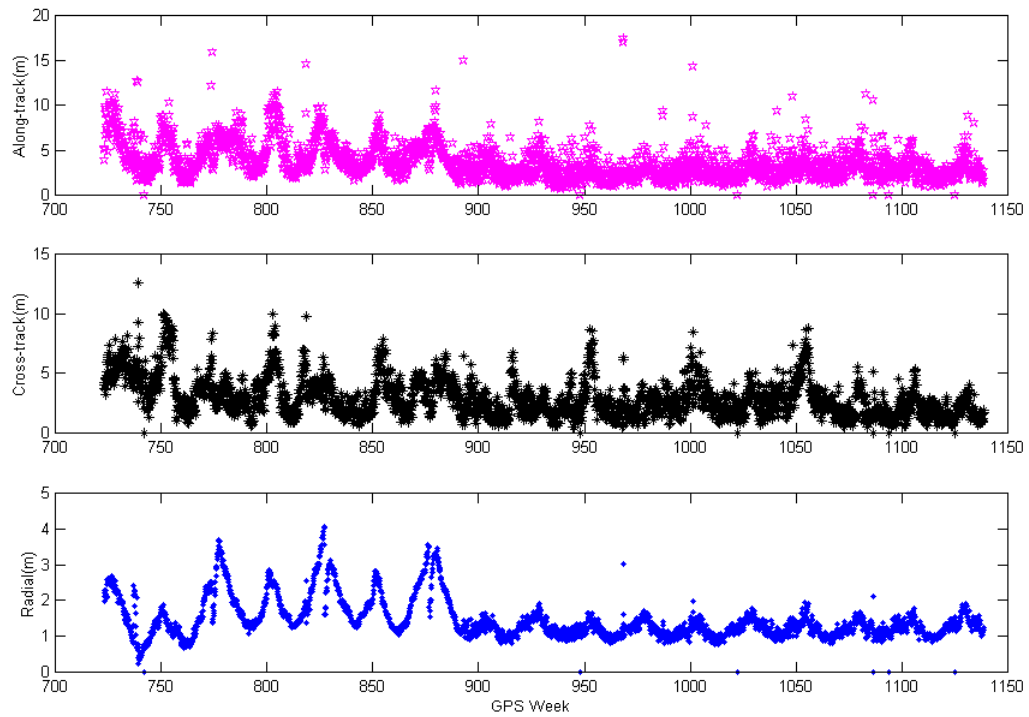
PRN 25 – SVN 25 (Block II)



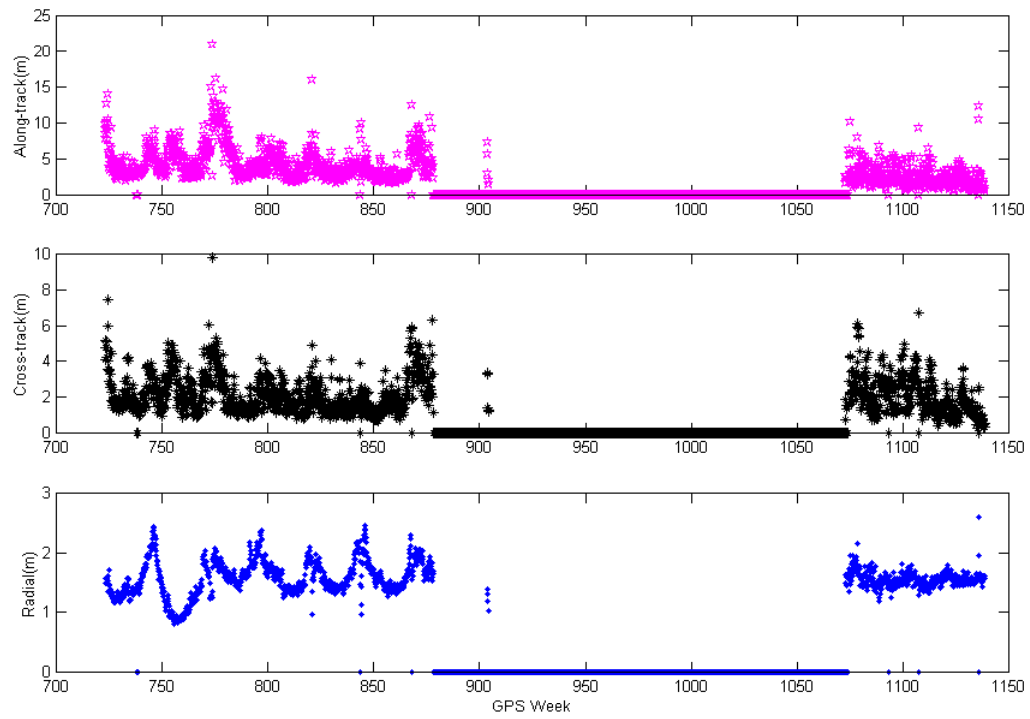
PRN 26 – SVN 26 (Block II)



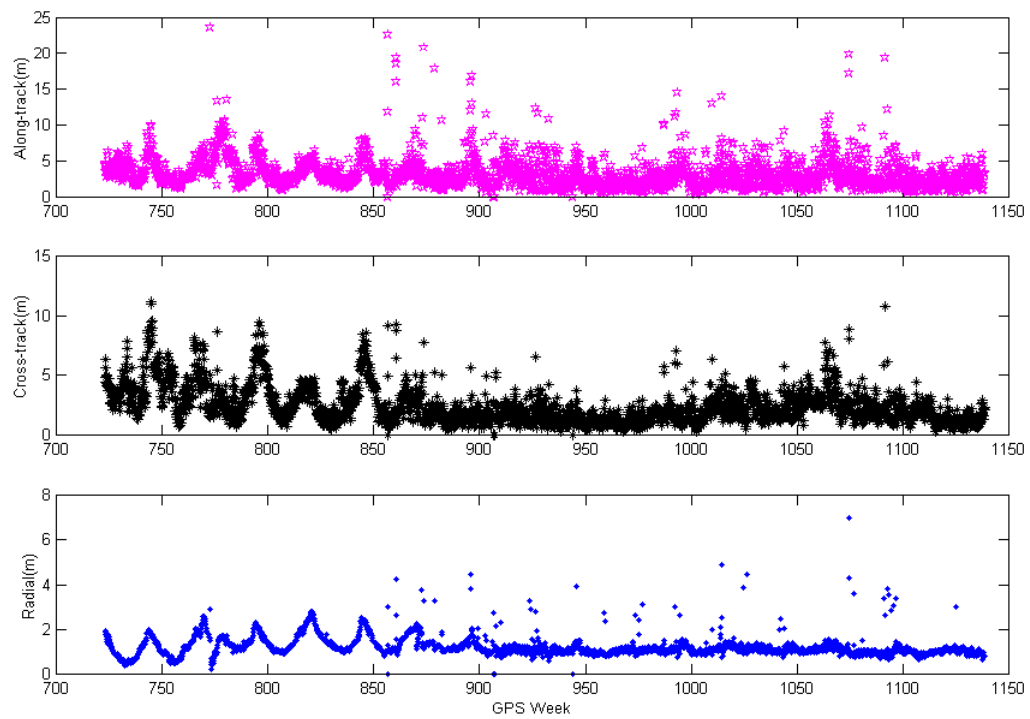
PRN 27 – SVN 27 (Block II)



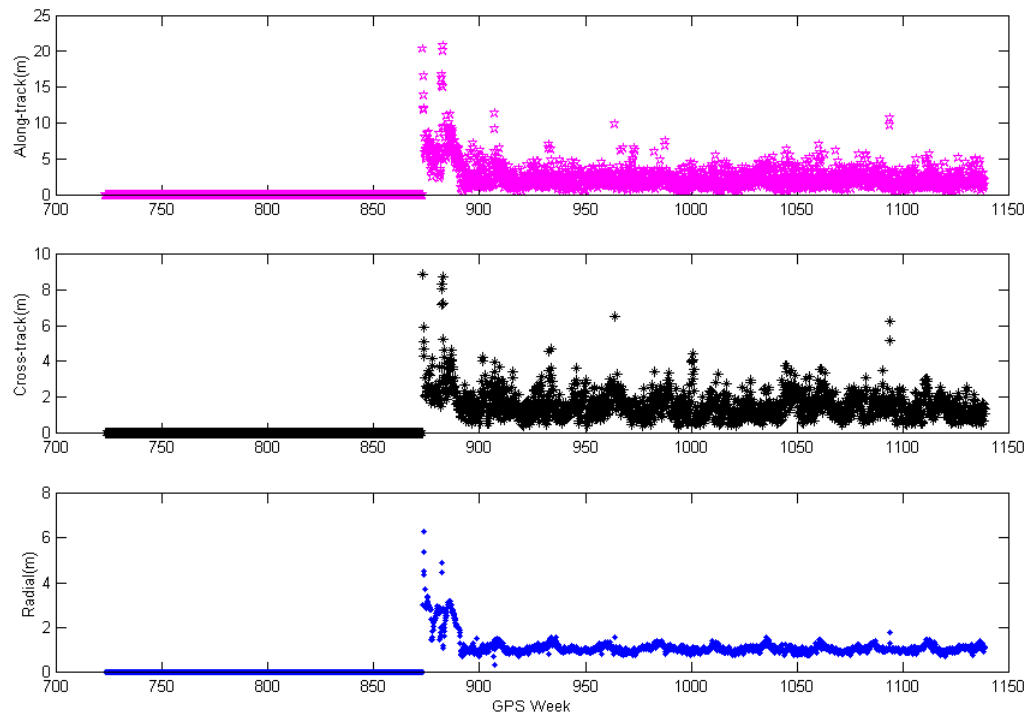
PRN 28 – Prior to week 870 – SVN 28 (Block II). After week 1080 – SVN 44 (Block II-R)



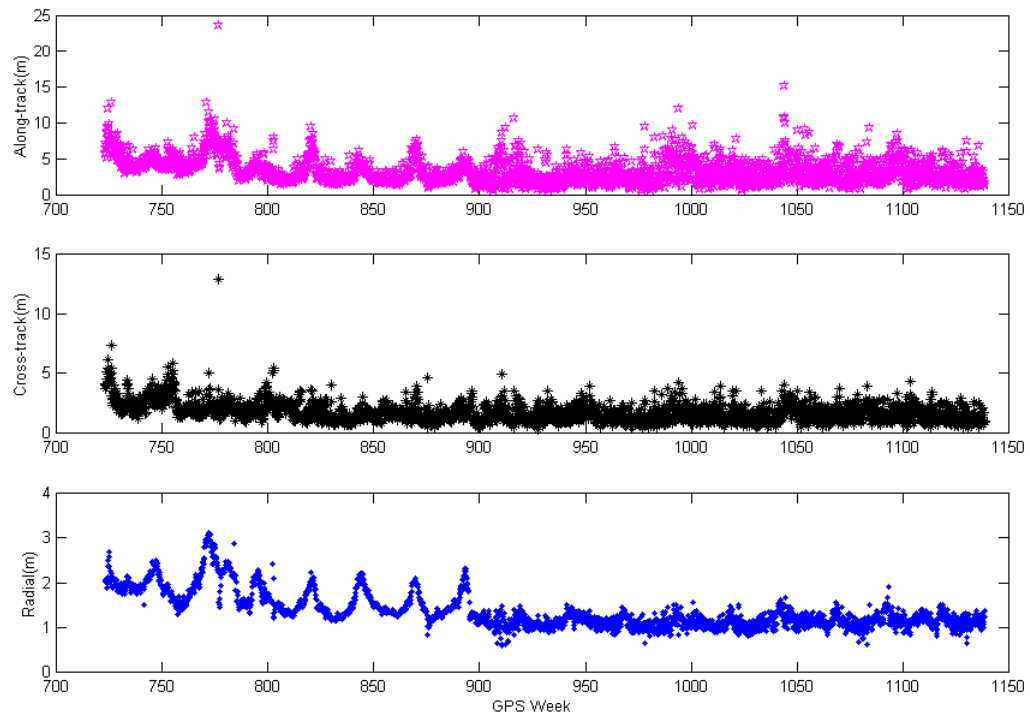
PRN 29 – SVN 29 (Block II)



PRN 30 – SVN 30 (Block II)

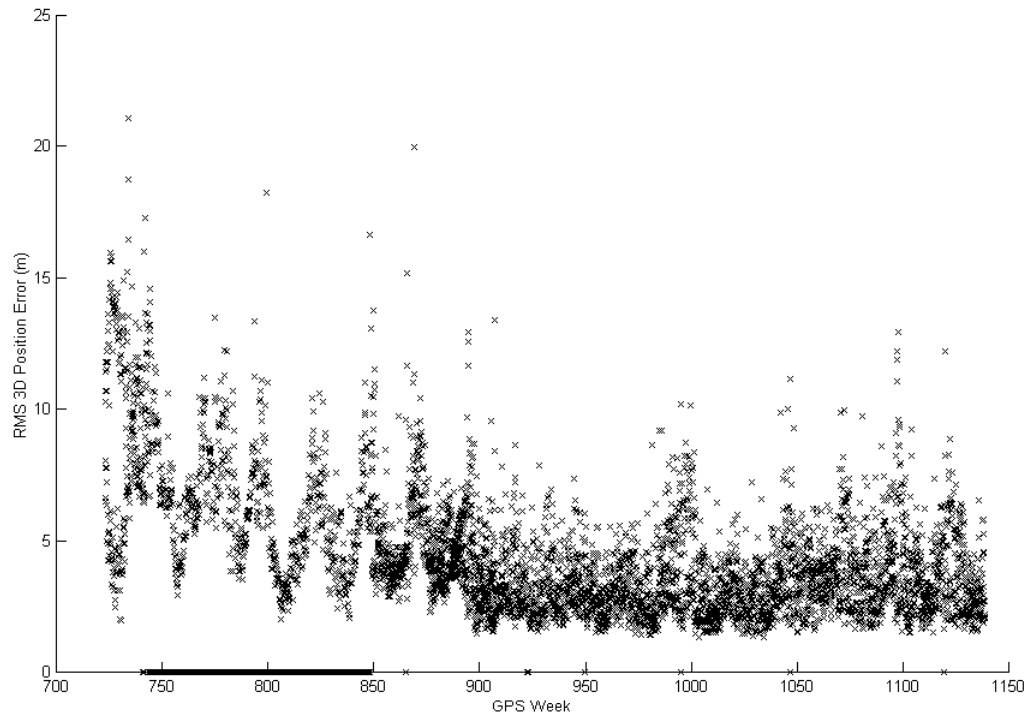


PRN 31 – SVN 31 (Block II)

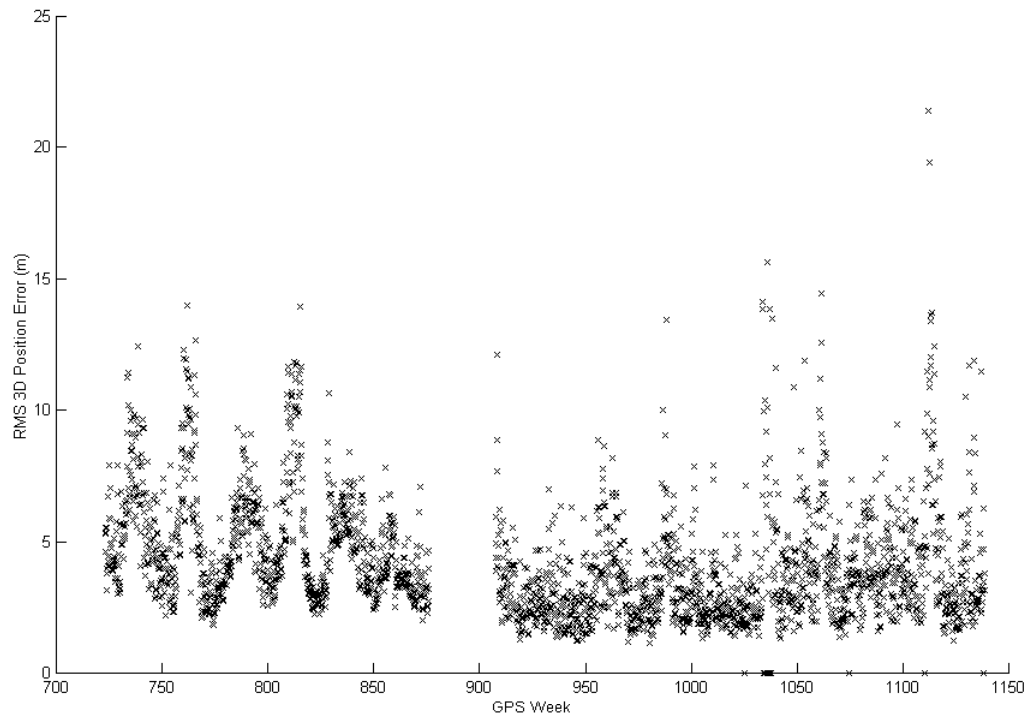


Appendix D: 3D ACR Broadcast Position Error

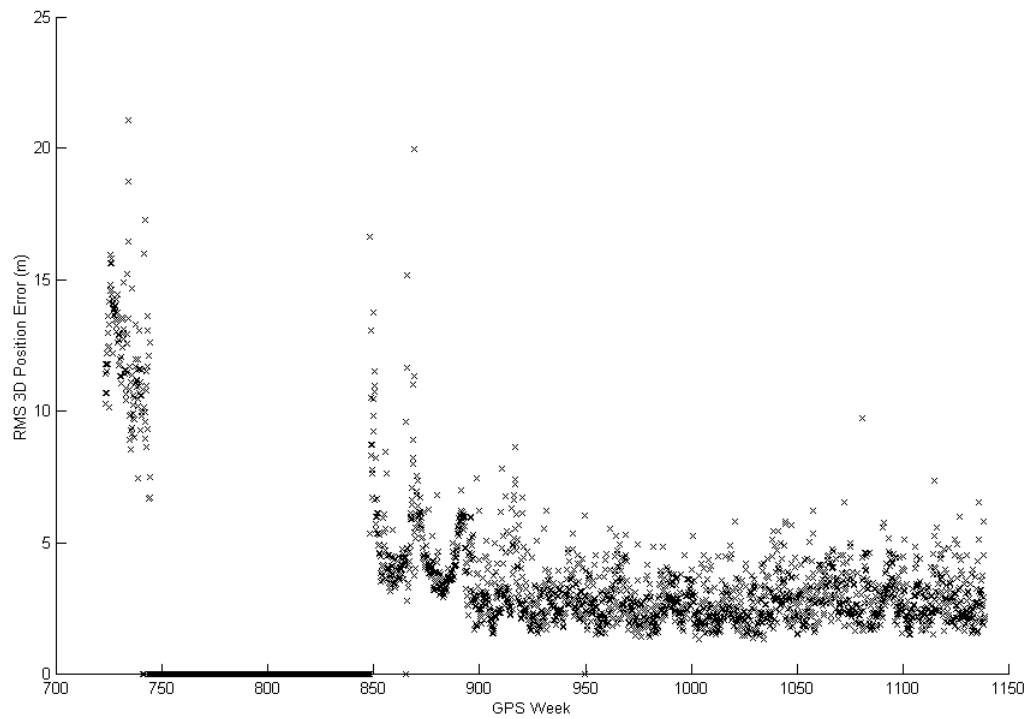
PRN 1 – SVN 32 (Block II)



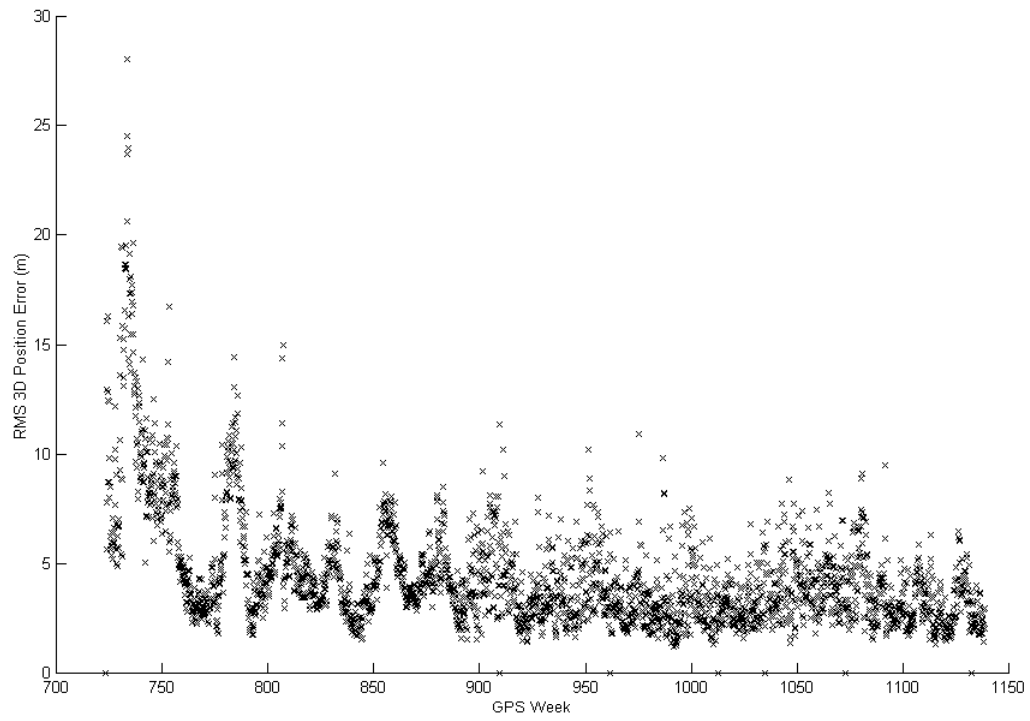
PRN 2 – SVN 13 (Block II)



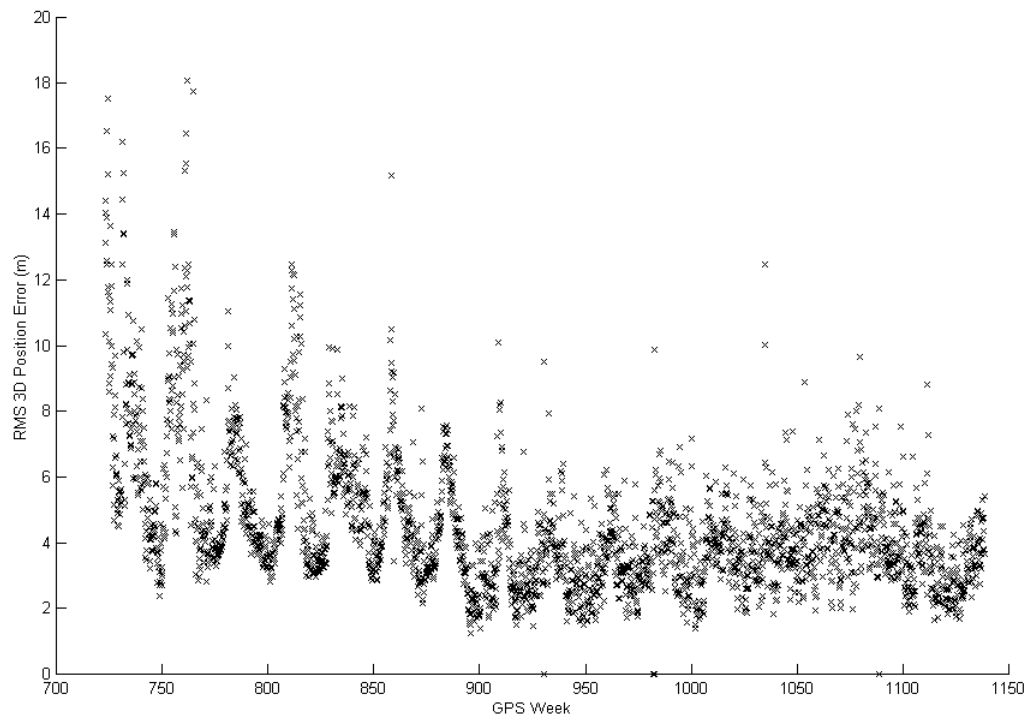
PRN 3 – Prior to week 740 - SVN 11 (Block I). After week 850 – SVN 33 (Block II)



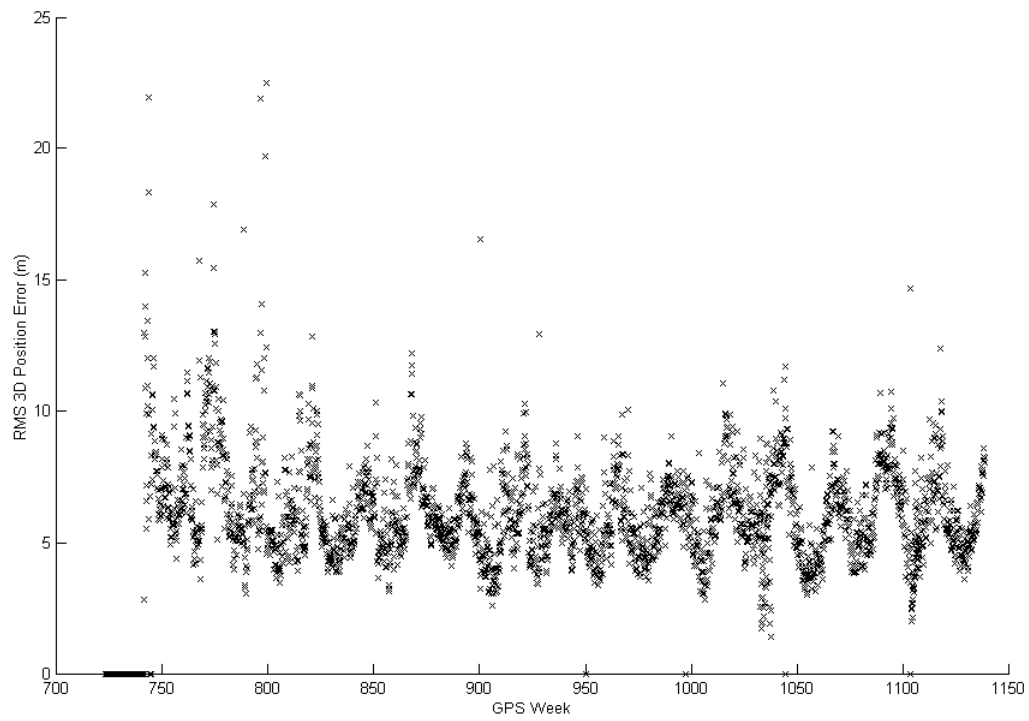
PRN 4 – SVN 34 (Block II)



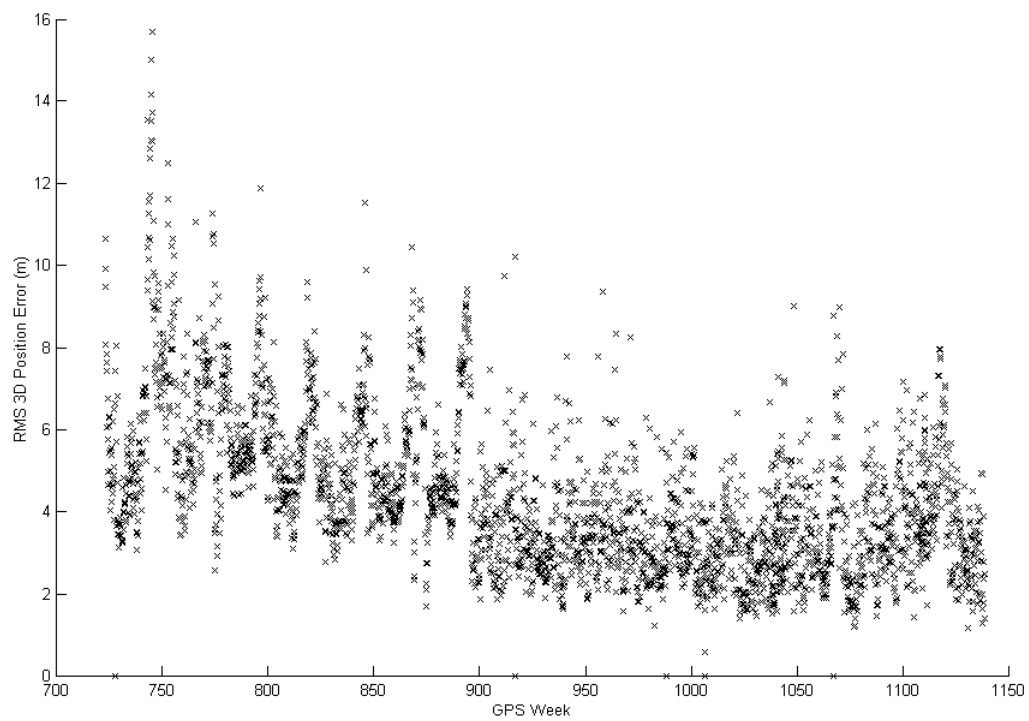
PRN 5 – SVN 35 (Block II)



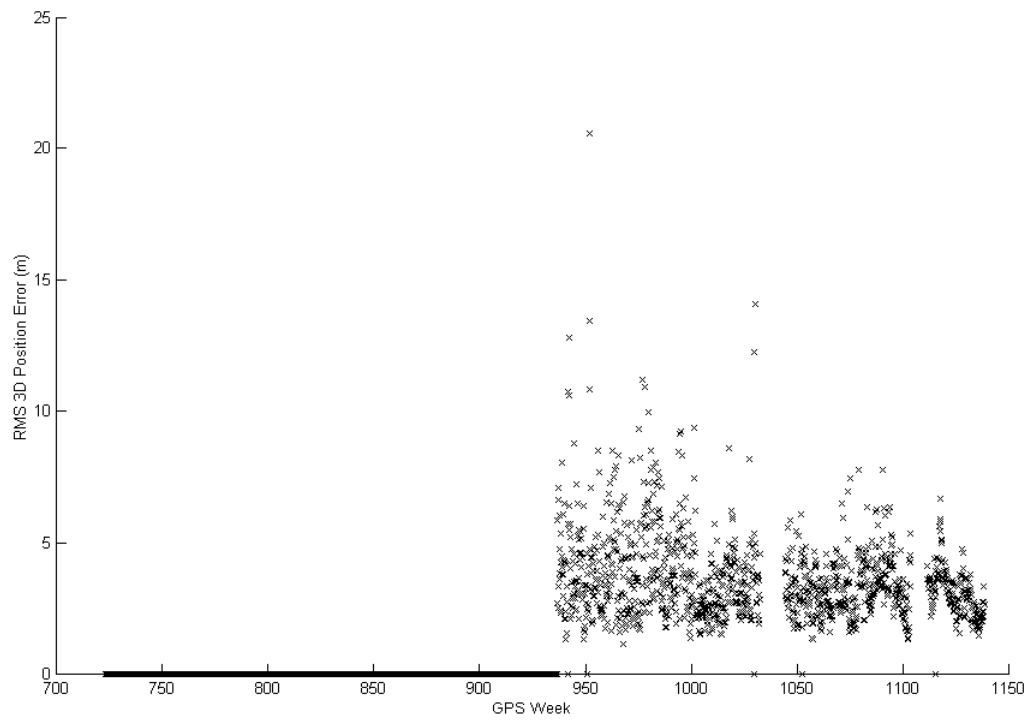
PRN 6 – SVN 36 (Block II)



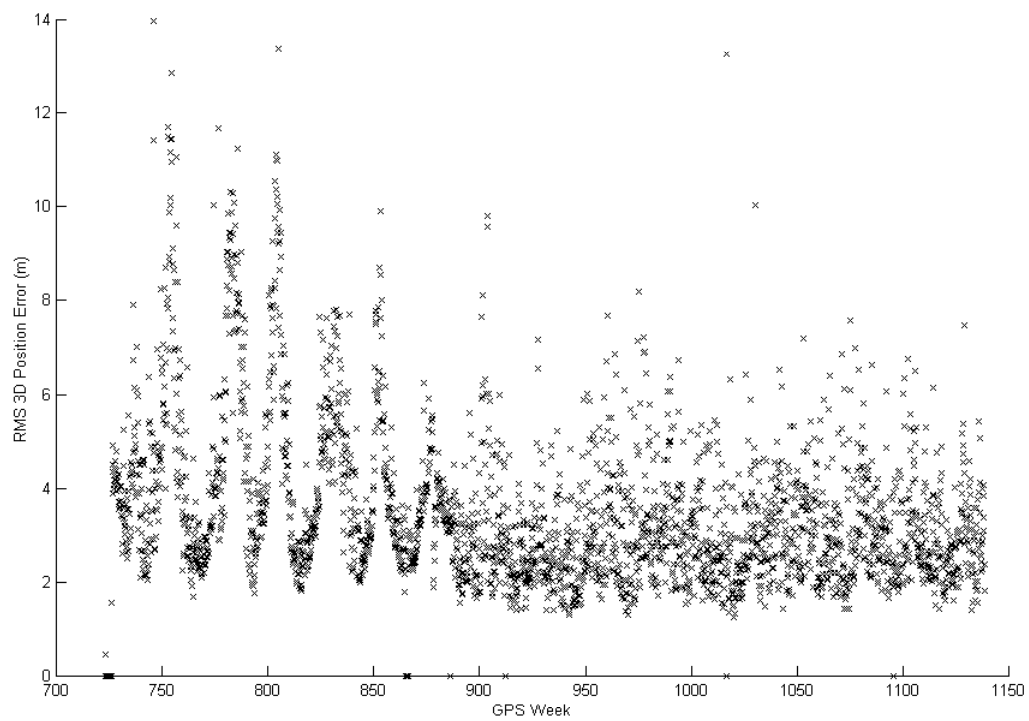
PRN 7 – SVN 37 (Block II)



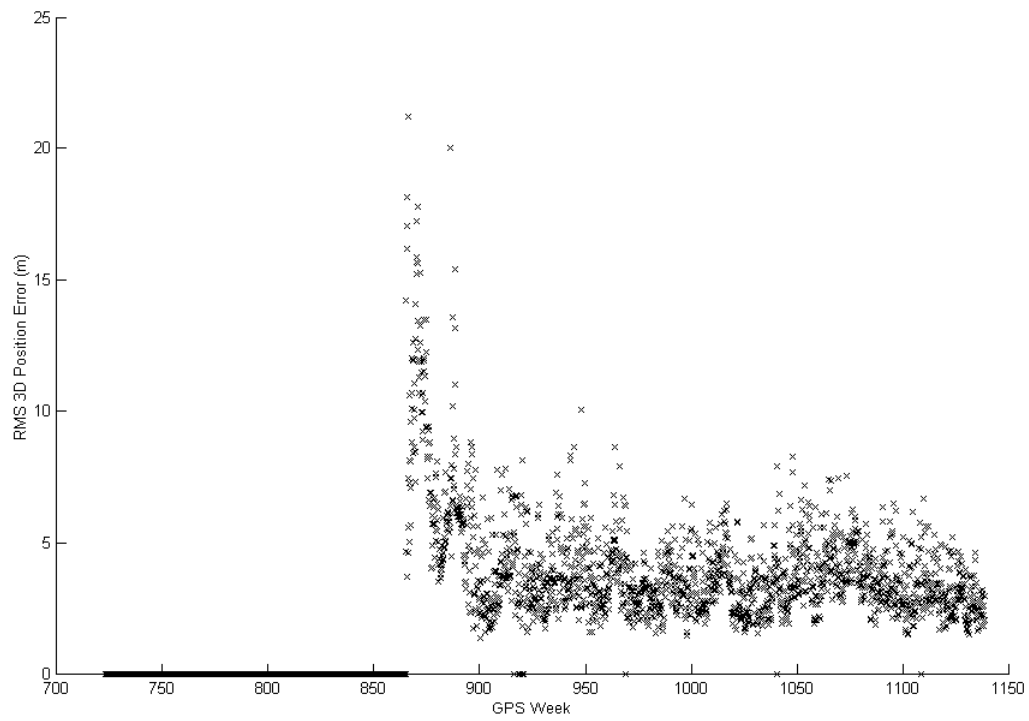
PRN 8 – SVN 38 (Block II)



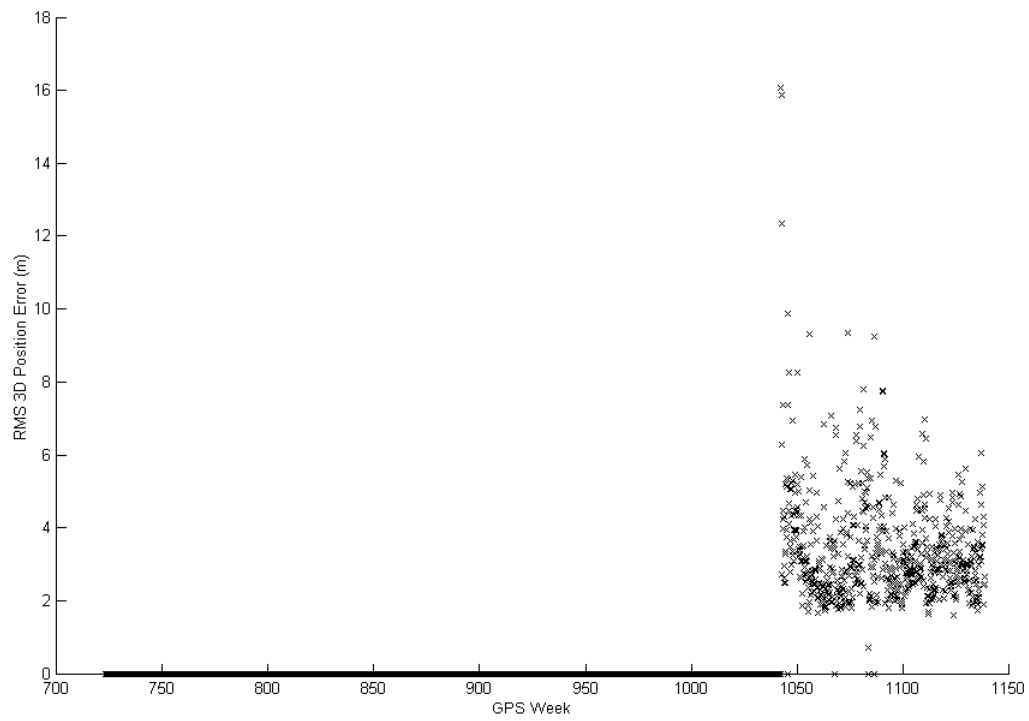
PRN 9 – SVN 39 (Block II)



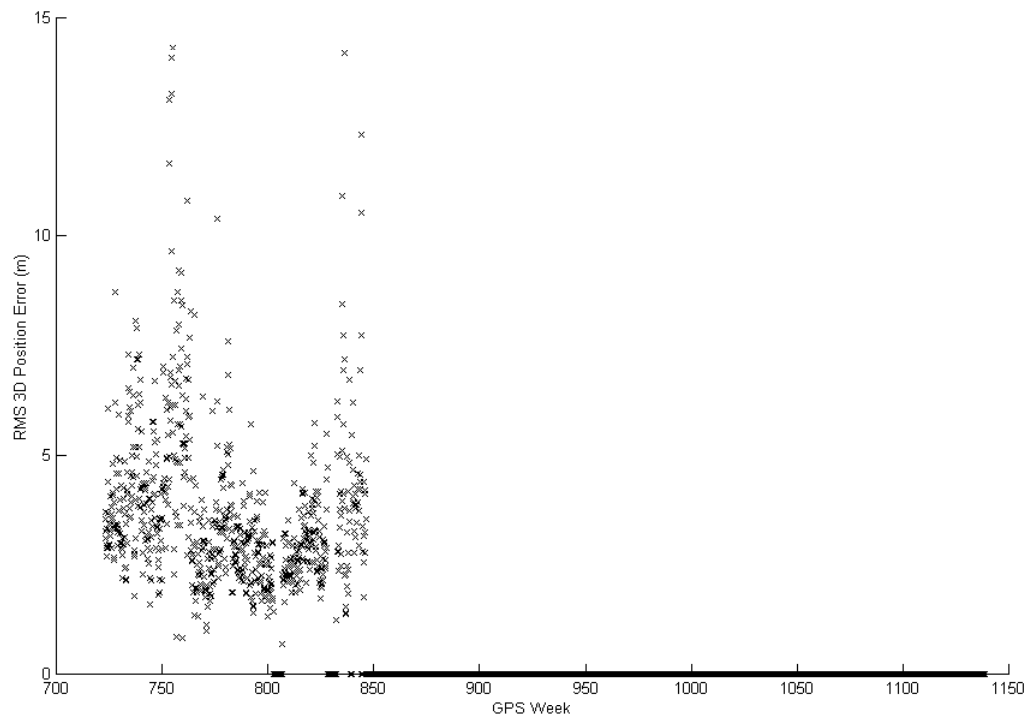
PRN 10 – SVN 40 (Block II)



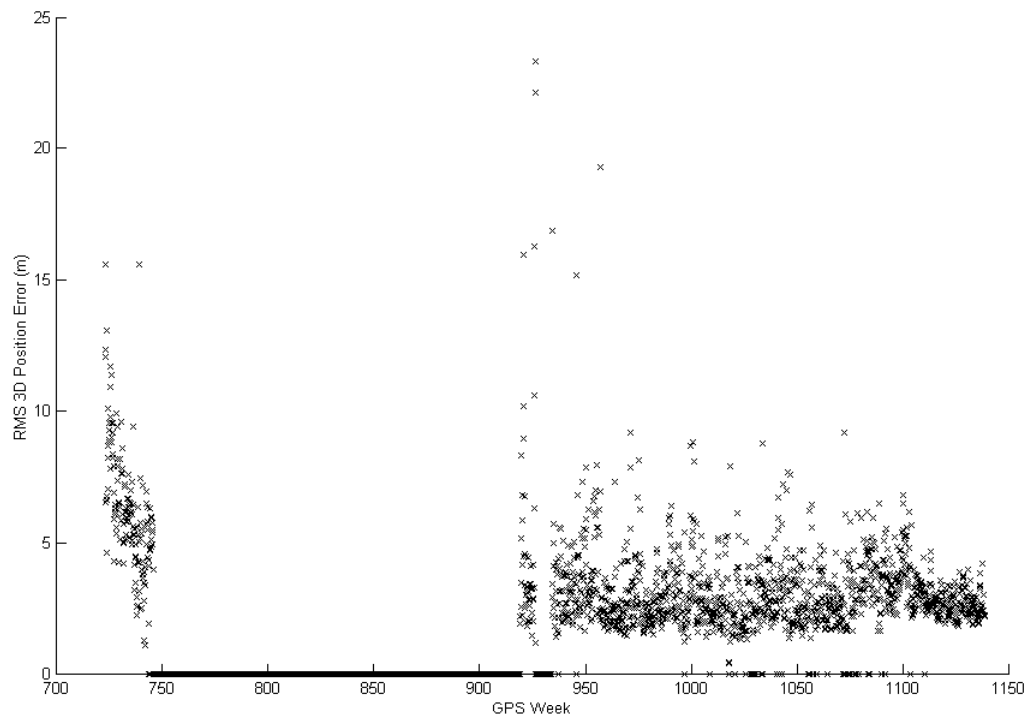
PRN 11 – SVN 46 (Block II-R)



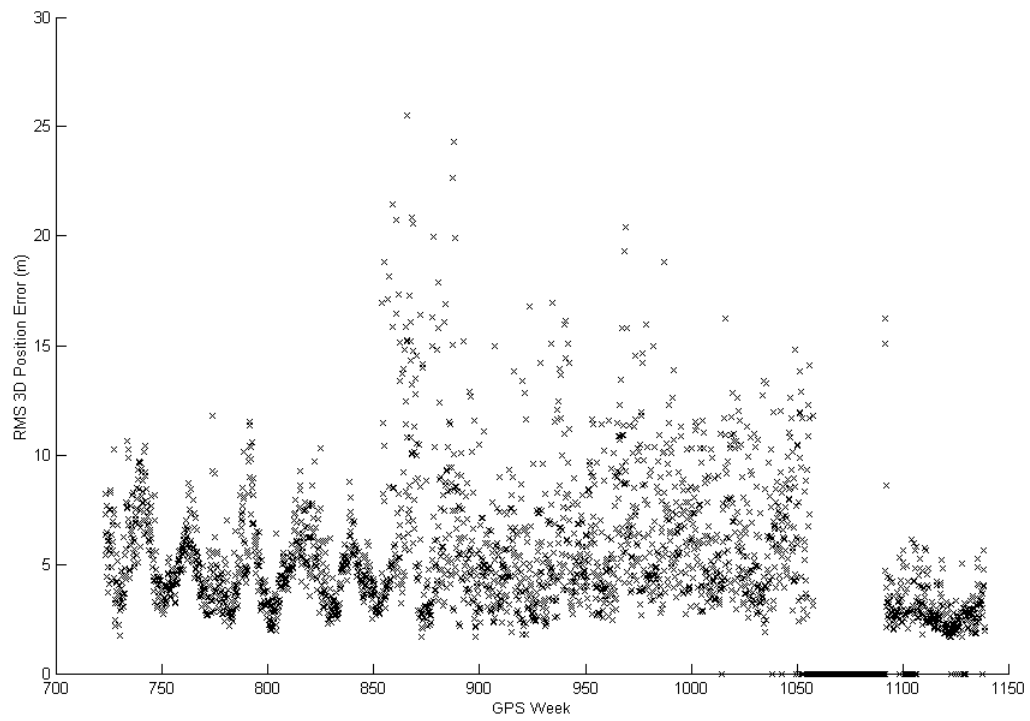
PRN 12 – SVN 10 (Block I)



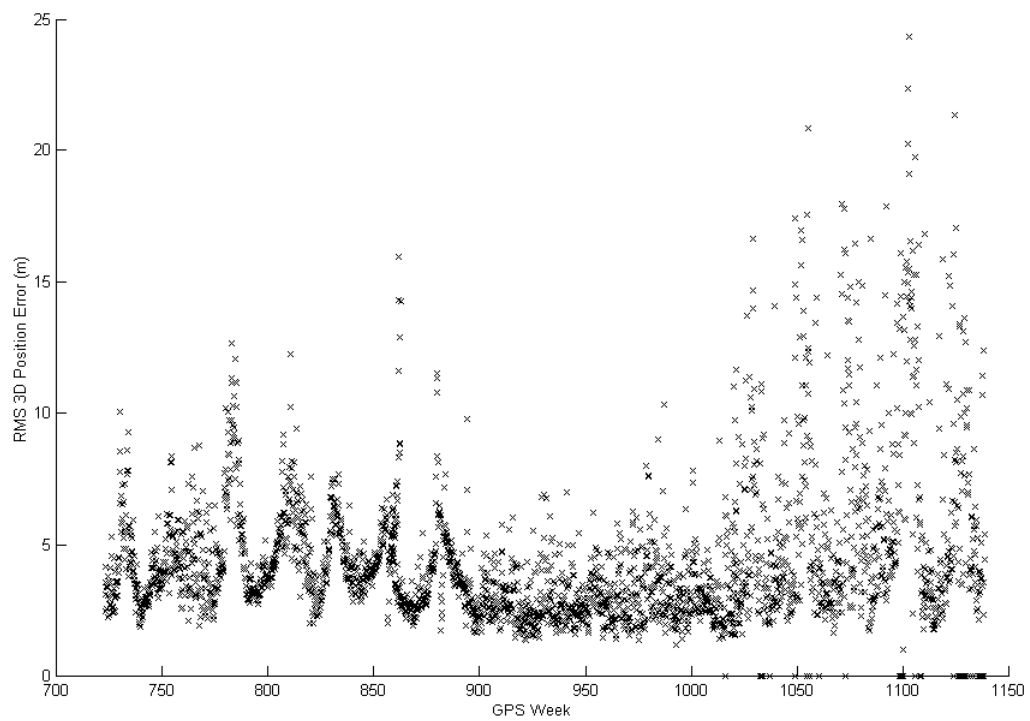
PRN 13 – Prior to week 750 – SVN 9 (Block I). After week 920 – SVN 43 (Block II-R)



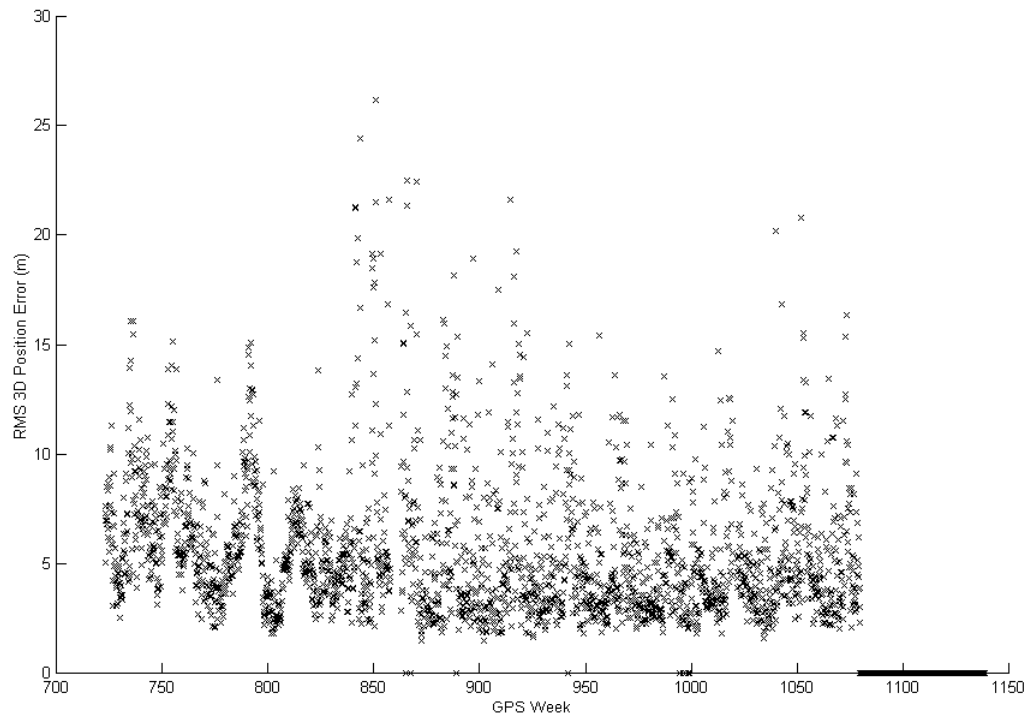
PRN 14 – Prior to week 1060 – SVN 14 (Block II). After week 1090 – SVN 41 (Block II-R)



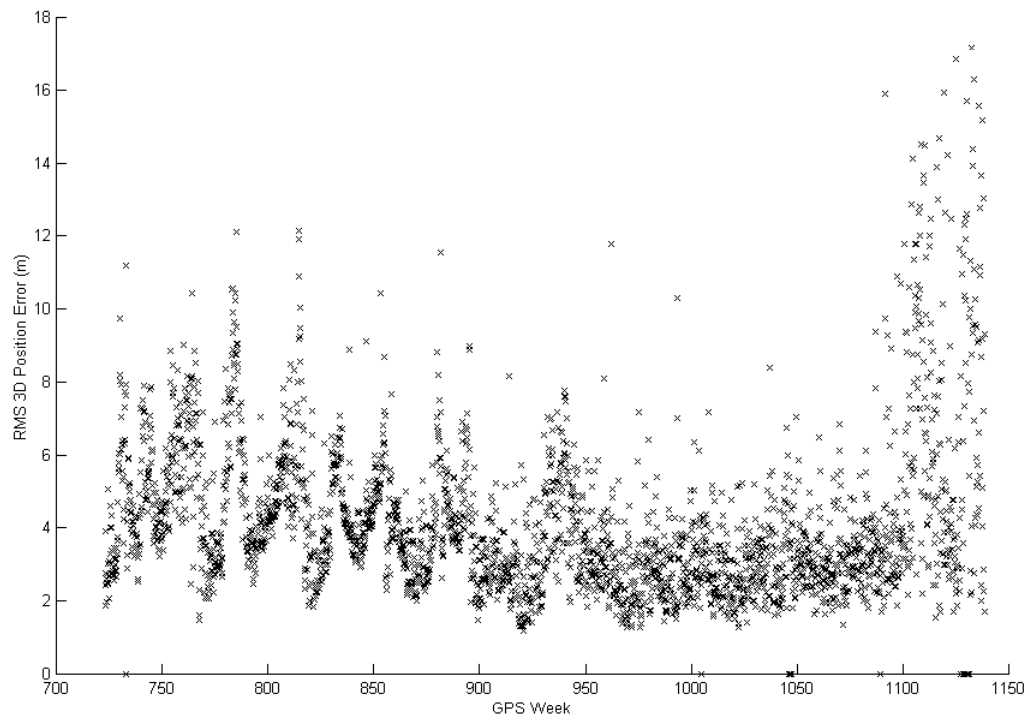
PRN 15 – SVN 15 (Block II)



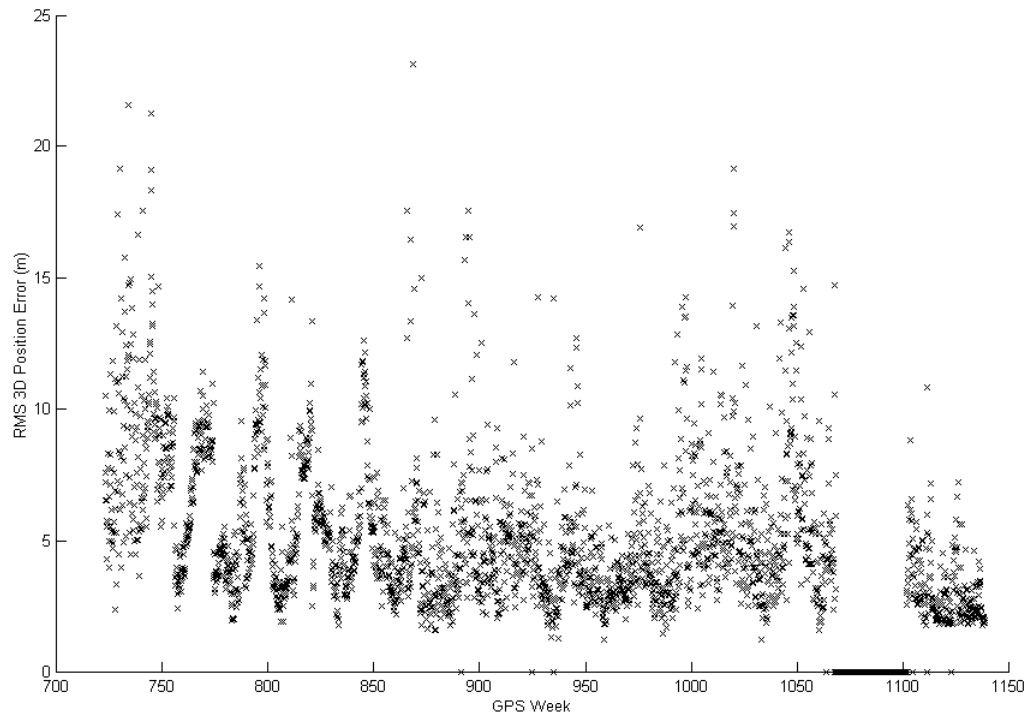
PRN 16 – SVN 16 (Block II)



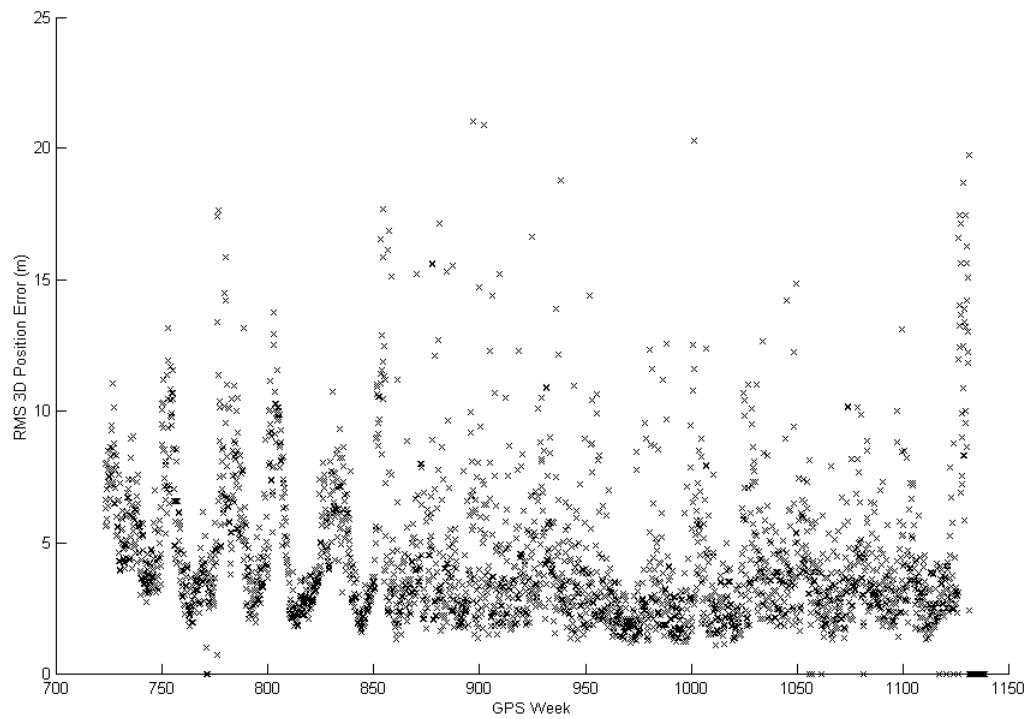
PRN 17 – SVN 17 (Block II)



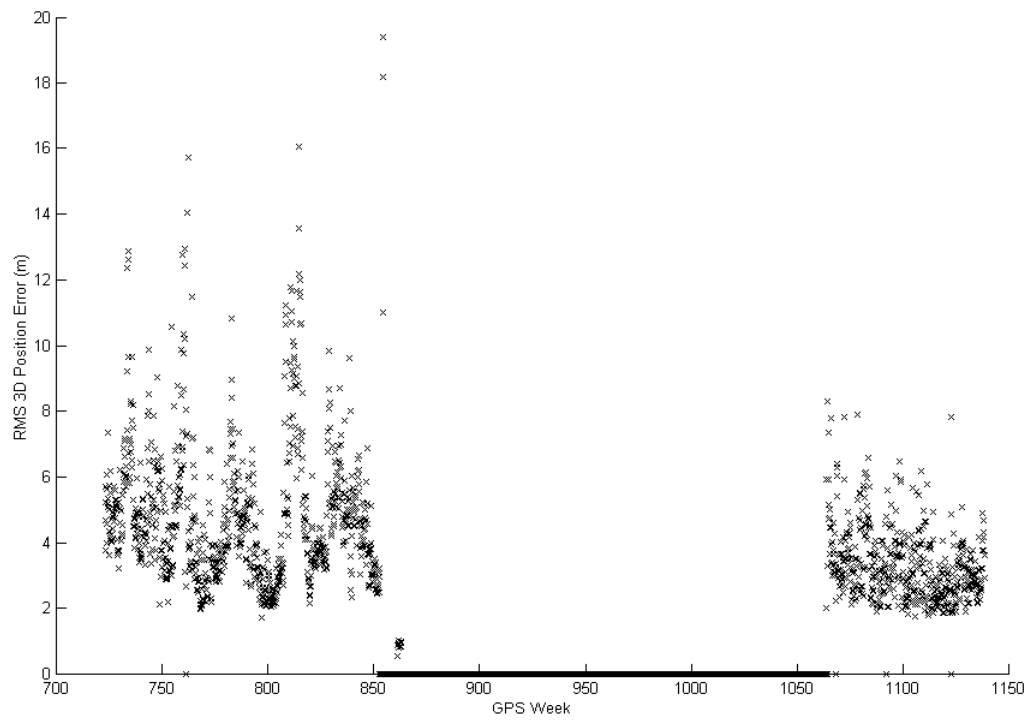
PRN 18 – SVN 18 (Block II)



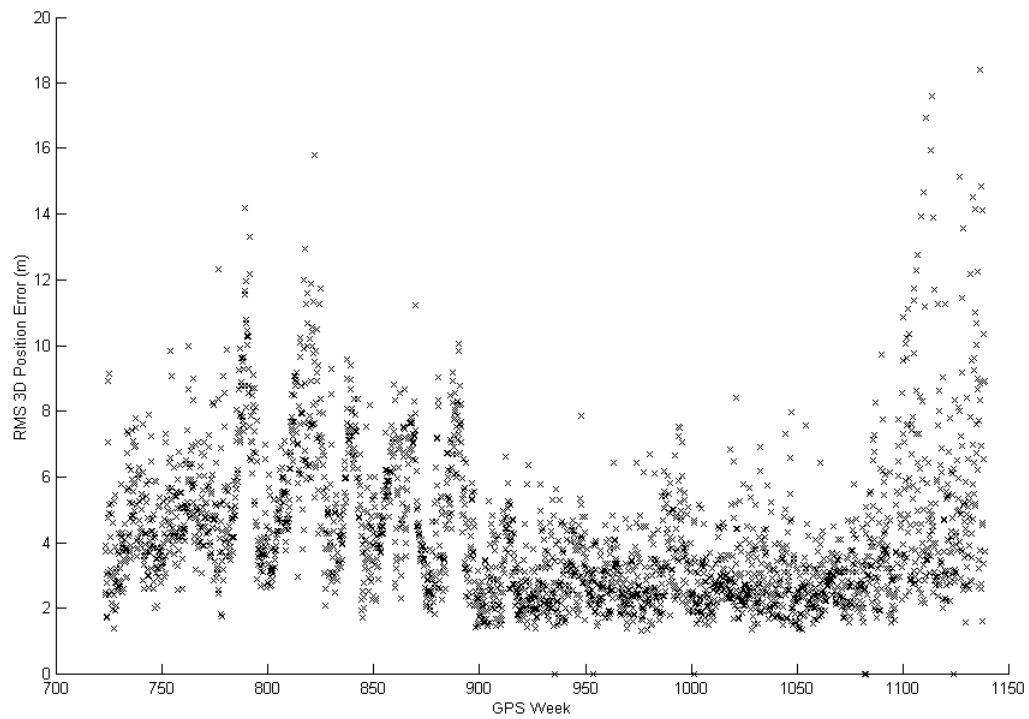
PRN 19 – SVN 19 (Block II)



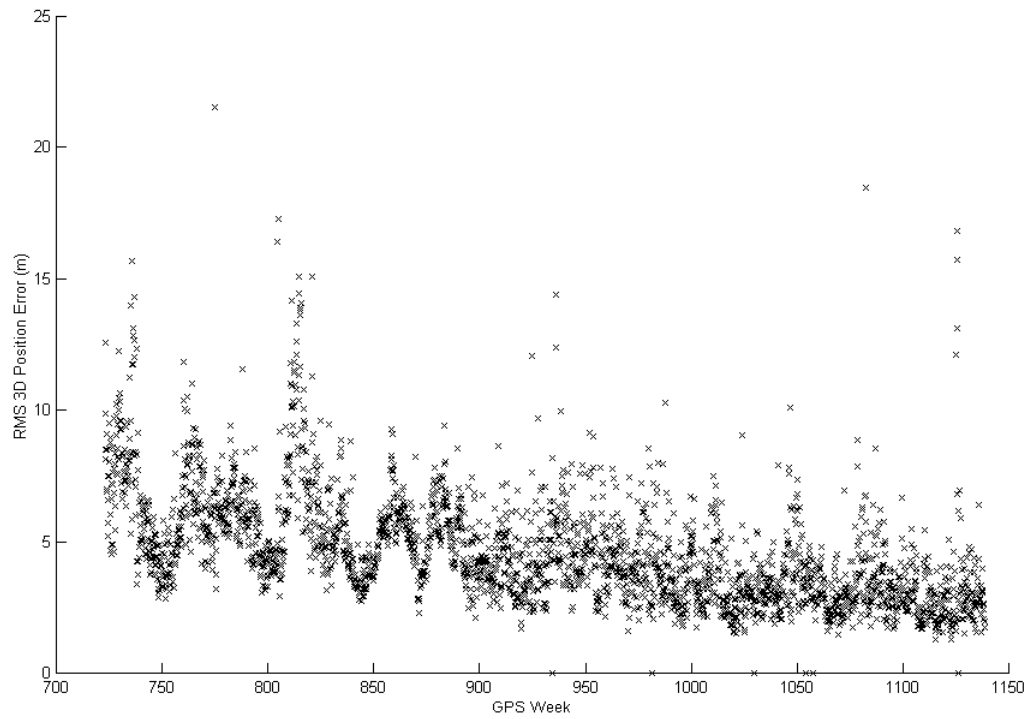
PRN 20 – Prior to week 860 – SVN 20 (Block II). After week 1060 – SVN 51 (Block II-R)



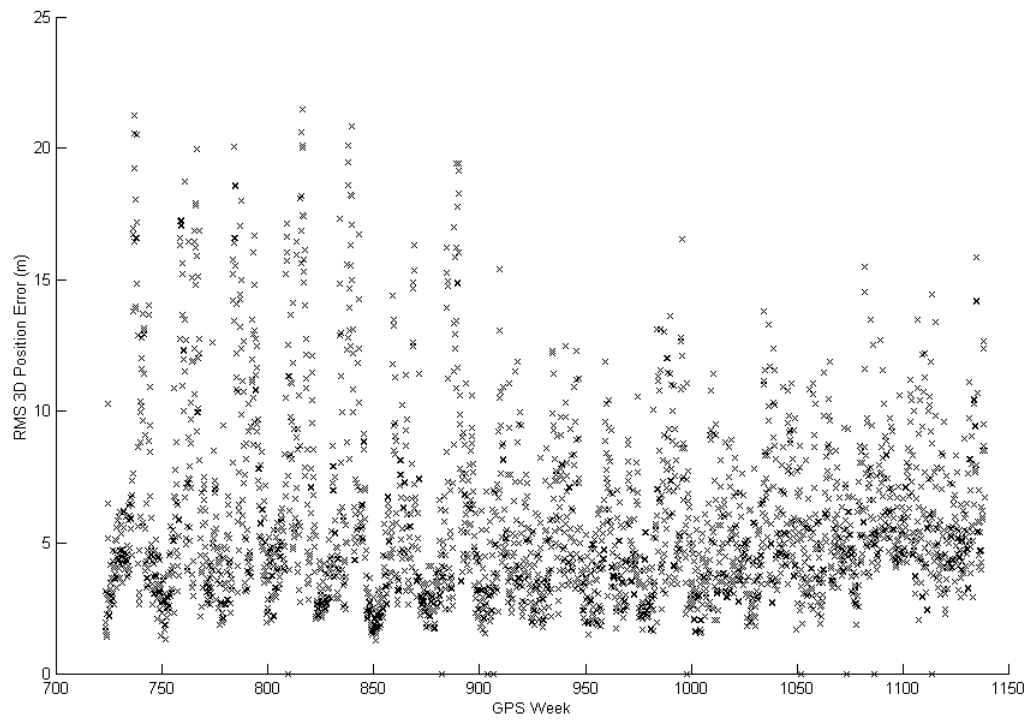
PRN 21 – SVN 21 (Block II)



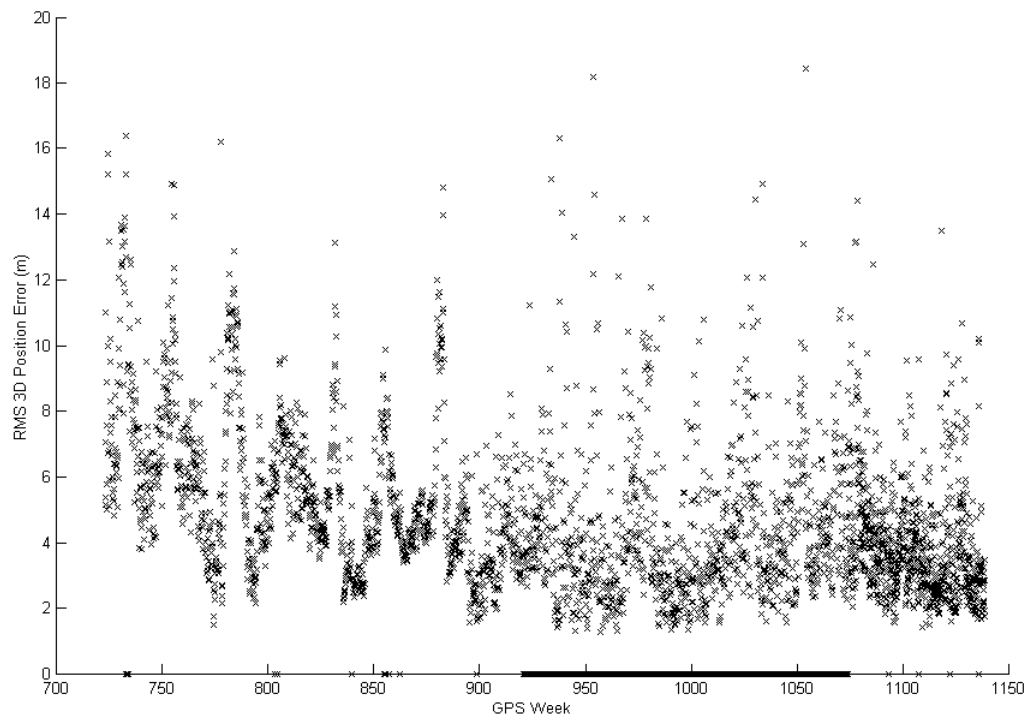
PRN 22 – SVN 22 (Block II)



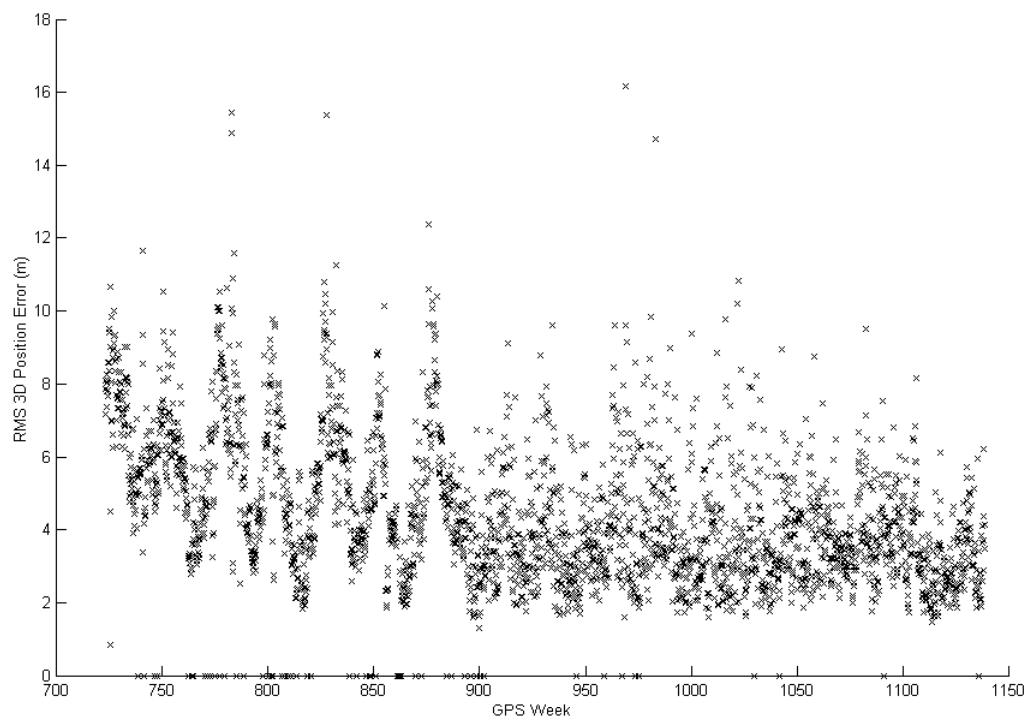
PRN 23 – SVN 23 (Block II)



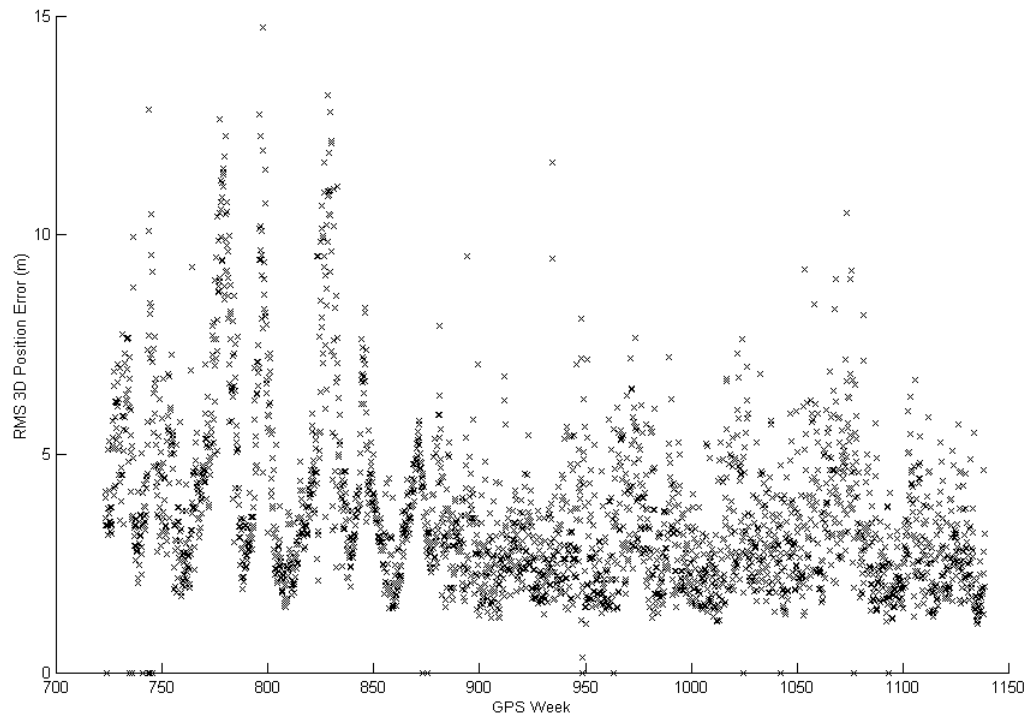
PRN 24 – SVN 24 (Block II)



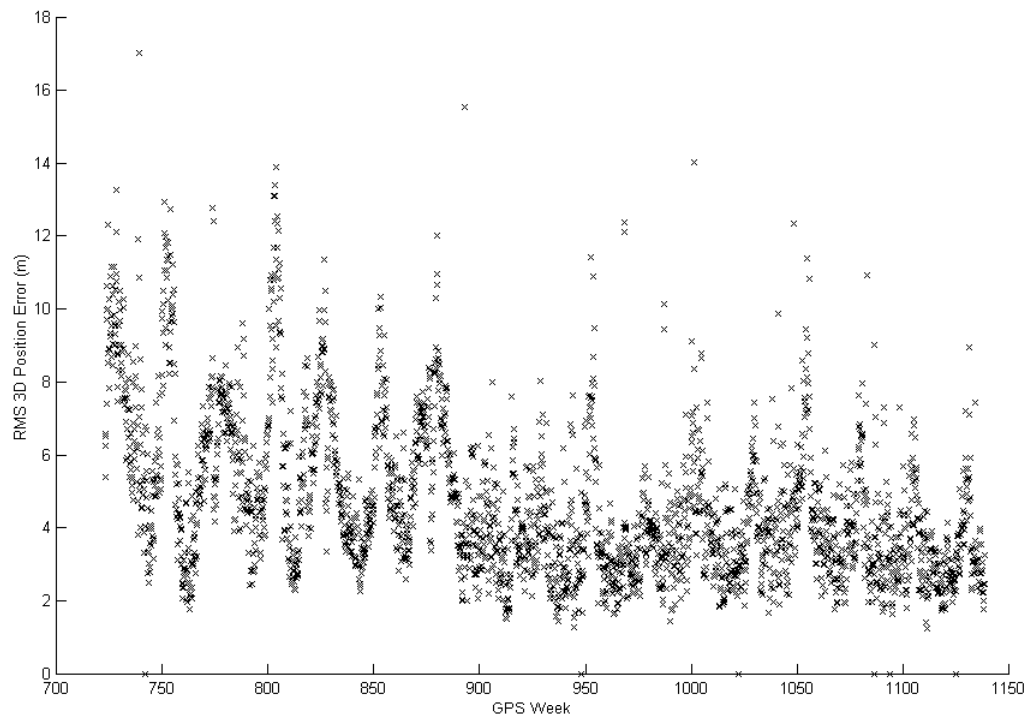
PRN 25 – SVN 25 (Block II)



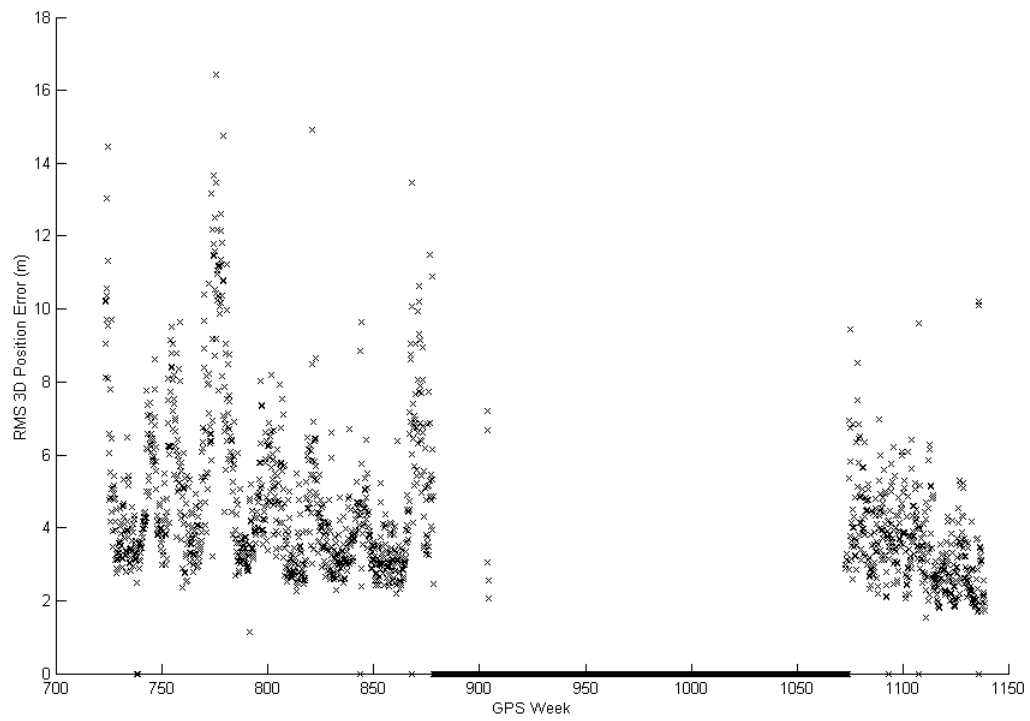
PRN 26 – SVN 26 (Block II)



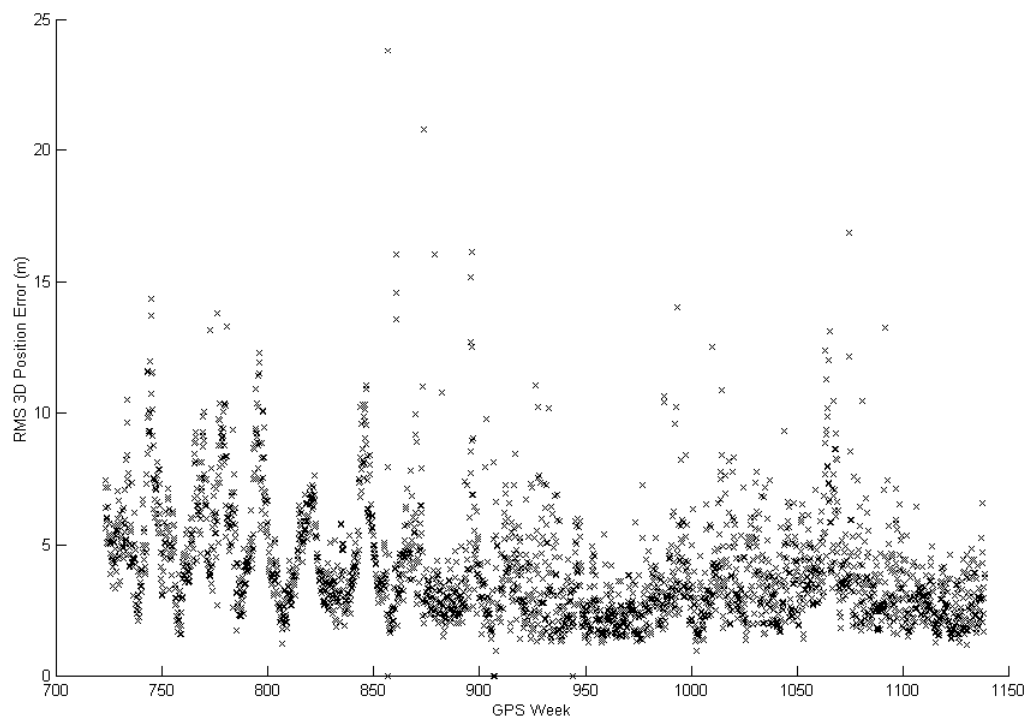
PRN 27 – SVN 27 (Block II)



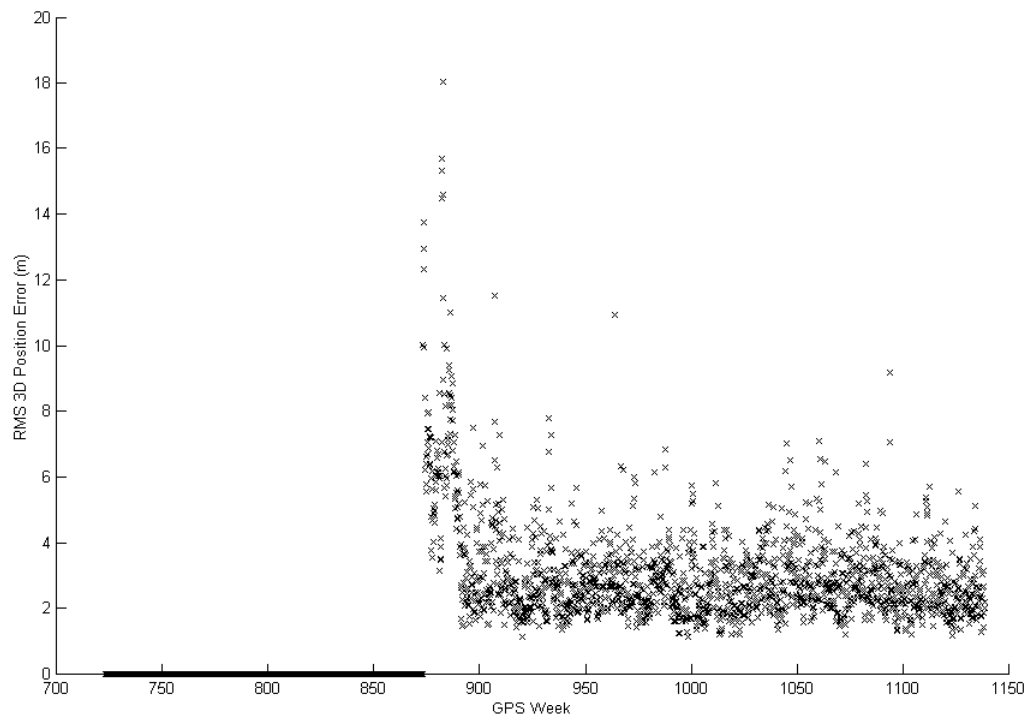
PRN 28 – Prior to week 870 – SVN 28 (Block II). After week 1080 – SVN 44 (Block II-R)



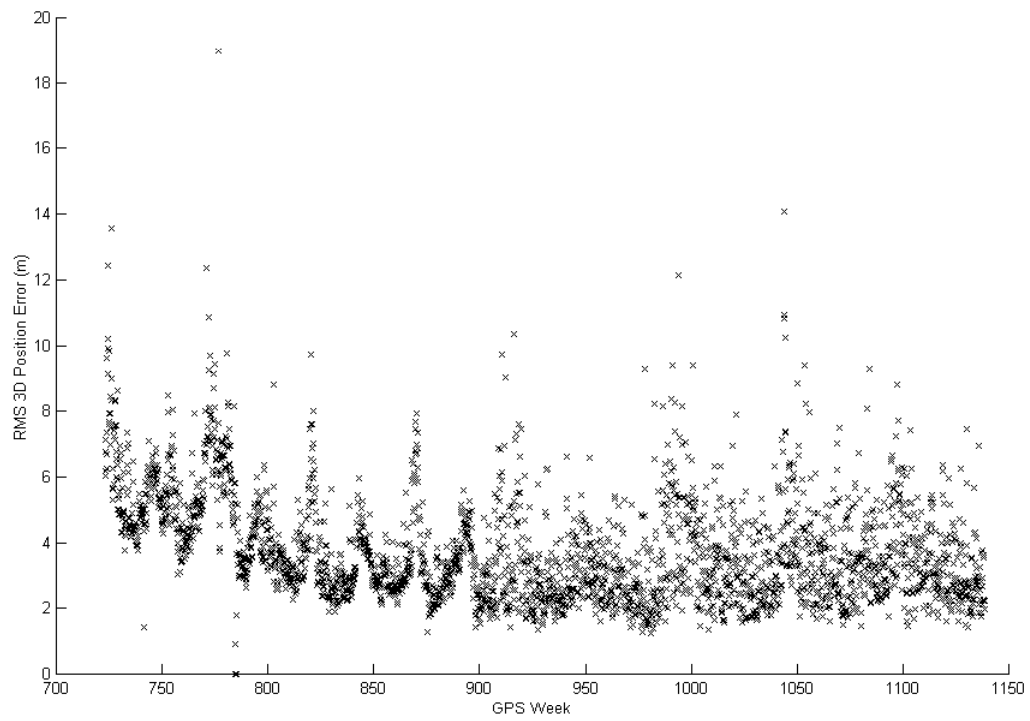
PRN 29 – SVN 29 (Block II)



PRN 30 – SVN 30 (Block II)

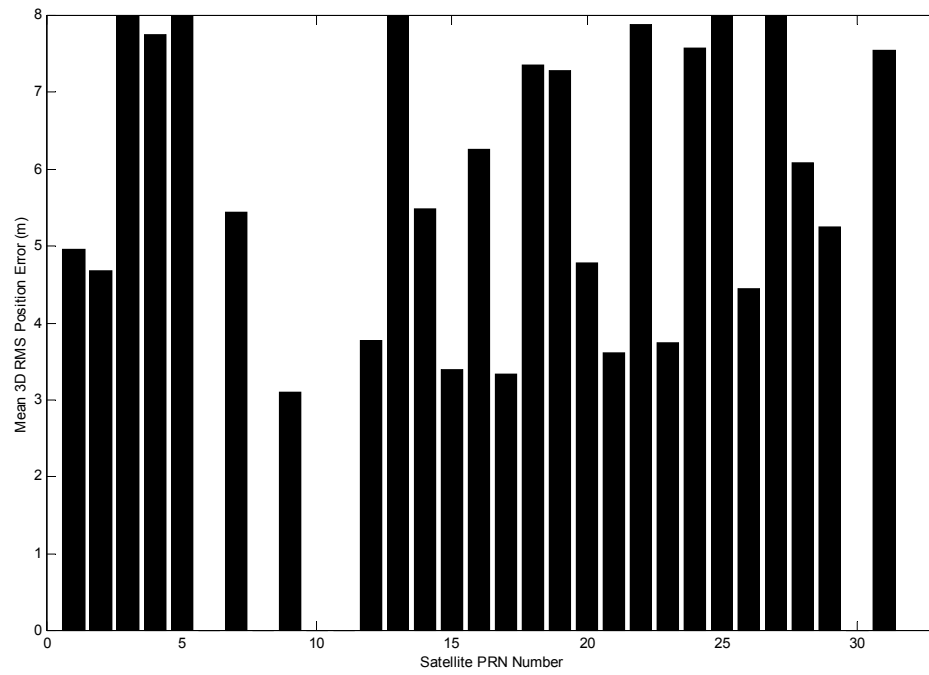


PRN 31 – SVN 31 (Block II)

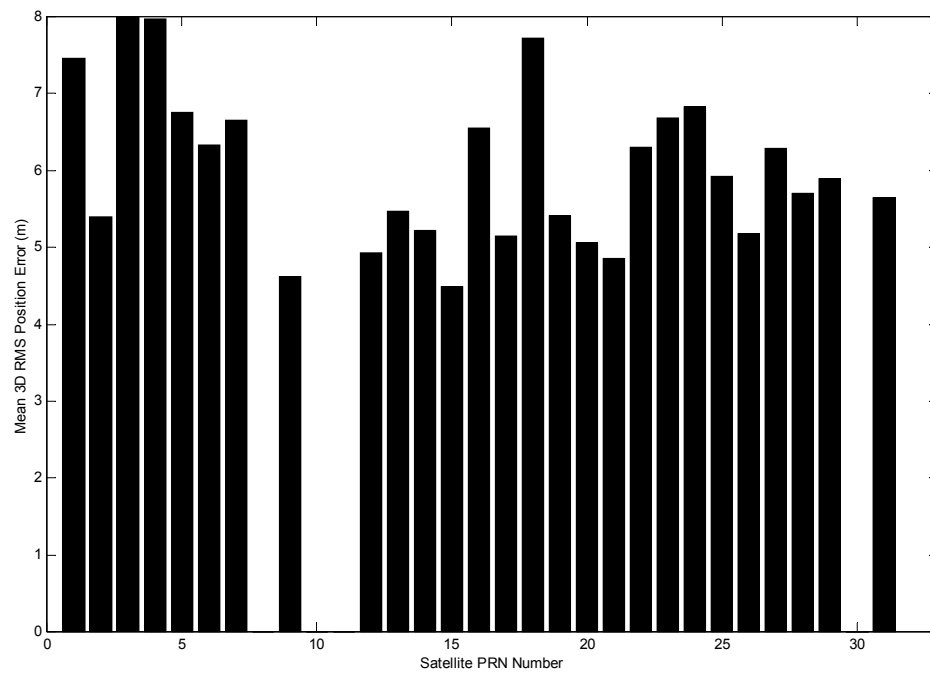


Appendix E: Mean 3D ACR Broadcast Position Error

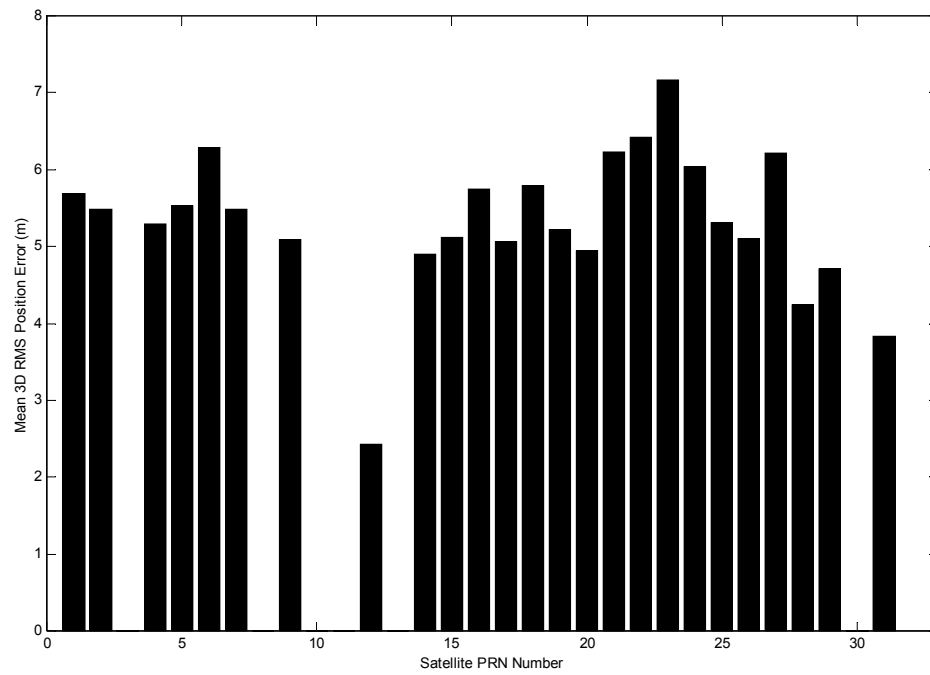
1993



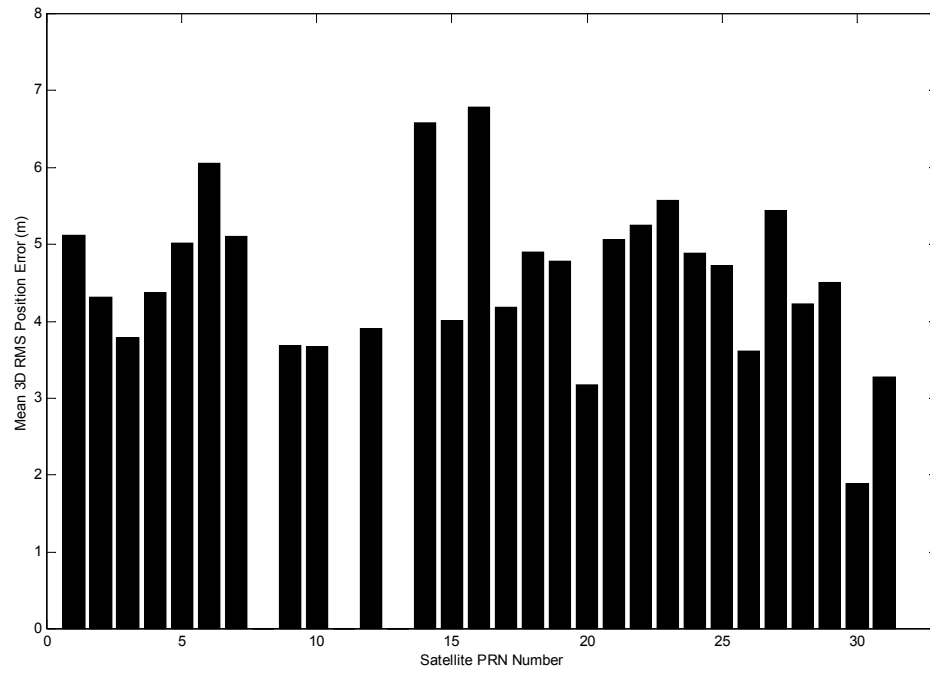
1994



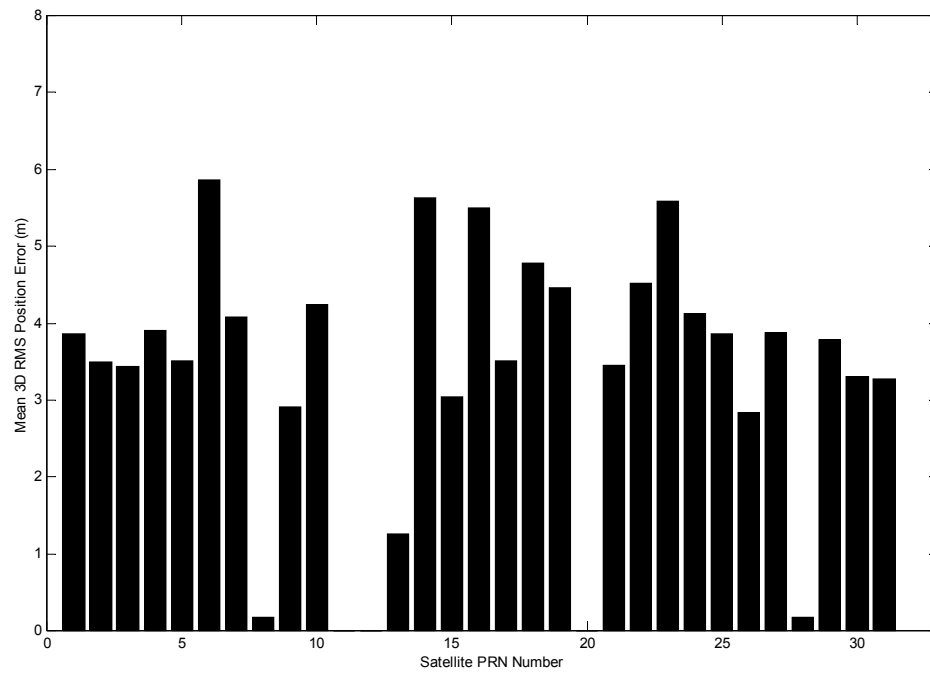
1995



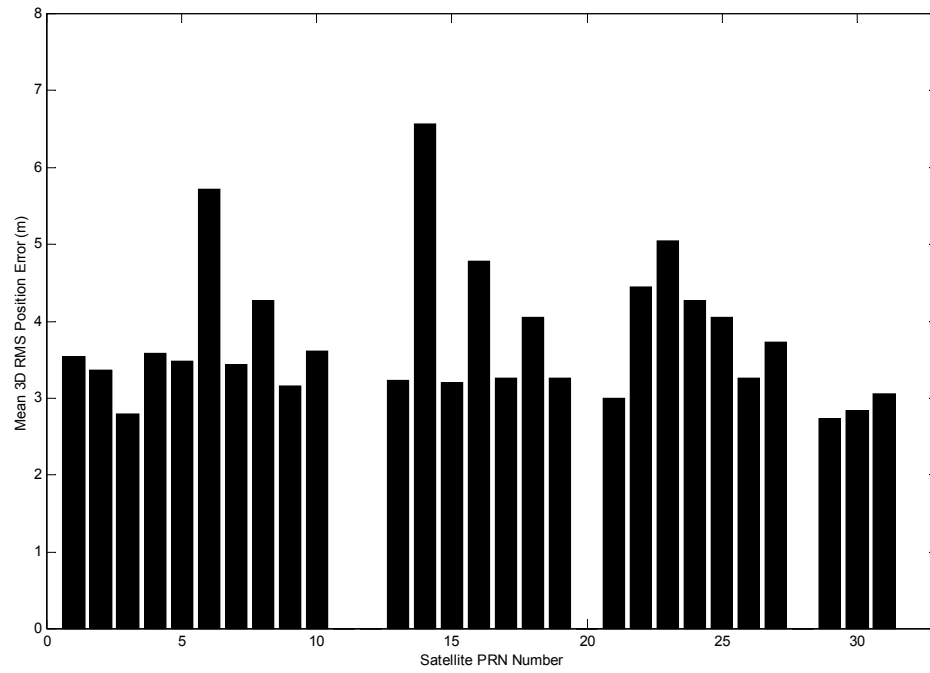
1996



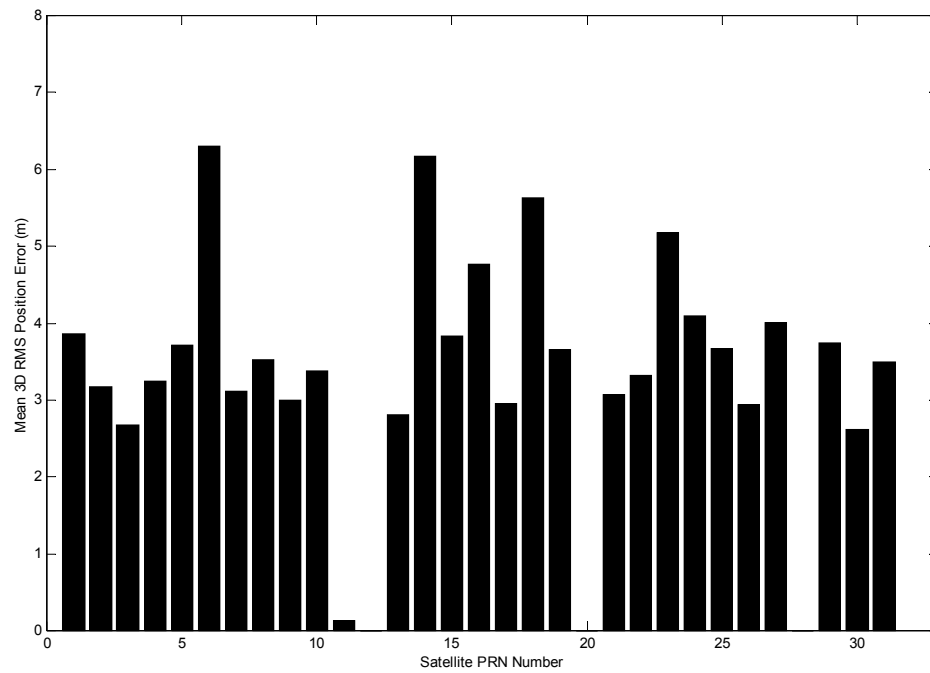
1997



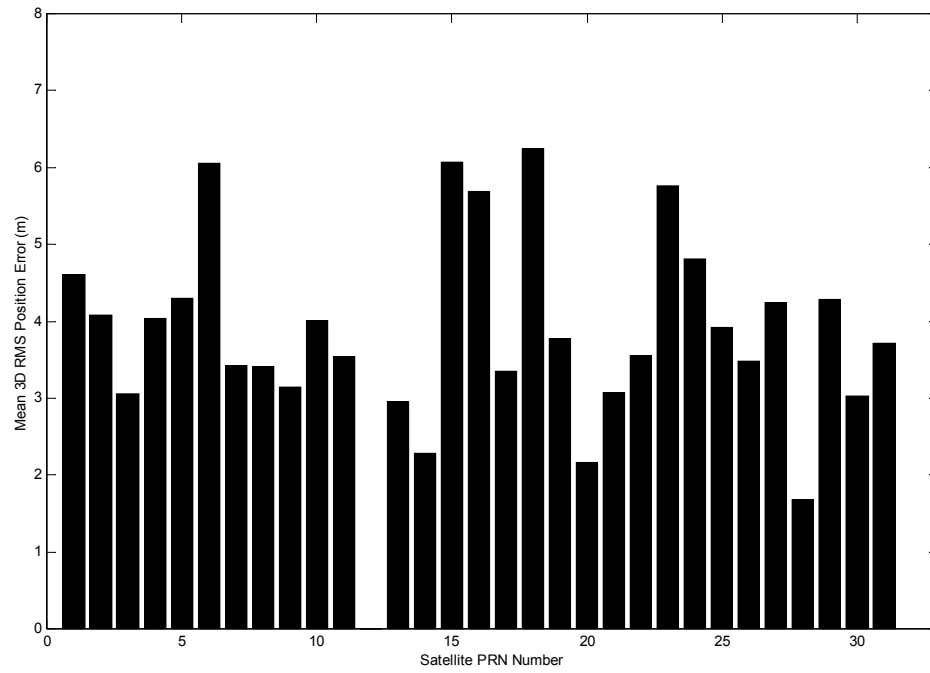
1998



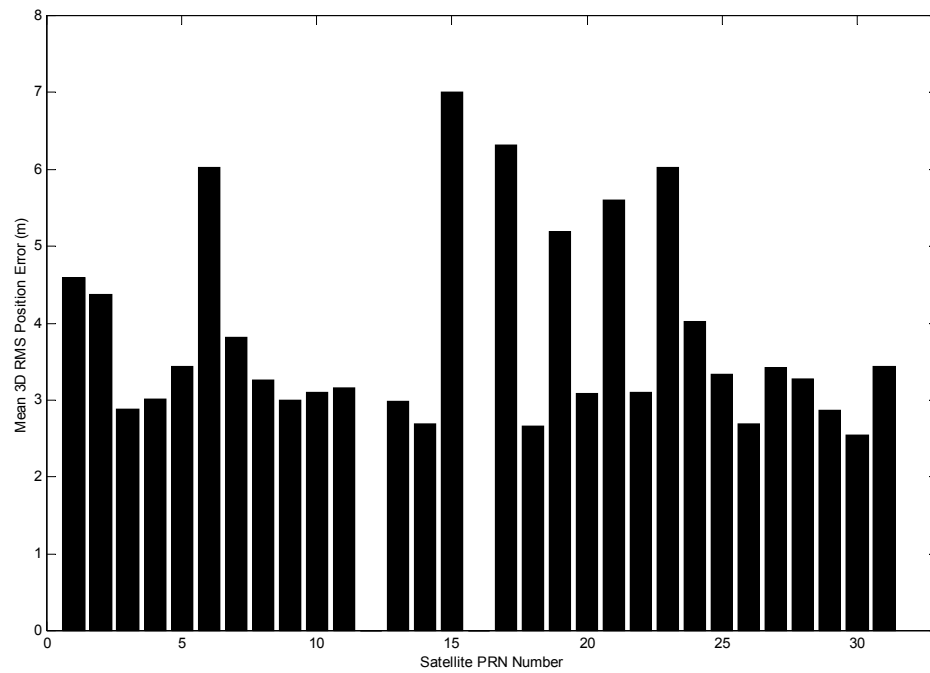
1999



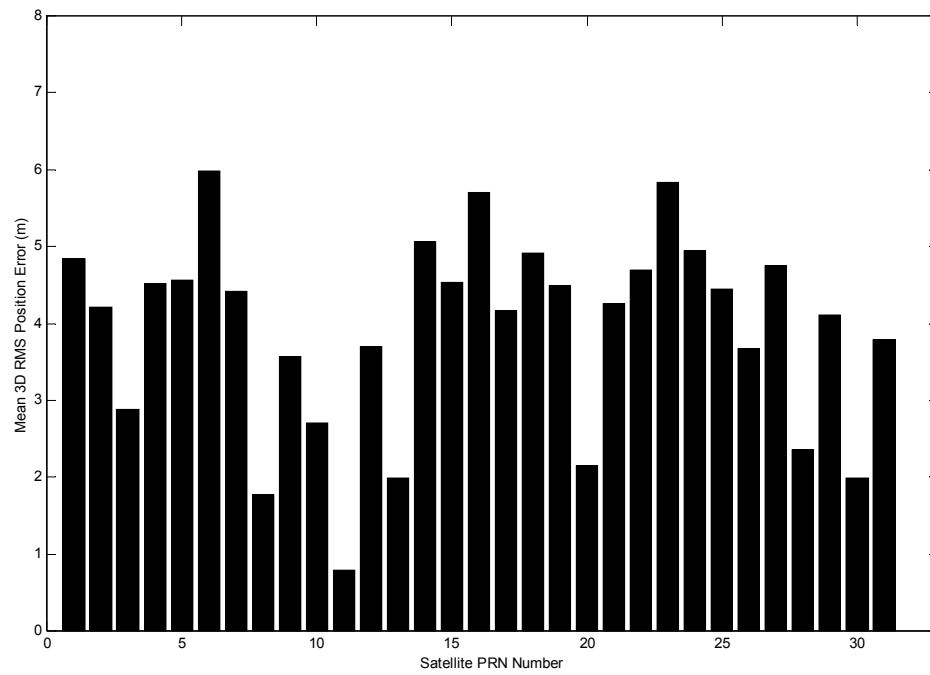
2000



2001



14 Nov 1993 to 1 Nov 2001



Bibliography

- Beutler, G., H. Bock, R. Dach, P. Fridez, W. Gurtner, U. Hugentobler, D. Ineichen, M. Meindl, L. Mervart, M. Rothacher, and S. Schaer, *Bernese GPS Software Introduction Course – Orbit Part*, October 2001.
- “Boeing: Products – GPS – General Data”, Boeing, www.boeing.com/defense-space/space/gps/m_gen.html, 2002.
- Conley, R., “Results of the GPS JPO’s GPS Performance Baseline Analysis: The GOSPAR Project”, *Proceedings of the Institute of Navigation Conference Global Positioning System 2000*, pp 365 – 375, 2000.
- Cook, Dayne.G. Major, USAF., *Solar Radiation Pressure Modelling Issues For High Altitude Satellites*, MS Thesis, US Department of the Air Force, Air University, AFIT, March 2001.
- Crowe, Ken SGNLDR, RAAF, *A Comparative Analysis of the Iridium and Globalstar Satellite Transmission Paths*, MS Thesis, US Department of the Air Force, Air University, AFIT, March 1999.
- Crum, J, Lt. USAF, *2SOPS Ephemeris Enhancement Endeavour Briefing Notes*, 1997.
- “Crustal Dynamics Data Information System (CDDIS) FTP Site”, <ftp://cddisa.gsfc.nasa.gov/pub/gps/gpsdata/brdc/>, January 2002.
- Crustal Dynamics Data Information System (CDDIS) Web Site, “RINEX Format”, <ftp://cddisa.gsfc.nasa.gov/pub/formats/rinex.format>, January 2002.
- Crustal Dynamics Data Information System (CDDIS) Web Site, “SP3 Format History”, <ftp://cddisa.gsfc.nasa.gov/pub/formats/orbits.format>, January 2002.
- “Description of Mission”, www.tsgc.utexas.edu/spacecraft/topex/pod.html, 2002.
- Dias, B., “GPS”, www.giswww.pok.ibm.com/gps/gpsweb.html, 2002.
- “Garmin – About GPS”, <http://www.garmin.com/aboutGPS/>, 2002.
- “GPS 35 – 36”, www.ilrs.gsfc.gov/gps.html, 2002.
- “GPS Info”, http://www.gpsdata.com/GPS_INFO.htm#spacesegment, GPS USA Ltd, 2002.
- “GPS Operational Advisory, 270.OA1”, www.navcen.uscg.gov, 27 Sep 2001.
- “GPS Overview”, www.forestry.umat.edu/academics/courses/X495/GPS_Overview.htm, 2002.
- “GPS Tutor Introduction”, Mercator Inc, www.mercat.com/QUEST/Intro.htm, 2002.
- Hofman-Wellenhof .B., H. Lichtenegger, and J. Collins, *GPS – Theory and Practice*, 3rd Edition, Springer-Verlag Wein New York, 1994.
- “International GPS Service for Geodynamics (IGS) Website”, <http://igsb.jpl.nasa.gov>, January 2002.
- International GPS Service for Geodynamics (IGS) Website. “IGS Analysis Centres”, <ftp://igsb.jpl.nasa.gov/pub/center/analysis>, January 2002.
- International GPS Service for Geodynamics (IGS) Website, “Data Formats”, ftp://igsb.jpl.nasa.gov/igsb/data/format/sp3_docu.txt, January 2002.

- International GPS Service for Geodynamics (IGS) Website, “Products Page”,
<http://igsb.jpl.nasa.gov/components/prods.html>, January 2002.
- Jefferson, D.C., and Y.E. Bar-Sever, “Accuracy and Consistency of Broadcast GPS Ephemeris Data”, *Proceeding of the Institute of Navigation Conference Global Positioning System 2000*, pp 391 – 395, 2000.
- Kelso, T.S., “NORAD Two-Line Element Sets”, <http://celestrak.com/NORAD/elements>, 2002.
- Langley, R.B., H. Jannasch, B. Peeters, and S. Bisnath, “The GPS Broadcast Orbits: An Accuracy Analysis”, *Proceedings of the 33rd COSPAR Scientific Assembly*, Warsaw, July 2000.
- Lockheed Martin Federal Systems, *GPS OCS Performance Analysis and Reporting (GOSPAR) Project Final Report*, September 30, 1996.
- Malys, Stephen., Margaret Larezos, Stephen Gottschalk, Shawn Monns, Bryant Wim, William Fess, Michael Menn, Everett Swift, Michael Merrigan and William Mathon, “The GPS Accuracy Improvement Initiative”, *Proceedings of the Institute of Navigation Global Positioning System Conference 1997*, 1997.
- Malys, S., J. Slater, R. Smith, L. Kunz, and S. Kenyan, “Refinements of The World Geodetic System 1984”, *Proceeding of the Institute of Navigation Conference Global Positioning System 1997*, pp 841-850, 1997.
- Nelson, Robert.A., Dr. “The Global Positioning System: A detailed look at the miracle of modern navigation”, Satellite Engineering Research Corporation,
www.atcourses.com/global_positioning_system.htm, 2002.
- National Imaging and Mapping Agency (NIMA) Web Site, “SP3 Format”,
<http://164.214.2.59/GandG/sathtml/sp3format.html>, January 2002.
- Notice Advisory to NAVSTAR Users 121-92282, DTG 011354ZJUL91.
- Pace, Scott, Gerald Frost, Irving Lachow, David Frelinger, Donna Fossum, D.K. Wassem, and Monica Pinto, *The Global Positioning System – Assessing National Policies*, RAND Critical Technologies Institute, Appendix B, 1995.
- Parkinson, Bradford.W., “Introduction and Heritage of NAVSTAR, the Global Positioning System”, *Global Positioning System: Theory and Applications, Volume 1*, Chap 1, Progress in Astronautics and Aeronautics, Volume 163, American Institute of Astronautics and Aeronautics Inc, 1996.
- Pollock, Peter SQLNDR, RAAF, *A Model to Predict Diffraction Attenuation Resulting From Signal Propagation Over Terrain in Low Earth Orbit Satellite Systems*, MS Thesis, US Department of the Air Force, Air University, AFIT, March 2001.
- Roulston, A., N. Talbot, and K. Zhang, “An Evaluation of Various GPS Satellite Ephemerides”, *Proceedings of the Institute of Navigation Conference Global Positioning System 2000*, pp 45 – 54, 2000.
- Russell, S.S., and J.H. Schaibly, “Control Segment and User Performance”, *Global Positioning System - Papers in Navigation, Volume 1*, Institute of Navigation, 1980.
- Spilker, J.J Jr., and Bradford W. Parkinson, “Overview of GPS Operation and Design”, *Global Positioning System: Theory and Applications, Volume 1*, Chap 2, Progress in Astronautics and Aeronautics, Volume 163, American Institute of Astronautics and Aeronautics Inc, 1996.

- Spilker, J.J Jr., "GPS Signal Structure and Performance Characteristics", *Global Positioning System: Papers in Navigation, Volume I*, Institute of Navigation, 1980.
- Spilker, J.J Jr., "GPS Navigation Data", *Global Positioning System: Theory and Applications, Volume I*, Chap 2, Progress in Astronautics and Aeronautics, Volume 163, American Institute of Astronautics and Aeronautics Inc, 1996.
- Springer, T.A., G. Beutler and M. Rothacher, "A New Solar Radiation Pressure Model for GPS", *Advance in Space Research*, 1999.
- Tascione, T.F., *Introduction to the Space Environment*, 2nd Edition, Orbit Foundation Series, Krieger Publishing Company, Florida, 1994.
- The Global Positioning System: A Shared National Asset*, National Research Council (NRC), Washington, 1995.
- "Tidal Forces", <http://www.dur.ac.uk/~dph0rms/solar-system/lectures/notes/node35.html>, 2002.
- "US Coast Guard Navigation Centre GPS Almanac Website", <http://www.navcen.uscg.gov/gps/defaulttxt.htm#Almanacs>, January 2002.
- US Coast Guard Web Site, "SEM Format", <http://www.navcen.uscg.gov/GPS/gpssem.htm>, January 2002.
- US Coast Guard Web Site, "YUMA Format", <http://www.navcen.uscg.gov/GPS/gpsyuma.htm>, January 2002.
- United States Naval Observatory (USNO) Website, "NAVSTAR Global Positioning System", www.tycho.usno.navy.mil/gpsinfo.html, 2002.
- Van Dierendonck, A.J., S.S. Russell, E.R. Kopitzke, and M. Birnbaum, "The GPS Navigational Message", *Global Positioning System - Papers in Navigation, Volume I*, Institute of Navigation, 1980.
- Wertz, James.R., and W.J. Larson, *Space Mission Analysis and Design*, 3rd Edition, Space Technology Series, Microcosm Press and Kluwer Academic Publishers, 1999.
- Weisal, W.E., *Spaceflight Dynamics*, 2nd Edition, Irwin McGraw-Hill, 1995.
- Weiss, M.A., G. Petit, and S. Shattil, "A Comparison of GPS Broadcast and DMA Precise Ephemeris", *Proceedings of the Precise Time and Time Interval (PTTI) Systems and Applications Meeting*, pp 293-306, 1994.
- Zumberge, J.F., and W.I. Bertiger, "Ephemeris and Clock Navigation Message Accuracy, In:" B. Parkinson, and J.J. Spilker (Editor), *Global Positioning System: Theory and Application*, pp 585-599, 1996.

Vita

Squadron Leader David Warren was born in Newcastle, Australia. He joined the Royal Australian Air Force as an Engineering Officer Cadet in January 1989 and graduated from the Australian Defence Force Academy in Canberra, Australia in 1992 with a Bachelor Degree in Electronics Engineering. From 1992 to 2000 he occupied a series of positions relating to simulation, logistics, engineering development and project management within the F/A-18 Hornet support environment. In August 2000, he entered the Graduate School of Engineering at the Air Force Institute of Technology.

REPORT DOCUMENTATION PAGE				Form Approved OMB No. 074-0188	
<p>The public reporting burden for this collection of information is estimated to average 1 hour per response, including the time for reviewing instructions, searching existing data sources, gathering and maintaining the data needed, and completing and reviewing the collection of information. Send comments regarding this burden estimate or any other aspect of the collection of information, including suggestions for reducing this burden to Department of Defense, Washington Headquarters Services, Directorate for Information Operations and Reports (0704-0188), 1215 Jefferson Davis Highway, Suite 1204, Arlington, VA 22202-4302. Respondents should be aware that notwithstanding any other provision of law, no person shall be subject to a penalty for failing to comply with a collection of information if it does not display a currently valid OMB control number.</p> <p>PLEASE DO NOT RETURN YOUR FORM TO THE ABOVE ADDRESS.</p>					
1. REPORT DATE (DD-MM-YYYY) 26 Mar 2002		2. REPORT TYPE Thesis		3. DATES COVERED (From – To) 8 Aug 2000 – 26 Mar 2002	
4. TITLE AND SUBTITLE BROADCAST VS PRECISE GPS EPHEMERIDES: A HISTORICAL PERSPECTIVE				5a. CONTRACT NUMBER	
				5b. GRANT NUMBER	
				5c. PROGRAM ELEMENT NUMBER	
6. AUTHOR(S) Warren, David.L.M., Squadron Leader, RAAF				5d. PROJECT NUMBER	
				5e. TASK NUMBER	
				5f. WORK UNIT NUMBER	
7. PERFORMING ORGANIZATION NAMES(S) AND ADDRESS(S) Air Force Institute of Technology Graduate School of Engineering and Management (AFIT/ENY) 2950 P Street, Building 640 WPAFB OH 45433-7765				8. PERFORMING ORGANIZATION REPORT NUMBER AFIT/GSO/ENG/02M-01	
9. SPONSORING/MONITORING AGENCY NAME(S) AND ADDRESS(ES) Major David Goldstein, SMC/CZE 2435 Vela Way Suite 1613, El Segundo, CA 90245-5500 Tel DSN 833-1208 Comm (310) 363-1208 Fax (310) 363-6387				10. SPONSOR/MONITOR'S ACRONYM(S) SMC/CZE	
				11. SPONSOR/MONITOR'S REPORT NUMBER(S)	
12. DISTRIBUTION/AVAILABILITY STATEMENT APPROVED FOR PUBLIC RELEASE; DISTRIBUTION UNLIMITED.					
13. SUPPLEMENTARY NOTES					
14. ABSTRACT <p>The Global Positioning System (GPS) Operational Control Segment (OCS) generates predicted satellite ephemerides and clock corrections that are broadcast in the navigation message and used by receivers to estimate real-time satellite position and clock corrections for use in navigation solutions. Any errors in these ephemerides will directly impact the accuracy of GPS based positioning. This study compares the satellite position computed using broadcast ephemerides with the precise position provided by the International GPS Service for Geodynamics (IGS) Final Orbit solution. Similar comparisons have been undertaken in the past, but for only short periods of time. This study presents an analysis of the GPS broadcast ephemeris position error on a daily basis over the entire period 14 Nov 1993 through to 1 Nov 2001. The statistics of these errors were also analysed. In addition, the satellite position computed using the almanac ephemeris was compared to the IGS precise final orbit to determine the long-term effect of using older almanac data. The results of this research provide an independent method for the GPS Joint Program Office (JPO) and the OCS to gauge the direct impact of Kalman filter modifications on the accuracy of the navigational information available to the GPS users. GPS engineers can compare future Kalman filter changes to the historical baseline developed by this thesis and readily assess the significance of each proposed engineering change.</p>					
15. SUBJECT TERMS GPS, Global Positioning, Ephemeris, Ephemerides, Navigation, Error, Almanac, Broadcast					
16. SECURITY CLASSIFICATION OF:			17. LIMITATION OF ABSTRACT UU	18. NUMBER OF PAGES 182	19a. NAME OF RESPONSIBLE PERSON Raquet, J.F.K, Major, USAF, john.raquet@afit.edu
. REPORT ^a U	. ABSTRACT ^b U	. THIS PAGE ^c U			19b. TELEPHONE NUMBER (Include area code) (937) 785-3636 x4580

Standard Form 298 (Rev. 8-98)
Prescribed by ANSI Std. Z39-18

Form Approved
OMB No. 074-0188